

Advancing Membrane Technologies for Recovery of Phosphorus and Nitrogen from Human  
Urine

Stephanie Nicole McCartney

Submitted in partial fulfillment of the  
requirements for the degree of  
Doctor of Philosophy  
under the Executive Committee  
of the Graduate School of Arts and Sciences

COLUMBIA UNIVERSITY

2022

© 2022

Stephanie Nicole McCartney

All Rights Reserved

## **Abstract**

Advancing Membrane Technologies for Recovery of Phosphorus and Nitrogen from Human  
Urine

Stephanie Nicole McCartney

The existing linear economy approach to nutrient management has clear shortcomings including high expenditures for nutrient extraction and production of fertilizer as well as additional costs for nutrient removal at downstream waste water treatment plants (WWTPs) to prevent the pollution of aquatic environments. In a circular nutrient economy, phosphorus (P) and nitrogen (N) are removed from waste streams and captured as valuable fertilizer products in order to more sustainably reuse the resources in closed-loops and simultaneously protect receiving aquatic environments from harmful P and N emissions. The overarching aim of this thesis is to understand strategic approaches for nutrient recovery from wastewater and advance membrane technologies for P and N reclamation. The studies i.) approach nutrient recovery on a system-level to recognize optimal waste streams to target for P and N separation, ii.) advance membrane-based processes for nutrient recovery, and iii.) examine the economic viability of the nutrient recovery techniques.

The thesis presents a thermodynamic and energy analysis of nutrient recovery from various waste streams of fresh and hydrolyzed urine, greywater, domestic wastewater, and secondary treated wastewater effluent. The analysis revealed comparative advantages in theoretical energy

intensities for P and N recovery from nutrient-dense waste streams, such as fresh and hydrolyzed urine, compared to other more dilute sources. The thesis quantifies efficiencies required by separation techniques for nutrient reclamation to be competitive with the energy requirements of the prevailing industrial fertilizer production methods, i.e., phosphate mining and nitrogen fixation by the Haber-Bosch process.

The dissertation examines and advances the performance of membrane-based processes for separation and recovery of P and N from diverted human urine. Donnan dialysis (DD), an ion-exchange membrane-based process, can capture and enrich orthophosphate,  $H_xPO_4^{(3-x)-}$ , from source-separated urine. This work demonstrates the transport of  $Cl^-$  driver ions down a concentration gradient, across an ion-exchange membrane to set up an electrochemical potential gradient that drives the transport of target  $H_xPO_4^{(3-x)-}$  in the opposite direction, enabling P capture. Importantly,  $H_2PO_4^-$  is transported against an orthophosphate concentration gradient, which achieves uphill transport of P. The thesis also provides a framework to better understand the impact of different ions in the water matrix on P recovery potential and kinetics.

The thesis presents a novel operation of membrane distillation (MD) — *isothermal* membrane distillation with *acidic collector* (IMD-AC) — to selectively recover volatile ammonia,  $NH_3$ , from hydrolyzed urine. The innovative isothermal and acidic collector features, respectively, suppressed undesired water permeation and enhanced ammonia vapor flux relative to conventional membrane distillation (CMD). The elimination of water flux in IMD-AC resulted in  $\approx 95\%$  savings in vaporization energy consumption relative to CMD. Critically, IMD-AC achieved uphill transport of ammoniacal nitrogen, i.e., transport against a concentration gradient, demonstrating the promising potential of the technique for N recovery.

The dissertation proposes an integrated bipolar membrane electrodialysis (BPM-ED), DD, and IMD-AC system to drive the separation and recovery of orthophosphate and ammoniacal nitrogen from human urine. This work elucidates the role of pH and nutrient speciation (i.e.,  $\text{H}_2\text{PO}_4^-$  versus  $\text{HPO}_4^{2-}$  and  $\text{NH}_4^+$  versus  $\text{NH}_3$ ) on the performance of DD and IMD-AC. In the proposed configuration, BPM-ED generates acids and bases *in situ* to strategically control the pH of urine streams to benefit DD and IMD-AC performances. Strategic pH modification can enhance orthophosphate transport and selectivity in DD as well as ammonia transport and recovery potential in IMD-AC. Importantly, the analysis quantifies comparable specific energy consumptions of the proposed integrated membrane-based process to the existing approaches to P and N management.

This thesis presents a preliminary economic assessment of onsite nutrient recovery employing DD and IMD-AC for respective P and N recovery from diverted urine. The analysis reveals opportunities to utilize widely-available waste chemical streams and recovered thermal energy to improve the economic viability of nutrient recovery. The largest capital expenditures are urine diversion toilets and additional piping for source-separation. Preliminary analysis demonstrates that employing urine diversion in public sanitation rooms, as opposed to private bathrooms, can reduce these capital expenditures. Furthermore, realizing savings from avoided costs for downstream nutrient removal at centralized wastewater treatment plants in addition to fertilizer revenue can enhance the economic viability of the approach.

Overall, this dissertation critically informs nutrient recovery approaches and advances membrane-based processes for P and N reclamation to facilitate a paradigm shift from an inefficient linear nutrient economy to a sustainable circular nutrient economy. The work reveals opportunities to minimize energy intensity for nutrient separation, advance the performance of

membrane-based techniques for selective and energy-efficient nutrient recovery from urine, and enhance the cost-competitiveness of nutrient reclamation. The findings of this work support nutrient recovery efforts and provide important insights that can be applied to other separation and resource recovery endeavors.

# Table of Contents

List of Figures .....	v
List of Tables .....	xiii
Acknowledgements .....	xvii
Chapter 1: Introduction .....	1
1.1 Motivation .....	1
1.2 Objectives and Scope of Dissertation.....	6
1.3 Thesis Structure.....	7
1.4 Key Contributions .....	10
Chapter 2: Emerging Investigator Series: Thermodynamic and Energy Analysis of Nitrogen and Phosphorous Recovery from Wastewaters .....	13
Chapter Abstract.....	13
2.1 Introduction .....	14
2.2 Minimum Energy of Nutrient Recovery .....	17
2.3 Energy Requirement for Nutrient Recovery .....	20
2.4 Implications.....	39
Chapter 3: Donnan Dialysis for Phosphate Recovery from Diverted Urine.....	42
Chapter Abstract.....	42
3.1 Introduction .....	43
3.2 Working Principles of Donnan Dialysis.....	45

3.3 Materials and Methods .....	48
3.4 Results and Discussion.....	52
3.5 Implications.....	76
Chapter 4: Novel Isothermal Membrane Distillation with Acidic Collector for Selective and Energy-Efficient Recovery of Ammonia from Urine .....	
Chapter Abstract.....	79
4.1 Introduction .....	80
4.2 Isothermal Membrane Distillation with Acidic Collector.....	82
4.3 Experimental Section .....	86
4.4 Results and Discussion.....	88
4.5 Implications.....	102
Chapter Abstract.....	105
5.1 Introduction .....	106
5.2 Working Principles.....	108
5.3 Materials and Methods .....	115
5.4 Results and Discussion.....	121
5.5 Implications.....	145
Chapter 6: Evaluation of Costs and Benefits of Nutrient Recovery in Onsite Wastewater Management.....	
Chapter Abstract.....	150
6.1 Introduction .....	151

6.2 Description of Onsite Nutrient Recovery .....	152
6.3 Assessment Methods and Assumptions .....	156
6.4 Implementation of Nutrient Recovery.....	160
6.5 Implications.....	171
Chapter 7: Conclusions.....	176
7.1 Summary .....	176
7.2 Novel Contributions .....	179
7.3 Resulting Publications.....	182
7.4 Implications and Future Directions.....	183
References.....	190
Appendix A: Supporting Information for Chapter 2.....	213
A.1 Methodology to Determine Molar Minimum Energy of Recovery .....	213
A.2 Molar Minimum Energy Equations.....	217
A.3 Activity Coefficient Models.....	227
A.4 Methodology to Determine the Molar Minimum Energy to Recover N from Hydrolyzed Urine at $Y > 0$ .....	234
A.5 Impact of Recovery Yield on Molar Minimum Energy of Recovery .....	236
Appendix B: Supporting Information for Chapter 3.....	241
B.1 Donnan Equilibrium .....	241
B.2 Simulated Waste Water Softening Regenerant Rinse .....	245
B.3 Simulated Dilute Bittern.....	247

B.4 Sorption Experimental Protocol .....	252
Appendix C: Supporting Information for Chapter 4.....	255
C.1 Determination of Vapor Pressure .....	255
C.2 Vaporization Enthalpy of Ammonia from Aqueous Solutions .....	262
Appendix D: Supporting Information for Chapter 5.....	266
D.1 Specific Energy Consumption of BPM-ED .....	267
Appendix E: Supporting Information for Chapter 6.....	271
E.1 Thermal Energy in Membrane Distillation.....	273

## List of Figures

Figure 1.1. A) Harmful algal blooms in Lake Erie on September 3, 2011. B) Eutrophication and hypoxic dead-zones in North America, particularly along the coast. ....2

Figure 1.2. The current linear economy management of N and P requires high energy to produce nutrients and demands high energy and chemicals downstream for nutrient removal. In contrast is a circular nutrient economy management, where nutrients are recovered from waste streams and re-entered into the food-chain, closing the nutrient “loop.”.....3

Figure 2.1. A) Illustrative representation of wastewater sources and streams. B) Concentration range of total ammoniacal nitrogen, TAN, and total orthophosphate, TOP, for waste streams of greywater, fresh urine, hydrolyzed urine, domestic WW, and secondary (2°) WW effluent.....15

Figure 2.2. Molar minimum energy,  $\bar{E}_{\min}$ , to recover nutrient product of pure liquid ammonia as a function of waste stream TAN concentration for recovery yields,  $Y$ , of 1 and 0.....21

Figure 2.3. Molar minimum energy,  $\bar{E}_{\min}$ , to recover A) TAN as products of liquid ammonia,  $\text{NH}_{3(l)}$ , 10, 5.0, and 1.0 M aqueous ammonia solutions, and ammonium sulfate solid,  $(\text{NH}_4)_2\text{SO}_{4(s)}$ ; and B) TOP as mineral products of potassium magnesium phosphate,  $\text{KMgPO}_4 \cdot 6(\text{H}_2\text{O})$ , struvite,  $\text{NH}_4\text{MgPO}_4 \cdot 6\text{H}_2\text{O}$ , potassium phosphate,  $\text{KH}_2\text{PO}_4$ , and monoammonium phosphate,  $\text{NH}_4\text{H}_2\text{PO}_4$ .....24

Figure 2.4. Molar minimum energy,  $\bar{E}_{\min}$ , to recover TAN product of 1.0 M  $\text{NH}_{3(aq)}$  and TOP product of struvite,  $\text{NH}_4\text{MgPO}_4 \cdot 6\text{H}_2\text{O}_{(s)}$ , from greywater at pH of 5.0 and 9.0.....35

Figure 2.5. Molar minimum energy,  $\bar{E}_{\min}$ , to recover  $\text{NH}_3$  as products of liquid ammonia,  $\text{NH}_{3(l)}$ , or 1.0 M  $\text{NH}_{3(aq)}$  aqueous solution from secondary wastewater effluent and hydrolyzed urine as a function of recovery yield,  $Y$ .....30

Figure 2.6. Molar minimum energy,  $\bar{E}_{\min}$ , to recover different N products from waste streams of secondary wastewater effluent and fresh urine. Products recovered from 2° WW effluent are 1.0 M  $\text{KNO}_{3(aq)}$ , 1.0 M  $\text{NH}_4\text{NO}_{3(aq)}$ ,  $\text{KNO}_{3(s)}$ , and  $\text{NH}_4\text{NO}_{3(s)}$ , whereas products reclaimed from fresh urine are 1.0 M aqueous urea solution,  $\text{CO}(\text{NH}_2)_{2(aq)}$ , and solid urea,  $\text{CO}(\text{NH}_2)_{2(s)}$ .....33

Figure 2.7. Practical molar energy,  $\bar{E}_{\text{prac}}$  as a function of efficiency,  $\eta$ , for an actual process to recover A) TAN from hydrolyzed urine and secondary wastewater effluent as 1.0 M  $\text{NH}_{3(aq)}$  and  $\text{NH}_{3(l)}$  and B) TOP from fresh urine and secondary wastewater effluent as  $\text{KMgPO}_4 \cdot 6\text{H}_2\text{O}_{(s)}$  and  $\text{KH}_2\text{PO}_4_{(s)}$ .....37

Figure 3.1. Schematic depicting Donnan dialysis recovery of orthophosphates.....47

Figure 3.2. Concentrations of  $\text{H}_2\text{PO}_4^-$  and  $\text{Cl}^-$  in the FS and  $\text{H}_2\text{PO}_4^-$  concentration in the RS as a function of time during DD orthophosphate recovery. ....53

Figure 3.3. A)  $[\text{H}_x\text{PO}_4^{(3-x)-}]_{\text{RS},f}$  and  $[\text{Cl}^-]_{\text{FS},f}$  (patterned blue and gray columns, respectively) in DD with different initial NaCl concentrations in the receiver solution. Predicted  $[\text{H}_x\text{PO}_4^{(3-x)-}]_{\text{RS},f}$  at Donnan equilibrium, calculated using eq **Error! Reference source not found.**, are depicted by the empty blue columns. Labels above the columns indicate the percentage of predicted  $[\text{H}_x\text{PO}_4^{(3-x)-}]_{\text{RS},f}$  experimentally captured in the RS. B) Experimental and predicted orthophosphate recovery yields,  $Y$ , in DD with the different  $[\text{Cl}^-]_{\text{RS},0}$ . ....56

Figure 3.4. Receiver solution final TOP concentration,  $[\text{H}_x\text{PO}_4^{(3-x)-}]_{\text{RS},f}$ , and orthophosphate recovery yields,  $Y$ , as a function of  $V_{\text{FS}}/V_{\text{RS}}$ . .....59

Figure 3.5. A) Final RS concentrations,  $[\text{H}_x\text{PO}_4^{(3-x)-}]_{\text{RS},f}$ ,  $[\text{SO}_4^{2-}]_{\text{RS},f}$ , and  $[\text{HCO}_3^-]_{\text{RS},f}$ , and B) orthophosphate recovery yields in TOP recovery experiments with different urine matrices as initial feed solutions.....62

Figure 3.6.  $\text{H}_x\text{PO}_4^{(3-x)-}$ ,  $\text{SO}_4^{2-}$ , and  $\text{HCO}_3^-$  anion fluxes from FS to RS,  $J_i$ , in kinetic experiments with different urine matrices as initial feed solutions. The anions of the five FS are: i) orthophosphate only, ii) orthophosphate and sulfate, iii) orthophosphate and chloride, iv) orthophosphate, sulfate, and chloride (fresh urine), and v) orthophosphate, sulfate, bicarbonate, and chloride (hydrolyzed urine). .....67

Figure 3.7. A) Orthophosphate and sulfate molar fluxes from feed solution to receiver solution,  $J_i$ , and B) flux selectivity in DD kinetic experiments for conventional anion exchange membrane, AMV, and monovalent ion selective membrane, ASVN. ....72

Figure 3.8. Fluxes of  $\text{H}_x\text{PO}_4^{(3-x)-}$  and  $\text{SO}_4^{2-}$  (blue and orange columns, respectively) in kinetic experiments with different initial receiver solutions of simulated aqueous potash solution (APS,  $[\text{Cl}^-] = 600 \times 10^{-3} \text{ mol/L}$ ), simulated waste water softening regenerant rinse, (WWSRR,  $[\text{Cl}^-] = 643 \times 10^{-3} \text{ mol/L}$ ), and simulated diluted bittern (DB,  $[\text{Cl}^-] = 615 \times 10^{-3} \text{ mol/L}$ ).....75

Figure 4.1. Temperature and vapor pressure profiles for A) conventional and B) isothermal MD with acidic collector. ....84

Figure 4.2. Ammonia and water vapor fluxes for four different MD operations: CMD-DI with 40 °C feed and 20 °C DI water collector, CMD-AC with 40 °C feed and 20 °C acidic collector,

IMD-DI with 40 °C feed and 40 °C DI water collector, and IMD-AC with 40 °C feed and 40 °C acidic collector. ....	89
Figure 4.3. Relative molar flux of water to ammonia for the four operations, CMD-DI, CMD-AC, IMD-DI, and IMD-AC. IMD-DI and IMD-AC exhibit negative relative fluxes because water vapor permeation was in opposite direction, from collector to feed side.....	91
Figure 4.4. Experimental IMD-AC ammonia and water vapor fluxes as a function of operating temperature. ....	94
Figure 4.5. Total ammoniacal nitrogen, TAN, concentration in the feed and collector streams in IMD-AC operation at 40 °C as a function of time.....	97
Figure 4.6. Vaporization energy for ammonia and water (green patterned and blue solid columns, respectively) per mole of ammonia separated and recovered in CMD-DI, CMD-AC, IMD-DI, and IMD-AC.....	100
Figure 5.1. Schematic of the integrated membrane technology approach of Donnan dialysis (DD) for $H_xPO_4^{(3-x)-}$ recovery, isothermal membrane distillation (IMD) for $NH_3$ recovery, and bipolar membrane electrodialysis (BPM-ED) to strategically modify the pH of various streams.....	114
Figure 5.2. Flux of orthophosphate, $J_P$ , and flux of sulfate, $J_S$ , (patterned blue and orange columns, respectively) in Donnan dialysis kinetic experiments with initial simulated urine feed solutions at pHs of 6.0 and 9.2.....	122
Figure 5.3. Concentration of key species (left vertical axis) of $HPO_4^{2-}$ and $H_2PO_4^-$ (A), $NH_3$ and $NH_4^+$ (B), and $H_2SO_4$ (C), as well as pH (right vertical axis) of the product solution during BPM-ED operation in different modes over time.....	125

Figure 5.4. Ion fluxes  $J_P$  and  $J_S$  (A, patterned blue and orange columns, respectively), and relative fluxes,  $J_P/J_S$  (B, patterned blue column), in DD kinetic experiments with different feed solutions of  $FU_0$  (simulated fresh urine, pH = 6.75),  $FU_1$  (simulated fresh urine +  $6.25 \times 10^{-3}$  mol/L HCl, pH = 6.5),  $FU_2$  (simulated fresh urine +  $7.50 \times 10^{-3}$  mol/L HCl, pH = 6.1), and  $FU_3$  (simulated fresh urine +  $12.5 \times 10^{-3}$  mol/L HCl, pH = 5.75).....129

Figure 5.5. A: concentration of ammoniacal nitrogen species of  $NH_3$ , depicted as a dashed red line, and  $NH_4^+$ , depicted as a dot-dashed blue line and ammonia vapor pressure in the solution,  $P_{F,A}$ , depicted as a solid green line as a function of IMD initial feed solution pH. B: experimental ammonia vapor flux from feed to collector,  $J_A$ , versus ammonia vapor pressure gradient across the membrane,  $P_{F,A} - P_{C,A}$ , in operation with constant collector solution of DI water and varied hydrolyzed urine feed solution pHs.....131

Figure 5.6. A:  $NH_3$  vapor flux,  $J_A$ , (left vertical axis, patterned red columns) and specific energy consumption,  $\overline{SEC}$ , of the BPM-ED step in isothermal membrane distillation experiments with different initial hydrolyzed urine feed solutions of  $HU_0$ ,  $HU_1$ , and  $HU_2$  as a function of BPM-ED current density. B: TAN recovery potentials in batch operations of isothermal membrane distillation with various feed and collector solutions of equal volumes.....135

Figure 5.7. Specific energy consumption,  $\overline{SEC}$ , (MJ/mol-P or N) for nutrient recovery technologies is depicted as patterned red columns.....141

Figure 6.1. Schematic of the proposed onsite nutrient recovery system.....155

Figure 6.2. Contribution of different components toward the total capital cost (CAPEX) for implementation of nutrient recovery. Note that the analysis does not consider retrofit costs because it considers nutrient recovery to be implemented in a new building with the Solaire as a model...161

Figure 6.3. Operating cost (OPEX) of P and N recovery via Donnan dialysis (2A) and membrane distillation (2B), respectively, under different operations..... 162

Figure 6.4. Annualized capital cost (CAPEX), operating cost (OPEX) separated into P recovery and N recovery components, revenue separated into P and N recovery components, and net profit for the implementation of nutrient recovery systems under different operations..... 165

Figure 6.5. Annualized capital cost (CAPEX), operating cost (OPEX), revenue, and net profit for the implementation of non-potable water reuse, non-potable water reuse + thermal energy recovery, and non-potable water reuse + thermal energy recovery + nutrient recovery in a building modeling the Solaire. Revenue for non-potable water reuse is calculated as reduction in OPEX relative to a baseline building without non-potable water reuse (i.e., savings) and for thermal energy recovery as reduction in OPEX relative to a baseline building without either water reuse or thermal energy recovery. Profit is calculated as revenue – total cost..... 269

Figure A.1. Molar minimum energy,  $\bar{E}_{\min}$ , as a function of recovery yield to recover  $\text{NH}_{3(0)}$  from hydrolyzed urine and the contributing terms *A*, *B*, *C*, and *D*..... 238

Figure B.1. Theoretical  $[\text{H}_x\text{PO}_4^{(3-x)-}]_{\text{RS},f}$  in DD operation with FS containing different anions. The decreases in  $[\text{H}_x\text{PO}_4^{(3-x)-}]_{\text{RS},f}$  relative to the FS containing  $\text{H}_x\text{PO}_4^{(3-x)-}$  only are displayed as labels above the columns.  $V_{\text{FS}}/V_{\text{RS}}$  equal to 2 and receiver solution is  $600 \times 10^{-3}$  mol/L NaCl..... 248

Figure B.2. Orthophosphate ion flux,  $J_P$ , normalized by  $[\text{H}_x\text{PO}_4^{(3-x)-}]_{\text{FS},0} - [\text{H}_x\text{PO}_4^{(3-x)-}]_{\text{FS},f}$  in DD kinetic experiments with four FS of 1)  $30 \times 10^{-3}$  mol- $\text{H}_x\text{PO}_4^{(3-x)-}$ /L, 2)  $30 \times 10^{-3}$  mol- $\text{H}_x\text{PO}_4^{(3-x)-}$ /L and  $16 \times 10^{-3}$  mol- $\text{SO}_4^{2-}$ /L, 3)  $30 \times 10^{-3}$  mol- $\text{H}_x\text{PO}_4^{(3-x)-}$ /L and  $100 \times 10^{-3}$  mol- $\text{Cl}^-$ /L, and 4)  $30 \times 10^{-3}$  mol- $\text{H}_x\text{PO}_4^{(3-x)-}$ /L,  $100 \times 10^{-3}$  mol- $\text{Cl}^-$ /L, and  $16 \times 10^{-3}$  mol- $\text{SO}_4^{2-}$ /L..... 251

Figure B.3. Sorption coefficient,  $X$ , for orthophosphate, sulfate, and chloride into AMV membrane for FS of: 1)  $30 \times 10^{-3}$  mol- $H_xPO_4^{(3-x)-}/L$ , 2)  $30 \times 10^{-3}$  mol- $H_xPO_4^{(3-x)-}/L$  and  $16 \times 10^{-3}$  mol- $SO_4^{2-}/L$ , 3)  $30 \times 10^{-3}$  mol-  $H_xPO_4^{(3-x)-}/L$  and  $100 \times 10^{-3}$  mol- $Cl^-/L$ , and 4)  $30 \times 10^{-3}$  mol-  $H_xPO_4^{(3-x)-}/L$ ,  $100 \times 10^{-3}$  mol- $Cl^-/L$ , and  $16 \times 10^{-3}$  mol- $SO_4^{2-}/L$ , i.e., fresh urine.....253

Figure C.1. Concentration of ammonia,  $NH_3$ , and ammonium,  $NH_4^+$ , as a function of pH. Total ammoniacal nitrogen, TAN, concentration of the solution is 500 mM and  $pK_a$  is 9.25 for temperature of 25 °C.....256

Figure C.2. Bench-scale membrane distillation setup utilized in all experiments.....257

Figure C.3. Temperature and vapor pressure profiles in isothermal MD, accounting for temperature polarization at the solution-membrane interfaces.....258

Figure C.4. Relative vapor flux of water to ammonia, kg- $H_2O/mol-NH_3$ , for the four operations, CMD-DI, CMD-AC, IMD-DI, and IMD-AC.....259

Figure C.5. Collector solution pH as a function of time for CMD-DI, CMD-AC, IMD-DI, and IMD-AC experimental runs.....260

Figure C.6. Relative molar flux of water to ammonia in IMD-AC as a function of solution temperature.....261

Figure D.1. Schematic depicting the setup and working principles of bipolar membrane electrodialysis.....266

Figure E.1. Costs of natural gas, energy use in non-potable water treatment (NPWT), electricity for the hydronic loop, and total energy cost (sum of the aforementioned 3 components) for different scenarios of a reference building without water reuse or thermal energy recovery, the Solaire

building with non-potable water reuse (i.e., water recovery), and the Solaire building with non-potable water reuse and thermal energy recovery (i.e., water + thermal energy recovery).....280

Figure E.2. Annualized CAPEX and OPEX broken into energy, water service, and other components for different scenarios of a reference building without water reuse or thermal energy recovery, the Solaire building with non-potable water reuse (i.e., water recovery), and the Solaire building with non-potable water reuse and thermal energy recovery (i.e., water + thermal energy recovery).....281

## List of Tables

Table 3.1. Anion compositions and pHs of feed solution containing only orthophosphate, simulated fresh urine, and simulated hydrolyzed urine.....	50
Table 5.1. BPM-ED experimental operating conditions and target solutions utilized in downstream processes of Donnan dialysis and isothermal membrane distillation. Note mode 1 products are generated at constant current density and varied duration, while mode 2 products are generated at varied current density for a constant duration.....	117
Table A.1. Range in pH of each waste stream and resultant speciation of TAN and TOP. $\alpha_i$ is the fraction of TAN or TOP present as the species denoted by the subscript. The pH range is presented with “H” signifying the high-end and “L” signifying the low-end. Note that only $\text{H}_2\text{PO}_4^-$ and $\text{HPO}_4^{2-}$ forms of TOP are presented because $\text{H}_3\text{PO}_4$ and $\text{PO}_4^{3-}$ concentrations are negligible in the waste streams.....	215
Table A.2. Concentration of active species (components of products in the analysis), other forms of N, and passive species (components in the waste streams, but not in products) in waste streams examined in the analysis. Ranges are provided when available in the literature.....	216
Table A.3. Standard state Gibbs free energy of formation for species in an aqueous solution.....	247
Table A.4. Standard state Gibbs free energy of formation for liquid and solid products. <sup>1-3</sup> For urea, $\text{CO}(\text{NH}_2)_2$ , the Gibbs free energy of dissolution, or the change in Gibbs free energy from $\text{CO}(\text{NH}_2)_2(\text{aq})$ to $\text{CO}(\text{NH}_2)_2(\text{s})$ , $G_{f,\text{CO}(\text{NH}_2)_2(\text{s})}^\circ - G_{f,\text{CO}(\text{NH}_2)_2(\text{aq})}^\circ$ is presented.....	230
Table A.5. Molar minimum energies of recovery, $\bar{E}_{\text{min}}$ , for TAN products from each waste stream presented in Figure 1.3A. $\bar{E}_{\text{min}}$ values are calculated at low and high TAN concentrations in the	

waste stream and low and high waste stream pH, i.e., four  $\bar{E}_{\min}$  values calculated for each recovery scenario.....231

Table A.6. Molar minimum energies of recovery,  $\bar{E}_{\min}$ , for TOP products from each waste stream presented in Figure 1.3B.  $\bar{E}_{\min}$  values are calculated at low and high TOP and co-species concentrations in the waste stream and low and high waste stream pH, i.e., four  $\bar{E}_{\min}$  values calculated for each recovery scenario.....232

Table A.7. Model hydrolyzed urine solution composition consisting of typical TAN,  $\text{HCO}_3^-$ ,  $\text{SO}_4^{2-}$ , and TOP concentrations found in hydrolyzed urine. The target pH, 9.1, is the mid-range pH of hydrolyzed urine.....233

Table A.8. Visual Minteq outputs for hydrolyzed urine feed and retentate streams in  $\text{NH}_3(\text{l})$  product recovery scenarios at various recovery yields.....234

Table A.9. Visual Minteq outputs for hydrolyzed urine feed and retentate streams in 1.0 M  $\text{NH}_3(\text{aq})$  product recovery scenarios at various recovery yields.....234

Table A.10. The change in the sum of the standard state Gibbs free energy of individual ions between the final state (product and retentate) and initial state (waste stream feed).....239

Table A.11. Molar minimum energy for recovery of select products,  $\text{NH}_3(\text{l})$  and 1.0 M  $\text{NH}_3(\text{aq})$ , from waste streams of secondary wastewater effluent and hydrolyzed urine calculated with the exclusion and inclusion of passive species,  $\text{Na}^+$  and  $\text{Cl}^-$  .....240

Table B.1. Specifications for commercially available water softening products from PuroLite...245

Table B.2. Calculated values based on material flow using the specifications in Table 1.....245

Table B.3. Composition of a typical waste water softening regenerant rinse, determined using the specifications in Table 1 and calculated values in Table 2.....246

Table B.4. Typical ion concentrations in bittern brine.....247

Table B.5 Selemion AMV and ASVN membrane characteristics.....249

Table B.6.  $\Delta[\text{H}_x\text{PO}_4^{(3-x)-}]$  in the feed solution, in operation with FS containing different anions.  $\Delta[\text{H}_x\text{PO}_4^{(3-x)-}] \equiv [\text{H}_x\text{PO}_4^{(3-x)-}]_{\text{FS},0} - [\text{H}_x\text{PO}_4^{(3-x)-}]_{\text{FS},f}$  is defined as the difference between initial and final (at Donnan equilibrium) total orthophosphate concentrations in the feed solution.....250

Table B.7. Area specific resistance of Selemion AMV and ASVN membranes for different electrolytes.....254

Table D.1. Experimental voltage drops across the BPM-ED stack in different BPM-ED operations, which are described by the streams produced, operating mode, and current density. Predicted voltage drops based on a more optimized BPM-ED stack based on eqs S2–3 and assumptions presented in Table S2.....268

Table D.2. Assumptions utilized for the prediction of voltage drop across the membrane in an optimized BPM-ED stack.....270

Table E.1. Assumptions in the calculation of CAPEX for onsite nutrient recovery using Donnan dialysis (DD) for P recovery and membrane distillation (MD) for N recovery.....271

Table E.2. Overall heat transfer coefficient,  $U$ , for operations with urine, assumed to have essentially equivalent properties to water, as the target stream to be warmed (i.e., the cold stream) and either steam as the hot stream or hot waste water as the hot stream.....271

Table E.3. Temperature of hot stream at the inlet of the heat exchanger,  $T_{H,in}$ , temperature of the cold stream to be warmed at the inlet of the heat exchanger,  $T_{C,in}$ , and target temperature of the warmed stream at the exit of the heat exchanger,  $T_{C,out}$  in heat exchanger operations with steam or hot waste water as the hot stream.....272

Table E.4. Assumptions for determining the amortization factor that is required for calculating annualized CAPEX.....272

Table E.5. Assumptions in the calculation of OPEX of the Donnan dialysis (DD) system for P recovery. Note that KCl is the chemical utilized in the “baseline” operation.....272

Table E.6. Assumptions in the calculation of electricity for pumping in the Donnan dialysis and membrane distillation systems.....273

Table E.7. Assumptions in the calculation of OPEX of the membrane distillation (MD) system for N recovery.....276

Table E.8. High and low prices of various P and N fertilizer normalized by kg of target nutrient, P or N.....277

Table E.9. Assumptions for determining the annualized capital cost of the Solaire non-potable water treatment system and thermal energy recovery unit.....278

Table E.10. Average values of potable water demand, reuse flow from the non-potable water treatment system, and wastewater sent to WWTP at the Solaire from Dec. 2017 to Feb. 2022. For comparison, the same metrics for a reference building (without water reuse) are provided..... 278

Table E.11. Assumptions for determining operating costs for water service, water heating, non-potable water treatment, and thermal energy recovery systems at the Solaire.....279

## **Acknowledgements**

I would like to express my gratitude to the people and organizations that have guided and supported me throughout my studies. First, I feel quite privileged to have worked with Dr. Ngai Yin Yip throughout my graduate studies. Dr. Yip fostered a lab environment that valued collaboration, scientific curiosity, and community outreach. He pushed me to become a better researcher and a stronger scientific writer. He has been an excellent teacher, mentor, and role-model. I have the greatest appreciation for the time and efforts that Dr. Yip has dedicated to my education.

I am also grateful to the time and guidance of the other members of my thesis committee: Dr. Pierre Gentine, Dr. Raymond Farinato, Dr. Christopher Durning, and Dr. Sheng Chu. Additionally, I would like to thank the staff and faculty of the Department of Earth and Environmental Engineering at Columbia University for their support during my studies and research work. I believe that the work in this thesis greatly benefited from courses taught by Dr. Upmanu Lall, Dr. William Becker, Dr. Wade McGillis, and Dr. Ngai Yin Yip. I appreciate the people and organizations that shared their resources to benefit the work in this thesis. Dr. Brian Mailloux at Barnard College and members of the Earth and Environmental Engineering Laboratory shared access to analytical resources, ion-chromatographer and spectrophotometer, which were essential to this research. Also, I am grateful to my collaborators at Natural Systems Utilities, Dr. Sheng Chu, Zach Gallagher, and Edward Clerico, for their time and dedication to the work in this thesis. Dr. Sheng Chu has been an excellent mentor and I am quite grateful to his insights and guidance.

I also thank my other collaborators and coauthors: Dr. Chanhee Boo, Dr. Xi Chen, Hanqing Fan, Yuxuan Huang, Natalie Williams, and Nobuyo Watanabe for their commitment to the research projects. Contributions from Dr. Chanhee Boo, Dr. Xi Chen, and Natalie Williams were

indispensable to Chapter 4. Contributions from Hanqing Fan and Yuxuan Huang were incredibly beneficial to Chapters 3 and 5. Nobuyo Watanabe has been very dedicated to nutrient recovery projects and her work has contributed to Chapter 2, 3, and 5. It has been such an honor working with Nobuyo and I am excited to see what is ahead for her as a scientist. I am grateful to every member of Dr. Yip's Technologies for Water-Energy-Environment Nexus lab for exposing me to new ideas and for their advice over the years. Ian Billinge, Kinnari Shah, Elizabeth Dach, and Amar Bhardwaj provided indispensable feedback on research, scientific writing, and presentations over the years.

I would like to thank the Columbia University, Graduate School of Arts and Sciences, and the Fu Foundation School of Engineering and Applied Science communities. Additionally, I am grateful for the opportunity to work as a CTV Fellow at Columbia University Ventures. In this role, I was introduced to and inspired by the innovative technologies invented in Columbia's laboratories.

I would next like to acknowledge the Lafayette College community for fostering the best undergraduate education and experience that I could have imagined. The Chemical and Biomolecular Engineering Department staff and faculty delivered a rich education full of research opportunities and engaging projects. I would like to thank Dr. Lindsay Soh and Dr. Michael Senra for their guidance and mentorship. Also, I deeply value the friendships that I made during my time at Lafayette College. My friends have been a source of great emotional support and companionship over the years. Also, my good friend, Cara Abecunas, has provided extensive and invaluable feedback on my scientific writing throughout my studies.

My research has benefited from the support of the National Science Foundation (NSF), the NSF-INTERN program, the American Membrane Technology Association (AMTA), the United States Bureau of Reclamation (USBR), and American Chemical Society (ACS).

I would also like to express gratitude to my friends and family for their love and support. My sisters and brothers, Ashley and Michael Bixler and Lauren and Donald Potter, have been my biggest cheerleaders throughout this journey. My dogs, Chip, Jewel, and Rosie provided emotional support and companionship. I also thank the Kovar and Burrill families for their support. Thanks to Stephanie Kovar, Christina Kovar, and Isabel Emanuel, for providing outside perspectives and for proofreading my writing. I want to express deep appreciation for my life partner, Thomas Kovar, for his endless support and love. Tom has always taken an interest in my research and has provided feedback on numerous practice presentations over the years. He has celebrated every victory with me and I am forever grateful for his friendship and partnership. I also thank my grandmother, Frances Jordan, for helping to support me during my undergraduate studies. Finally, I thank my mom and dad, Elizabeth and Patrick McCartney, for their guidance, support, and sacrifices over the years. Without their love this thesis would have been impossible.

# Chapter 1: Introduction

## 1.1 Motivation

**Challenges with Existing Nutrient Management.** Nitrogen and phosphorous are vital macronutrients and principal components of fertilizer. Global food security is dependent on sufficient access to bioavailable forms of nutrients: N as ammoniacal nitrogen ( $\text{NH}_3/\text{NH}_4^+$ ) and P as phosphate ( $\text{H}_x\text{PO}_4^{(3-x)-}$ ). In the conventional approach for production of N fertilizer, ammonia ( $\text{NH}_3$ ) is fixed from the atmosphere through the Haber-Bosch process, which is energy intensive as it requires 8.9–19.3 kWh/kg-N and totals to  $\approx 1\text{--}2\%$  of the world's annual energy use.<sup>4-6</sup> Similarly, phosphate rock mining, the prevailing technique for P fertilizer production, has a high energy cost of 0.80-1.66 kWh/kg-P.<sup>7,8</sup> Additionally, phosphate rock reserves are diminishing and are projected to last only 50–100 more years with peak phosphate production predicted in 2033.<sup>9</sup> <sup>10</sup> Furthermore, phosphorous fertilizer manufacturing plants present inherent safety concerns related to the production of toxic and radioactive byproducts, such as phosphogypsum, during the manufacturing process.<sup>11, 12</sup> These hazards were starkly demonstrated in March 2021 when the Piney Point, Florida production plant leaked phosphogypsum into Tampa Bay due to an engineering failure in the aged infrastructure.<sup>12</sup> The immense energy requirements, resource-limitation, and hazardous practices of current fertilizer production practices underscore the lack of sustainability and motivate alternative methods for nutrient capture.

Downstream, nutrients utilized in fertilizer move through the food-chain, and are eventually excreted in human urine and feces. Anthropogenic nutrients in municipal wastewater are often not adequately removed during U.S. wastewater treatment (WWT) and are consequently discharged into surface waters. Nutrient accumulation in aquatic environments leads to

eutrophication, growth of harmful algal blooms (Figure 1.1A), and hypoxic dead zones (Figure 1.1B), which harm aquatic biodiversity.<sup>13-15</sup> Additionally, harmful algae produce toxins and cyanobacteria, which can cause illness or be fatal to humans and pets using contaminated recreational waterbodies.<sup>16, 17</sup> Furthermore, these toxins can infiltrate drinking water because conventional water treatment is not equipped to sufficiently remove algal toxins.<sup>18-20</sup> The devastating impacts of harmful algae were demonstrated by the 2014 Toledo, OH algal blooms, where water supplies were contaminated with toxins leaving half a million residents without water service.<sup>21-23</sup>

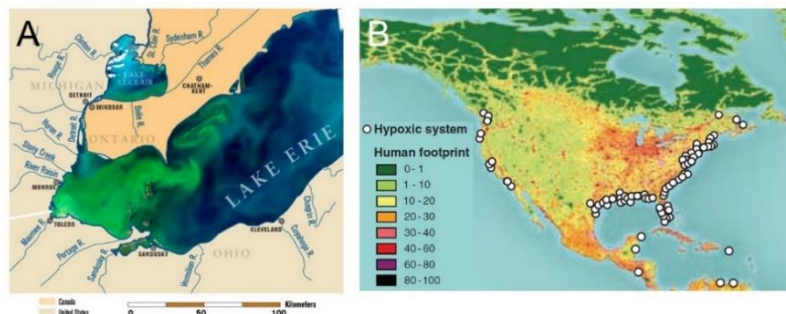


**Figure 1.1** A) Harmful algal blooms in Lake Erie on September 3, 2011.<sup>10</sup> B) Eutrophication and hypoxic dead-zones in North America, particularly along the coast.<sup>12</sup>

For these reasons, the biogeochemical flows of N and P are flagged as exceeding the safe operating space for humanity and pose high risks under the planetary boundaries framework.<sup>24</sup> The current approach for nutrient management has clear shortcomings and a new paradigm for sustainable management is urgently needed. Improvements in the efficiency of nutrient usage can reduce fertilizer demand and alleviate some challenges posed by industrial fertilizer production and nutrient discharge.<sup>25-27</sup> Improved agricultural practices, such as strategically timing fertilizer application, can benefit nutrient use efficiency and also reduces nutrient discharge from farms to surface waters (another cause of eutrophication and harmful algal blooms).<sup>25-27</sup> Additionally,

reducing food waste and improving nutrient utilization across the food-chain can lessen P and N loss to the environment.<sup>25-27</sup>

Another vital nutrient management strategy is to control nutrient loading from wastewater treatment plant effluent.<sup>21, 28-30</sup> Unfortunately, most WWT plants (WWTPs) are not equipped with tertiary or advanced treatment, i.e., dedicated stage for nutrient removal, because advanced treatment systems require substantial energy and chemical expenditures.<sup>31</sup> There has been considerable efforts to develop and advance nutrient removal technologies in WWTPs,<sup>32-39</sup> but most methods aim to remove nutrients from the wastewater without recovery. This approach still relies on the unsustainable practices for fertilizer production and an inefficient linear nutrient economy. The red arrows of Figure 1.2 demonstrate the linear economy approach to nutrient management: nutrients are produced/extracted at high energy and chemical cost, utilized by the food-chain, excreted in wastewater, and excess nutrients in wastewater are treated, incurring further expenditure, to prevent nutrient loading to aquatic environments.

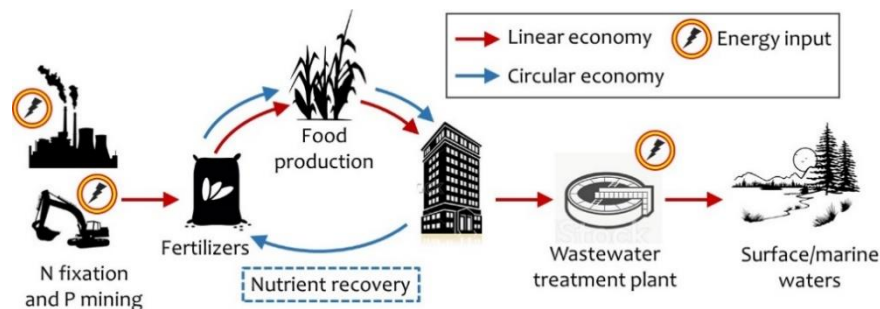


**Figure 1.2.** The current linear economy management of N and P (red arrows) requires high energy to produce nutrients and demands high energy and chemicals downstream for nutrient removal. In contrast is a circular nutrient economy management (blue arrows), where nutrients are recovered from waste streams and re-entered into the food-chain, closing the nutrient “loop.”

**Circular Nutrient Economy Approach.** A more forward-looking approach is the simultaneous removal and recovery of nutrients from wastewaters. In a circular economy approach, nutrients can be recovered from waste sources and re-entered into the food chain (blue arrows in Figure

1.2), closing the nutrient “loop.” This approach can ease the requirement for N fixation and P mining, which are currently practiced at unsustainable levels. Concurrently, this approach reduces nutrient loading to aquatic environments and protects ecosystems from eutrophication and harmful algal blooms. Nutrient recovery from wastewater and its reuse in fertilizer marks a paradigm shift towards more sustainable nutrient management.

Land applications of biosolids, i.e., treated sewage sludge being used directly as fertilizer, is a prevailing practice for nutrient reuse. However, the method risks contamination from heavy metals, pharmaceuticals, per- and polyfluoroalkyl substances (PFAS), and pathogens.<sup>40, 41</sup> For this reason, the application of biosolids faces societal and legal hurdles, particularly when used on crops for human consumption.<sup>40, 41</sup> Decentralized nutrient recovery efforts that target source-separated urine have gained traction because urine is rich in nutrients and essentially pathogen free.<sup>42-46</sup> However, it remains unclear if such approaches are a more competitive than conventional centralized efforts. Additionally, high-performance technologies capable of achieving high nutrient yield and cost-effectiveness are lacking.<sup>47-50</sup> These critical gaps have hindered the progress towards a circular nutrient economy and the adoption of nutrient recovery practices.

**Problem Statement #1: Rigorous Quantitative Analysis can Guide Nutrient Recovery.** Conventional sanitation infrastructure collects all streams of waste, including urine, feces, and greywater in centralized treatment facilities. However, combining waste streams high in N and P, such as urine, with less concentrated streams dilutes the concentration of valuable nutrients over 100× increasing the challenge of nutrient recovery. Intuitively, the separation of N and P nutrient rich streams should enable higher recovery efficiency and effectiveness than recovery from diluted streams.<sup>44, 51, 52</sup> Therefore, a promising approach can be nutrient recovery from isolated urine, which contains ~80% of N and up to 80% of P excreted from humans.<sup>42-46</sup> It is important to

consider that a paradigm switch from the existing wastewater infrastructure to decentralized systems of urine source-separation and resource recovery will require capital investment and a shift in societal sanitation practices. Therefore, the benefits of urine separation for nutrient recovery must be informed not on an intuitive basis, but on a quantitative level. An analysis of thermodynamics and energy requirements for N and P separation from waste streams can inform strategic approaches for nutrient recovery from waste streams. Such analysis can identify ideal waste streams and nutrient products to minimize energy requirements for nutrient recovery.

**Problem Statement #2: High Performance Techniques for Capturing Nutrients are Needed.**

Equally critical to strategic selection of waste stream and fertilizer product is the need for technologies capable of achieving selective nutrient recovery with high yields and efficient energy utilization. Membrane filtration allows for the separation of valuable nutrients from harmful components in waste streams such as pathogens, pharmaceuticals, endocrine disrupting compounds, and personal care products. However, for P recovery from urine, the state-of-the-art techniques involve precipitation of minerals, such as struvite or potassium magnesium phosphate, rather than membrane-based approaches. Phosphate mineral precipitation potentially introduces some risks from pathogen, pharmaceutical, and heavy metal contamination. An alternative practice is the use of sorbents, e.g., metal (oxy)hydroxide sorbents,<sup>53-57</sup> to separate phosphate from urine; however, sorbent regeneration is expensive and produces waste brines that cannot be easily disposed.<sup>58</sup> Anion-exchange membrane processes offer promising options to separate  $H_xPO_4^{(3-x)-}$  from the other constituents in urine without the need for regeneration. However, there are critical gaps in the fundamental understanding of the transport of ions and selectivity for  $H_xPO_4^{(3-x)-}$ . For N recovery, membrane distillation is a promising method for volatile  $NH_3$  separation from urine, but the current state-of-the-art process has low selectivity for  $NH_3$  over  $H_2O$  and requires

significant energy. High-performance membrane technologies for both P and N recovery from urine are urgently needed.

**Problem Statement #3: Nutrient Recovery must be Cost-Effective.** The shift toward a circular nutrient economy requires that the nutrient recovery methods be competitive with existing approaches to fertilizer production and nutrient removal at WWTP (i.e., the linear nutrient economy) across key metrics, most notably cost and sustainability, which are both heavily influenced by energy and chemical inputs. While thermodynamically strategic approaches to nutrient recovery and high-performance membrane techniques can minimize energy requirements, there is also an opportunity to utilize waste sources of thermal energy to further enhance cost-effectiveness. Commercial and residential sources of waste heat, such as warm bathwater runoff and cooling water for computer servers, can be tapped to power nutrient recovery efforts.<sup>59-61</sup> Additionally, avenues for application of low-cost or recycled chemical resources, such as seawater and desalination brine, in place of costly inputs should be explored. Harnessing low-cost and waste sources of heat and chemicals can improve the sustainability and cost-competitiveness of nutrient recovery.

## **1.2 Objectives and Scope of Dissertation**

The overarching aim of this thesis is to understand strategic approaches for nutrient recovery from wastewater and advance membrane technologies for P and N recovery.

More specifically, the goals of this work are:

- i. Assess thermodynamic and energy requirements of various nutrient recovery schemes encompassing a variety of waste streams, different fertilizer products, and spanning product yields to guide strategic efforts for capturing P and N from waste.

- ii. Examine the performance potential of Donnan dialysis (DD) to capture and enrich phosphate from human urine, and systematically study the impacts of different ions in the urine matrix on recovery potential and transport kinetics.
- iii. Develop a novel isothermal membrane distillation with acidic collector (IMD-AC) technology for selective and energy efficient capture of  $\text{NH}_3$  from human urine by measuring  $\text{NH}_3$  and water flux under different operating conditions of feed and collector temperature and collector composition.
- iv. Explore opportunities to employ pH manipulation using bipolar membrane electrodialysis (BPM-ED) to feed and product streams of DD and IMD-AC systems to enhance the performance of these techniques.
- v. Conduct a techno-economic analysis of onsite nutrient recovery to determine the feasibility of this approach and guide future research and development initiatives.

### **1.3 Thesis Structure**

This thesis examines strategic opportunities to recover nutrients from waste streams and advances membrane technologies for capturing P and N from urine. Chapter 2 presents a thermodynamic and energy analysis for harvesting fertilizers from various waste streams of fresh and hydrolyzed urine, greywater, domestic wastewater, and secondary treated wastewater effluent. This chapter utilizes the Gibbs free energy of separation to determine the theoretical minimum energy to recover various fertilizer products from these waste streams at different yields. The chapter investigates strategic configurations for nutrient recovery to minimize energy demands and sheds light on potential practical energy demands for various nutrient recovery schemes. The benefits of targeting nutrient-dense waste streams, such as human urine, are highlighted on a thermodynamic and

energy basis. Additionally, the chapter presents a first-order analysis of potential energy savings that can be achieved through supplementing fertilizer production with nutrient capture from urine.

Chapter 3 advances the understanding of ion transport in Donnan dialysis, an ion-exchange membrane-based process, and assesses the performance potential of the technique for orthophosphate recovery from human urine. In Donnan dialysis, the transport of “driver” ions across an ion-exchange membrane from solutions of high to low concentrations (termed receiver and feed, respectively), sets up an electrochemical potential that drives the transport of “target” ions in the opposite direction. The chapter outlines the exchange of  $\text{H}_2\text{PO}_4^-$ , i.e., target ions, in urine and  $\text{Cl}^-$ , i.e., driver ions, in an electrolyte receiver solution across an anion-exchange membrane in Donnan dialysis, which enables the capture of orthophosphate in the receiver solution. The chapter establishes that Donnan dialysis operation at higher feed to receiver solution volume ratios is capable of enriching orthophosphate in the receiver solution, or product stream. The study also examines the influence of other anions in urine on orthophosphate transport and presents challenges with the selectivity for orthophosphate over other anions; however, the use of a monovalent ion permselective membrane is shown to improve selectivity for orthophosphate. The chapter also highlights the applicability of widely available low-cost or waste streams, such as seawater, desalination brine, bittern solution, and waste water softening regenerant rinse, as chemical inputs to the receiver stream.

Chapter 4 proposes and develops isothermal membrane distillation with acidic collector, a novel technology driving the selective and energy-efficient capture of ammonia from human urine. Membrane distillation drives the permeation of volatile components, such as  $\text{NH}_3$ , across a hydrophobic microporous membrane toward a collector solution, while nonvolatile species are retained by the membrane and remain in the feed solution. However, conventional membrane

distillation suffers from simultaneous and undesired water permeation that dilutes the  $\text{NH}_3$  fertilizer product and increases the energy requirements of the technique. This chapter examines the transport of  $\text{NH}_{3(g)}$  and  $\text{H}_2\text{O}_{(g)}$  in different membrane distillation configurations, conventional and isothermal, and demonstrates enhanced selectivity for  $\text{NH}_3$  permeation over  $\text{H}_2\text{O}$  with the novel isothermal membrane distillation operation. The study also highlights that the use of an acidic stream as the collector increases the flux of  $\text{NH}_3$  and enables uphill transport of  $\text{NH}_3$  against an ammoniacal nitrogen concentration gradient. The vaporization energy-savings achievable by novel isothermal membrane distillation with acidic collector relative to conventional membrane distillation are highlighted and energy requirements are compared against the linear economy approach to N management.

Chapter 5 presents an integrated membrane approach to capture both orthophosphate and ammonia from human urine utilizing Donnan dialysis, isothermal membrane distillation with acidic collector, and bipolar membrane electrodialysis. Bipolar membrane electrodialysis is introduced as a technique for *in situ* acid and base production, which is leveraged to control the pH of streams in the other membrane techniques (Donnan dialysis and isothermal membrane distillation) to enhance performance. The influence of bipolar membrane electrodialysis operation duration and current density on the performance of Donnan dialysis and isothermal membrane distillation are presented and the impact on energy requirements are discussed. The chapter also provides the specific energy consumption of each membrane technique compared against the linear nutrient economy approaches.

Chapter 6 provides a preliminary economic assessment of the aforementioned membrane techniques for P and N recovery from human urine (Donnan dialysis and isothermal membrane distillation with acidic collector, respectively) if applied at the Solaire building in New York City.

The chapter additionally presents a techno-economic assessment of the existing water reuse and thermal energy recovery infrastructure in the Solaire compared against a baseline building without water, energy, or nutrient recovery. Environmental implications of incorporating water reuse, thermal energy recovery, and nutrient recovery in high-density buildings, such as the Solaire, are highlighted.

Finally, Chapter 7 summarizes the key findings of this work and highlights the significant contributions of the thesis. This chapter discusses the implications of this work on nutrient recovery as well as on broader applications to membrane science and the water sector. Future work for advancement of membrane techniques and decentralized resource recovery efforts are recommended.

#### **1.4 Key Contributions**

This section briefly describes contributions of this thesis, while more in-depth discussion and implications are presented in Chapter 7. **This work elucidates strategic approaches for nutrient recovery, advances membrane technologies to capture P and N from human urine, and assesses the economic feasibility of incorporating nutrient recovery into decentralized wastewater management.** Outside of nutrient recovery, the findings in this dissertation **present a thermodynamic framework to determine the minimum energy of separation and provide new insights of transport in membrane processes**, which future development of separation processes can utilize.

The quantitative thermodynamic and energy analysis of nutrient recovery from various waste streams demonstrates that **P and N capture from nutrient rich sources, such as human urine, has lower energy requirements than recovery from more dilute sources.** A first-order analysis underlines the potential energy savings achievable by nutrient recovery from human urine

compared with the existing linear economy approach. **The framework to determine the minimum energy of separation can be applied to other resource recovery efforts to guide the strategic selection of waste streams and products.**

Donnan dialysis (DD) with a high driver ion content in the receiver solution is utilized to enable **orthophosphate recovery against a concentration gradient, i.e., uphill transport**, and can **enrich orthophosphate in the receiver solution** by leveraging feed and receiver volumes. The systematic exploration of anion transport from feed solutions containing multiple anions provides strong evidence that **ions compete to partition into the ion exchange membrane, which contributes to competitive ion transport**. Selectivity for monovalent ions, here in this thesis  $\text{H}_2\text{PO}_4^-$ , over multivalent ions can be enhanced using monovalent ion selective membranes.

The thesis **presents a novel operation of membrane distillation, isothermal membrane distillation with acidic collector (IMD-AC), as a promising and energy-efficient technique for selective recovery of ammonia from human urine**. The isothermal feature, i.e., equal feed and collector operating temperatures, removes the driving force for water vapor permeation and resultingly **suppresses undesired  $\text{H}_2\text{O}$  transport and improves selectivity for  $\text{NH}_3$** . The acidic collector feature drives the protonation of  $\text{NH}_3$  to  $\text{NH}_4^+$  and **enables the transport of  $\text{NH}_3$  vapor against an ammoniacal nitrogen concentration gradient, i.e., IMD-AC can achieve uphill transport of N**. By suppressing water vapor transport **IMD-AC achieves 95% savings in vaporization energy consumption relative to conventional MD**.

Donnan dialysis and isothermal membrane distillation with acidic collector can be practiced in conjunction to capture both P and N from human urine. **Nutrient speciation, i.e.,  $\text{H}_2\text{PO}_4^-/\text{HPO}_4^{2-}$  and  $\text{NH}_4^+/\text{NH}_3$ , in urine is pH-dependent and can be favorably leveraged to improve DD and IMD-AC performance**. The thesis applies **bipolar membrane electro dialysis**

**to generate acids and bases *in situ* and strategically control the pHs of streams in DD and IMD-AC. As a result, orthophosphate flux and selectivity in DD can be favorably increased and NH<sub>3</sub> vapor flux in IMD-AC is enhanced. At the same time, an acidic stream benefiting N recovery is produced *in situ* with BPM-ED using low-cost/waste salt solutions.**

The techno-economic assessment of implementing DD and IMD-AC for nutrient recovery from source-separated urine into onsite wastewater management **reveals opportunities to improve the economic viability for decentralized nutrient recovery. Utilization of waste resources, such as waste low-grade heat and recycled chemicals, significantly decreases costs of operation.** Additionally, realizing the benefits of nutrient recovery to downstream wastewater treatment plants can potentially improve the feasibility of nutrient recovery.

# **Chapter 2: Emerging Investigator Series: Thermodynamic and Energy Analysis of Nitrogen and Phosphorous Recovery from Wastewaters**

## **Chapter Abstract**

In a circular nutrient economy, nitrogen and phosphorous are removed from waste streams and captured as valuable fertilizer products, to more sustainably reuse the resources in closed-loops and simultaneously protect receiving aquatic environments from harmful N and P emissions. For nutrient reclamation to be competitive with the existing practices of N fixation and P mining, the methods of recovery must achieve at least comparable energy consumption. This study employed the Gibbs free energy of separation to quantify the minimum energy required to recover various N and P fertilizer products from waste streams of fresh and hydrolyzed urine, greywater, domestic wastewater, and secondary treated wastewater effluent. The comparative advantages in theoretical energy intensities for N and P recovery from nutrient-dense waste streams, such as fresh and hydrolyzed urine, were assessed against the other more dilute sources. For examples, compared to reclaiming the nutrients from treated wastewater effluent at centralized wastewater treatment plants, the minimum energy to recover 1.0 M  $\text{NH}_{3(\text{aq})}$  from source-separated hydrolyzed urine can be  $\approx 40\text{--}68\%$  lower, whereas recovering  $\text{KH}_2\text{PO}_{4(\text{s})}$  from diverted fresh urine can, in principle, be  $\approx 13\text{--}34\%$  less energy intense. The study also evaluated the efficiencies required by separation techniques for the energy demand of N and P recovery to be lower than the current production approaches of Haber-Bosch process and phosphate rock mining. For instance, the most energetically favorable ammoniacal nitrogen and orthophosphate reclamation schemes, which target hydrolyzed and fresh urine, respectively, require energy efficiencies  $>7\%$  and  $>39\%$ . This

study highlights that strategic selection of waste stream and fertilizer product can enable the most expedient recovery of nutrients and realize a circular economy model for N and P management.

## 2.1 Introduction

The challenges facing current nutrient management practices, detailed in Chapter 1, offer opportunities for synergistic solutions. A circular economy model advocates for the simultaneous removal and recovery of nutrients from waste-sources.<sup>62-65</sup> N and P captured from wastewater can be recycled back into the food chain to close the nutrient loop, easing the demand for nitrogen fixation and phosphorus mining, and simultaneously alleviating potential harms to the environment and public health. The recovery of nutrients from waste streams for reuse is, therefore, a paradigm shift to a more sustainable approach for nutrient management.

The recovery of nutrients from various waste streams of the cycle, including urine,<sup>51, 52, 66-77</sup> greywater,<sup>78</sup> domestic wastewater,<sup>79-83</sup> and WWTP effluent,<sup>84-88</sup> has been investigated in previous studies. A simplified schematic of the wastewater cycle and the principal streams are depicted in Figure 2.1A. Note that the main form of nitrogen in fresh urine is urea,  $\text{CO}(\text{NH}_2)_2$ , which undergoes hydrolysis by naturally present urease enzymes to form ammoniacal nitrogen and bicarbonate, yielding hydrolyzed urine after  $\approx 2-7$  d.<sup>89, 90</sup> As the waste streams undergo biological, chemical, and physical transformations along the cycle and combine with other flows, the compositions and aqueous chemistries are significantly altered.<sup>89, 91-97</sup> Similarly, the nutrient content can vary drastically. Figure 2.1B shows the concentration range of total ammoniacal nitrogen, TAN, and total orthophosphate, TOP, (shaded green and patterned red bars, respectively) for the different waste streams. The TAN and TOP concentrations span over five orders of magnitude, with the general trend, in increasing order of nutrient content, being greywater < secondary (2°) WW effluent < domestic WW < fresh and hydrolyzed urine. Therefore, the various

recovery technologies are targeting sources with widely disparate nutrient contents and with N and P in different chemical forms (e.g., nitrogenous compounds include ammonia, nitrate, nitrite, and urea).

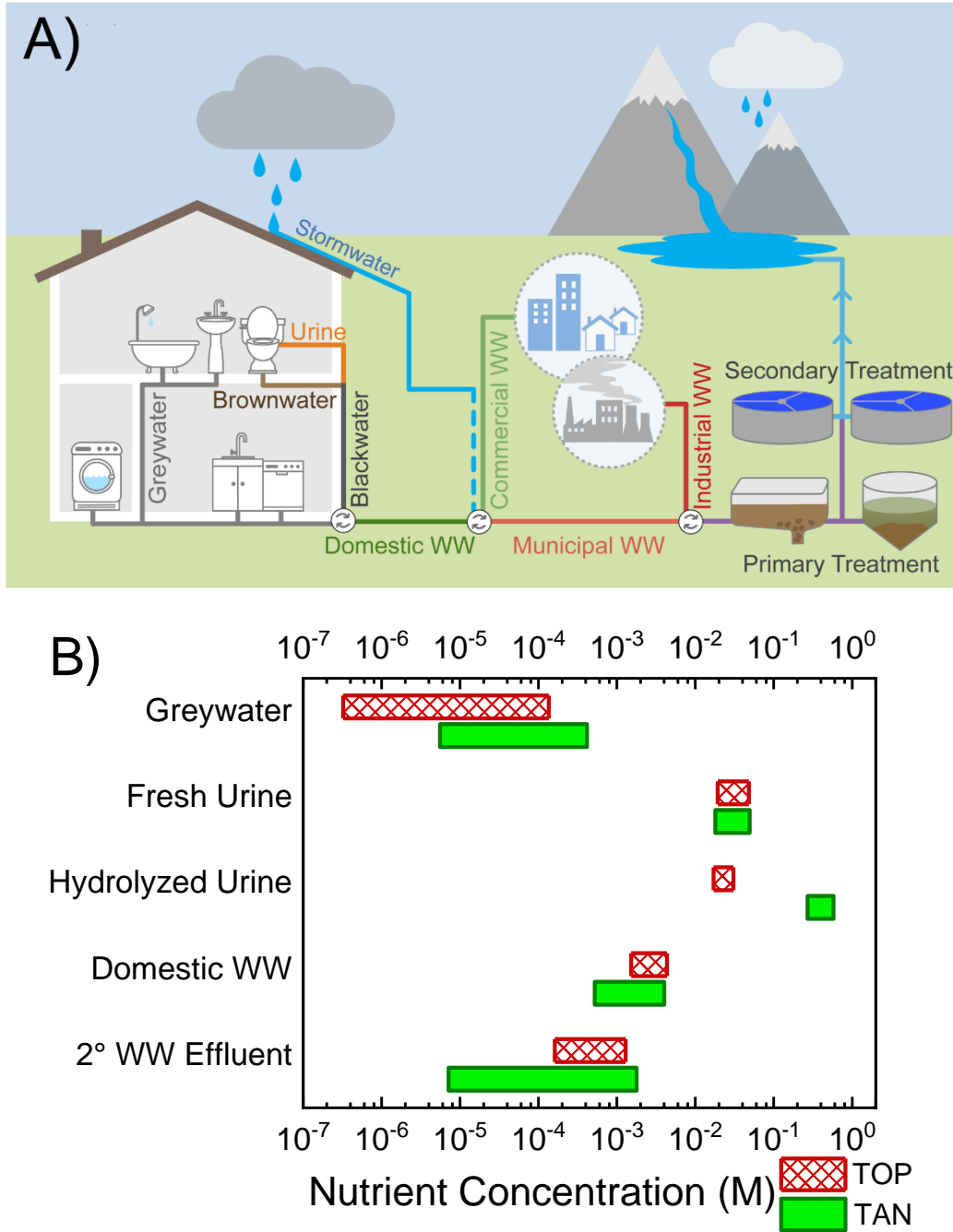


**Figure 2.1.** A) Illustrative representation of wastewater sources and streams. The constituents of domestic wastewater (WW) are blackwater, the mixture of brownwater and urine, and greywater.

Domestic WW combines with waste streams from commercial and industrial sources, and may be diluted by stormwater runoff in combined sewer systems before treatment at centralized facilities. Treated effluent is eventually discharged to the environment. B) Concentration range of total ammoniacal nitrogen, TAN, and total orthophosphate, TOP, (shaded green and patterned red bars, respectively) for waste streams of greywater, fresh urine, hydrolyzed urine, domestic WW, and secondary (2°) WW effluent.<sup>89, 91-97</sup>

Waste streams that are richer in nutrients should, intuitively, favor recovery efficiency and effectiveness. The advantages of high nutrients content for recovery have been qualitatively discussed in literature,<sup>44, 51, 52</sup> but there are currently no rigorous quantitative analyses to more precisely value the benefits. In contrast, energy analyses had been conducted for other environmentally-relevant separations, such as, reverse osmosis desalination, conventional thermal distillation, and membrane distillation,<sup>98-101</sup> to reveal intrinsic limitations and thermodynamic insights of the processes. Applying similar analytical approaches to nutrient recovery can enhance fundamental understanding and shed light on the thermodynamic principles governing the separation, which can in turn inform efforts to capture N and P from the waste streams.

In this study, we conduct a thermodynamic analysis of nutrient recovery from different waste streams. First, governing equations for the theoretical minimum energy required to recover nutrients, determined using the Gibbs free energy of separation, are presented. The minimum energy to recover ammonia and phosphate are quantitatively assessed for different waste streams spanning a range of nutrient content, namely source-separated urine (fresh and hydrolyzed), greywater, domestic WW, and 2° WW effluent. Energy requirements to reclaim products of different nutrient species and concentrations are then examined. The impact of recovery yield on energy demand is evaluated and practical considerations are discussed. The energy to separate and capture other forms of N, specifically, nitrate and urea, is also explored. Next, we analyze the practical efficiency needed from actual processes for nutrient recovery from wastewaters to be

competitive with conventional methods of N and P production, i.e., NH<sub>3</sub> fixation by Haber-Bosch and phosphate mining. Finally, implications of ammonia and phosphate separation from wastewaters are discussed and the benefits of nutrient recovery are highlighted.

## 2.2 Minimum Energy of Nutrient Recovery

**Gibbs Free Energy of Separation is the Minimum Energy to Recover Nutrients.** In the recovery of nutrients from waste streams, the desired nutrient components of N and P are separated from the dilute feed to yield a nutrient-rich product, leaving a wastewater retentate stream less concentrated in N or P. The theoretical minimum energy required to achieve this nutrient recovery,  $E_{\min}$ , is equal to the Gibbs free energy of separation,  $\Delta G_{\text{sep}}$ , which is the difference between the Gibbs free energy of the product and retentate (resultant streams), and the wastewater (initial feed), as described by eqn (2.1):

$$E_{\min} = \Delta G_{\text{sep}} = N_{\text{P}}G_{\text{P}} + N_{\text{R}}G_{\text{R}} - N_{\text{F}}G_{\text{F}} \quad (2.1)$$

where  $G$  is the molar Gibbs free energy,  $N$  is the total number of moles in each stream, and subscripts P, R, and F, denote the product, retentate, and feed streams, respectively.

The molar Gibbs free energy of a mixed solution is the sum of the partial molar Gibbs free energy of the constituent species:<sup>102, 103</sup>

$$G = \sum x_i G_i^0 + RT \left[ \sum x_i \ln(\gamma_i x_i) \right] \quad (2.2)$$

where  $x$  and  $\gamma$  are mole fraction and activity coefficient of species  $i$ ,  $G^0$  is Gibbs free energy of formation in the aqueous solution at standard state,  $R$  is the gas constant, and  $T$  is absolute temperature.

By applying eqns (2.1) and (2.2), the Gibbs free energy of separation per mole of nutrient recovered,  $\Delta\bar{G}_{\text{sep}}$ , can be expressed as:

$$\Delta\bar{G}_{\text{sep}} = \frac{1}{x_{1,P}} \left\{ \begin{array}{l} \sum x_{i,P} G_{i,P} + RT \sum x_{i,P} \ln(\gamma_{i,P} x_{i,P}) \\ + \frac{N_R}{N_P} \left[ \sum x_{i,R} G_{i,R} + RT \sum x_{i,R} \ln(\gamma_{i,R} x_{i,R}) \right] \\ - \frac{N_F}{N_P} \left[ \sum x_{i,F} G_{i,F} + RT \sum x_{i,F} \ln(\gamma_{i,F} x_{i,F}) \right] \end{array} \right\} = \bar{E}_{\text{min}} \quad (2.3)$$

where subscript 1 denotes the targeted nutrient component, i.e., N or P species. Therefore, with the composition and relative proportion of the feed, product, and retentate streams, the theoretical minimum energy to reclaim a mole of nutrient,  $\bar{E}_{\text{min}}$ , can be determined using eqn (2.3). Note that for pure products, i.e., solid minerals or unmixed liquids, the product  $\sum x \ln \gamma x$  term vanishes and  $x_{1,P}$  can be replaced with  $n_{1,P}$ , the number of N or P atoms in the chemical structure of the pure liquid/solid mineral product ( $n_{1,P} = 1$  for all products except for  $(\text{NH}_4)_2\text{SO}_4$ , where  $n_{1,P} = 2$ ). Recovery yield,  $Y$ , is defined as the fraction of nutrient available in the initial feed captured in the product stream, and can be described by:

$$Y_{i,P} = \frac{x_{1,P} N_P}{x_{1,F} N_F} \quad (2.4)$$

Note that, again, for solids and pure liquid products,  $x_{1,P}$  is replaced with  $n_{1,P}$ .

**Analysis of Minimum Energy for Nutrient Recovery.** Detailed methodology to determine the molar minimum energy of nutrient recovery,  $\bar{E}_{\text{min}}$ , is discussed in Appendix A and briefly presented here. Typical ranges of nutrient species mole fraction concentrations and pHs of the greywater, domestic WW, 2° WW effluent, fresh urine, and hydrolyzed urine feed waste

streams are based on literature data (Table A.1),<sup>89, 91-96</sup> whereas  $x_{1,P}$  and  $n_{1,P}$  are dependent on the concentration and chemical structure of the product, respectively. Typical concentration ranges of other species in the waste streams relevant to the analysis is presented in Table A.2.<sup>89, 91-97</sup> For a certain  $Y$  (and corresponding  $x_{1,P}$  or  $n_{1,P}$ ), the retentate composition is determined by mole balance and accounting for speciation due to pH and concentration changes. I.e., the approach incorporates the effects of protonation/deprotonation on  $x$  of orthophosphates and ammoniacal nitrogen ( $\text{H}_3\text{PO}_4/\text{H}_2\text{PO}_4^-/\text{HPO}_4^{2-}/\text{PO}_4^{3-}$  and  $\text{NH}_4^+/\text{NH}_3(\text{aq})$ , respectively). To understand the influence of recovery yield on  $\bar{E}_{\min}$ ,  $Y$  of 0.005, 0.2, 0.5, 0.8, and 1.0 are modeled for select wastewater matrices of 2° WW effluent and hydrolyzed urine. In that analysis, the presence of carbonate species in hydrolyzed urine is considered. Because the complete water chemistry of most wastewater feeds are not fully known (i.e., species composition and buffering capacity), the analysis is able to only consider the capture of an infinitesimally small amount of nutrient, i.e.,  $Y \rightarrow 0$ , such that the feed and retentate compositions are effectively identical. The complete equations utilized to determine the molar Gibbs free energy of separation for all scenarios in the analysis are presented in Appendix A, eqns (A.5)–(A.20).

All calculations model recovery at  $T = 298$  K. Non-ideal behavior in solutions was accounted for using activity coefficients,  $\gamma_i$ , which were determined using the Davies approximation,<sup>67</sup> nonrandom two-liquid method,<sup>104, 105</sup> or experimental data reported in literature,<sup>106</sup> as described in Appendix A.  $G^0$  for each species  $i$  in aqueous solution can be found in Table A.3 in Appendix A. For pure liquids and solid minerals, the Gibbs free energy of the product is equal to the Gibbs free energy of formation at standard state,  $G_p = G_{f,p}^0$  (values are presented in Table A.4 of Appendix A).

## 2.3 Energy Requirement for Nutrient Recovery

**Harvesting Ammonia from More Concentrated Waste Streams Requires Less Energy.** The molar minimum energy (i.e., per mole of  $\text{NH}_3$  captured) to recover liquid ammonia,  $\text{NH}_{3(l)}$ , from different waste streams of varying TAN concentrations is calculated using eqn (A.5) of Appendix A and presented in Figure 2.2. Yields of 1 and 0, representing complete recovery of N in the product and capture of an infinitesimally small amount of N from the feed, respectively, were analyzed (solid and dashed lines). Typical TAN concentration ranges in the various waste streams are shown as floating bars and correspond to the horizontal axis (logarithmic scale). To isolate the impact of [TAN] on  $\bar{E}_{\min}$ , the analysis for  $Y = 1$  assumes the feed waste streams to have  $\text{pH} \ll \text{p}K_a$  of  $\text{NH}_4^+$  (9.24) and inexhaustible buffering capacity, such that the predominant form of TAN in both the feed and retentate is  $\text{NH}_4^+$ ; the influence of  $\text{NH}_4^+/\text{NH}_{3(aq)}$  speciation is considered in the next subsection. We note that the pH of all waste streams examined in this study, except for hydrolyzed urine, are usually well below 9.24 and, hence, TAN is mostly present as ammonium.<sup>89</sup>

91-97

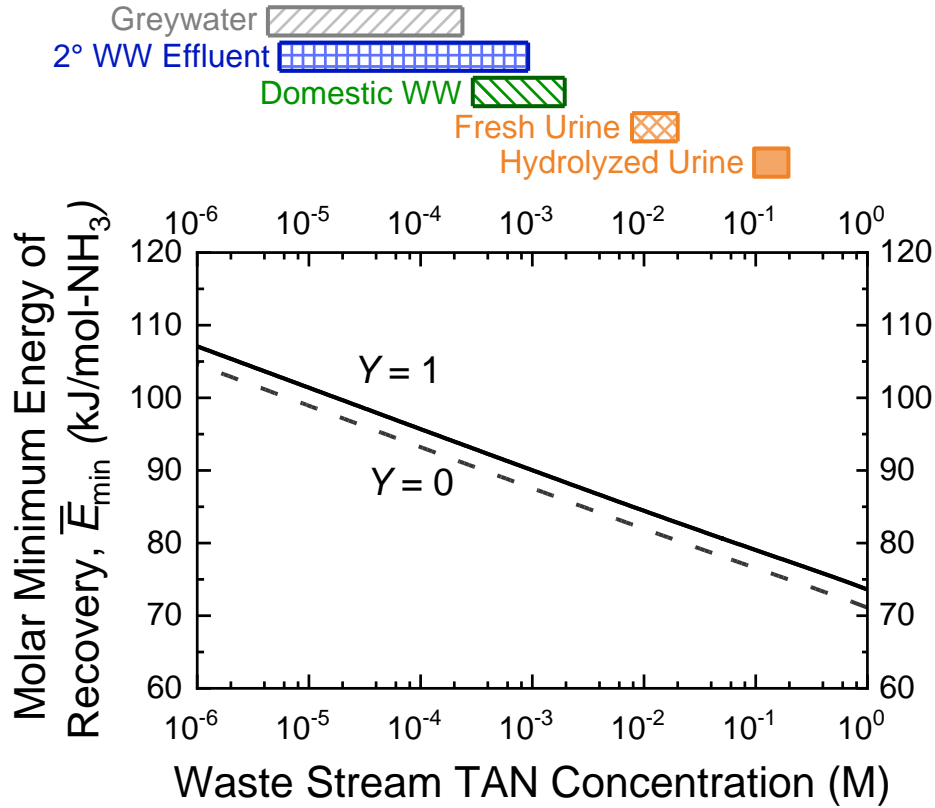


**Figure 2.2.** Molar minimum energy,  $\bar{E}_{\min}$ , to recover nutrient product of pure liquid ammonia as a function of waste stream TAN concentration for recovery yields,  $Y$ , of 1 and 0 (solid and dashed lines, respectively). Floating bars, corresponding to the horizontal axis (on logarithmic scale), represent the TAN concentration ranges for waste streams of greywater, secondary wastewater effluent, domestic wastewater, fresh urine, and hydrolyzed urine. For simplification of analysis, all TAN in the waste streams was assumed to be present as  $\text{NH}_4^+$ .

As expected, Figure 2.2 demonstrates that to minimize the theoretical minimum energy to capture  $\text{NH}_{3(l)}$ , it is advantageous to target waste streams with high TAN concentrations. This trend is consistent with thermodynamic assessments of desalination, where  $\bar{E}_{\min}$  for water recovery increases with feed salinity.<sup>98, 99</sup> The minimum energy to reclaim  $\text{NH}_{3(l)}$  essentially decreases linearly with increasing logarithm of TAN concentration in the waste stream, i.e.,  $\bar{E}_{\min} \approx \infty - \log[\text{TAN}]$ , primarily due to the  $\ln x$  terms of eqn (2.3). The slight deviation from perfect linearity

is attributed to the non-linear dependence of  $\gamma_{\text{NH}_4^+}$  on ionic strength (Davies approximation, eqn (A.21) in Appendix A).<sup>67</sup> In other words, the reduction in  $\bar{E}_{\text{min}}$  is not proportional to the increase in [TAN] of the feed stream. Concentrated streams, such as hydrolyzed and fresh urine, have orders of magnitude more TAN than diluted streams of domestic wastewater, secondary wastewater effluent, and greywater; however,  $\bar{E}_{\text{min}}$  is not orders of magnitude higher when capturing N from the diluted streams compared to the more concentrated streams. For example, hydrolyzed urine is  $\approx 140\text{--}520\times$  more concentrated in TAN than domestic wastewater, but  $\bar{E}_{\text{min}}$  for product of  $\text{NH}_3(\text{l})$  at  $Y = 0$  is only  $1.13\text{--}1.22\times$  greater for domestic WW.

Recovery yields of 1 and 0 exhibit similar trends, with  $\bar{E}_{\text{min}}$  for  $Y = 1$  approximately 3% higher than  $Y = 0$  across the TAN concentrations investigated. As  $Y$  increases,  $\text{NH}_3$  is separated from a progressively more dilute feed stream, thus requiring more energy and the averaged molar energy of separation rises. Again, parallels can be drawn to the increasing specific energy of desalination for larger water recovery yields.<sup>15, 16</sup> However, the magnitude of  $\bar{E}_{\text{min}}$  increase for higher nutrient recoveries is drastically smaller than for desalination, where energy requirement almost doubles when  $Y$  is raised from 0 to 0.5. Because  $\bar{E}_{\text{min}}$  for  $Y = 1$  and  $Y = 0$  only differ by  $\approx 3\%$ , examination of  $\bar{E}_{\text{min}}$  for  $Y = 0$  closely translates to higher recovery yields. The impact of recovery yield on  $\bar{E}_{\text{min}}$  will be discussed in depth in a latter section.

**Feed Stream pH Affects  $\bar{E}_{\text{min}}$  by Influencing Speciation.**  $\bar{E}_{\text{min}}$  values to recover select ammonia and phosphate products from various waste streams are shown in Figures 2.3A and B, respectively. The N products of liquid ammonia,  $\text{NH}_3(\text{l})$ , aqueous ammonia solutions at 10, 5.0,

and 1.0 M, and solid precipitate of ammonium sulfate,  $(\text{NH}_4)_2\text{SO}_{4(s)}$ , are common commercial fertilizers.<sup>107-110</sup> Likewise, solid precipitate P products of potassium magnesium phosphate,  $\text{KMgPO}_4 \cdot 6(\text{H}_2\text{O})$ , struvite,  $\text{NH}_4\text{MgPO}_4 \cdot 6\text{H}_2\text{O}$ , potassium phosphate,  $\text{KH}_2\text{PO}_4$ , and monoammonium phosphate,  $\text{NH}_4\text{H}_2\text{PO}_4$ , are also conventional fertilizers available in the market.<sup>110-117</sup> Because each waste stream can be highly heterogeneous in nutrients content, concentrations of product co-species (e.g.,  $\text{SO}_4^{2-}$  is co-species for  $(\text{NH}_4)_2\text{SO}_{4(s)}$  product), and pH, the resultant energy requirement spans a range of values (according to eqn (2.3)). The top and bottom of the floating bars represent the highest and lowest  $\bar{E}_{\min}$ , respectively, for each waste stream and product pair. Detailed  $\bar{E}_{\min}$  values for all conditions, calculated using eqns (A.5)–(A.12), can be found in Tables A.5 and A.6 of Appendix A.

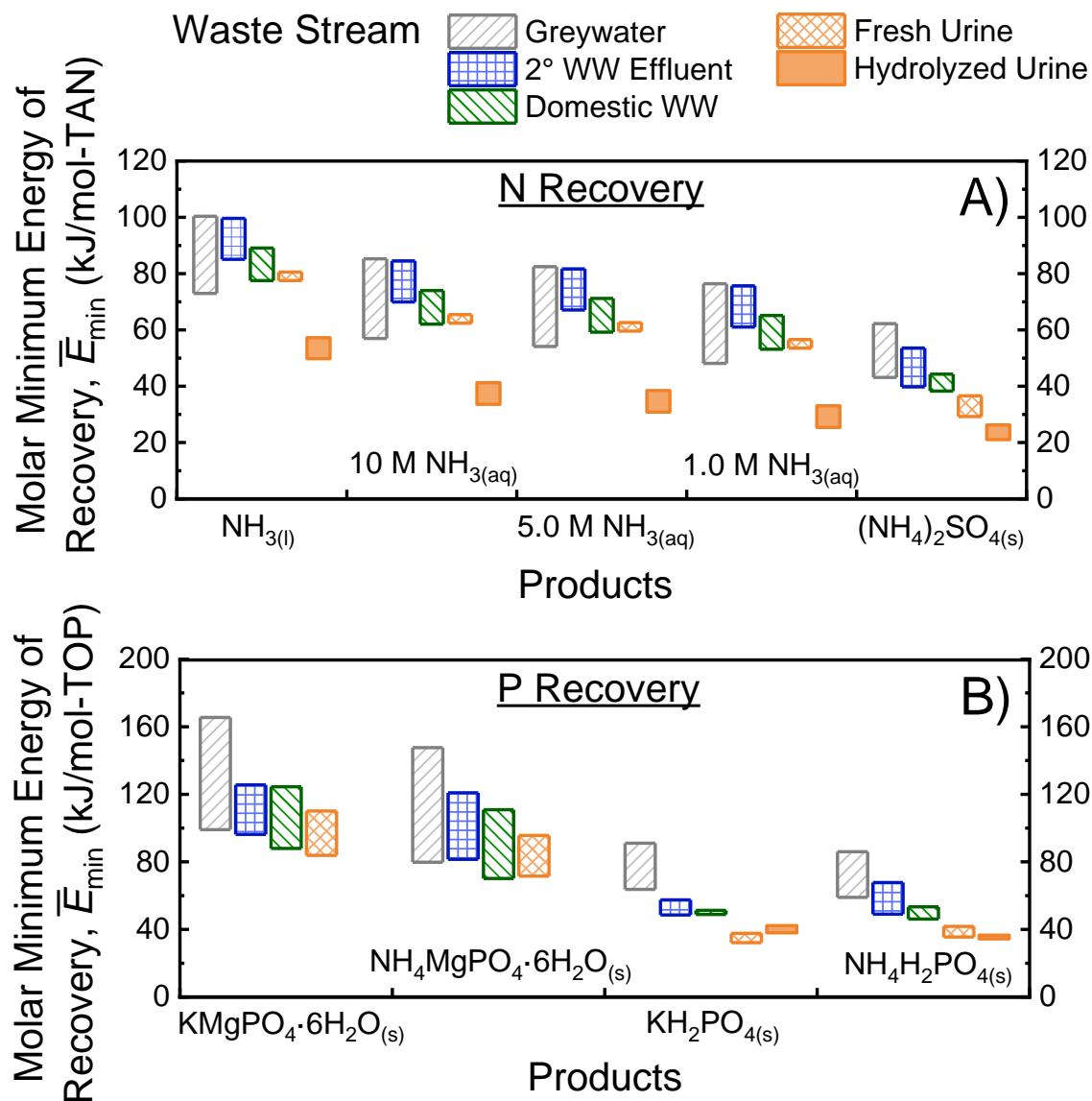


**Figure 2.3.** Molar minimum energy,  $\bar{E}_{\min}$ , to recover A) TAN as products of liquid ammonia,  $\text{NH}_3(\text{l})$ , 10, 5.0, and 1.0 M aqueous ammonia solutions, and ammonium sulfate solid,  $(\text{NH}_4)_2\text{SO}_4(\text{s})$ ; and B) TOP as mineral products of potassium magnesium phosphate,  $\text{KMgPO}_4 \cdot 6(\text{H}_2\text{O})$ , struvite,  $\text{NH}_4\text{MgPO}_4 \cdot 6\text{H}_2\text{O}$ , potassium phosphate,  $\text{KH}_2\text{PO}_4$ , and monoammonium phosphate,  $\text{NH}_4\text{H}_2\text{PO}_4$ . Waste stream sources are greywater, secondary wastewater effluent, domestic wastewater, fresh urine, and hydrolyzed urine. Floating columns indicate the  $\bar{E}_{\min}$  ranges that correspond to the typical span of nutrient content, product co-species concentrations, and pH reported for the waste streams. The analysis considered recovery yield of 0 for all products, i.e., an infinitesimally minute amount of nutrient is recovered from the waste stream.

As previously discussed, TAN concentration in the waste stream is a primary factor influencing  $\bar{E}_{\min}$ : minimum energy to capture ammonia products is generally lower when targeting waste streams of higher [TAN], such as hydrolyzed urine, compared to more diluted streams. Additionally,  $\bar{E}_{\min}$  is also dependent on the pH of the waste stream. For a certain waste stream [TAN],  $\bar{E}_{\min}$  values for the selected products are lower in N recovery scenarios with higher waste stream pH (Table A.5). As an illustration, Figure 2.4 presents  $\bar{E}_{\min}$  for products recovered from greywater with [TAN] =  $2.11 \times 10^{-4}$  M (midpoint of concentration range), but at different pH values.

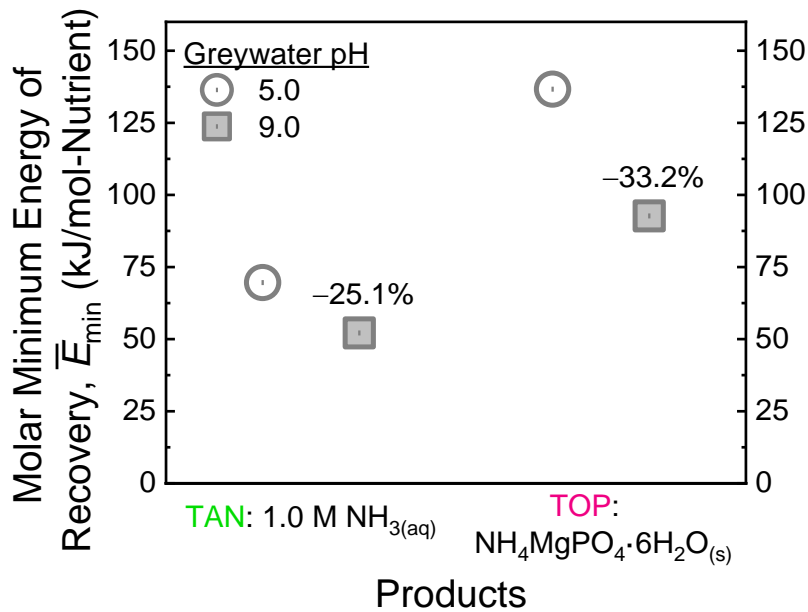


**Figure 2.4.** Molar minimum energy,  $\bar{E}_{\min}$ , to recover TAN product of 1.0 M  $\text{NH}_3(\text{aq})$  and TOP product of struvite,  $\text{NH}_4\text{MgPO}_4 \cdot 6\text{H}_2\text{O}(\text{s})$ , from greywater at pH of 5.0 and 9.0 (open circle and filled square symbols, respectively). Labels above the symbols indicate the percent decrease in  $\bar{E}_{\min}$  from feed pH of 5.0 to 9.0. Mid-range greywater TAN and TOP concentrations of  $2.11 \times 10^{-4}$  M and  $6.80 \times 10^{-5}$  M, respectively, are utilized in this analysis and recovery yield of the product is 0 (i.e., an infinitesimally small quantity of nutrient is recovered from the waste stream).

$\bar{E}_{\min}$  to recover 1.0 M  $\text{NH}_{3(\text{aq})}$  from greywater at pH of 9.0 is 25.1% less than at pH of 5.0. Because ammonia is a weak base, which can protonate to form ammonium, the fraction of TAN present as  $\text{NH}_{3(\text{aq})}$  rises with increasing pH (eqn (A.1) in Appendix A). The standard-state molar Gibbs free energy of formation of  $\text{NH}_{3(\text{aq})}$  is higher than that of  $\text{NH}_4^+$  ( $-26.6$  kJ/mol compared to  $-79.3$  kJ/mol, Table A.3) and, thus, the Gibbs free energy of separation is lower for  $\text{NH}_{3(\text{aq})}$  than  $\text{NH}_4^+$ , as per eqn (2.3). Hence, recovery of the N products is thermodynamically more favorable if TAN is present as  $\text{NH}_{3(\text{aq})}$  in more basic waste streams. The theoretical minimum energy to reclaim N from hydrolyzed urine is significantly lower than other waste streams (Figure 2.3A) because of the two advantages of higher pH and greater TAN concentration. Hydrolyzed urine pH range is 9–9.2, close to or at the  $\text{pK}_a$  of 9.24 for ammonium, whereas pH of the other waste streams are mostly  $\approx 5$ –8.5. Also, [TAN] is 0.270–0.578 M for hydrolyzed urine, at least  $67\times$  greater than other N sources aside from fresh urine (still  $5.5$ – $32.2\times$  higher). However, the energy benefits for  $(\text{NH}_4)_2\text{SO}_{4(\text{s})}$  recovery from hydrolyzed urine are less pronounced (Figure 2.3A), because N is captured as  $\text{NH}_4^+$ . Converting  $\text{NH}_{3(\text{aq})}$ , the predominant TAN species in hydrolyzed urine, to ammonium increases  $\Delta G_{\text{sep}}$  and offsets the beneficial  $G^0$  effect. Overall, waste streams with both high TAN concentration and pH offer the smallest  $\bar{E}_{\min}$  to overcome for N recovery; of the waste streams examined here, hydrolyzed urine is the most optimal.

Among the N products evaluated,  $\bar{E}_{\min}$  is generally highest for  $\text{NH}_{3(\text{l})}$ , followed by 10 M  $\text{NH}_{3(\text{aq})}$ , 5.0 M  $\text{NH}_{3(\text{aq})}$ , 1.0 M  $\text{NH}_{3(\text{aq})}$ , and then  $(\text{NH}_4)_2\text{SO}_{4(\text{s})}$  (Figure 2.3A). For the aqueous ammonia solutions,  $\bar{E}_{\min}$  decreases with lower product concentration. This is reflected in eqn (A.7) and also intuitively understood: a more dilute product stream requires less separation from the feed and, hence, demands less energy. For the pure products of  $\text{NH}_{3(\text{l})}$  and  $(\text{NH}_4)_2\text{SO}_{4(\text{s})}$ ,  $\bar{E}_{\min}$  is largely

dependent on the Gibbs free energy of formation of the product,  $G_{f,P}^0$  (Table A.4), with a lower  $G_{f,P}^0$  contributing to a smaller  $\bar{E}_{\min}$ . Because  $G_{f,(NH_4)_2SO_4(s)}^0 \ll G_{f,NH_3(l)}^0$ , recovering  $(NH_4)_2SO_4(s)$  is thermodynamically more favorable than  $NH_3(l)$ .

**Rational Selection of Waste Stream Feed and Products Minimizes Energy for Nutrient Recovery.** Similar trends are also observed for TOP recovery (Figures 2.3B and 2.4). Note that because magnesium precipitates out from urine, as struvite, magnesium phosphates, and  $Mg(OH)_2$ , during hydrolysis,<sup>89, 90, 118</sup>  $[Mg^{2+}]$  in hydrolyzed urine is practically negligible and, hence, recovery of Mg-based P products,  $NH_4MgPO_4 \cdot 6H_2O(s)$ , and  $KMgPO_4 \cdot 6H_2O(s)$ , were not analyzed. Higher concentrations of TOP and product co-species (TAN,  $K^+$ , and  $Mg^{2+}$ ) in the waste stream lowered  $\bar{E}_{\min}$ . TOP concentrations in the waste stream follow the trend: greywater < secondary wastewater effluent < domestic wastewater < hydrolyzed urine < fresh urine, resulting in  $\bar{E}_{\min}$  values largely following the reverse trend, i.e., P recovery from fresh urine generally has the lowest  $\bar{E}_{\min}$ . However, one deviation is the separation of  $NH_4H_2PO_4(s)$  from hydrolyzed urine. This is due to the low concentration of the product co-species,  $NH_4^+$ , significantly contributing to  $\bar{E}_{\min}$ . Although fresh urine is richer in TOP (1.13–1.57 $\times$ ), [TAN] is only 0.067–0.085 that of hydrolyzed urine.

Despite fresh urine having significantly higher [TOP], the molar minimum energies of recovery for struvite,  $NH_4MgPO_4 \cdot 6H_2O(s)$ , and potassium magnesium phosphate (KMP),  $KMgPO_4 \cdot 6H_2O(s)$ , are comparable with the lower  $\bar{E}_{\min}$  range for the more dilute streams of domestic WW, 2<sup>o</sup> WW effluent, and greywater. This is because P is present in struvite and KMP as  $PO_4^{3-}$ , the least protonated form of phosphate, and a greater portion of TOP in the feed exists

as  $\text{PO}_4^{3-}$  at higher pHs. The pH range for fresh urine (6–7.5) is lower than domestic wastewater and secondary-treated wastewater effluent (6.5–8.5 and 6.8–7.7, respectively) and is considerably below the high-end of greywater (pH = 9). In the recovery of struvite and KMP from fresh urine, the deprotonation of  $\text{H}_2\text{PO}_4^-$  (predominant species below pH of 7.2) to  $\text{PO}_4^{3-}$  increases  $\Delta G_{\text{sep}}$ , and partially nullifies the benefits of the high [TOP]. Therefore,  $\bar{E}_{\text{min}}$  is not substantially lower than other waste streams at higher pH (Table A.6). The impact of pH on  $\bar{E}_{\text{min}}$  is further illustrated by Figure 2.4, which shows  $\bar{E}_{\text{min}}$  of struvite recovery from greywater at pH = 5.0 and 9.0.  $\bar{E}_{\text{min}}$  at pH = 9.0 is markedly depressed (-33.2%) relative to pH of 5.0. As the dominant forms of phosphate at pH = 5.0 and 9.0 are  $\text{H}_2\text{PO}_4^-$  and  $\text{HPO}_4^{2-}$ , respectively, less energy is required for the conversion to  $\text{PO}_4^{3-}$  with the more basic feed stream. This trend is observed for struvite and KMP across the different waste streams (Table A.6) and also corroborated by experimental observations that the two minerals precipitate more readily in higher pH solutions.<sup>119</sup> In contrast, the effect of pH on  $\bar{E}_{\text{min}}$  is negligible for  $\text{KH}_2\text{PO}_4$  and  $\text{NH}_4\text{H}_2\text{PO}_4$ , where P is present as  $\text{H}_2\text{PO}_4^-$  (Table A.6).

The most thermodynamically favorable products for P recovery are  $\text{KH}_2\text{PO}_{4(\text{s})}$  and  $\text{NH}_4\text{H}_2\text{PO}_{4(\text{s})}$ , followed by  $\text{NH}_4\text{MgPO}_4 \cdot 6\text{H}_2\text{O}_{(\text{s})}$  and  $\text{KMgPO}_4 \cdot 6\text{H}_2\text{O}_{(\text{s})}$ , with  $\bar{E}_{\text{min}}$  primarily affected by the phosphate identity ( $\text{H}_2\text{PO}_4^-$  or  $\text{PO}_4^{3-}$ ) and feed concentrations of product co-species (specifically  $\text{Mg}^{2+}$ ). The acid dissociation constants of phosphoric acid are 2.2, 7.2, and 12.4. For the waste streams investigated here, the typical pH ranges between 5 and 9.2. Hence, the predominant phosphate species are  $\text{H}_2\text{PO}_4^-$  or  $\text{HPO}_4^{2-}$ . Because the conversion of the predominant phosphate species to  $\text{H}_2\text{PO}_4^-$  (no reaction or protonation of one  $\text{H}^+$ ) needed to form  $\text{KH}_2\text{PO}_{4(\text{s})}$  and  $\text{NH}_4\text{H}_2\text{PO}_{4(\text{s})}$  requires less energy than the conversion to  $\text{PO}_4^{3-}$  (deprotonation of one or two  $\text{H}^+$ ),  $\bar{E}_{\text{min}}$  is larger for struvite and KMP. Furthermore, the formation of struvite and KMP require  $\text{Mg}^{2+}$

in addition to  $\text{NH}_4^+$  and  $\text{K}^+$ , respectively. The separation of  $\text{Mg}^{2+}$  from waste streams with low  $[\text{Mg}^{2+}]$  adds to the energy cost, hence, contributing to the greater  $\bar{E}_{\min}$  for  $\text{NH}_4\text{MgPO}_4 \cdot 6\text{H}_2\text{O}_{(s)}$  and  $\text{KMgPO}_4 \cdot 6\text{H}_2\text{O}_{(s)}$ .

For nutrient recovery from waste streams, it is advantageous to minimize energy requirements, thus a low  $\bar{E}_{\min}$  is desirable. The main factors influencing the molar minimum energy for nutrient recovery are: nutrient concentrations in the feed, waste stream pH, and co-species in the product. To minimize  $\bar{E}_{\min}$ , waste streams and products can be strategically targeted. Hydrolyzed urine and fresh urine, which contain the highest concentrations of TAN and TOP, respectively, are almost always the most optimal streams for TAN and TOP recovery. However, depending on the product, certain waste streams may be better suited because of the more favorable pH and co-species concentration. Therefore, the selection of product should be informed by the pH, availability of nutrients, and co-species in the specific waste stream.

**Impact of Nutrient Recovery Yields on Minimum Energy of Recovery.** Previous analysis modeled  $\bar{E}_{\min}$  for capturing various products from different waste streams at  $Y = 0$ . However, actual nutrient recovery will have nonzero recovery yields. Figure 2.5 shows  $\bar{E}_{\min}$  of select ammonia products of 1.0 M  $\text{NH}_3$  aqueous solution and  $\text{NH}_3(l)$  (open and filled symbols, respectively) from two waste streams of secondary wastewater effluent and hydrolyzed urine (blue square and orange circle symbols, respectively) as a function of  $\text{NH}_3$  recovery yield. As discussed previously, at  $Y = 0$ , i.e., infinitesimally small  $\text{NH}_3$  recovery, the pH and TAN speciation in the feed and retentate are essentially equal. However, at higher recovery yields, the pH and TAN speciation in the retentate stream differ significantly from the feed stream. Therefore, to calculate  $\bar{E}_{\min}$  for  $Y > 0$ , the speciation of TAN (i.e., fraction of TAN as  $\text{NH}_3(\text{aq})$  and  $\text{NH}_4^+$ , denoted by  $\alpha_{\text{NH}_3}$

and  $\alpha_{\text{NH}_4^+}$ , respectively) in both the feed and retentate stream must be considered in conjunction with the TAN material balance (i.e.,  $x_{\text{TAN},F}N_F + x_{\text{TAN},\text{RXN}}N_{\text{RXN}} = x_{\text{TAN},P}N_P + x_{\text{TAN},R}N_R$ ).

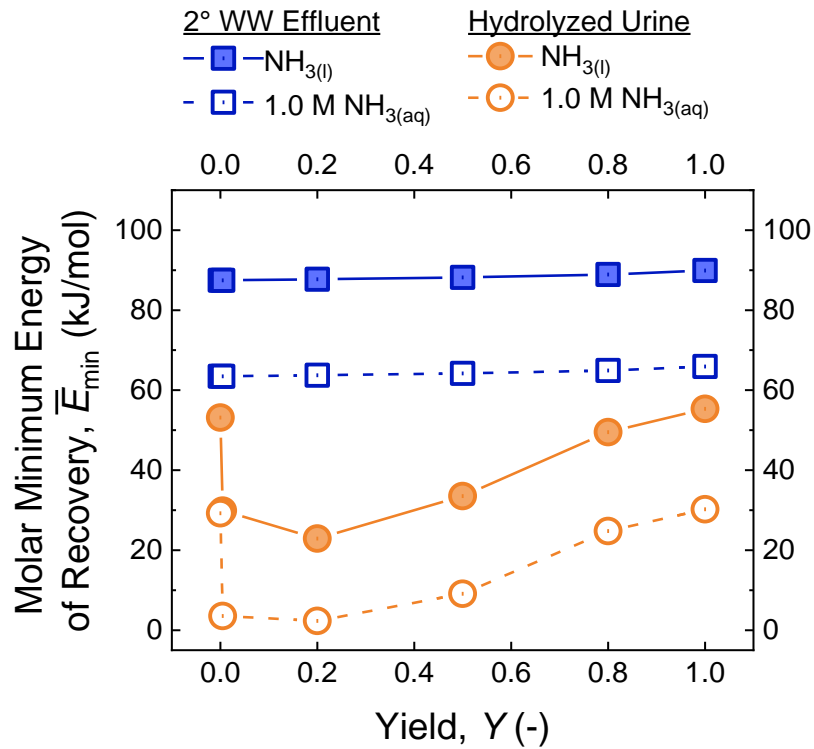


**Figure 2.5.** Molar minimum energy,  $\bar{E}_{\min}$ , to recover  $\text{NH}_3$  as products of liquid ammonia,  $\text{NH}_{3(l)}$ , or 1.0 M  $\text{NH}_{3(aq)}$  aqueous solution (filled and open symbols, respectively) from secondary wastewater effluent and hydrolyzed urine (blue square and orange circle symbols, respectively) as a function of recovery yield,  $Y$  (0, 0.005, 0.2, 0.5, 0.8, and 1). The mid-range TAN and pH of 2° WW effluent and hydrolyzed urine were utilized for this analysis.

For scenarios with secondary wastewater effluent (blue square symbols), the feed stream  $\text{pH} \ll \text{pK}_a$ , which results in nearly complete predominance of  $\text{NH}_4^+$  over  $\text{NH}_{3(aq)}$  (i.e.,  $\alpha_{\text{NH}_4^+} \approx 1$  and  $\alpha_{\text{NH}_3} \approx 0$ ). Because removing basic  $\text{NH}_3$  leaves the remaining solution more acidic, pH of the retentate stream is always lower than the feed stream pH. Therefore, TAN speciation in the feed and retentate streams for 2° WW effluent are essentially equal, with  $\alpha_{\text{NH}_4^+,R} \approx \alpha_{\text{NH}_4^+,F} \approx 1$  and  $\alpha_{\text{NH}_3,R} \approx \alpha_{\text{NH}_3,F} \approx 0$ . Increasing  $Y$  results in a slight increase in  $\bar{E}_{\min}$  for both  $\text{NH}_{3(l)}$  and 1.0 M

$\text{NH}_{3(\text{aq})}$  recovery. This trend is consistent with Figure 2.2, which also simulated waste streams with  $\text{NH}_4^+$  as the predominant form of TAN. Importantly,  $\bar{E}_{\text{min}}$  only marginally increases ( $< 4\%$ ) between  $Y = 0$  and 1. Thus, actual nutrient recovery applications can take advantage of this by striving for higher yields without significantly raising the theoretical energy requirement.

For hydrolyzed urine (orange circle symbols in Figure 2.5), the feed pH is near the  $\text{p}K_a$  of ammonium, such that  $\alpha_{\text{NH}_3} \neq 0$ . Thus at  $Y > 0$ , TAN speciation in the feed and retentate streams differ significantly, i.e.,  $\alpha_{\text{NH}_3,\text{R}} \neq \alpha_{\text{NH}_3,\text{F}}$  and  $\alpha_{\text{NH}_4^+,\text{R}} \neq \alpha_{\text{NH}_4^+,\text{F}}$ . An in-depth discussion of methodology to account for this differing speciation can be found in Appendix A. In contrast to 2° WW effluent, the trends for  $\bar{E}_{\text{min}}$  of  $\text{NH}_{3(\text{l})}$  and 1.0 M  $\text{NH}_{3(\text{aq})}$  recovery from hydrolyzed urine are not monotonic, but instead exhibit L-shaped rebounds with initial sharp decreases and followed by gradual increases. This signifies that reclaiming the first molecule of  $\text{NH}_3$  from hydrolyzed urine requires, in theory, more energy than the next molecules until a certain amount of ammonia is recovered and, thereafter, capturing every additional  $\text{NH}_3$  molecule requires more energy than the last. In contrast to secondary wastewater effluent,  $\bar{E}_{\text{min}}$  of hydrolyzed urine changes significantly as a function of recovery yield. The distinction between  $\bar{E}_{\text{min}}$  trends of the two waste streams is due to the disparate speciation of TAN in the retentates. For 2° WW effluent scenarios,  $\alpha_{\text{NH}_4^+,\text{R}}$  and  $\alpha_{\text{NH}_3,\text{R}}$  are effectively independent of  $Y$  and, therefore, the concentration of both  $\text{NH}_4^+$  and  $\text{NH}_{3(\text{aq})}$  in the retentate consistently decrease with higher yields. However, for hydrolyzed urine scenarios, pH of the retentate significantly declines at higher yields and, thus,  $\alpha_{\text{NH}_4^+,\text{R}}$  increases and  $\alpha_{\text{NH}_3,\text{R}}$  decreases (see Tables A.8 and A.9 for pH and speciation in the feed and retentate at different  $Y$ , for products of  $\text{NH}_{3(\text{l})}$  and 1.0 M  $\text{NH}_{3(\text{aq})}$ , respectively). Because the magnitude of the

Gibbs free energy of formation for  $\text{NH}_4^+$  is much greater than  $\text{NH}_{3(\text{aq})}$  ( $-79.3$  and  $-26.6$  kJ/mol, respectively),  $\text{NH}_4^+$  is the thermodynamically preferred form of TAN in solution. This results in competing factors affecting  $\bar{E}_{\text{min}}$ : TAN in the retentate decreases with increasing yield, which drives  $\bar{E}_{\text{min}}$  to increase, but this is countered by the reduction in  $\bar{E}_{\text{min}}$  as the fraction of TAN present as  $\text{NH}_4^+$  in the retentate increases with increasing yield. At low  $Y$ , the latter factor is more dominant, thus explaining the initial dip in  $\bar{E}_{\text{min}}$ . With greater  $Y$ , retentate pH drops and  $\text{NH}_4^+$  becomes increasingly predominant over  $\text{NH}_{3(\text{aq})}$ . Beyond a certain point, the former factor dominates and  $\bar{E}_{\text{min}}$  increases. Further quantitative analysis and a more detailed discussion can be found in Appendix A.

**Nitrate and Urea are Other Forms of Nitrogen Suitable for Recovery.** In addition to ammoniacal products of  $\text{NH}_{3(\text{l})}$ ,  $\text{NH}_{3(\text{aq})}$ , and  $\text{NH}_4\text{SO}_{4(\text{s})}$ , N can be recovered in other forms, such as nitrate,  $\text{NO}_3^-$ , and urea,  $\text{CO}(\text{NH}_2)_2$ .<sup>108, 110</sup> Nitrate is present in greywater, domestic wastewater, and secondary wastewater effluent (but is only present in negligible amounts in fresh or hydrolyzed urine), whereas urea is excreted in fresh urine (upon storage, the compound hydrolyzes into TAN and bicarbonate and, thus, urea is not present in significant quantities in the other waste streams). Figure 2.6 shows the range of molar minimum energies to reclaim aqueous and solid products containing  $\text{NO}_3^-$  from 2° WW effluent, as well as aqueous and solid urea from fresh urine. Based on compiled literature data, nitrate concentration in secondary wastewater effluent spans from 0.0714–1.42 mM and urea concentration range in fresh urine is 126–265 mM (252–530 mM-N).<sup>89, 91-97</sup> To calculate  $\bar{E}_{\text{min}}$  for 1.0 M  $\text{KNO}_{3(\text{aq})}$ , 1.0 M  $\text{NH}_4\text{NO}_{3(\text{aq})}$ ,  $\text{KNO}_{3(\text{s})}$ , and  $\text{NH}_4\text{NO}_{3(\text{s})}$  recovery from 2° WW effluent, eqns (A.13), (A.14), (A.15), and (A.16) were used, respectively; to calculate  $\bar{E}_{\text{min}}$  to recover 1.0 M  $\text{CO}(\text{NH}_2)_{2(\text{aq})}$  and  $\text{CO}(\text{NH}_2)_{2(\text{s})}$  from fresh urine, eqns (A.17) and (A.18)

were utilized, respectively. Note that, for every mole of product,  $\text{CO}(\text{NH}_2)_2$  and  $\text{NH}_4\text{NO}_3$  contain 2 moles of N, whereas  $\text{KNO}_3$  has only 1 mole of N.

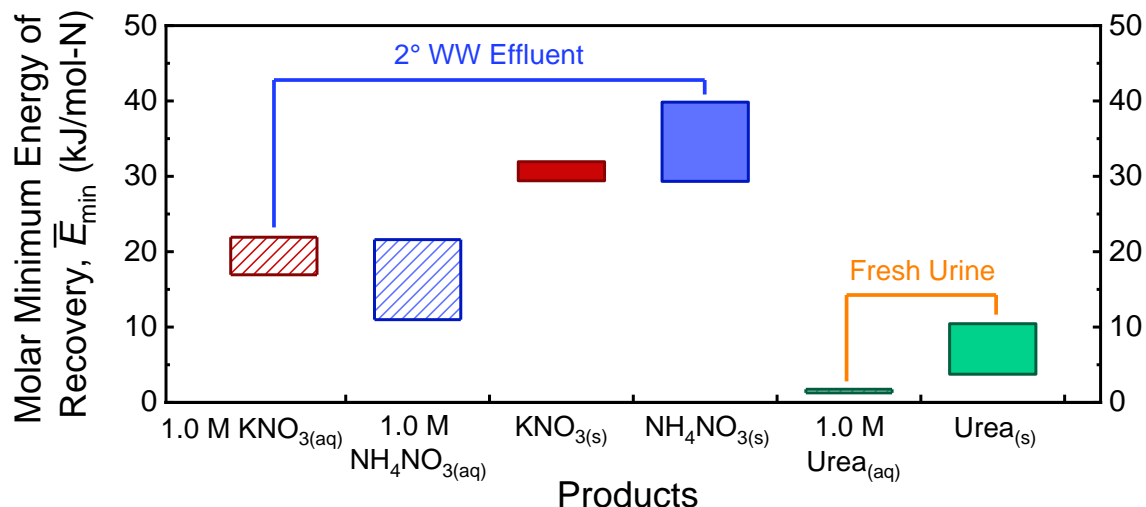


**Figure 2.6.** Molar minimum energy,  $\bar{E}_{\min}$ , to recover different N products from waste streams of secondary wastewater effluent and fresh urine. Products recovered from 2° WW effluent are 1.0 M  $\text{KNO}_3$ (aq), 1.0 M  $\text{NH}_4\text{NO}_3$ (aq),  $\text{KNO}_3$ (s), and  $\text{NH}_4\text{NO}_3$ (s), whereas products reclaimed from fresh urine are 1.0 M aqueous urea solution,  $\text{CO}(\text{NH}_2)_2$ (aq), and solid urea,  $\text{CO}(\text{NH}_2)_2$ (s). Patterned and shaded columns denote aqueous and solid products, respectively. Floating columns indicate the  $\bar{E}_{\min}$  ranges that correspond to the typical span of nutrient content, product co-species concentrations, and pH reported for the waste streams. The recovery yield is 0 for all products, i.e., an infinitesimally minute amount of nutrient is recovered from the waste stream.

The recovery of urea products from fresh urine is less energy demanding than the recovery of nitrate products from secondary wastewater effluent. This is attributed to urea being over 100-fold more concentrated in fresh urine than nitrate and the product co-species ( $\text{NH}_4^+$  and  $\text{K}^+$ ) are in 2° WW effluent. As discussed previously,  $\bar{E}_{\min}$  is lower when capturing products from a more concentrated waste stream. For the aqueous products,  $\bar{E}_{\min}$  is lowest for  $\text{CO}(\text{NH}_2)_2$ (aq) followed by  $\text{NH}_4\text{NO}_3$ (aq), then  $\text{KNO}_3$ (aq). For solid products,  $\text{NH}_4\text{NO}_3$ (s) recovery from secondary wastewater effluent has the highest  $\bar{E}_{\min}$ . This is because the Gibbs free energy required to form solid  $\text{NH}_4\text{NO}_3$

from the initial species of aqueous  $\text{NH}_4^+$  and  $\text{NO}_3^-$  in the feed is greater than for  $\text{CO}(\text{NH}_2)_2(\text{s})$  and  $\text{KNO}_3(\text{s})$  (Table A.10). Generally, the recovery of 1.0 M aqueous products are thermodynamically more favorable than pure solids. This can be intuitively understood: producing solids requires the separation of all the water from the minerals, whereas less water needs to be removed to yield aqueous solutions. Furthermore, ordering free ions in aqueous solution into a solid crystal lattice incurs an additional entropic energy penalty, which further raises  $\bar{E}_{\text{min}}$ . However, there can be exceptions to the rule. Specific scenarios of pH-dependent speciation in the feed and Gibbs free energy of formation of the solid product can yield opposite trends. An example of such a deviation is the higher  $\bar{E}_{\text{min}}$  for the recovery of 1.0 M  $\text{NH}_3(\text{aq})$  than for  $\text{NH}_4\text{SO}_4(\text{s})$  (Figure 2.3).

The  $\bar{E}_{\text{min}}$  values to reclaim aqueous nitrate products, 1.0 M  $\text{KNO}_3(\text{aq})$  and 1.0 M  $\text{NH}_4\text{NO}_3(\text{aq})$ , from 2° WW effluent are less than 1.0 M  $\text{NH}_3(\text{aq})$  recovery from hydrolyzed urine, which is the lowest  $\bar{E}_{\text{min}}$  for aqueous TAN recovery in Figure 2.3.  $\bar{E}_{\text{min}}$  values to recover solid nitrate products,  $\text{KNO}_3(\text{s})$  and  $\text{NH}_4\text{NO}_3(\text{s})$ , from 2° WW effluent are also comparable to or lower than recovery of TAN product  $(\text{NH}_4)_2\text{SO}_4(\text{s})$  from all waste streams other than fresh and hydrolyzed urine. These comparisons suggest that, in principle, recovering nitrate from 2° WW effluent may be an equally or more favorable alternative to TAN recovery. However, the Gibbs free energy to reduce nitrate to the bio-preferred form of N—ammonia,  $\text{NH}_3$ —is 591 kJ/mol.<sup>6</sup> The additional energy requirement to reduce the oxidation state of N from +5 to -3 (8 electrons) is an order of magnitude higher than  $\bar{E}_{\text{min}}$  for TAN recovery. The better suitability of  $\text{NH}_3$  as a fertilizer and the huge energy cost to convert nitrate to ammonia, thus, indicate that targeting TAN over  $\text{NO}_3^-$  would be more prudent for nutrient recovery.  $\bar{E}_{\text{min}}$  values to capture urea as aqueous and solid products from fresh urine are significantly lower than the different TAN product and waste stream pairing

examined here. Specific pros and cons of different nitrogen fertilizers aside,<sup>120-122</sup> the theoretically less energy-intensive path provides impetus to pursue the realization of urea recovery from fresh urine.

**Presence of Other Species in Wastewater Matrix Marginally Increases Energy Demand for Nutrient Recovery.** Analyses presented earlier consider the feed streams as simplified solutions containing only species required for the product (i.e., nutrients and co-species), in addition to H<sub>2</sub>O, OH<sup>-</sup>, and H<sup>+</sup>. However, actual waste streams are complex water matrices with many other solutes, including different ions and neutral compounds. Na<sup>+</sup> and Cl<sup>-</sup> are two prominent ionic species universally present in all the examined waste streams (e.g., NaCl concentrations in secondary wastewater effluent and hydrolyzed urine are 1.41–17.4 and 64.9–119 mM, respectively). The purity of the product and the presence of undesired species, such as Na<sup>+</sup> and Cl<sup>-</sup>, are important metrics for fertilizer products. To quantify the influence of species passive to the nutrient recoveries, such as NaCl,  $\bar{E}_{\min}$  values are evaluated for the capture of NH<sub>3(l)</sub> and 1.0 M NH<sub>3(aq)</sub> from secondary wastewater effluent and hydrolyzed urine using eqns (A.6) and (A.7) (with 0 mM NaCl) and eqns (A.19) and (A.20) (with 9.40 and 88.9 mM NaCl in the feeds, respectively). Note that the recovered products do not contain the passive species NaCl. In this analysis, mid-range TAN content, NaCl concentration, and pH of the waste streams were utilized. Detailed results are presented in Table A.11 in Appendix A.

The inclusion of passive species in the determination of  $\bar{E}_{\min}$  results in only miniscule added energy requirements of 0.10–1.89% across the investigated scenarios. When NaCl in the waste stream is considered,  $\bar{E}_{\min}$  is marginally higher due to the additional energy to separate TAN from Na<sup>+</sup> and Cl<sup>-</sup>, in addition to H<sub>2</sub>O. However, because NaCl is present at substantially lower

concentrations compared to H<sub>2</sub>O at ≈55 mol/L (i.e., the waste streams are >99% water, even for the most saline feeds), this increase is minimal. Therefore, the ubiquitous presence of passive species in the waste streams has a negligible impact on the theoretical energy to recover N and P nutrients.

**Energy Intensity of N and P Recovery from Waste Streams can be Competitive with Conventional Nutrient Production.** The energy demand discussed so far is the theoretical minimum, but in practical nutrient recovery processes, the actual energy required to capture N and P will be higher than  $\bar{E}_{\min}$  due to inevitable inefficiencies of the recovery techniques. This analysis examines the practical molar energy of recovery,  $\bar{E}_{\text{prac}}$ , defined as the energy required to recover a mole of nutrient using a putative practical process with an assumed efficiency of  $\eta$ , i.e.,  $\bar{E}_{\text{prac}} = \bar{E}_{\min} / \eta$ . Figures 2.7A and B present  $\bar{E}_{\text{prac}}$  as a function of  $\eta$  for harvesting TAN and TOP products, respectively, from different waste streams. For each nutrient, two products  $\bar{E}_{\min}$  were selected to illustrate a range of energy demand, namely pure liquid ammonia and 1.0 M aqueous ammonia solution for N and solid precipitates of potassium magnesium phosphate and potassium phosphate for P. For the waste streams, a centralized source of secondary wastewater effluent and a decentralized source of either hydrolyzed urine or diverted fresh urine for N and P, respectively, were selected for quantitative comparisons. Mid-range  $\bar{E}_{\min}$  values from Figure 2.3 were used and recovery yield  $Y \rightarrow 0$ , i.e., an infinitesimally small amount of nutrient is reclaimed from the waste stream. The ranges of energy costs for conventional linear economy approaches to nutrient production, i.e., Haber-Bosch for N-fixation<sup>4-6</sup> and mining and beneficiation for phosphate,<sup>8, 123</sup> are also depicted as shaded green regions.

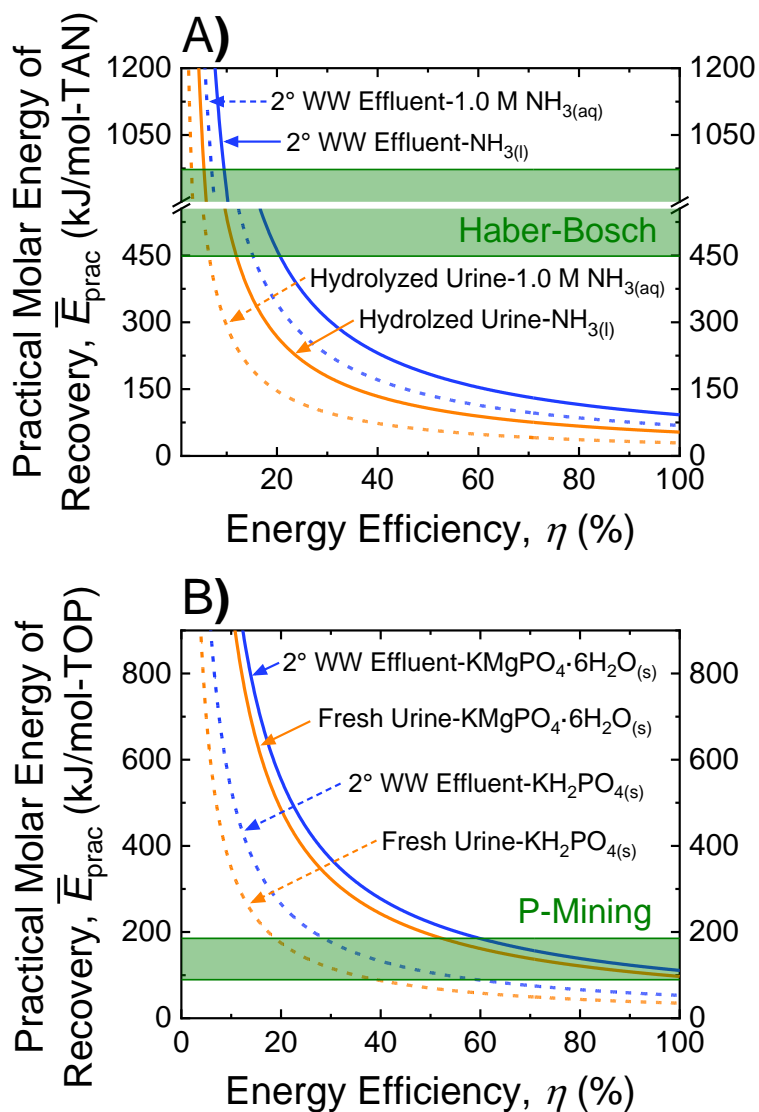


**Figure 2.7.** Practical molar energy,  $\bar{E}_{\text{prac}}$  as a function of efficiency,  $\eta$ , for an actual process to recover A) TAN from hydrolyzed urine and secondary wastewater effluent as 1.0 M  $\text{NH}_3(\text{aq})$  and  $\text{NH}_3(\text{l})$  and B) TOP from fresh urine and secondary wastewater effluent as  $\text{KMgPO}_4 \cdot 6\text{H}_2\text{O}(\text{s})$  and  $\text{KH}_2\text{PO}_4(\text{s})$ . Mid-range  $\bar{E}_{\text{min}}$  values were used and  $Y \rightarrow 0$ , i.e., an infinitesimally small amount of nutrient is recovered from the waste stream, for all scenarios. Note that  $\bar{E}_{\text{prac}}$  at  $\eta = 100\%$  is equivalent to  $\bar{E}_{\text{min}}$ . For comparison, the range of energy costs required for N-fixation by the Haber-Bosch process (448–973 kJ/mol-N)<sup>4-6</sup> and phosphate rock mining and beneficiation (89–185 kJ/mol-P)<sup>8, 123</sup> are shown as shaded green areas in A and B, respectively.

The high energy intensity of nitrogen fixation by the Haber-Bosch process and the relatively low  $\bar{E}_{\min}$  signify that TAN recovery from the different waste streams can be competitive across a large range of process efficiencies (lines below green shaded region of Figure 2.7A). Harvesting TAN as 1.0 M  $\text{NH}_{3(\text{aq})}$  from hydrolyzed urine requires  $\eta$  as low as  $\approx 7\%$  (dashed orange line, Figure 2.7A). Even the more energy demanding recovery of  $\text{NH}_{3(\text{l})}$  from secondary wastewater effluent can be competitive with separation techniques of efficiencies  $>25\%$  (solid blue line). As comparisons, the energy efficiencies of reverse osmosis desalination and liquid-liquid extraction are around 25% (for 10-fold concentration, approximately equivalent to recovery yield of 0.9).<sup>124</sup> We note that the  $\bar{E}_{\min}$  values utilized for this analysis are for  $Y \rightarrow 0$ . Even for practical recovery yields  $\gg 0$ , the elevation of  $\bar{E}_{\min}$  is only marginal at most, as previously discussed (Figures 2.2 and 2.5), and, hence, the increase in required energy efficiencies of the actual processes are expected to be modest.

In contrast, the substantially lower energy cost of conventional P production significantly constrains the energy efficiencies for recovery techniques to be competitive.  $\text{KH}_2\text{PO}_{4(\text{s})}$  recovery from fresh urine and 2° WW effluent need  $\eta$  greater than 39% and 59%, respectively, to have lower energy requirements than current phosphate mining and beneficiation (dashed orange and blue lines, Figure 2.7B). However, for  $\text{KMgPO}_4 \cdot 6\text{H}_2\text{O}_{(\text{s})}$  recovery, the energy requirement can, at best, be comparable with the conventional approach for P production, even with highly efficiency methods of  $\eta > 60\%$  (solid orange and blue lines). Therefore, the strategic selection of waste stream and nutrient product are imperative to maximize the chances of success for competitive phosphate recovery.

## 2.4 Implications

A circular economy espouses cyclical material flows.<sup>125</sup> The approach, hence, promotes the recovery of nutrients from discard streams for reuse, to lower industrial N production and P mining from the current unsustainable levels, and concomitantly protect aquatic environments from harmful N and P emissions. To realize viable implementation, the methods for nutrient recovery from waste streams must be competitive with existing practices across key metrics, including energy requirements. This study analyzed the thermodynamics of the separations to identify the minimum energy requirements for various nutrient recovery schemes employing different waste streams as the feed, targeting diverse fertilizer products, and achieving a range of recovery yields. The analysis quantified lower theoretical energy intensities of N and P recovery from nutrient-rich sources, such as diverted fresh and hydrolyzed urine, and indicates that waste stream pH and speciation of components are important factors affecting the separation that need to be considered in the product selection and design of actual nutrient recovery processes. The analytical approach for thermodynamic evaluation presented here can inform the strategic selection of waste stream, fertilizer product, and recovery yield, to enhance the competitiveness of nutrient recovery on the energy-intensity metric. The results and/or approach for determination of energetic constraints can be employed in nutrient recovery life-cycle assessments, which consider other constraints, such as capital and infrastructure costs and practical constraints.

The study also sheds light on the potential practical energy requirements of actual nutrient recovery using technologies with various efficiencies. Importantly, the separation processes need to operate above certain efficiencies for energy demand of N and P recovery to be lower than the conventional linear economy production methods, i.e., Haber-Bosch for N fixation and phosphate rock mining. For instance, ammoniacal nitrogen recovery from hydrolyzed urine, generally the

least energy-intensive TAN reclamation among the scenarios investigated here, only requires efficiency >7%. The use of urine as the feed source has additional benefits of reduced pathogen and heavy metal concentrations compared to other waste streams.<sup>44, 126, 127</sup> Further, urine contains approximately 80% and 50% of the N and P in human excretions, respectively.<sup>44, 127</sup> Thus, N and P recovery from urine can enable significant reductions in nutrient loading to WWTPs and, ultimately, aquatic environments. Compared to nitrogen recycling, phosphorous reuse is more challenging. Because concentrations in the waste streams are inherently lower and typical fertilizer products are pure solid minerals, the theoretical minimum energy of phosphate recovery is significantly greater. The relatively smaller energy cost of current P mining practices further compounds to the difficulty of the task, necessitating recovery processes to have higher efficiencies in order to be competitive. Technologies with energy efficiencies >39% are needed even for the least demanding orthophosphate separation and capture from fresh urine. However, with phosphate reserves unceasingly depleting and high-grade ores rapidly exhausted, energy expenditures for mining are expected to surge.<sup>10, 128</sup> Furthermore, nutrient recovery has the additional benefit of environmental protection. Therefore, P recovery from waste streams will likely become increasingly attractive compared to the conventional linear economy approach. Nevertheless, the development of more energy efficient technologies will enhance the accessibility of nutrient recovery from waste streams.

To put in perspective the benefits of a circular economy approach for nutrient management over the existing linear economy model, we performed a first-order estimation of the potential energy savings achievable through supplementing current fertilizer production with nutrient recovery from waste streams. In 2017, the International Fertilizer Association estimated global nutrient demands of  $7,930 \times 10^9$  mol-N and  $148 \times 10^9$  mol-P.<sup>129</sup> Given the respective concentrations

of N and P in hydrolyzed and fresh urine, the world population of 7.6 billion in 2017,<sup>130</sup> and 1–2 L/d of urine produced per person, around  $748\text{--}3,208 \times 10^9$  mol-N and  $54\text{--}267 \times 10^9$  mol-P were excreted in urine annually. Therefore, in principle, 9–40% and 36–180% of the N and P fertilizer markets, respectively, could be supplemented by TAN and TOP reclaimed from urine. The recovery of half of the available TAN in hydrolyzed urine as 1.0 M  $\text{NH}_{3(\text{aq})}$  using techniques achieving 50% efficiency can notionally reduce the global energy demand for industrial N production by 4.6–20.0%. Similarly, using recovery technologies that are 50% efficient to capture half of the TOP in fresh urine as  $\text{KH}_2\text{PO}_{4(\text{s})}$  can presumably reduce the energy required to produce P fertilizer by 4.0–15.9%. The sizable energy savings and significant environmental benefits of capturing N and P from waste streams, particularly urine, for reuse provide compelling justification for the broad implementation of nutrient recovery.

# Chapter 3: Donnan Dialysis for Phosphate Recovery from Diverted Urine

## Chapter Abstract

There is a critical need to shift from existing linear phosphorous management practices to a more sustainable circular P economy. Closing the nutrient loop can reduce our reliance on phosphate mining, which has well-documented environmental impacts, while simultaneously alleviating P pollution of aquatic environments from wastewater discharges that are not completely treated. The high orthophosphate,  $H_xPO_4^{(3-x)-}$ , content in source-separated urine offers propitious opportunities for P recovery. This study examines the use of Donnan dialysis (DD), an ion-exchange membrane-based process, for the recovery of orthophosphates from fresh and hydrolyzed urine matrixes.  $H_2PO_4^-$  transport against an orthophosphate concentration gradient was demonstrated and orthophosphate recovery yields up to 93% were achieved. By adopting higher feed to receiver volume ratios, DD enriched orthophosphate in the product stream as high as  $\approx 2.5\times$  the initial urine feed concentration. However, flux, selectivity, and yield of orthophosphate recovery were detrimentally impacted by the presence of  $SO_4^{2-}$  and  $Cl^-$  in fresh urine, and the large amount of  $HCO_3^-$  rendered hydrolyzed urine practically unsuitable for P recovery using DD. The detrimental effects of sulfate ions can be mitigated by utilizing a monovalent ion permselective membrane, improving selectivity for  $H_2PO_4^-$  transport over  $SO_4^{2-}$  by  $3.1\times$  relative to DD with a conventional membrane; but the enhancement was at the expense of reduced orthophosphate flux. Critically, widely available and low-cost/waste resources with sufficiently high  $Cl^-$  content, such as seawater and waste water softening regenerant rinse, can be employed to improve the economic viability of orthophosphate recovery. This study shows the promising potential of DD for P recovery and enrichment from source-separated urine.

### 3.1 Introduction

For the reasons presented in Chapter 1, the biogeochemical flow of phosphate is flagged as exceeding the safe operating space for humanity and poses high risks under the planetary boundaries framework.<sup>24</sup> The current approach for P management has clear shortcomings and a new paradigm that is more sustainable is urgently needed.<sup>131-133</sup> Orthophosphate,  $H_xPO_4^{(3-x)-}$ , can be simultaneously removed and recovered from anthropogenic wastewaters within a circular economy model, specifically, phosphorous is captured from wastewater and recycled back into the food chain.<sup>62-65, 74</sup> Closing the nutrient loop can ease the demand for phosphate mining to strengthen food security and alleviate P pollution of aquatic environments, thereby representing a transformative evolution to a more sustainable approach for phosphorous management.

As presented in Chapter 2, the theoretical minimum energy for P recovery, governed by thermodynamic principles, is substantially lower for the feed of source-separated urine (i.e., the liquid is diverted away from black water and isolated) compared with other wastewaters.<sup>134</sup> For instance, recovery of orthophosphate from urine is  $\approx 13-34\%$  less energy-intensive than treated wastewater effluent.<sup>134</sup> This is because urine is rich in P (total orthophosphate, TOP =  $19-48 \times 10^{-3}$  mol/L),<sup>44, 89, 92, 96</sup> whereas treated wastewater effluent is over 1–2 orders of magnitude more dilute. There has been considerable efforts to study the recovery of orthophosphates from urine and significant strides have been made, with the primary approach being mineral precipitation of slow-release fertilizers, such as struvite and magnesium potassium phosphate.<sup>67, 68, 72, 89, 90, 114, 115, 135</sup> However, the technique has potential risks for contamination by pharmaceuticals, endocrine disrupting compounds, and pathogens.<sup>136-141</sup> Alternatively, sorbents, e.g., metal (oxy)hydroxide,<sup>53-57</sup> can be used to separate orthophosphate from other constituents in urine. But sorbent regeneration

is chemically costly and the technique is further disadvantaged by the unavoidable generation of waste brines that cannot be easily disposed.<sup>58</sup>

Ion exchange membrane (IEM) processes offer viable options for orthophosphate separation from urine without being encumbered by the above limitations. Donnan dialysis (DD) using IEMs has demonstrated promising potential for orthophosphate separation from other wastewaters besides urine, achieving high recovery yields (up to 98.4%).<sup>142-144</sup> However, the previous studies examined orthophosphate recovery from solutions containing only orthophosphate anions, i.e., no other co-ions are included in the water chemistry.<sup>142-144</sup> Actual waste streams, including urine, are complex water matrices with many anions, cations, and uncharged species. In particular, the ionic composition of urine is uniquely different from, say, raw sewage or treated secondary effluent, with significantly greater amounts of  $\text{SO}_4^{2-}$ ,  $\text{Cl}^-$ , and  $\text{HCO}_3^-$ . Based on the general understanding of Donnan equilibrium theory, the presence of other anions in addition to orthophosphate is expected to have non-negligible and potentially detrimental effects on the process. In a past DD study, the presence of co-ions was shown to have deleterious impacts on arsenate removal from groundwater,<sup>145</sup> underscoring the need to better understand these effects to enable P recovery from urine using DD.

In this study, the performance of Donnan dialysis to drive the separation and recovery of orthophosphate from diverted human urine is assessed. First, the working principles of anion exchange membranes and Donnan dialysis are introduced. The exchange of  $\text{H}_2\text{PO}_4^-$  and  $\text{Cl}^-$  across an anion-exchange membrane is then examined with DD experiments driven by the ion concentration gradients between an orthophosphate feed solution and a receiver solution of high chloride content. Next, the impact of receiver solution chloride concentration on P recovery is analyzed using simulated streams of brackish water, seawater, and desalination brine. The

capability of DD to enrich orthophosphate in the receiver solution above the initial urine feed concentration is evaluated by adopting higher feed to receiver volume ratios. Then, the influence of other anions in urine on orthophosphate flux and recovery yield is studied, specifically,  $\text{SO}_4^{2-}$  and  $\text{Cl}^-$  in fresh urine, and  $\text{SO}_4^{2-}$ ,  $\text{Cl}^-$ , and  $\text{HCO}_3^-$  in hydrolyzed urine. Enhancements in selectivity for orthophosphate transport over other anions using a monovalent ion permselective membrane are assessed and the potential of DD to harvest fertilizer products of aqueous orthophosphate solutions is investigated. Finally, implications of Donnan dialysis for P separation and recovery from urine are discussed.

### 3.2 Working Principles of Donnan Dialysis

**Ion Exchange in Donnan Dialysis.** In Donnan dialysis, DD, flux of driver ions down a concentration gradient, across an ion-exchange membrane (IEM), sets up an electrochemical potential to drive the transport of target ions in the opposite direction.<sup>146-148</sup> IEMs are polymeric thin-films with a high density of charged functional groups to allow the selective permeation of oppositely-charged counterions, while retaining like-charged co-ions (cation and anion exchange membranes, CEMs and AEMs, are selective for cation and anion transport, respectively).<sup>149, 150</sup> The IEM separates the feed solution (FS) and receiver solution (RS). Driver counterions permeate from the higher concentration RS to the lower concentration FS. Because co-ions are rejected by the charge-selective membrane, target counterions in the FS migrate across the membrane in the opposite direction, into the RS, to preserve electroneutrality.<sup>142, 143, 146, 151-154</sup> I.e., the electrochemical potential gradient across the IEM drives the exchange of counterions between the FS and RS in DD, with co-ions retained in the initial solutions.<sup>146</sup> Note that the charge fluxes of driver and target ions must be equal to maintain electroneutrality. Importantly, an adequately large

driver ion concentration difference across the membrane can enable migration of target ions against a concentration gradient, to achieve “uphill” transport.<sup>148</sup>

In DD recovery of orthophosphates,  $\text{H}_x\text{PO}_4^{(3-x)-}$ , an AEM is employed to exchange  $\text{H}_x\text{PO}_4^{(3-x)-}$  target ions from the FS with driver anions in the RS.<sup>142-144</sup> Chloride is a suitable driver ion because  $\text{Cl}^-$  is present in high concentrations in low-cost or waste streams that are widely available, such as brackish water, seawater, desalination brine, and waste effluent from water softening regeneration. Critically,  $\text{Cl}^-$  concentrations in these streams are significantly higher than in urine ( $>200 \times 10^{-3}$  mol/L, compared to  $\approx 100 \times 10^{-3}$  mol/L), to establish a sufficiently large electrochemical potential gradient across the AEM for uphill transport of  $\text{H}_x\text{PO}_4^{(3-x)-}$ . Therefore, this study will investigate DD recovery of orthophosphates using chloride as the RS driver counterion. Figure 3.1 depicts the DD separation of orthophosphates from other constituents in urine feed solution and capture in the chloride-rich receiver solution:  $\text{H}_x\text{PO}_4^{(3-x)-}$  in the FS exchanges with  $\text{Cl}^-$  in the RS across the AEM, while cations,  $\text{M}^+$ , are rejected by the charge-selective membrane. Note that one  $\text{H}_x\text{PO}_4^{(3-x)-}$  ion exchanges with  $(3-x)$   $\text{Cl}^-$  ion(s) to maintain electroneutrality and that the ions moving across the membrane are hydrated.

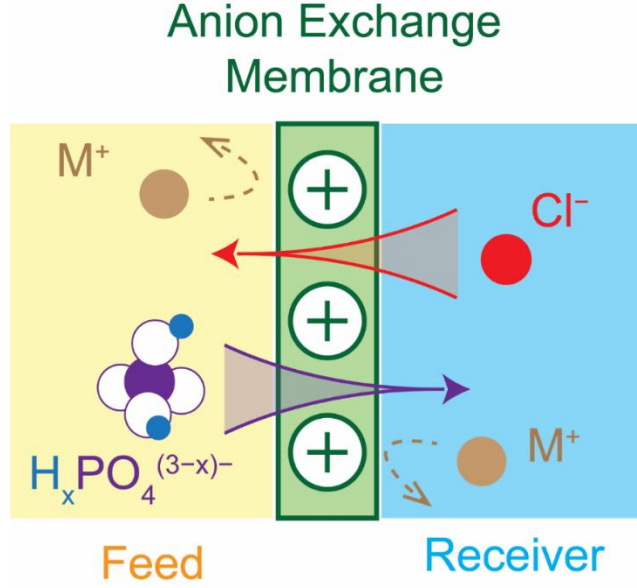


**Figure 3.1.** Schematic depicting Donnan dialysis recovery of orthophosphates. Exchange of counterions (anions) across an anion exchange membrane (AEM) is driven by an electrochemical potential gradient across the membrane, while co-ions (cations,  $M^+$ ) are rejected by the charge-selective membrane and retained in initial solutions. Driver ions,  $Cl^-$ , transport down a concentration gradient from the high concentration RS to low concentration FS. The positively-charged AEM excludes  $M^+$  cations. Therefore, to maintain electroneutrality, target ions,  $H_xPO_4^{(3-x)-}$ , transport in the opposite direction, i.e., from FS to RS. The charge fluxes of driver and target ions must be equal to maintain electroneutrality, i.e.,  $H_xPO_4^{(3-x)-}$  exchanges with  $(3-x) Cl^-$  ions.

**Orthophosphate Recovery at Donnan Equilibrium.** Target and driver counterions in the FS and RS exchange until Donnan equilibrium is reached, i.e., electrochemical potential gradient across the membrane = 0. For the system with  $H_xPO_4^{(3-x)-}$  and  $Cl^-$  as target and driver ions, respectively, concentrations in the FS and RS at Donnan equilibrium are governed by (3.**Error! Reference source not found.**), derivation is detailed in eqs (B.1)–(B.4) of Appendix B:

$$\frac{[H_xPO_4^{(3-x)-}]_{FS,f}}{[H_xPO_4^{(3-x)-}]_{RS,f}} = \left( \frac{[Cl^-]_{FS,f}}{[Cl^-]_{RS,f}} \right)^{(3-x)} \quad (3.1)$$

where subscripts FS and RS denote feed and receiver solutions, respectively, and  $f$  signifies final equilibrium. Note that eqn (3.1) assumes perfect cation rejection and negligible water transport across the AEM.

To determine final target and driver ion concentrations at Donnan equilibrium using known initial concentrations, the principles of electroneutrality and material balances can be applied and are represented by eqns (B.5–B.8) of Appendix B. For equivalent FS and RS volumes (i.e.,  $V_{FS} = V_{RS}$ ),  $H_xPO_4^{(3-x)-}$  as the sole initial anion in the FS, and  $Cl^-$  as the sole initial anion in the RS, eqn (3.2) describes the relationship between initial concentrations and final concentrations at Donnan equilibrium:

$$\frac{[H_xPO_4^{(3-x)-}]_{FS,0} - [H_xPO_4^{(3-x)-}]_{RS,f}}{[H_xPO_4^{(3-x)-}]_{RS,f}} = \left( \frac{(3-x)[H_xPO_4^{(3-x)-}]_{RS,f}}{[Cl^-]_{RS,0} - (3-x)[H_xPO_4^{(3-x)-}]_{RS,f}} \right)^{(3-x)} \quad (3.2)$$

$[H_xPO_4^{(3-x)-}]_{RS,f}$  can be determined using initial concentrations  $[H_xPO_4^{(3-x)-}]_{RS,0}$  and  $[Cl^-]_{FS,0}$ . The moles of orthophosphate recovered is the product of concentration and volume of the final RS solution,  $[H_xPO_4^{(3-x)-}]_{RS,f}V_{RS}$ . Eqns (B.9)–(B.17) of Appendix B are the Donnan equilibrium expressions for systems with different initial conditions, specifically multiple anions in the FS ( $H_xPO_4^{(3-x)-}$ ,  $SO_4^{2-}$ , and  $Cl^-$ ) and non-equivolume scenarios ( $V_{FS} \neq V_{RS}$ ).

### 3.3 Materials and Methods

**Materials and Chemicals.** Commercial anion exchange membranes of Selemion AMV and Selemion ASVN, a monovalent ion-selective AEM, were procured from Asahi Glass Co. (Japan); membrane specifications provided in Table B5 of Appendix B. Four DD cells with different chamber volumes were fabricated using Mars Pro MSLA 3D Printer acquired from Elegoo (China). The feed and receiver chamber volumes, respectively, are: 20 and 20 mL; 40 and 20 mL;

80 and 20 mL; and 40 and 40 mL, for feed to receiver solution volume ratios of 1:1, 2:1, 4:1, and 2:2, respectively. The effective membrane areas in all cells are 9.0 cm<sup>2</sup>. Na<sub>2</sub>HPO<sub>4</sub>·7H<sub>2</sub>O, Na<sub>3</sub>PO<sub>4</sub>·12H<sub>2</sub>O, NaCl, MgCl<sub>2</sub>·6H<sub>2</sub>O, MgSO<sub>4</sub>·7H<sub>2</sub>O, and NH<sub>4</sub>Cl salts were obtained from Alfa Aesar (Ward Hill, MA). KCl salt, 85% H<sub>3</sub>PO<sub>4</sub> solution, and 2.5 M H<sub>2</sub>SO<sub>4</sub> were acquired from Lab Chem (Zelienople, PA), Fisher Scientific (Waltham, MA), and Titripur (St. Louis, MO), respectively. All chemicals are ACS grade and were used as received. All solutions were prepared using deionized (DI) water from a Milli-Q ultrapure water purification system (Millipore Co., Burlington, MA).

**Orthophosphate and Chloride Exchange in Donnan Dialysis.** To demonstrate the exchange of H<sub>2</sub>PO<sub>4</sub><sup>-</sup> in a feed solution, FS, with Cl<sup>-</sup> in a receiver solution, RS, DD experiments were conducted with 30×10<sup>-3</sup> mol/L H<sub>2</sub>PO<sub>4</sub><sup>-</sup> initial FS (16.5×10<sup>-3</sup> mol/L Na<sub>2</sub>HPO<sub>4</sub>·7H<sub>2</sub>O and 13.5×10<sup>-3</sup> mol/L H<sub>3</sub>PO<sub>4</sub>; pH = 6.0) and 600×10<sup>-3</sup> mol/L Cl<sup>-</sup> (as NaCl) initial RS. The 20:20 mL cell was utilized. H<sub>2</sub>PO<sub>4</sub><sup>-</sup> concentrations in the FS and RS and Cl<sup>-</sup> concentrations in the RS were measured at 1.0 h intervals for 6.0 h. 175 µL samples were collected from each solution and the anion concentrations were analyzed using ion chromatography, IC (Dionex Aquion, Thermo Fisher Scientific, Waltham, MA).

**Characterization of Orthophosphate Recovery at Donnan Equilibrium.** Orthophosphate, sulfate, and bicarbonate transport from FS to RS and chloride transport from RS to FS were evaluated in different DD operations. Three FS were utilized in orthophosphate recovery experiments: i. feed solution with the total orthophosphate, TOP, concentration and pH of fresh urine,<sup>44, 89, 92, 96</sup> but without other anions (16.5×10<sup>-3</sup> mol/L Na<sub>2</sub>HPO<sub>4</sub>·7H<sub>2</sub>O and 13.5×10<sup>-3</sup> mol/L H<sub>3</sub>PO<sub>4</sub>; pH = 6.0), ii. simulated fresh urine with the TOP, sulfate, and chloride concentrations, and pH of actual fresh urine<sup>44, 89, 92, 96</sup> (24×10<sup>-3</sup> mol/L Na<sub>2</sub>HPO<sub>4</sub>·7H<sub>2</sub>O, 6×10<sup>-3</sup>

mol/L  $\text{Na}_3\text{PO}_4 \cdot 12\text{H}_2\text{O}$ ,  $100 \times 10^{-3}$  mol/L NaCl, and  $16 \times 10^{-3}$  mol/L  $\text{H}_2\text{SO}_4$ ), and iii. simulated hydrolyzed urine with the TOP, sulfate, chloride, and bicarbonate concentrations, and pH of actual hydrolyzed urine<sup>89, 96</sup> ( $30 \times 10^{-3}$  mol/L  $\text{Na}_2\text{HPO}_4 \cdot 7\text{H}_2\text{O}$ ,  $100 \times 10^{-3}$  mol/L NaCl,  $144 \times 10^{-3}$  mol/L  $\text{Na}_2\text{CO}_3$ , and  $106 \times 10^{-3}$  mol/L  $\text{NaHCO}_3$ ), as presented in Table 3.1. Note that hydrolyzed urine is formed when urea,  $\text{CO}(\text{NH}_2)_2$ , in urine hydrolyses to form ammoniacal nitrogen and bicarbonate, which in turn increases the pH from  $\approx 6.0$  to  $\approx 9.2$ .<sup>89, 90</sup> Three receiver solutions with NaCl concentrations of  $200 \times 10^{-3}$  mol/L,  $600 \times 10^{-3}$  mol/L, and  $1,000 \times 10^{-3}$  mol/L were utilized to simulate brackish water, seawater, and seawater desalination brine, respectively. DD cells with feed chamber volumes of 20, 40, and 80 mL were employed for orthophosphate recovery experiments with different feed to receiver solution volume ratios. In summary, FS anion composition and RS  $\text{Cl}^-$  concentration were the parameters assessed in different FS to RS volume ratios. Unless stated otherwise, AMV membranes were used in the experiments. Pressure and temperature were at ambient conditions in all experiments.

**Table 3.1.** Anion compositions and pHs of feed solution containing only orthophosphate, simulated fresh urine, and simulated hydrolyzed urine.

Simulated Feed Solution	Ion Concentration ( $\times 10^{-3}$ mol/L)				pH
	$[\text{H}_x\text{PO}_4^{(3-x)-}]$	$[\text{SO}_4^{2-}]$	$[\text{Cl}^-]$	$[\text{HCO}_3^-]$	
TOP-only	30	0	0	0	6.0
Fresh urine	30	16	100	0	6.0
Hydrolyzed urine	30	16	100	250	9.2

Total orthophosphate, sulfate, and bicarbonate concentrations in the FS and RS, and chloride concentration in the FS were sampled and analyzed using ion chromatography. The measurement intervals were 12, 24, or 48 h for experiments with FS to RS volume ratios of 1, 2, and 4, respectively, with longer time allotted for experiments with higher ratios to approach equilibrium. The experiments were considered to have effectively equilibrated when the moles of exchanged orthophosphate ions remained consistent over three consecutive measurements ( $< 5\%$

change). Note that the sampling times are relatively long because the solution volumes are large compared to the effective membrane area. Additionally, the equilibration is asymptotic and, hence, the ions exchange rates slow significantly as the process approaches equilibrium. Water transport was assessed by measuring feed and receiver solution volumes at the end of each experiment. Recovery yield,  $Y$ , is defined as the moles of TOP in the final RS normalized by the moles in the initial FS.

**Evaluation of Anion Transport Kinetics.** Anion fluxes from FS to RS were examined in DD kinetic experiments, i.e., final Donnan equilibria were not reached in the tests. Fluxes were determined from the rate of change of anion concentrations in the RS over 2.0 and 8.0 h for the AMV and ASVN membranes, respectively (the ASVN experiments required more time because anion fluxes are relatively lower). Water transport across the AEMs during the kinetic experiments was not observed and deemed to be practically negligible. The change in moles of anion in the RS over time normalized by the membrane area yields flux,  $J_i$ . Flux selectivity,  $J_i/J_T$ , is defined as  $J_i$  normalized by the sum of all anion fluxes from feed to receiver solution.

Anion fluxes and flux selectivities were assessed for the AMV membrane using  $600 \times 10^{-3}$  mol/L NaCl RS with the three FS of TOP-only solution, simulated fresh urine, and simulated hydrolyzed urine.  $J_i$  and  $J_i/J_T$  were determined for the ASVN membrane using simulated fresh and hydrolyzed urine as FS and RS of  $600 \times 10^{-3}$  mol/L NaCl. To demonstrate the potential of DD to recover orthophosphate and yield aqueous products, experiments were conducted using the ASVN membrane, simulated fresh urine as FS, and four different RS. The RS investigated are: i.  $600 \times 10^{-3}$  mol/L NaCl, ii.  $600 \times 10^{-3}$  mol/L KCl to simulate aqueous potash fertilizer, iii. waste water softening regenerant rinse, WWSRR ( $547 \times 10^{-3}$  mol/L KCl and  $48 \times 10^{-3}$  mol/L  $\text{MgCl}_2 \cdot 6\text{H}_2\text{O}$ ), iv. and simulated diluted bittern, DB ( $252 \times 10^{-3}$  mol/L  $\text{MgCl}_2 \cdot 6\text{H}_2\text{O}$ ,  $77 \times 10^{-3}$  mol/L KCl,  $25 \times 10^{-3}$

mol/L  $\text{MgSO}_4 \cdot 7\text{H}_2\text{O}$ ,  $26 \times 10^{-3}$  mol/L NaCl, and  $8 \times 10^{-3}$  mol/L  $\text{NH}_4\text{Cl}$ ). Further information on the composition of WSRW and DB can be found in Appendix B.

### 3.4 Results and Discussion

**Chloride Driver Ion Concentration Gradient Drives Transport of Orthophosphate Across the Anion Exchange Membrane.** Donnan dialysis experiments were conducted using an initial FS of  $30 \times 10^{-3}$  mol/L  $\text{H}_2\text{PO}_4^-$  and RS of  $600 \times 10^{-3}$  mol/L  $\text{Cl}^-$ . Note that the FS simulates the pH and  $[\text{H}_2\text{PO}_4^-]$  of fresh urine, with  $\text{H}_2\text{PO}_4^-$  being the predominant form of orthophosphate species at pH = 6.0. The RS replicates  $[\text{Cl}^-]$  in seawater. Figure 3.2 shows  $[\text{H}_2\text{PO}_4^-]$  in the feed and receiver solutions, indicated by subscripts FS and RS, respectively (solid blue square and open blue circle symbols), and  $[\text{Cl}^-]$  in the FS (open gray square symbols) as a function of time during DD operation. Because of the large driver ion concentration difference across the membrane, i.e.,  $[\text{Cl}^-]_{\text{RS},0} - [\text{Cl}^-]_{\text{FS},0}$ ,  $\text{Cl}^-$  permeates from the RS to the lower concentration FS.  $\text{Na}^+$  cations are rejected by the AEM; thus, to maintain electroneutrality, one  $\text{H}_2\text{PO}_4^-$  ion from the FS exchanges with one  $\text{Cl}^-$  ion from the RS, as demonstrated by nearly equal  $[\text{H}_2\text{PO}_4^-]_{\text{RS}}$  and  $[\text{Cl}^-]_{\text{FS}}$  throughout the DD experiment ( $< 1.5 \times 10^{-3}$  mol/L difference). Further,  $[\text{H}_2\text{PO}_4^-]_{\text{FS}}$  decreases at the same rate as  $[\text{H}_2\text{PO}_4^-]_{\text{RS}}$  increases, specifically,  $[\text{H}_2\text{PO}_4^-]_{\text{FS}} + [\text{H}_2\text{PO}_4^-]_{\text{RS}}$  is within 5% of  $[\text{H}_2\text{PO}_4^-]_{\text{FS},0}$ . As more  $\text{H}_2\text{PO}_4^-$  and  $\text{Cl}^-$  ions are exchanged, the electrochemical potential gradient across the AEM decreases. The reduced driving force lessens the rate of anion exchange, i.e., slopes of the concentration profiles become less steep. Importantly, even after  $[\text{H}_2\text{PO}_4^-]_{\text{RS}}$  exceeds  $[\text{H}_2\text{PO}_4^-]_{\text{FS}}$  (at  $\approx 3$  h),  $\text{H}_2\text{PO}_4^-$  continues to be transported from the feed to receiver solution, achieving uphill transport of orthophosphates. Approximately 73% of  $\text{H}_2\text{PO}_4^-$  from the FS was recovered in the RS after 6 h of DD operation in batch mode.

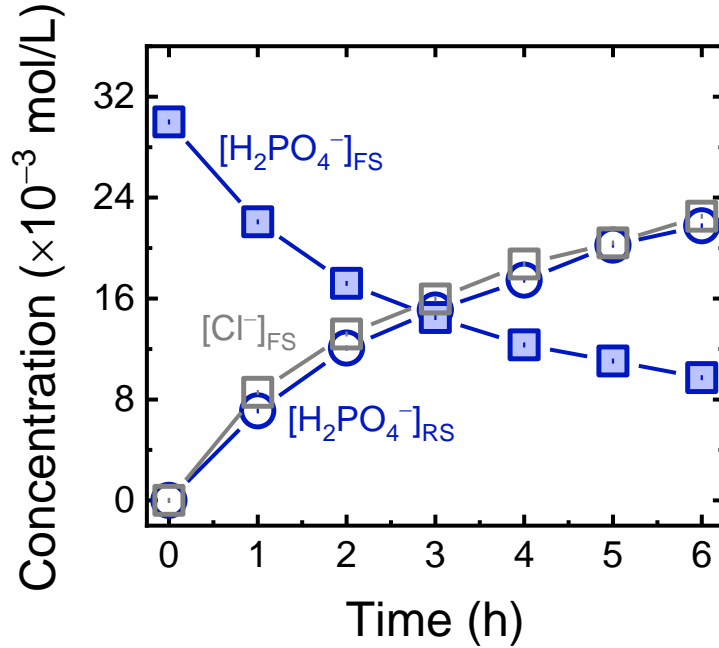


**Figure 3.2.** Concentrations of  $\text{H}_2\text{PO}_4^-$  and  $\text{Cl}^-$  in the FS (solid blue and open gray square symbols, respectively) and  $\text{H}_2\text{PO}_4^-$  concentration in the RS (open blue circles) as a function of time during DD orthophosphate recovery. Feed and receiver solution concentrations are denoted by subscripts FS and RS, respectively. The initial feed and receiver solutions consist of  $30 \times 10^{-3}$  mol/L  $\text{H}_2\text{PO}_4^-$  at pH = 6.0 ( $16.5 \times 10^{-3}$  mol/L  $\text{Na}_2\text{HPO}_4 \cdot 7\text{H}_2\text{O}$  and  $13.5 \times 10^{-3}$  mol/L  $\text{H}_3\text{PO}_4$ ) and  $600 \times 10^{-3}$  mol/L NaCl, respectively. Both feed and receiver solution volumes are 20 mL and effective AMV membrane area is  $9.0 \text{ cm}^2$ .

**Higher Receiver Solution Chloride Concentrations Increase Orthophosphate Recovery.** Donnan dialysis experiments were conducted using FS with  $30 \times 10^{-3}$  mol/L TOP, i.e., the  $\text{H}_x\text{PO}_4^{(3-x)-}$  concentration in fresh urine where  $\text{H}_2\text{PO}_4^-$  is the predominant orthophosphate species, and various initial  $[\text{Cl}^-]_{\text{RS}}$  to investigate the influence of chloride driver ion concentration on orthophosphate recovery. Receiver solutions of 200, 600, and  $1,000 \times 10^{-3}$  mol/L NaCl were utilized to simulate potential widely-available low-cost/waste streams of brackish water, seawater, and seawater desalination brine, respectively. Figure 3.2A presents experimental  $[\text{H}_x\text{PO}_4^{(3-x)-}]_{\text{RS},f}$  at the end of 72 h and predicted  $[\text{H}_x\text{PO}_4^{(3-x)-}]_{\text{RS},f}$  at Donnan equilibrium calculated using eqn (3.2) (patterned and empty blue columns, respectively). Labels above these columns denote percentage difference of experimental  $[\text{H}_x\text{PO}_4^{(3-x)-}]_{\text{RS},f}$  relative to the prediction at Donnan equilibrium.

Theoretical orthophosphates captured in the receiver solution at Donnan equilibrium increase with greater feed concentrations of driver chloride ions: predicted  $[\text{H}_x\text{PO}_4^{(3-x)-}]_{\text{RS},f}$  are 26.1, 28.6, and  $29.1 \times 10^{-3}$  mol/L for  $[\text{Cl}^-]_{\text{RS},0}$  of 200, 600, and  $1,000 \times 10^{-3}$  mol/L, respectively. The FS is constant across all operations. Therefore, higher  $[\text{Cl}^-]_{\text{RS},0}$  generates larger driver ion concentration gradients, i.e.,  $[\text{Cl}^-]_{\text{RS}} - [\text{Cl}^-]_{\text{FS}}$ , and results in increased driving forces for  $\text{Cl}^-$  permeation from the high concentration FS to the lower concentration RS. Correspondingly, there is a greater exchange of  $\text{H}_x\text{PO}_4^{(3-x)-}$  ions to the RS, eqn (3.2). The DD experiments exhibited this increasing trend of  $[\text{H}_x\text{PO}_4^{(3-x)-}]_{\text{RS},f}$  with larger  $[\text{Cl}^-]_{\text{RS},0}$  (patterned blue columns of Figure 3.2A). However, the observed  $[\text{H}_x\text{PO}_4^{(3-x)-}]_{\text{RS},f}$  were below the predicted values by  $\approx 8\text{--}15\%$ , with the improvements being less marked at greater  $[\text{Cl}^-]_{\text{RS},0}$ , e.g., raising  $[\text{Cl}^-]_{\text{RS},0}$  from 200 to  $1,000 \times 10^{-3}$  mol/L increases  $[\text{H}_x\text{PO}_4^{(3-x)-}]_{\text{RS},f}$  by 3.7%, lower than the theoretical enhancement of 11.3%.

$[\text{H}_x\text{PO}_4^{(3-x)-}]_{\text{RS},f}$  for the three different  $[\text{Cl}^-]_{\text{RS},0}$  are lower than theoretical final concentrations due to dilution by simultaneous water transport from FS to RS and imperfect cation exclusion by the AEM. The high concentration of NaCl in the RS generates an osmotic pressure gradient that drives water permeation from FS to RS, i.e., osmosis. Additionally, electro-osmosis, where water molecules are dragged along with the permeating charged ions, contributes to water transport.<sup>102, 155, 156</sup> Electro-osmosis due to  $\text{H}_x\text{PO}_4^{(3-x)-}$  flux from FS to RS is opposite in direction to water transport by  $\text{Cl}^-$  flux (and  $\text{Na}^+$  flux, explained next) from RS to FS. Net electro-osmosis is  $<10\%$  of the measured water permeation; therefore, the contribution from the phenomenon is relatively minor and osmosis is the primary driver of water transport. The RS volume increased by 5.3–21% at the end of the DD experiments performed here. Water flux dilutes the RS and consequently lowers the TOP concentration. Additionally, co-ions are not completely rejected by ion-exchange membranes.<sup>157, 158</sup> The  $\text{Na}^+$  concentration gradient set up by the high [NaCl] in the

RS results in  $\text{Na}^+$  permeation from RS to FS, i.e., co-ion (cation) leakage. To maintain electroneutrality, every  $\text{Na}^+$  ion that leaks across the AEM compels one  $\text{Cl}^-$  ion to permeate in the same direction; therefore  $\text{H}_2\text{PO}_4^-$  and  $\text{Cl}^-$  are transported at slightly below equimolar ratio and  $[\text{Cl}^-]_{\text{FS},f} + [\text{H}_x\text{PO}_4^{(3-x)-}]_{\text{FS},f} > [\text{H}_x\text{PO}_4^{(3-x)-}]_{\text{FS},0}$ . The cation leakage reduces  $\text{Cl}^-$  ions in RS that are available to exchange with  $\text{H}_x\text{PO}_4^{(3-x)-}$  ions in the FS, thus detrimentally lowering  $[\text{H}_x\text{PO}_4^{(3-x)-}]_{\text{RS},f}$ . Both water and co-ion leakage are not accounted for in eqn (3.2) and cause the experimental  $[\text{H}_x\text{PO}_4^{(3-x)-}]_{\text{RS},f}$  to deviate below the predicted Donnan equilibrium. Note that transport of  $\text{Cl}^-$  from RS to FS and  $\text{H}_2\text{PO}_4^-$  from FS to RS were nearly identical during the 6 h of DD operation presented in Figure 3.2; however, given the relatively longer duration of the phosphate recovery experiments presented in Figure 3.3A (72 h), cumulative co-ion transport is more pronounced.

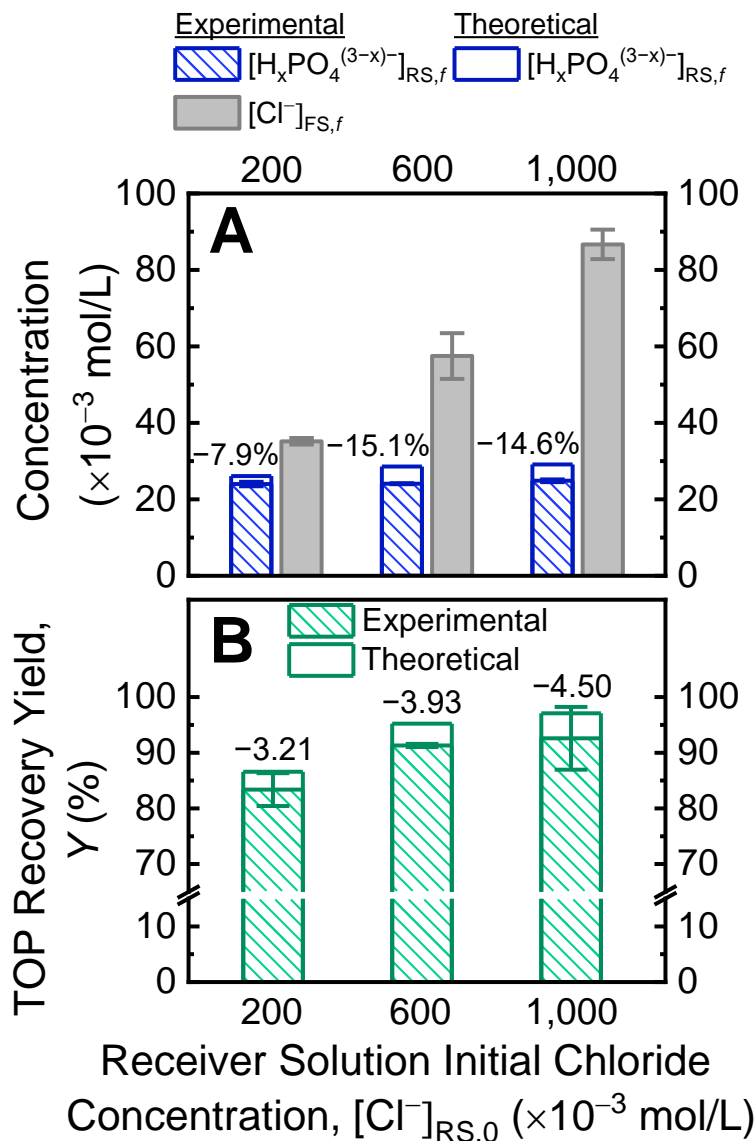


**Figure 3.3.** A)  $[H_xPO_4^{(3-x)-}]_{RS,f}$  and  $[Cl^-]_{FS,f}$  (patterned blue and gray columns, respectively) in DD with different initial NaCl concentrations in the receiver solution. Predicted  $[H_xPO_4^{(3-x)-}]_{RS,f}$  at Donnan equilibrium, calculated using eqn (3.2), are depicted by the empty blue columns. Labels above the columns indicate the percentage of predicted  $[H_xPO_4^{(3-x)-}]_{RS,f}$  experimentally captured in the RS. B) Experimental and predicted orthophosphate recovery yields,  $Y$ , (patterned and empty green columns, respectively) in DD with the different  $[Cl^-]_{RS,0}$ . The experimental  $Y$  were calculated from measured  $[H_xPO_4^{(3-x)-}]_{RS,f}$  and accounting for osmotic water flux the FS to the RS. Labels above the columns signify the percent decrease of moles of  $H_xPO_4^{(3-x)-}$  experimentally captured in the RS relative to theoretical prediction, based on eqn (3.2). Initial feed solution contains  $30 \times 10^{-3}$  mol/L  $H_2PO_4^-$  at pH = 6.0 (i.e., same composition as the FS of Figure 3.2). Receiver solutions with initial concentrations of 200, 600, and  $1,000 \times 10^{-3}$  mol/L NaCl to simulate brackish water,

seawater, and seawater desalination brine, respectively, were investigated. In all operations  $V_{FS}/V_{RS}$  is 1:1. Data points and error bars are means and standard deviations, respectively, of duplicate experiments.

$H_xPO_4^{(3-x)-}$  experimentally captured in the RS are 7.91%, 15.1%, and 14.6% lower than predicted for  $[Cl^-]_{RS,0}$  of 200, 600, and  $1,000 \times 10^{-3}$  mol/L, respectively. Deviations of the experimental  $[H_xPO_4^{(3-x)-}]_{RS,f}$  from theoretical values, eqn (3.2), are larger with  $[Cl^-]_{RS,0}$  of 600 and  $1,000 \times 10^{-3}$  mol/L compared to  $200 \times 10^{-3}$  mol/L. The greater deficits are due to both water permeation from FS to RS and cation leakage from RS to FS being more prominent in operations with higher  $[Cl^-]_{RS,0}$ . Osmotic pressure is essentially proportional to  $[NaCl]$  and are 9.91, 29.7, and 49.6 bar for 200, 600, and  $1,000 \times 10^{-3}$  mol/L NaCl, respectively. As a result of the greater osmotic pressure difference between the RS and FS, increased water permeation is observed when  $[Cl^-]_{RS,0}$  is higher; net water fluxes are  $1.93 \times 10^{-2}$ ,  $6.37 \times 10^{-2}$ , and  $7.10 \times 10^{-2}$  L/m<sup>2</sup>h for initial RS of 200, 600, and  $1,000 \times 10^{-3}$  mol/L NaCl, respectively. Additionally,  $Na^+$  leakage is more exacerbated with conditions of higher initial RS  $[NaCl]$  due to increased  $Na^+$  concentration gradients.<sup>157, 158</sup> Consequently, the undesired co-permeation of  $Cl^-$  is elevated. In principle,  $[Cl^-]_{FS,f}$  (gray columns in Figure 3.3A) should be equivalent to  $[H_xPO_4^{(3-x)-}]_{RS,f}$  because the predominant form of orthophosphate in the FS is monovalent  $H_2PO_4^-$ , and therefore electroneutrality dictates a 1:1 exchange of  $Cl^-$  and  $H_2PO_4^-$ . However, experimentally,  $[Cl^-]_{FS,f} > [H_xPO_4^{(3-x)-}]_{RS,f}$  due to the  $Na^+$  and  $Cl^-$  leakage from RS to FS and water flux from FS to RS. Furthermore, the divergences between  $[Cl^-]_{FS,f}$  and  $[H_xPO_4^{(3-x)-}]_{RS,f}$  are larger at higher  $[Cl^-]_{RS,0}$  as co-ion leakage and osmosis, are more exacerbated. Although increasing  $[Cl^-]_{RS,0}$  resulted in higher TOP concentrations recovered in the receiver solution, the greater deviations between experimental and predicted DD performance also indicate that the inefficiencies of water and co-ion leakage are more pronounced.

Recovery yield,  $Y$ , is defined as the percentage of orthophosphate moles from the initial FS that are recovered in the RS and is presented in Figure 3.3B, with patterned and empty green columns denoting experimental and predicted  $Y$ , respectively. Experimental  $Y$  is calculated using the product of TOP concentration and solution volume at the end of the test ( $[\text{H}_x\text{PO}_4^{(3-x)-}]_{\text{RS},f}V_{\text{RS},f}$ ), i.e., the effects of osmotic and electro-osmotic water transport are accounted for. Labels above the columns are the differences between experimental and predicted  $Y$ . The experimental orthophosphate recovery yields are very close to  $Y$ s predicted at Donnan equilibrium using eqn (3.2) (within 5%). The minor shortfalls in recovery yield are attributed to  $\text{Na}^+$  leakage and  $\text{Cl}^-$  co-permeation. Despite the imperfect permselectivity of the AEM, experimental  $Y$ s are high and exceed 90% for  $[\text{Cl}^-]_{\text{RS},0}$  of  $600 \times 10^{-3}$  and  $1,000 \times 10^{-3}$  mol/L. Even the lowest  $[\text{Cl}^-]_{\text{RS},0}$  of  $200 \times 10^{-3}$  mol/L produced  $Y$  of 83%. The high yields achieved signify that DD can be a promising technique for orthophosphate recovery. Increasing  $[\text{Cl}^-]_{\text{RS},0}$  improves  $Y$ , but with diminishing returns. For example, raising  $[\text{Cl}^-]_{\text{RS},0}$  from  $200 \times 10^{-3}$  to  $600 \times 10^{-3}$  mol/L increases experimental  $Y$  by 9.5%. However, further increasing  $[\text{Cl}^-]_{\text{RS},0}$  to  $1,000 \times 10^{-3}$  mol/L only marginally improved the orthophosphate recovery yield by 1.4%; this trend is also predicted by the Donnan equilibrium theory of eqn (3.2). Subsequent phosphate recovery experiments will, thus, utilize  $[\text{Cl}^-]_{\text{RS},0} = 600 \times 10^{-3}$  mol/L.

**Donnan Dialysis can Enrich Orthophosphate in the Receiver Solution.** It is advantageous to produce concentrated orthophosphate solutions to be utilized in downstream applications as fertilizer. Orthophosphate can be enriched in the RS (i.e.,  $[\text{H}_x\text{PO}_4^{(3-x)-}]_{\text{RS},f} > [\text{H}_x\text{PO}_4^{(3-x)-}]_{\text{FS},0}$ ) by using a smaller RS volume relative to FS, based on the Donnan equilibrium (eqns (B.14)–(B.17) of Appendix B). DD experiments were conducted using different  $V_{\text{FS}}/V_{\text{RS}}$  of 1, 2, and 4. The FS contains  $30 \times 10^{-3}$  mol/L of  $\text{H}_x\text{PO}_4^{(3-x)-}$  and the RS has  $600 \times 10^{-3}$  mol/L of  $\text{Cl}^-$ .

Figure 3.4 presents experimental  $[\text{H}_x\text{PO}_4^{(3-x)-}]_{\text{RS},f}$  as patterned blue columns, and predicted  $[\text{H}_x\text{PO}_4^{(3-x)-}]_{\text{RS},f}$  are indicated by the blue dashed line (left vertical axis). Labels in the columns denote enrichment factors, defined as  $[\text{H}_x\text{PO}_4^{(3-x)-}]_{\text{RS},f}/[\text{H}_x\text{PO}_4^{(3-x)-}]_{\text{FS},0}$ . Experimental and predicted recovery yields of  $\text{H}_x\text{PO}_4^{(3-x)-}$ ,  $Y$ , are green square symbols and green dashed line, respectively (right vertical axis).

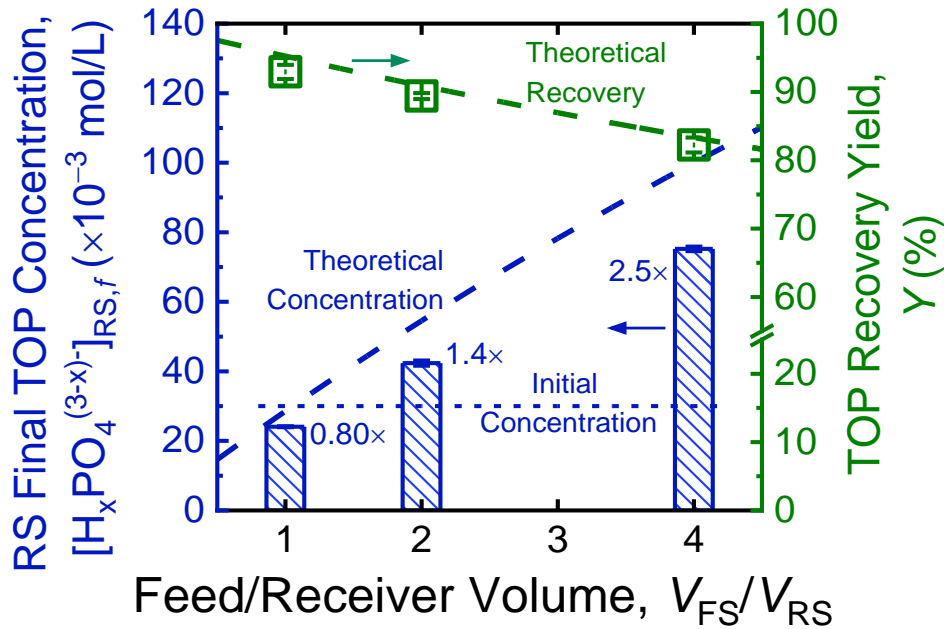


**Figure 3.4.** Receiver solution final TOP concentration,  $[\text{H}_x\text{PO}_4^{(3-x)-}]_{\text{RS},f}$  (blue columns, left vertical axis), and orthophosphate recovery yields,  $Y$  (green square symbols, right vertical axis), as a function of  $V_{\text{FS}}/V_{\text{RS}}$ . Experimental  $Y$  is calculated using  $[\text{H}_x\text{PO}_4^{(3-x)-}]_{\text{RS},f}V_{\text{RS},f}$  and, therefore, accounts for water transport from the FS to the RS due to osmosis and electro-osmosis. Predicted  $[\text{H}_x\text{PO}_4^{(3-x)-}]_{\text{RS},f}$  and recovery yields at Donnan equilibrium, calculated using eqns (B.14)–(B.17) in Appendix B, are depicted as blue and green dashed lines, respectively. The initial feed and receiver solutions are the same as the FS and RS of Figure 3.2. For comparison, the initial total orthophosphate concentration in the simulated urine feeds is depicted as a dotted blue line. Enrichment factors, defined as  $[\text{H}_x\text{PO}_4^{(3-x)-}]_{\text{RS},f}/[\text{H}_x\text{PO}_4^{(3-x)-}]_{\text{FS},0}$ , are indicated in the blue columns. Experimental  $Y$  is  $[\text{H}_x\text{PO}_4^{(3-x)-}]_{\text{RS},f}V_{\text{RS},f}$  and, therefore, accounts for osmotic water flux from the FS to the RS. Data points and error bars are means and standard deviations, respectively, of duplicate experiments.

Because DD can enable uphill transport of ions from FS to RS, the recovered orthophosphate can be concentrated in a small volume of RS. Enrichment factors of 1.4 and 2.5

were achieved in experiments with  $V_{FS}/V_{RS}$  of 2 and 4, respectively. However, experimental  $[\text{H}_x\text{PO}_4^{(3-x)-}]_{RS,f}$  and enrichment factors are lower than predictions by Donnan equilibrium. Eqn (B.8) predicts enrichment factors of 1.8 and 3.3 at Donnan equilibrium with  $V_{FS}/V_{RS} = 2$  and 4, respectively. These deviations are primarily due to water permeation diluting the orthophosphates captured in the RS. Furthermore, the dilution effect is more pronounced at higher  $V_{FS}/V_{RS}$ , where osmotic water flux from FS to RS mixes with relatively smaller volumes of RS. As a result, the deviations of experimental  $[\text{H}_x\text{PO}_4^{(3-x)-}]_{RS,f}$  from predicted values are detrimentally elevated with increased  $V_{FS}/V_{RS}$  and are  $-15.7\%$ ,  $-22.3\%$ , and  $-24.8\%$  for  $V_{FS}/V_{RS}$  of 1, 2, and 4, respectively. However, similar to the results presented in Figure 3.3, experimental recovery yields (green square symbols in Figure 3.4) are comparable to theoretical  $Y$  at Donnan equilibrium ( $<3\%$  difference between green square symbols and green dashed lines), as water permeation is accounted for in the determination of moles of TOP recovered. This minor difference is attributed to  $\text{Na}^+$  leakage and  $\text{Cl}^-$  co-permeation, i.e., imperfect AEM permselectivity,<sup>157, 158</sup> which results in reduced driving force available for  $\text{H}_x\text{PO}_4^{(3-x)-}$  transport.

Varying  $V_{FS}/V_{RS}$  produces a tradeoff between enrichment and recovery yield, as predicted by the Donnan equilibrium theory, eqns (B.14)–(B.17): increasing  $V_{FS}/V_{RS}$  enhances the enrichment factor, but the recovery yield is slightly compromised (dashed blue line and dashed green line in Figure 3.4 exhibit positive and negative slopes, respectively). This is because with a relatively smaller receiver solution volume, the initial ratio of moles of  $\text{Cl}^-$  in the RS to moles of  $\text{H}_x\text{PO}_4^{(3-x)-}$  in the FS (i.e.,  $[\text{Cl}^-]_{RS}:[\text{H}_x\text{PO}_4^{(3-x)-}]_{FS,0}V_{FS}$ ) is lower. Therefore, there are fewer available driver  $\text{Cl}^-$  ions to exchange with target  $\text{H}_2\text{PO}_4^-$  ions, and the achievable  $Y$  is decreased. Nevertheless, it can be overall advantageous to use a higher  $V_{FS}/V_{RS}$ , if the benefit from a greater enrichment factor outweighs the loss in recovery yield. For example, compared to  $V_{FS}/V_{RS} = 1$ ,

experimental enrichment factor increased by 76.0% and 212.4% at  $V_{FS}/V_{RS}$  of 2 and 4, respectively, while experimental  $Y$  only decreased by 5.9% and 11.7%. Furthermore, the highest enrichment factor (at  $V_{FS}/V_{RS} = 4$ ) was still achieved with adequately high orthophosphate recovery  $>80\%$ .

**Competing Anions in the Urine Feed Solutions Lower Orthophosphate Transport and Recovery.** Results presented thus far utilized a feed solution with TOP concentration of fresh urine, i.e., orthophosphate as the sole anion. However, actual fresh urine contains orthophosphate, sulfate, and chloride anions, and hydrolyzed urine additionally has significant bicarbonate concentration.<sup>44, 89, 92, 96</sup> To examine the effects of other anions on orthophosphate recovery, DD experiments were conducted using simulated fresh urine and hydrolyzed urine (anion compositions are summarized in Table 3.1), for comparison with the TOP-only solution. In all operations, the RS has  $600 \times 10^{-3}$  mol/L of  $\text{Cl}^-$ . Figure 3.5A shows experimental  $[\text{H}_x\text{PO}_4^{(3-x)-}]_{RS,f}$ ,  $[\text{SO}_4^{2-}]_{RS,f}$ , and  $[\text{HCO}_3^-]_{RS,f}$  as patterned blue, orange, and red columns, respectively. Empty columns of the respective colors signify concentrations in the RS at Donnan equilibrium (determined using eqns (B.9)–(B.13) of Appendix B). Labels above the arrows designate the percent reduction in experimental  $[\text{H}_x\text{PO}_4^{(3-x)-}]_{RS,f}$  achieved in DD relative to orthophosphate-only feed solution.

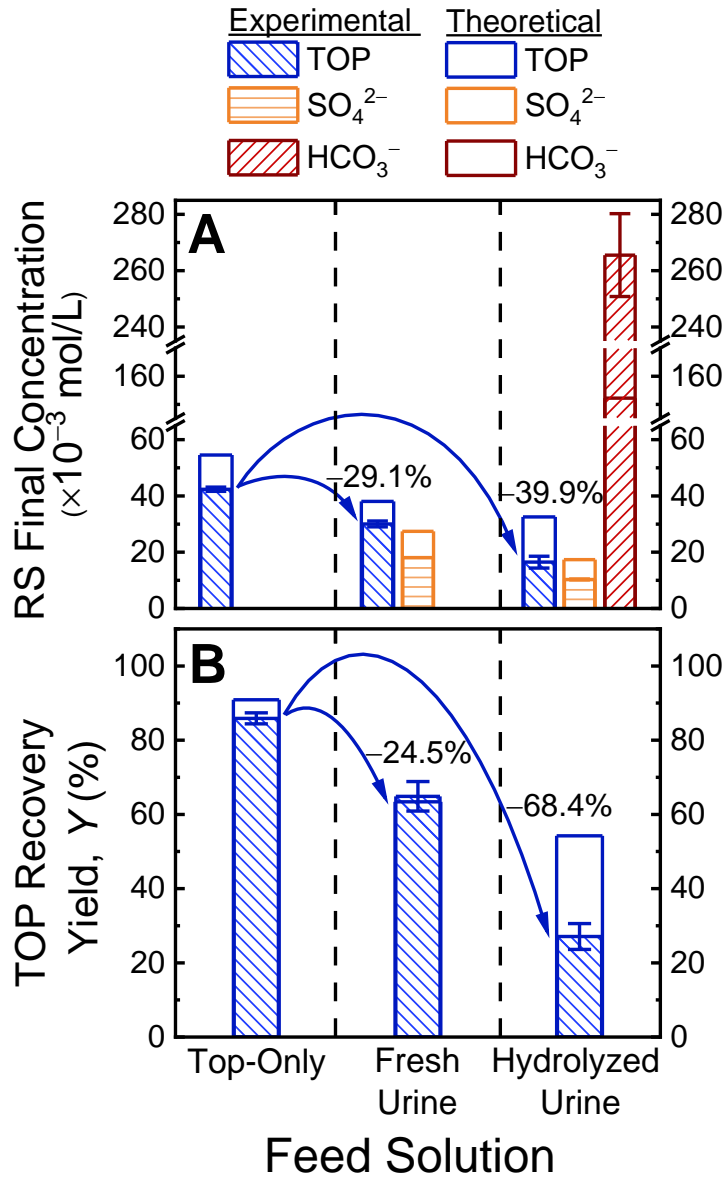


**Figure 3.5.** A) Final RS concentrations,  $[\text{H}_x\text{PO}_4^{(3-x)-}]_{\text{RS},f}$ ,  $[\text{SO}_4^{2-}]_{\text{RS},f}$ , and  $[\text{HCO}_3^-]_{\text{RS},f}$ , and B) orthophosphate recovery yields in TOP recovery experiments with different urine matrices as initial feed solutions. The three FS are: orthophosphate anion-only, fresh urine, and hydrolyzed urine.  $[\text{H}_x\text{PO}_4^{(3-x)-}]_{\text{FS},0}$  of all three FS are  $30 \times 10^{-3}$  mol/L. Simulated fresh urine contains  $16 \times 10^{-3}$  mol/L  $\text{SO}_4^{2-}$  and  $100 \times 10^{-3}$  mol/L  $\text{Cl}^-$  anions as well as  $\text{H}_x\text{PO}_4^{(3-x)-}$ , whereas simulated hydrolyzed urine additionally has  $250 \times 10^{-3}$  mol/L  $\text{HCO}_3^-$ . Note that the transport of water from feed solution to receiver solution is accounted for in the experimental orthophosphate recovery yields. Predicted final RS concentrations and predicted orthophosphate recovery yields at Donnan equilibrium, calculated using eqns (B.14)–(B.17) in Appendix B, are depicted as empty columns. The labels above the columns indicate the change relative to the orthophosphate-only FS. All experiments were operated with  $V_{\text{FS}}/V_{\text{RS}}$  equal to 2 and

$600 \times 10^{-3}$  mol/L NaCl as the receiver solution. Data points and error bars are means and standard deviations, respectively, of duplicate experiments.

Theoretical  $[\text{H}_x\text{PO}_4^{(3-x)-}]_{\text{RS},f}$  are 30.3% and 40.3% lower in operations with fresh and hydrolyzed urine, respectively, relative to TOP-only FS (empty blue columns in Figure 3.5A). In DD with fresh urine, both  $\text{SO}_4^{2-}$  and  $\text{H}_x\text{PO}_4^{(3-x)-}$  ions can transport from the FS to the RS to balance  $\text{Cl}^-$  transport from RS to FS and maintain net electroneutrality. Therefore,  $\text{SO}_4^{2-}$  ions compete with target  $\text{H}_x\text{PO}_4^{(3-x)-}$  ions to exchange with  $\text{Cl}^-$  ions. Moreover,  $\text{SO}_4^{2-}$  is a divalent anion. Thus, two  $\text{Cl}^-$  ions are required to exchange with one  $\text{SO}_4^{2-}$  ion to achieve charge balance, which further limits  $\text{Cl}^-$  ions available to exchange with  $\text{H}_x\text{PO}_4^{(3-x)-}$ . Additionally, the inclusion of  $\text{Cl}^-$  ions in the fresh urine matrix also decreases the chloride concentration gradient,  $[\text{Cl}^-]_{\text{RS}} - [\text{Cl}^-]_{\text{FS}}$ , which lowers the total  $\text{Cl}^-$  ions that will be transported from RS to FS at Donnan equilibrium. The decreased driver ion transport further decreases the transport of target ion  $\text{H}_x\text{PO}_4^{(3-x)-}$  from the FS to RS. Thus, both the competition with  $\text{SO}_4^{2-}$  ions and the weakened driving force give rise to the decline of predicted  $[\text{H}_x\text{PO}_4^{(3-x)-}]_{\text{RS},f}$  in operations with fresh urine relative to TOP-only.

In DD with hydrolyzed urine,  $\text{HCO}_3^-$  ions pose additional competition for exchange with the driver  $\text{Cl}^-$  ions, which leads to further reduction of predicted  $[\text{H}_x\text{PO}_4^{(3-x)-}]_{\text{RS},f}$  relative to FS of TOP-only. For the same reason, predicted  $[\text{SO}_4^{2-}]_{\text{RS},f}$  in operations with hydrolyzed urine is 36.7% lower than with fresh urine ( $\text{HCO}_3^-$  ion competition also impacts  $\text{SO}_4^{2-}$  transport). The concentration of  $\text{HCO}_3^-$  in hydrolyzed urine,  $250 \times 10^{-3}$  mol/L, is nearly 1 order of magnitude higher than  $\text{H}_x\text{PO}_4^{(3-x)-}$  and over 1 order of magnitude higher than  $\text{SO}_4^{2-}$  ( $30 \times 10^{-3}$  mol/L and  $16 \times 10^{-3}$  mol/L, respectively). As a result, the exchange of  $\text{HCO}_3^-$  with  $\text{Cl}^-$  is expected to dominate over the exchange with other anions in the FS, yielding predicted  $[\text{HCO}_3^-]_{\text{RS},f} \gg [\text{H}_x\text{PO}_4^{(3-x)-}]_{\text{RS},f} > [\text{SO}_4^{2-}]_{\text{RS},f}$ .

To uncouple the relative impact of these three factors (i.e., i) competition with  $\text{SO}_4^{2-}$  ions, ii) competition with  $\text{HCO}_3^-$  ions, and iii) the weakened driving force due to  $\text{Cl}^-$  ions in the FS) on orthophosphate recovery, theoretical  $[\text{H}_x\text{PO}_4^{(3-x)-}]_{\text{RS},f}$  were additionally calculated for DD with FS containing i)  $\text{H}_x\text{PO}_4^{(3-x)-}$  and  $\text{SO}_4^{2-}$ , ii)  $\text{H}_x\text{PO}_4^{(3-x)-}$  and  $\text{HCO}_3^-$ , and iii)  $\text{H}_x\text{PO}_4^{(3-x)-}$  and  $\text{Cl}^-$ . These calculated values are presented in Figure B.1 of Appendix B, together with the theoretical  $[\text{H}_x\text{PO}_4^{(3-x)-}]_{\text{RS},f}$  with FS of TOP-only, fresh urine, and hydrolyzed urine. When included in the FS,  $\text{H}_x\text{PO}_4^{(3-x)-}$ ,  $\text{SO}_4^{2-}$ ,  $\text{Cl}^-$ , and  $\text{HCO}_3^-$  ion concentrations are  $30 \times 10^{-3}$ ,  $16 \times 10^{-3}$ ,  $100 \times 10^{-3}$ , and  $250 \times 10^{-3}$  mol/L, respectively. Inclusion of  $\text{Cl}^-$  ions to the feed matrix lowers  $[\text{H}_x\text{PO}_4^{(3-x)-}]_{\text{RS},f}$  by more than 2 $\times$  compared to the inclusion of  $\text{SO}_4^{2-}$  (23.3% and 10.4% reductions for iii and i, respectively, relative to TOP-only feed solution). Therefore, the decrease in  $\text{Cl}^-$  concentration gradient driving force impacts orthophosphate recovery more than the competition posed by  $\text{SO}_4^{2-}$  ions in urine. The introduction of  $\text{HCO}_3^-$  ions, as in hydrolyzed urine, substantially lowers  $[\text{H}_x\text{PO}_4^{(3-x)-}]_{\text{RS},f}$  by 32.0% compared with the TOP-only FS, which is even larger than the 30.3% reduction observed with the combined inclusion of  $\text{SO}_4^{2-}$  and  $\text{Cl}^-$  ions, i.e., fresh urine. Therefore, the competition posed by  $\text{HCO}_3^-$  in hydrolyzed urine is the main reason projected  $[\text{H}_x\text{PO}_4^{(3-x)-}]_{\text{RS},f}$  is significantly lower than in DD with TOP-only FS.

Consistent with the Donnan equilibrium predictions, experimental  $[\text{H}_x\text{PO}_4^{(3-x)-}]_{\text{RS},f}$  in DD with fresh and hydrolyzed urine are 29.1% and 39.9% lower, respectively, relative to TOP-only feed solution (Figure 3.5A). However, all experimental  $[\text{H}_x\text{PO}_4^{(3-x)-}]_{\text{RS},f}$  are lower than theoretical values at Donnan equilibrium (-22.3%, -21.0%, and -49.4% with TOP-only FS, fresh urine, and hydrolyzed urine, respectively). Similarly,  $[\text{SO}_4^{2-}]_{\text{RS},f}$  in operations with fresh and hydrolyzed urine are 34.1% and 40.5% lower, respectively, than predicted. As discussed earlier, these

differences are caused by water permeation from FS to RS diluting the ions captured in the RS and co-ion leakage of  $\text{Na}^+$  from RS to FS lowering anion transport from FS to RS.

However, experimental  $[\text{HCO}_3^-]_{\text{RS},f}$  with hydrolyzed urine is significantly higher than predicted (+60.9%, red columns in Figure 3.5A). At the same time, experimental  $[\text{H}_x\text{PO}_4^{(3-x)-}]_{\text{RS},f}$  in DD with hydrolyzed urine resulted in considerably larger deviations from Donnan equilibrium values (-49.4%) than with TOP-only feed solution and fresh urine (-22.3% and -21.0%, respectively). One possible explanation for these observations is that the hydrolyzed urine experiments were terminated prior to actual equilibrium. The experimental protocol used  $[\text{H}_x\text{PO}_4^{(3-x)-}]_{\text{RS}}$  to assess the progress of ions transport in DD, with test runs ending when orthophosphate concentrations stagnated (< 5% change over three consecutive measurements). If the transport of  $\text{HCO}_3^-$  ions from the FS to RS is much faster than the transport of  $\text{H}_x\text{PO}_4^{(3-x)-}$  ions in the same direction,  $[\text{H}_x\text{PO}_4^{(3-x)-}]_{\text{RS}}$  can appear to level-off and trigger premature termination of the experiments. Ion transport kinetics will be further evaluated in the following subsection. To explore this postulation,  $\left( \frac{[\text{H}_x\text{PO}_4^{(3-x)-}]_{\text{FS}}}{[\text{H}_x\text{PO}_4^{(3-x)-}]_{\text{RS}}} \right)^{1/(3-x)}$  and  $[\text{HCO}_3^-]_{\text{FS}}/[\text{HCO}_3^-]_{\text{RS}}$  were calculated using concentrations at the end of the experimental runs (note that the predominant form of  $\text{H}_x\text{PO}_4^{(3-x)-}$  in hydrolyzed urine of pH = 9.2 is  $\text{HPO}_4^{2-}$  and, therefore,  $x = 1$ ). At Donnan equilibrium, the fractions should be equal. However, the values for  $\text{HPO}_4^{2-}$  and  $\text{HCO}_3^-$  are 1.15 and 0.445, respectively, indicating that the system has not fully equilibrated at the end point of the experiment. Furthermore,  $[\text{HCO}_3^-]_{\text{FS}}/[\text{HCO}_3^-]_{\text{RS}} < \left( \frac{[\text{HPO}_4^{2-}]_{\text{FS}}}{[\text{HPO}_4^{2-}]_{\text{RS}}} \right)^{1/2}$  suggests that experimental  $[\text{HCO}_3^-]_{\text{RS}}$  at end of the test run is higher than theoretical concentration at Donnan equilibrium. Allowing the DD experiments to proceed further can possibly result in

redistribution of the ions between the FS and RS, such that  $[\text{HCO}_3^-]_{\text{FS}}/[\text{HCO}_3^-]_{\text{RS}}$  and  $([\text{HPO}_4^{2-}]_{\text{FS}}/[\text{HPO}_4^{2-}]_{\text{RS}})^{1/2}$  are similar.

Figure 3.5B presents experimental and predicted orthophosphate recovery yields,  $Y$  (patterned and empty blue columns, respectively); note that  $Y$  accounts for water transport (as discussed earlier). Labels above the arrows designate the percent reduction in experimental  $Y$  relative to orthophosphate-only FS. Recovery yield trends are generally similar to  $[\text{H}_x\text{PO}_4^{(3-x)-}]_{\text{RS},f}$  trends. Specifically,  $Y$  are 24.5% and 68.4% lower with fresh and hydrolyzed urine, respectively, relative to DD with TOP-only FS, which qualitatively agrees with theoretical predictions of 30.3% and 40.3% reduction. Experimental DD with TOP-only feed solutions and fresh urine deviate slightly from predicted  $Y$  at Donnan equilibrium (<3%). As previously discussed,  $\text{Na}^+$  leakage from RS to FS results in less  $\text{H}_x\text{PO}_4^{(3-x)-}$  ion transport from FS to RS, which explains the experimental  $Y$  being slightly lower than the predicted value for DD with TOP-only FS. For fresh urine, co-ion leakage is lower because the  $\text{Na}^+$  present in the FS reduces the  $\text{Na}^+$  concentration gradient, which drives co-ion permeation. Therefore, the experimental and predicted  $Y$ s are comparable for DD with fresh urine (minor difference is due to unavoidable experimental uncertainties). In contrast,  $Y$  is significantly lower than the theoretical recovery yield at Donnan equilibrium for hydrolyzed urine (50.0% lower). As conjectured in the preceding paragraph, the substantially greater discrepancy is possibly explained by the premature termination of the DD experiment before the ion concentrations were fully equilibrated.

**Orthophosphate Fluxes are Diminished by the Competing Anions.** Parallel DD kinetics experiments were conducted with the same initial feed solutions presented in Figure 3.5, i.e., TOP-only FS, fresh urine, and hydrolyzed urine. To elucidate the impacts of individual ionic species in

the urine matrix on ion fluxes, additional DD kinetic experiments were carried out with feed solutions of  $\text{H}_x\text{PO}_4^{(3-x)-} + \text{SO}_4^{2-}$  and  $\text{H}_x\text{PO}_4^{(3-x)-} + \text{Cl}^-$ . In all operations, the RS has  $600 \times 10^{-3}$  mol/L of  $\text{Cl}^-$  and  $V_{\text{FS}}/V_{\text{RS}} = 1$ . Figure 3.6 shows molar ion fluxes,  $J_i$ , of  $\text{H}_x\text{PO}_4^{(3-x)-}$ ,  $\text{SO}_4^{2-}$ , and  $\text{HCO}_3^-$  from FS to RS (subscript  $i$  is P, S, and C, respectively) as patterned blue, orange, and red columns, respectively; labels above blue columns indicate reduction in  $J_P$  relative to DD with the orthophosphate-only FS.

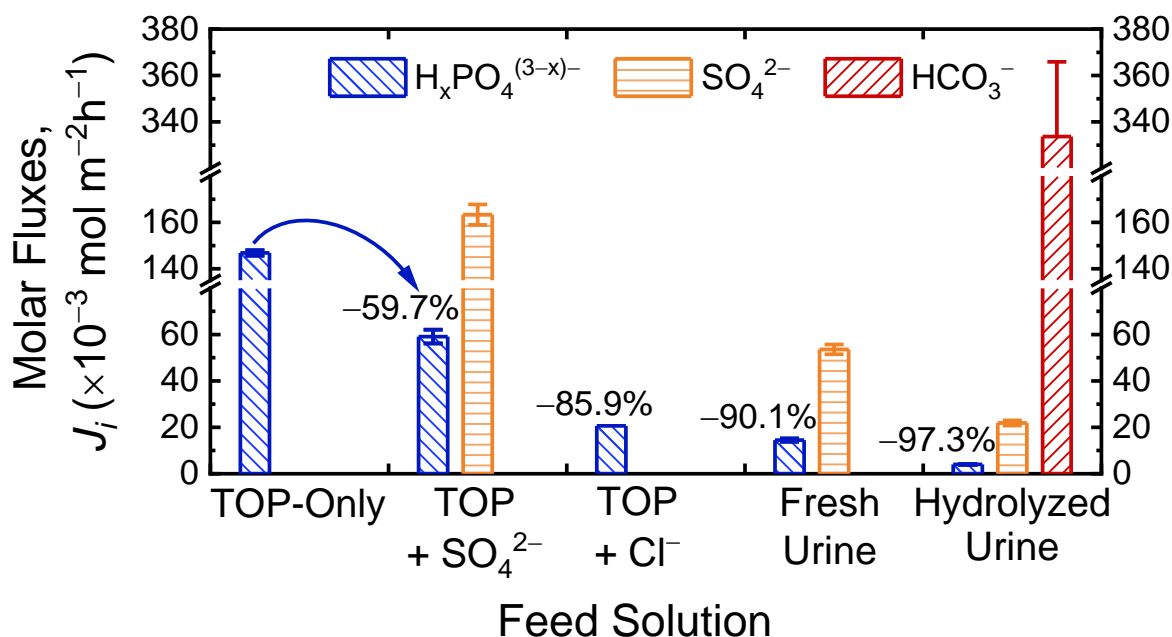


**Figure 3.6.**  $\text{H}_x\text{PO}_4^{(3-x)-}$ ,  $\text{SO}_4^{2-}$ , and  $\text{HCO}_3^-$  anion fluxes from FS to RS,  $J_i$ , in kinetic experiments with different urine matrices as initial feed solutions. The anions of the five FS are: i) orthophosphate only, ii) orthophosphate and sulfate, iii) orthophosphate and chloride, iv) orthophosphate, sulfate, and chloride (fresh urine), and v) orthophosphate, sulfate, bicarbonate, and chloride (hydrolyzed urine). Labels above the columns indicate the change in flux relative to the orthophosphate-only feed solutions.  $[\text{H}_x\text{PO}_4^{(3-x)-}]_{\text{FS},0}$  of all FS are  $30 \times 10^{-3}$  mol/L. When present in the FS,  $\text{SO}_4^{2-}$ ,  $\text{Cl}^-$ , and  $\text{HCO}_3^-$  concentrations are  $16 \times 10^{-3}$ ,  $100 \times 10^{-3}$ , and  $250 \times 10^{-3}$  mol/L, respectively.  $V_{\text{FS}}/V_{\text{RS}} = 1$  and receiver solutions are  $600 \times 10^{-3}$  mol/L NaCl for all experiments. Data points and error bars are means and standard deviations, respectively, of duplicate experiments.

As observed with experimental  $[\text{H}_x\text{PO}_4^{(3-x)-}]_{\text{RS},f}$  and  $Y$  (Figures 3.5A and B),  $J_P$  is reduced in DD with simulated fresh or hydrolyzed urine relative to orthophosphate-only FS (90.1% and

97.3% lower, respectively). However, the decreases in anion fluxes with the inclusion of  $\text{SO}_4^{2-}$ ,  $\text{Cl}^-$ , and  $\text{HCO}_3^-$  are more drastic than the observed decreases in  $[\text{H}_x\text{PO}_4^{(3-x)-}]_{\text{RS},f}$  and  $Y$ . Introducing  $\text{SO}_4^{2-}$  to the FS containing only orthophosphate ions diminishes  $J_P$  by 59.7%, whereas the isolated inclusion of  $\text{Cl}^-$  decreases  $J_P$  by 85.9%. These reductions in  $J_P$  qualitatively mirror the reductions in  $[\text{H}_x\text{PO}_4^{(3-x)-}]_{\text{RS},f}$  at Donnan equilibrium, i.e., presence of  $\text{Cl}^-$  and  $\text{SO}_4^{2-}$  in the FS both lower fluxes and final concentrations, but the influence of  $\text{Cl}^-$  ions is greater in magnitude. The effects of the competing ions on  $J_P$  are similar to the impacts on  $[\text{H}_x\text{PO}_4^{(3-x)-}]_{\text{RS},f}$ : the presence of  $\text{SO}_4^{2-}$  poses competition for  $\text{H}_x\text{PO}_4^{(3-x)-}$  permeation from FS to RS, whereas  $\text{Cl}^-$  in the FS reduces the electrochemical potential gradient driving  $\text{Cl}^-$  transport from RS to FS and consequently lowers  $\text{H}_x\text{PO}_4^{(3-x)-}$  permeation.

The inclusion of anions other than  $\text{H}_x\text{PO}_4^{(3-x)-}$  in the feed solution lowers the orthophosphate that can be theoretically recovered in DD (Figure 3.5A) by reducing the driving force for  $\text{H}_x\text{PO}_4^{(3-x)-}$  transport. To quantitatively explore the impact of the reduced driving force on  $\text{H}_x\text{PO}_4^{(3-x)-}$  fluxes,  $J_P$ , we examine  $\Delta[\text{H}_x\text{PO}_4^{(3-x)-}] \equiv [\text{H}_x\text{PO}_4^{(3-x)-}]_{\text{FS},0} - [\text{H}_x\text{PO}_4^{(3-x)-}]_{\text{FS},f}$ , defined as the difference between initial and final (at Donnan equilibrium) TOP concentrations in the feed solution.  $\Delta[\text{H}_x\text{PO}_4^{(3-x)-}]$  can be intuitively understood as the equivalent amount of ions that should be transported to the RS in Donnan dialysis. Table B.6 in Appendix B displays  $\Delta[\text{H}_x\text{PO}_4^{(3-x)-}]$  and the percentage decrease in  $\Delta[\text{H}_x\text{PO}_4^{(3-x)-}]$  relative to DD with  $\text{H}_x\text{PO}_4^{(3-x)-}$ -only FS for different ions in the feed solution. The inclusion of  $\text{SO}_4^{2-}$  and  $\text{Cl}^-$  lower  $\Delta[\text{H}_x\text{PO}_4^{(3-x)-}]$  by 5.26% and 13.7%, respectively, while having both ions decreases the driving force by 18.0%. However, the reductions in  $J_P$  with additional ions in the FS are drastically more pronounced (60–90%) than reductions in  $\Delta[\text{H}_x\text{PO}_4^{(3-x)-}]$  (5.3–18%). Importantly, normalizing the ion fluxes of Figure 3.6 by  $\Delta[\text{H}_x\text{PO}_4^{(3-x)-}]$  gave vastly dissimilar values for the different FS anion compositions (Figure B.2

of Appendix B), providing strong evidence that the lessened  $\Delta[\text{H}_x\text{PO}_4^{(3-x)-}]$  does not fully explain the diminished  $J_P$ .

Instead, the observed differences in  $J_P$  could possibly be explained by different affinities of the various ions to sorb into the anion exchange membrane. Specifically, if other anions in the FS, such as  $\text{SO}_4^{2-}$  and  $\text{Cl}^-$ , more preferentially partition into the membrane than  $\text{H}_x\text{PO}_4^{(3-x)-}$ , the relative concentration of orthophosphate ions within the IEM will be disproportionately lower compared to the feed solution.<sup>159</sup> As flux is directly proportional to the ion concentration in the IEM,  $J_P$  will consequently be depressed. Additionally, the higher charge of multivalent ions favors sorption into the charged membrane more than monovalent ions.<sup>160</sup> Hence, partitioning of  $\text{H}_2\text{PO}_4^-$ , the predominant orthophosphate species, into the IEM matrix can be further hindered by the presence of divalent  $\text{SO}_4^{2-}$ . To assess this postulation, sorption experiments were conducted for each of the feed solutions (method detailed in Appendix B). Figure B.3 in Appendix B presents sorption coefficients,  $X_i$ , for  $\text{H}_x\text{PO}_4^{(3-x)-}$ ,  $\text{SO}_4^{2-}$ , and  $\text{Cl}^-$  (subscript  $i$  is P, S, and Cl, respectively) with feed solutions containing different anions. Sorption coefficient is defined as ions sorbed into a unit volume of the membrane normalized by molar concentration in the feed solution. If the AEM does not differentiate between the different ions and ion sorption is solely determined by ion concentrations in the feed solution,  $X_i$  should be similar for the three ions ( $\text{H}_x\text{PO}_4^{(3-x)-}$ ,  $\text{SO}_4^{2-}$ , and  $\text{Cl}^-$ ) and across different feed solution compositions. However, experiments utilizing fresh urine FS result in different sorption coefficients with  $X_{\text{Cl}} > X_{\text{S}} > X_{\text{P}}$ . These results demonstrate relative affinities of each ion to the AEM, e.g., sorption coefficient for  $\text{SO}_4^{2-}$  is 4.26 $\times$  higher than  $\text{H}_x\text{PO}_4^{(3-x)-}$  in the fresh urine FS. Furthermore, the analysis reveals different sorption coefficients for the same ion across various feed solutions. For example,  $X_{\text{P}}$  is 85.0% and 92.8% lower in FS with  $\text{SO}_4^{2-}$  and  $\text{Cl}^-$ , respectively, relative to FS containing only orthophosphate. This supports the

postulation that  $\text{SO}_4^{2-}$  and  $\text{Cl}^-$  ions in the FS significantly outcompete  $\text{H}_x\text{PO}_4^{(3-x)-}$  ion sorption into the AEM. Aligned with the observed  $J_P$  trend, the addition of  $\text{Cl}^-$  ions suppresses orthophosphate sorption more than the addition of  $\text{SO}_4^{2-}$  ions.

The high concentration of  $\text{HCO}_3^-$  ions in hydrolyzed urine greatly suppresses  $J_P$ , with reductions of 97.3% and 72.4% in the orthophosphate fluxes relative to TOP-only feed solution and fresh urine, respectively (Figure 3.6). The high  $\text{HCO}_3^-$  content similarly affects  $J_S$  (59.2% lower with hydrolyzed urine than fresh urine). DD with hydrolyzed urine resulted in predominantly  $\text{HCO}_3^-$  and  $\text{Cl}^-$  exchange, with  $J_C > 8\times$  higher than  $J_P$  and  $J_S$ . As discussed in the preceding paragraph, anions in a multi-component FS compete to sorb into the AEM. In particular, the high concentration of  $\text{HCO}_3^-$  present in hydrolyzed urine<sup>89</sup> is expected to strongly favor the partitioning of bicarbonate anions into the AEM, which in turn hinders the fluxes of other ions. Importantly,  $J_C \gg J_P$  supports the earlier conjecture that bicarbonate transport from FS to RS significantly outpaced orthophosphate transport, which resulted in the apparent stagnation of  $[\text{H}_x\text{PO}_4^{(3-x)-}]_{\text{RS},f}$  before Donnan equilibrium was reached in the experiments. Compared to fresh urine as the feed solution, utilizing hydrolyzed urine resulted in lower  $[\text{H}_x\text{PO}_4^{(3-x)-}]_{\text{RS},f}$ , less orthophosphate recovery, more significant deviations from the Donnan equilibrium, and reduced  $J_P$  (Figures 3.5 and 3.6). For these reasons, it is more advantageous for DD to target fresh urine for orthophosphate recovery.

**Monovalent Ion Permselective Membranes can Improve Selectivity for  $\text{H}_2\text{PO}_4^-$  over other Anions in Urine.** Despite fresh urine having a higher concentration of  $\text{H}_2\text{PO}_4^-$  than  $\text{SO}_4^{2-}$ , sulfate flux in Donnan dialysis is still greater than orthophosphate flux (Figure 3.6). The conventional anion exchange membrane, Selemion AMV, preferentially permeates  $\text{SO}_4^{2-}$  over  $\text{H}_2\text{PO}_4^-$  primarily because the membrane has greater affinity to sorb divalent  $\text{SO}_4^{2-}$  than

monovalent  $\text{H}_2\text{PO}_4^-$  (Figure B.3). To selectively transport and capture  $\text{H}_x\text{PO}_4^{(3-x)-}$  over  $\text{SO}_4^{2-}$ , we investigate the use of monovalent ion permselective membranes (MIPMs), specifically Selemion ASVN, for DD recovery of orthophosphates from fresh urine. MIPMs are selective for transport of monovalent ions, such as  $\text{H}_2\text{PO}_4^-$ , over multivalent ions, such as  $\text{SO}_4^{2-}$  (details on the mechanisms of valence-selectivity can be found in literature).<sup>161-164</sup> Because the predominant orthophosphate species in fresh urine is  $\text{H}_2\text{PO}_4^-$ , DD with the ASVN MIPM is expected to improve selectivity for  $\text{H}_x\text{PO}_4^{(3-x)-}$  over  $\text{SO}_4^{2-}$  relative to the conventional AMV. DD kinetic experiments were conducted with the AMV and ASVN membranes using simulated fresh urines as FS,  $600 \times 10^{-3} \text{ mol/L Cl}^-$  for RS, and  $V_{\text{FS}}/V_{\text{RS}} = 1$ . Figure 3.7A presents the ion fluxes from FS to RS,  $J_i$ , and Figure 3.7B shows ion flux selectivity, defined as the molar ion flux normalized by the sum of two fluxes,  $J_i/J_{\text{T}}$ .  $\text{H}_2\text{PO}_4^-$  and  $\text{SO}_4^{2-}$  fluxes are denoted by blue and orange columns, respectively, whereas patterned and solid columns signify AMV and ASVN, respectively.

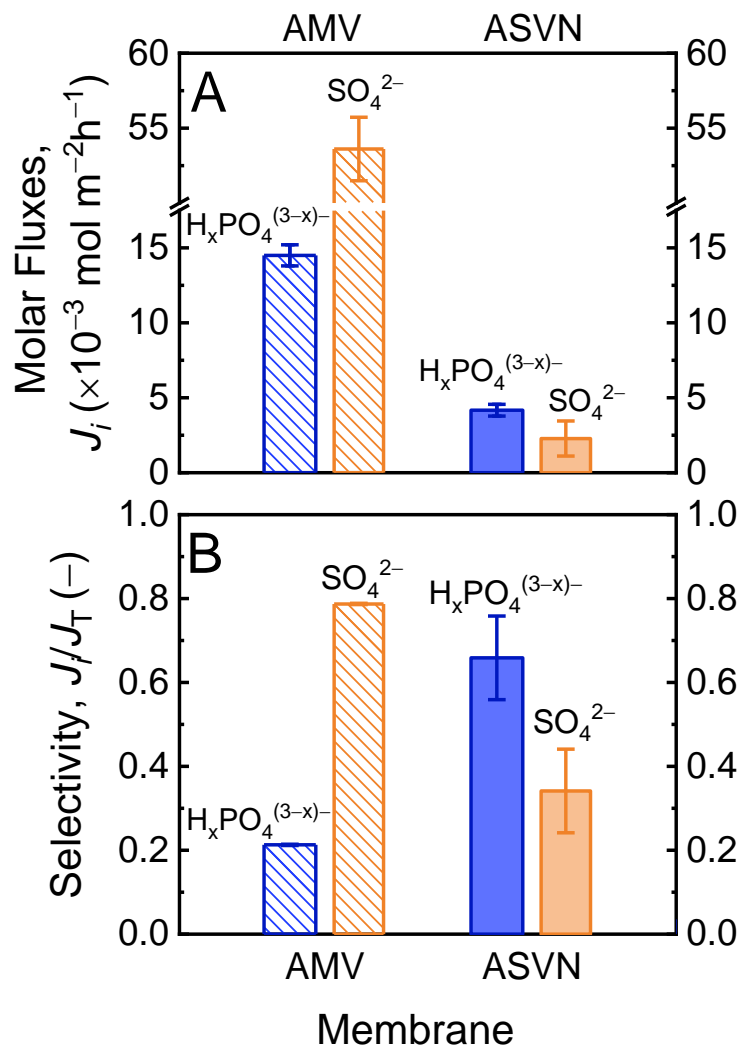


**Figure 3.7.** A) Orthophosphate and sulfate molar fluxes from feed solution to receiver solution,  $J_i$ , and B) flux selectivity in DD kinetic experiments for conventional anion exchange membrane, AMV, and monovalent ion selective membrane, ASVN. Flux selectivity,  $J_i/J_T$ , is defined as flux of the component,  $J_i$ , normalized by sum of the two anion fluxes. Blue and orange columns denote  $\text{H}_2\text{PO}_4^-$  and  $\text{SO}_4^{2-}$ , respectively, whereas patterned and solid columns signify AMV and ASVN, respectively. All experiments were operated with  $V_{FS}/V_{RS}$  of 1. The feed solution is simulated fresh urine, i.e.,  $30 \times 10^{-3}$  mol/L  $\text{H}_x\text{PO}_4^{(3-x)-}$ ,  $16 \times 10^{-3}$  mol/L  $\text{SO}_4^{2-}$ , and  $100 \times 10^{-3}$  mol/L  $\text{Cl}^-$  anions, and  $600 \times 10^{-3}$  mol/L NaCl was used as the receiver solution. Data points and error bars are means and standard deviations, respectively, of duplicate experiments.

Similar to the results presented in Figure 3.6, Figure 3.7A shows  $J_P < J_S$  in DD with the AMV membrane. Flux selectivity  $J_P/J_T$  is 0.21 (Figure 3.7B), which signifies approximately four

$\text{SO}_4^{2-}$  ions permeate across the AEM for every  $\text{H}_2\text{PO}_4^-$  ion recovered. In contrast, DD with the monovalent ion-selective ASVN membrane resulted in a reversal in the flux trend, i.e.,  $J_P > J_S$ , with flux selectivity for  $\text{H}_2\text{PO}_4^-$ ,  $J_P/J_T = 0.66$ . That is, for every two  $\text{H}_2\text{PO}_4^-$  ions recovered, roughly only one  $\text{SO}_4^{2-}$  anion permeated across. Overall, the ASVN membrane achieved  $3.1\times$  higher selectivity for  $\text{H}_2\text{PO}_4^-$  than the AMV membrane. Therefore, ASVN preferentially selected for  $\text{H}_2\text{PO}_4^-$  transport over  $\text{SO}_4^{2-}$ , resulting in  $\text{H}_2\text{PO}_4^-$  being the predominant anion exchanging from FS to RS with  $\text{Cl}^-$  in DD orthophosphate recovery.

However, it can be observed from Figure 3.7A that DD with the ASVN membrane resulted in lower  $\text{H}_2\text{PO}_4^-$  fluxes compared to operation with the AMV membrane. More generally, both ion fluxes are significantly diminished with the MIPM relative to the conventional AEM (71.3 and 95.8% lower for  $J_P$  and  $J_S$ , respectively). The monovalent ion selective coating on the ASVN membrane is composed of highly crosslinked resin, which creates additional steric hindrance for permeating ions.<sup>161-164</sup> Consequently, the overall ASVN membrane has greater resistance for ion transport compared to the AMV membrane (this is reflected in the manufacturer's specifications on resistance with various salt solutions, summarized in Table B.7). Thus, there exists a tradeoff between ion selectivity and permeability: using MIPMs instead of conventional AEMs yields improved monovalent ion selectivity but reduced ion fluxes. In applications of DD for orthophosphate recovery, MIPMs can improve TOP yield, but at the expense of slower kinetics; a lower  $J_P$  would necessitate larger membrane areas for the same productivity of orthophosphate recovery.

**Orthophosphate can be Captured as a Fertilizer Solution using Donnan Dialysis.** The previously presented results utilized receiver solutions with high  $\text{Cl}^-$  concentrations to demonstrate the potential of Donnan dialysis to separate orthophosphate from urine, which can have

contaminants, e.g., pharmaceuticals, endocrine disrupting compounds, and opportunistic pathogens, that prohibit the direct application of urine for fertilization. Orthophosphate was captured in receiver streams of NaCl solutions for the experiments. However, Na<sup>+</sup> is not well tolerated by most plant species at concentrations > 4.3–13×10<sup>-3</sup> mol/L,<sup>165, 166</sup> i.e., the eventual DD receiver solutions contain too much sodium. One option to exclude Na<sup>+</sup> is to precipitate phosphate fertilizers as mineral solids, such as struvite, NH<sub>4</sub>MgPO<sub>4</sub>·6H<sub>2</sub>O, and potassium magnesium phosphate, KMgPO<sub>4</sub>·6H<sub>2</sub>O, from the TOP-enriched RS by adding Mg<sup>2+</sup> and NH<sub>4</sub><sup>+</sup> or K<sup>+</sup>. As highlighted in the Introduction section, some studies reported the presence of contaminants in phosphate minerals directly precipitated from urine.<sup>136-141</sup> The anion exchange membrane in DD serves as a barrier, retaining the contaminants of concern in the urine feed.<sup>167-172</sup> Therefore, utilizing Donnan dialysis to separate orthophosphate from the urine matrix prior to mineral precipitation can sidestep the issue of possible pollutants contaminating the fertilizer products. Future studies need to be conducted to better understand the rejection of pharmaceuticals by AEMs.

An alternative method to circumvent both the sodium and product contamination issues is to recover the orthophosphates in DD receiver solutions with little or no Na<sup>+</sup>. In this approach, initial receiver solutions that contain sufficiently high concentrations of Cl<sup>-</sup> but with cations other than Na<sup>+</sup> are used. Additionally, the cations can be K<sup>+</sup> and NH<sub>4</sub><sup>+</sup> to further valorize nutrient content of the fertilizer product. For instance, aqueous solutions of potash fertilizer, KCl<sub>(aq)</sub>, can be used as the RS (simulated as 600 × 10<sup>-3</sup> mol/L KCl here), to draw additional value through the exchange of orthophosphate and Cl<sup>-</sup>. Another RS option is waste water softening regenerant rinse (WWSRR), which contains a high concentration of chloride anions and potassium and magnesium as the cations (approximately 547×10<sup>-3</sup> mol/L K<sup>+</sup>, 48×10<sup>-3</sup> mol/L Mg<sup>2+</sup>, and 643×10<sup>-3</sup> mol/L Cl<sup>-</sup>).

Diluted bittern (DB), a concentrated byproduct of table salt production from seawater, is yet another alternative. DB contains approximately  $77 \times 10^{-3} \text{ mol/L K}^+$ ,  $252 \times 10^{-3} \text{ mol/L Mg}^{2+}$ ,  $25 \times 10^{-3} \text{ mol/L SO}_4^{2-}$ ,  $8 \times 10^{-3} \text{ mol/L NH}_4^+$ ,  $615 \times 10^{-3} \text{ mol/L Cl}^-$ , and  $26 \times 10^{-3} \text{ mol/L Na}^+$ . Note that the concentration of  $\text{Na}^+$  in diluted bittern is sufficiently low and can be tolerated by some plant species, such as beets.<sup>165, 173</sup> DD experiments were conducted using simulated aqueous potash solutions (APS), WWSRR, and DB, with the ASVN membrane, simulated fresh urine as FS, and  $V_{\text{FS}}/V_{\text{RS}}$  of 1. Figure 3.8 presents fluxes of  $\text{H}_x\text{PO}_4^{(3-x)-}$  and  $\text{SO}_4^{2-}$  from FS to RS.

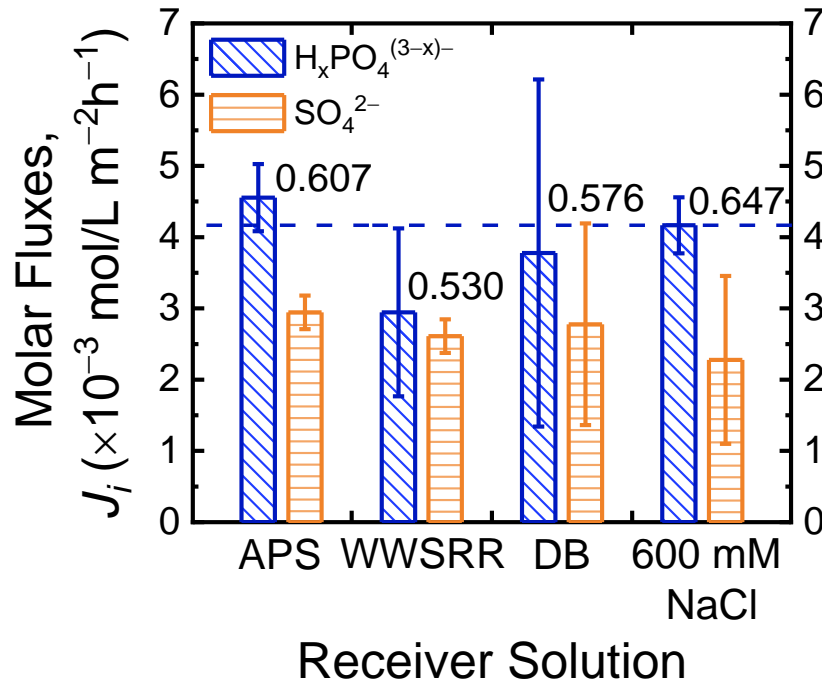


**Figure 3.8.** Fluxes of  $\text{H}_x\text{PO}_4^{(3-x)-}$  and  $\text{SO}_4^{2-}$  (blue and orange columns, respectively) in kinetic experiments with different initial receiver solutions of simulated aqueous potash solution (APS,  $[\text{Cl}^-] = 600 \times 10^{-3} \text{ mol/L}$ ), simulated waste water softening regenerant rinse, (WWSRR,  $[\text{Cl}^-] = 643 \times 10^{-3} \text{ mol/L}$ ), and simulated diluted bittern (DB,  $[\text{Cl}^-] = 615 \times 10^{-3} \text{ mol/L}$ ). Fluxes with RS of  $600 \times 10^{-3} \text{ mol/L NaCl}$  are included for comparison. For all experiments simulated fresh urine was used as the FS and  $V_{\text{FS}}/V_{\text{RS}} = 1$ . Labels above the  $\text{H}_x\text{PO}_4^{(3-x)-}$  columns denote the selectivity for orthophosphate,  $J_p/J_T$ . Horizontal line is orthophosphate flux in DD with  $600 \times 10^{-3} \text{ mol/L NaCl}$ . Data points and error bars are means and standard deviations, respectively, of duplicate experiments.

In general,  $J_P$  (and  $J_S$ ) of the different simulated receiver solutions are comparable with the  $600 \times 10^{-3}$  mol/L NaCl RS. Similar  $J_P$  are expected because all operations utilized the same FS and have fairly similar  $[Cl^-]_{RS,0}$  (< 7% difference). Importantly, DD with the monovalent ion selective membrane (ASVN) consistently achieved selectivity for  $H_xPO_4^{(3-x)-}$  flux over  $SO_4^{2-}$  for all the simulated receiver solutions ( $J_P/J_T = 0.53$ – $0.61$ ). This highlights the flexibility of DD to utilize different  $Cl^-$ -rich streams, including waste and low-cost sources, as the receiver solution for orthophosphate recovery from fresh urine.

### 3.5 Implications

The current P management practices are unsustainable. Phosphate is mined and processed from diminishing reserves at immense energy costs. P-rich excretions are heavily diluted in the traditional wastewater system, which contributes to the high energy and chemical expenditures in efforts to remove the phosphates from wastewaters. When not adequately removed, P is released into the environment, causing ecological harm and public health concerns. Further compounding to these issues are environmental problems associated with phosphate fertilizer manufacturing, in particular, the radioactive byproducts that are generated. Improper storage and management of the radioactive wastes pose leakage risks.<sup>11, 12</sup> These hazards were starkly exposed in March 2021 when the Piney Point, Florida, production plant leaked radioactive phosphogypsum into Tampa Bay because of an engineering failure in the aged infrastructure. Residents of the surrounding area were evacuated due to risks of contact with the contaminated waters.<sup>12</sup> The inefficient linear economy approach and this unfortunate incident underscore the need for a paradigm shift to a circular P economy with sustainable phosphate capture and reuse.

The high concentrations of orthophosphate anion in human urine offer propitious opportunities for recovery. Donnan dialysis can utilize driver ions to exchange for  $H_xPO_4^{(3-x)-}$  in

the urine feed, capturing P in the receiver solution for application as fertilizer. This study demonstrates that Donnan dialysis can i) recover orthophosphate from urine, ii) enrich orthophosphate in the receiver solution, iii) selectively capture orthophosphate over other anions by utilizing fresh urine and monovalent ion permselective membranes, and iv) leverage on widely available and low-cost/waste resources to drive orthophosphate recovery. Importantly, using receiver streams with adequately high driver ion concentrations in DD ( $\text{Cl}^-$  in this study) can enable orthophosphate transport against a concentration gradient and attain “uphill transport” to reach practically feasible recovery yields (> 80% demonstrated in this investigation). By employing a smaller receiver solution volume relative to the feed, DD can achieve enrichment of orthophosphate, i.e., P concentration in the product is higher than in fresh urine. A fertilizer product with high orthophosphate concentrations is of greater economic value and additionally facilitates transportation. The analysis also reveals the rationale for using fresh, rather than hydrolyzed urine, for P recovery. Specifically, the high bicarbonate content of the latter source is detrimental to orthophosphate flux and selectivity. This indicates that DD orthophosphate recovery should be performed immediately after urine diversion and collection, prior to urea hydrolysis. Alternatively, dosing with inhibitory compounds, electrochemical treatment, or acid/base addition can inactivate the urease enzyme,<sup>89,90,174-179</sup> thus suppressing bicarbonate formation. Besides bicarbonate, sulfate can compete with orthophosphate anions to exchange with driver chloride ions, hence reducing recovery efficiency. The study highlights the applicability of using monovalent ion permselective membrane to drive more selective transport of orthophosphate over sulfate. However, the improvements in selectivity are at the cost of decreased kinetics. Therefore, the overall DD process would need to simultaneously consider TOP recovery yields and membrane requirements, i.e., tradeoffs between with economic benefits with capital and operating costs. Thoughtful selection

of the receiver stream offers flexibility in tailoring the water chemistry and nutrient profile of the fertilizer product. Critically, economic viability of P recovery with DD can be enhanced by utilizing waste/low-cost streams as the receiver solution. For example, waste water softening regenerant rinse generated in residential buildings can be repurposed to supply the high chloride concentrated needed in the receiver solution, to drive DD recovery of orthophosphate from diverted urine from the same premises.

The insights from this study are broadly applicable to other DD processes for resource recovery or contaminant removal, particularly for streams with multiple anions and/or cations. Some examples are  $\text{NH}_4^+$  recovery from wastewater, metal ion recovery from electroplating rinse, and removal of  $\text{NO}_3^-$  and  $\text{H}_x\text{AsO}_4^{(3-x)-}$  from drinking water. The approach for determining ion concentrations in feed and receiver solutions at Donnan equilibrium presented here, eqns (B.9)–(B.13), can be utilized to project target ion recovery potential or contaminant removal efficiency from mixed electrolyte solutions. Furthermore, the systematic analysis of factors influencing fluxes of different ions underscores the role of competitive ion sorption on transport kinetics and can elucidate ion transport behavior in solutions with complex compositions. In applications where multivalent species are present together with the monovalent target ion, as in  $\text{NH}_4^+$  recovery from wastewater or  $\text{NO}_3^-$  removal from drinking water, MIPMs may be useful to improve selectivity for the target species with an acceptable sacrifice in permeation flux.

## **Chapter 4: Novel Isothermal Membrane Distillation with Acidic Collector for Selective and Energy-Efficient Recovery of Ammonia from Urine**

### **Chapter Abstract**

The high concentration of ammonia in source-separated urine offers propitious opportunities for N recovery. Membrane distillation (MD) can recover volatile ammonia from hydrolyzed urine, but conventional operation suffers from the simultaneous permeation of water vapor that results in poor selectivity for ammonia transport and high energy demand. Here, we present a novel operation of MD — *isothermal* membrane distillation with *acidic collector* (IMD-AC) — to overcome the limitations of conventional MD. The innovative isothermal operation, i.e., same feed and collector temperatures, effectively suppressed water vapor permeation while maintaining ammonia vapor flux and, thus, significantly improved selectivity for ammonia transport. The acidic collector further enhanced ammonia vapor flux by an average of 46.5% compared to using a deionized water collector. Against a total ammoniacal nitrogen concentration gradient, i.e., uphill transport, ammonia recovery of  $\approx 60\%$  was attained, highlighting the prospect of the technology for high-yield recovery. Critically, IMD-AC achieved approximately 95% savings in vaporization energy consumption relative to conventional MD by practically eliminating the evaporation of water. The resultant energy requirement of  $\approx 2.2$  kWh/kg-N is less than the Haber-Bosch process for N fixation and N removal by nitrification-denitrification (8.9-19.3 and 2.3-6.5 kWh/kg-N, respectively). This study shows the promising potential of IMD-AC for the selective and energy-efficient recovery of ammonia from source-separated urine.

## 4.1 Introduction

Management of nitrogen, an essential nutrient for life, has been recognized by the National Academy of Engineers as one of the Grand Challenges.<sup>180</sup> As elucidated in Chapter 1, the current practices of N production, consumption, and disposal are unsustainable.<sup>24</sup> Of particular concern are the energy-intensive and costly practices for industrial N fertilizer production and N removal from wastewater at centralized wastewater treatment plants (WWTPs). Nitrogen is fixed from the atmosphere through the energy-intensive Haber-Bosch process, requiring 8.9-19.3 kWh/kg-N, which accounts for  $\approx$ 1-2% of the world's energy use.<sup>6, 181, 182</sup> Downstream, conventional N removal by nitrification-denitrification at WWTPs demands 2.3-6.5 kWh/kg-N.<sup>48, 183-185</sup> For the reasons outlined in Chapter 1, the current linear economy approach is clearly untenable and a new paradigm for sustainable nitrogen management is urgently needed.<sup>131, 186, 187</sup>

Nitrogen in anthropogenic wastewaters can be recovered to promote a more sensible circular economy model. Approaches that separate N from WWTP wastewater for reuse were explored,<sup>81, 188-192</sup> but progress is thwarted by low recovery yields and high energy and chemical expenses of these techniques.<sup>193</sup> For instance, ammonia recovery from wastewater by precipitation of phosphate-based minerals is typically limited to only  $\approx$ 5-15% yield,<sup>81, 191</sup> and energy demand of N recovery methods range from approximately 5 to 18 kWh per kg of N.<sup>48, 81, 194, 195</sup> An underlying reason for the difficulties in implementing practical N harvesting at WWTPs is the inherently low nutrient concentration of the flows.

A more forward-looking approach is to recover N from source-separated urine,<sup>47, 196-198</sup> which contains  $\approx$ 80% of the nitrogen from human excretions.<sup>199-201</sup> Because urine isolated at-source is not diluted by flush water and grey water, the N concentration is two orders of magnitude greater than municipal wastewater, a significantly more favorable condition for separation and

capture as presented in Chapter 2.<sup>47, 69, 197, 198, 200, 202</sup> The N in fresh urine, present as urea ( $\text{CH}_4\text{N}_2\text{O}$ ), hydrolyzes during  $\approx 2-7$  d of storage to form ammoniacal nitrogen ( $\text{NH}_3/\text{NH}_4^+$ ) and bicarbonate.<sup>89</sup>  
<sup>90</sup> Various approaches to extract ammonia,  $\text{NH}_3$ , from urine have been explored, including vacuum distillation, stripping-adsorption, mineral precipitation, ion-exchange, and electrochemical methods.<sup>49, 203-208</sup> However, most efforts thus far have generally fallen short of cost-competitiveness with the Haber-Bosch process because the approaches were prohibitively capital-intensive and/or demanded high operating energy and chemical cost.<sup>47-49, 209, 210</sup>

Membrane distillation (MD), an emergent technology that utilizes low-temperature heat to drive the permeation of volatile compounds across a hydrophobic microporous membrane,<sup>211-213</sup> can take advantage of the intrinsic high volatility of ammonia.<sup>214-216</sup> Most MD studies focused on desalination, i.e., separation of water from saline feed streams,<sup>211-213, 217</sup> but potential of the technique for ammonia separation and recovery were recently investigated.<sup>214-216, 218-237</sup> However, harvesting ammonia from source-separated urine using MD is hampered by the indiscriminating transport of all volatile components, including water. The unavoidable permeation of  $\text{H}_2\text{O}$  along with  $\text{NH}_3$  is undesirable because of the additional energy demand to evaporate water and dilution of the product stream.<sup>218, 219</sup>

In this study, we demonstrate a novel operation of direct contact membrane distillation, termed isothermal membrane distillation with acidic collector (IMD-AC) to overcome the limitations of conventional MD in the separation and recovery of ammonia from simulated urine. The working principles of IMD-AC are first presented and the features differentiating the technique from conventional MD are highlighted. Vapor fluxes of ammonia and water in conventional and isothermal MD are compared, and the selectivity for  $\text{NH}_3$  permeation over  $\text{H}_2\text{O}$  is analyzed. The influence of an acidic solution as the collector stream on  $\text{NH}_3(\text{g})$  transport is

examined. Next, the study evaluated the effects of temperature on IMD-AC performance. Heat energy consumed to vaporize water and ammonia is then quantified to assess the energy savings of IMD-AC over conventional MD. The implications of IMD-AC for ammonia recovery from source-separated urine are discussed, and the potential utilization for other environmental applications are identified.

## 4.2 Isothermal Membrane Distillation with Acidic Collector

**Limitations of Conventional Membrane Distillation for Ammonia Recovery.** Membrane distillation (MD) is a separation process where volatile compounds are driven across a hydrophobic microporous membrane while nonvolatile components are retained in the feed stream. Working principles of MD are detailed in literature,<sup>211, 212</sup> and are briefly explained here with specific focus on ammonia recovery. In the conventional operation of direct contact MD, the feed stream is at a higher temperature than the permeate, or sweep/collector, stream, i.e.,  $T_F > T_C$  (subscripts F and C denote feed and collector streams, respectively). Because partial vapor pressure of volatile component  $i$ ,  $P_i$ , is exponentially dependent on the solution temperature, as described by the Clausius-Clapeyron relation,<sup>238</sup> the temperature difference sets up a vapor pressure gradient between the feed and collector sides at the solution-membrane interfaces. The transmembrane vapor pressure difference,  $P_{F,i} - P_{C,i}$  (subscripts F and C denote feed and collector sides, respectively), is the driving force for the compound to volatilize from the feed solution, permeate across the membrane, and eventually condense in the collector stream. Vapor flux of component  $i$ ,  $J_i$ , is described by eqn (4.**Error! Reference source not found.**):<sup>212</sup>

$$J_i = L_i (P_{F,i} - P_{C,i}) \quad (4.1)$$

where membrane vapor permeability coefficient,  $L_i$ , characterizes the transport of compound  $i$  per unit driving force and is dependent on the vapor molecule, membrane structural properties and membrane chemistry, feed and collector compositions, as well as operating conditions, such as temperature.<sup>211-213</sup>

Although MD is primarily employed for water recovery from saline feed streams, i.e., desalination,<sup>211, 212, 239</sup> the technique can also be used to separate volatile compounds, including ammonia, from aqueous solutions.<sup>214-216, 232, 240</sup> However, using conventional membrane distillation (CMD) for ammonia separation also unavoidably also vaporizes water, resulting in simultaneous permeation of water vapor together with  $\text{NH}_{3(g)}$  flux (Figure 4.1A). The indiscriminate transport of water limits the effectiveness of conventional MD in applications where selective permeation of one volatile component is desired. For  $\text{NH}_3$  recovery from urine, the incidental water vapor flux,  $J_w$ , unfavorably dilutes the ammonia concentration of the product (i.e., collector stream effluent).<sup>241</sup> More importantly, because evaporating water is very energy intensive (enthalpy of vaporization  $\approx 630 \text{ kWh/m}^3$ ), the concomitant  $J_w$  would detrimentally raise the thermal energy input required for the overall process. Note that column distillation is similarly encumbered by the disadvantage of inevitable water evaporation.

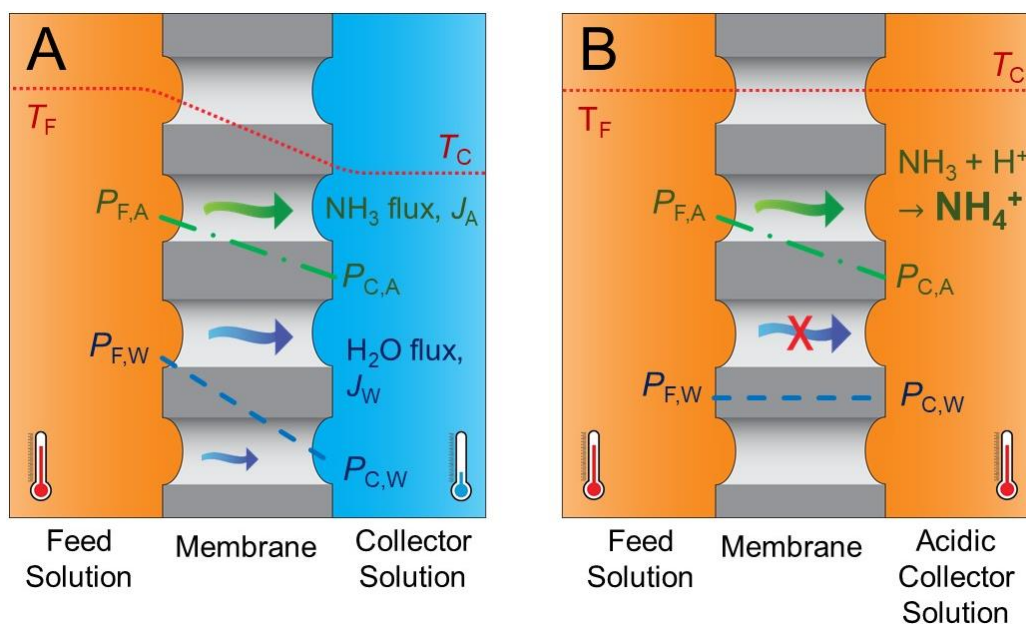


**Figure 4.1.** Temperature and vapor pressure profiles for A) conventional and B) isothermal MD with acidic collector. The temperature difference between the solution-membrane interfaces in CMD establishes a water vapor pressure gradient from feed to collector side, thus driving water vapor flux,  $J_W$  (blue arrow). Whereas the driving force for  $J_W$  is effectively zero in IMD, because the identical solution temperatures set up a constant water vapor pressure across the membrane. As  $NH_{3(g)}$  vapor pressure is linearly proportional to ammonia concentration in the aqueous solution (Henry's law), both CMD and IMD exhibit a gradient for ammonia vapor pressure from feed to collector side, thus driving  $NH_{3(g)}$  permeation,  $J_A$  (green arrows). Permeated  $NH_3$  that solubilizes in the acidic collector solution associates with  $H^+$  to form nonvolatile  $NH_4^+$ .

**Working Principles of Isothermal Membrane Distillation with Acidic Collector.** To overcome the limitations of conventional MD for separating volatile compounds from aqueous solutions, specifically the recovery of ammonia from hydrolyzed urine, we introduce *isothermal* membrane distillation (IMD), where the feed and collector streams are at the same temperature, i.e.,  $T_F = T_C$ . Note that the main form of nitrogen in fresh, i.e., unhydrolyzed urine, is urea,  $CO(NH_2)_2$ , which has a very low Henry's Law constant; urea undergoes hydrolysis by urease enzymes naturally present in urine to form bicarbonate and volatile ammonia, eventually yielding hydrolyzed urine,<sup>200</sup> i.e., MD is not applicable to fresh urine for N recovery. The equivalent temperature on both sides effectively eliminates the partial  $H_2O$  vapor pressure gradient, thus

ceasing the driving force for water vapor transport. Partial vapor pressure is linearly proportional to concentration of the volatile component in aqueous solution,  $c_i$ , as governed by Henry's and Raoult's laws (determination of vapor pressure of solutions of different composition and temperature is detailed in Appendix C.1).<sup>242</sup> Therefore for ammonia (and other volatile compounds), a driving force for permeation from feed to collector subsists for  $c_{F,A} > c_{C,A}$  (subscript A indicates ammonia,  $\text{NH}_3$ ), even when temperature profile across the membrane is flat, i.e., unlike conventional MD operation (Figure 4.1B). Critically, by curbing  $J_w$ , IMD avoids the heat energy input required to evaporate water that is unpreventable in conventional MD.

In the isothermal operation of MD, ammonia vapor permeates from feed to collector side when there is an  $\text{NH}_{3(\text{aq})}$  concentration gradient between the aqueous solutions, i.e.,  $c_{F,A} - c_{C,A} > 0$ . But as more ammonia is separated from the feed stream and captured in the collector stream,  $c_{F,A}$  decreases while  $c_{C,A}$  increases, thus gradually diminishing the driving force for ammonia vapor flux,  $J_A$ , eqn (4.1). Eventually ammonia recovery ceases as  $\text{NH}_{3(\text{aq})}$  concentration of the collector approaches the feed solution. To address this constraint, a second feature of acidic collector (AC) is incorporated to promote the speciation of volatile ammonia,  $\text{NH}_3$ , in the collector stream to ionic ammonium,  $\text{NH}_4^+$ , which is nonvolatile.<sup>214, 215, 218-231</sup> A weak acid in the collector solution maintains a low pH that is below the  $\text{p}K_A$  of ammonia (between 9.4 and 8.3 for solution temperatures of 20-60 °C),<sup>243</sup> effectively converting all  $\text{NH}_3$  that has permeated over to the collector to  $\text{NH}_4^+$  (Figure C.1 of Appendix C). Therefore,  $\text{NH}_{3(\text{aq})}$  concentration of the collector stream is practically negligible, i.e.,  $c_{C,A} \approx 0$ , even though the total ammoniacal nitrogen,  $\text{NH}_3 + \text{NH}_4^+$ , concentration increases. Therefore, a positive driving force for  $J_A$  is always sustained, i.e.,  $P_{F,A} - P_{C,A} > 0$ . Overall, the isothermal and acidic collector features of IMD-AC can, respectively, suppress the undesirable permeation of water vapor, thus reducing the heat energy

required to vaporize water, and eliminate the partial vapor pressure of ammonia in the collector solution, to maximize the driving force for  $\text{NH}_3$  flux and enable high recovery yields.

### 4.3 Experimental Section

**Materials and Chemicals.** Commercial microporous hydrophobic polyvinylidene fluoride (PVDF) membrane of 0.22  $\mu\text{m}$  pore-size, GVHP14250, was acquired from MilliporeSigma (Burlington, MA) and utilized for all membrane distillation experiments. The simulated urine feed solution comprised 250 mM ammonium hydroxide and 250 mM ammonium bicarbonate in deionized (DI) water from a Milli-Q ultrapure water purification system (MilliporeSigma), to mimic the total ammoniacal concentration and pH of hydrolyzed urine.<sup>47, 197, 198, 200, 201</sup> DI water was used for the collector stream in non-acidic MD experiments. To prepare the acidic collector solution, acetic acid was diluted in DI water. All chemicals utilized in the experiments are analytical grade and were purchased from ThermoFisher Scientific (Waltham, MA).

**Ammonia Separation and Recovery Experiments.** Ammonia and water vapor fluxes were evaluated in four different operating modes: conventional membrane distillation with DI water collector (CMD-DI), conventional MD with acidic collector (CMD-AC), isothermal MD with DI water collector (IMD-DI), and isothermal MD with acidic collector (IMD-AC). I.e., the parameters assessed are collector stream composition (DI water or acid) and conventional versus isothermal operation. Simulated hydrolyzed urine was consistently utilized as the feed solution. For CMD-AC and IMD-AC operations, 100 mM acetic acid was employed as the collector solution. In the conventional MD experiments, a 20 °C temperature differential was applied, with the feed and collector streams maintained at 40 and 20 °C, respectively. In the comparison analysis, the feed and collector streams of isothermal MD were operated at the same temperature of 40 °C (i.e., same temperature as feed solution of CMD). To investigate the effect of temperature on

performance, IMD-AC was additionally operated with  $T_F = T_C$  at 20, 30, 50, and 60 °C. Volume of the feed and collector solutions are approximately 2.0 L each.

All experiments were conducted in a bench-scale MD unit (Figure C.2 of Appendix C). The feed and collector streams were circulated countercurrently at crossflow velocities of 22.2 cm/s and 20.0 cm/s, respectively, across the active membrane area of 19.0 cm<sup>2</sup> in a custom-built membrane cell.  $T_F$  and  $T_C$  were regulated with heated and refrigerated circulators (PolyScience, Warrington, PA), respectively, through heat exchangers. Temperatures at the inlet and outlet of the membrane cell on the feed and collector sides were monitored using thermocouples (Omega Engineering, Norwalk, CT) and the solution within the cell is maintained within  $\pm 1.5$  °C of the target temperature throughout all experimental runs.

Ammonia vapor flux was determined from the rate of change of total ammoniacal nitrogen (TAN =  $\text{NH}_3 + \text{NH}_4^+$ ) in the collector stream. Four 1 mL samples were taken every 15 min, and TAN concentrations were measured following the Indophenol blue method.<sup>244</sup> Ammonia salicylate and ammonia cyanurate reagent powder were added in excess to DI water-diluted samples and analyzed using a calibrated colorimeter (ThermoFisher Scientific). The change in moles of ammonia over time normalized by the membrane area yields  $J_A$ . Additionally, pH of the collector stream was measured during sampling with a pH Meter (Orion Star, ThermoFisher Scientific). Water flux was calculated as the average rate of change in the feed and collector solution weights normalized by membrane area, accounting for the transferred ammonia and evaporative loss from bulk solution tanks. The change in weight of the feed and collector bulk solution tanks were automatically logged every 10 seconds using digital microbalances (AX5202, Ohaus, Parsippany, NJ).

To demonstrate the potential of IMD-AC for high-recovery of ammonia, an isothermal MD experiment was conducted at 40 °C with the feed and collector solutions at the same initial ammoniacal nitrogen concentration. The feed solution was simulated urine (i.e., 500 mM TAN), while the collector solution composition was 750 mM acetic acid and 500 mM ammonium chloride (a higher acetic acid concentration than the earlier described experiments was employed to ensure collector stream pH was maintained sufficiently lower than the  $pK_a$  of ammonia throughout the experiment duration). The experimental run was conducted for 6 h, with ammonia concentrations in the collector stream measured every 1.5 h.

#### 4.4 Results and Discussion

**Higher Ammonia Selectivity is Achieved using Isothermal MD.** Figure 4.2 shows ammonia and water vapor fluxes (green patterned columns, left vertical axis and blue solid columns, right vertical axis respectively) under CMD and IMD operation with DI water and acidic collector. For the same collector solution of DI water,  $J_A$  was practically consistent between conventional and isothermal MD (9.25 molm<sup>-2</sup>h<sup>-1</sup> for CMD-DI and 9.47 molm<sup>-2</sup>h<sup>-1</sup> for IMD-DI). At 40 °C, pH of the simulated urine feed solution is 8.8 whereas  $pK_a = 8.8$  and, thus, volatile  $NH_{3(aq)}$  and  $NH_4^+$  are of approximately equal concentrations ( $\approx 250$  mM). Isothermal operation of direct contact MD did not affect  $NH_{3(g)}$  transport as the driving force for ammonia vapor permeation,  $P_{F,A} - P_{C,A}$ , is essentially equal for IMD and CMD (excluding temperature polarization effects, which will be discussed later) because the feed composition and temperature were held constant and ammonia concentration in the collector is negligible throughout the relatively short experiment duration. A comparison between CMD-AC and IMD-AC also presented minimal difference in  $J_A$  (13.5 and 13.9 molm<sup>-2</sup>h<sup>-1</sup>, respectively), further validating that ammonia vapor flux is not affected by

warming the collector stream to  $T_F$  for isothermal MD operation. Effect of acidic collector on ammonia vapor fluxes is discussed in the next section.

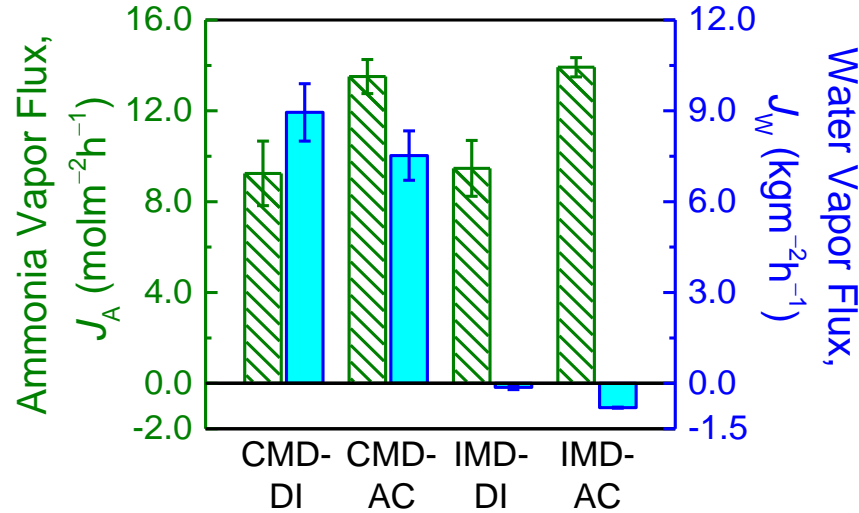


**Figure 4.2.** Ammonia and water vapor fluxes for four different MD operations: CMD-DI with 40 °C feed and 20 °C DI water collector, CMD-AC with 40 °C feed and 20 °C acidic collector, IMD-DI with 40 °C feed and 40 °C DI water collector, and IMD-AC with 40 °C feed and 40 °C acidic collector. The feed stream for all scenarios is simulated solution of hydrolyzed urine (250 mM  $\text{NH}_4\text{OH}$  and 250 mM  $\text{NH}_4\text{HCO}_3$ ), whereas acidic collector is 100 mM acetic acid. The green patterned columns correspond to ammonia vapor fluxes (left vertical axis) and the blue solid columns denote water vapor fluxes (right vertical axis). Error bars indicate standard deviations of duplicate experiments with different membrane coupons.

In contrast to ammonia vapor permeation, water vapor fluxes were drastically different between IMD and CMD operation. Under CMD operation, water flux in the direction of feed to collector was significant, measuring 8.9 and 7.5  $\text{kg m}^{-2} \text{h}^{-1}$  with DI water and acidic collector, respectively. The imposed 40-20 °C temperature differential in CMD set up a water vapor pressure gradient across the microporous membrane, which drove water vapor permeation from the feed to the collector side. On the other hand,  $J_w$  in IMD is markedly suppressed by over an order of magnitude to 0.13 and 0.80  $\text{kg m}^{-2} \text{h}^{-1}$  for DI water and acidic collector, respectively. Elevating  $T_C$  to match  $T_F$  in isothermal operation raised the water vapor pressure at the collector side to  $\approx P_{F,w}$

(Figure 4.1B). Note that the effect of solution composition (i.e., DI water or 100 mM acetic acid) on partial vapor pressure is negligible relative to the influence of temperature. The driving force for  $J_W$  is, therefore, effectively eliminated in IMD-DI and IMD-AC, i.e.,  $P_{F,W} - P_{C,W} = 0$ , and  $H_2O$  transport was almost fully inhibited, eqn (4.1).

Direction of the diminished  $J_W$  for IMD is opposite to CMD, i.e., water vapor permeated from collector to feed side (indicated as negative fluxes in Figure 4.2). The reversed water vapor flux is attributed to temperature polarization at the solution-membrane interfaces producing a slight local transmembrane temperature gradient toward the feed side. In  $NH_3$  transport, ammonia volatilizes from the feed stream at the membrane interface, permeates across the membrane, and solubilizes in the collector solution. These phase-changes necessary for  $NH_3$  transport in MD inevitably cools the feed and warms the collector solutions near the membrane surface, a phenomenon termed temperature polarization.<sup>245-247</sup> Hence, even though the bulk solution temperatures are similar in IMD, there is a water vapor pressure gradient from collector to feed side, i.e.,  $P_{C,W} > P_{F,W}$ , yielding negative  $J_W$  (illustrated in Figure C.3 of Appendix C). Temperature polarization likewise occurs in CMD, but the bulk solution temperature difference overwhelms the local deviations. Thus,  $P_F > P_C$  and water and ammonia vapor fluxes are always positive, i.e., from feed to collector side.

For the separation and recovery of ammoniacal nitrogen from hydrolyzed urine, high ammonia vapor permeation and minimal water vapor flux is desired to minimize energy required for vaporization enthalpy and limit watering down of the product (i.e., collector stream effluent). That is, selective transport of  $NH_3$  over  $H_2O$  is advantageous. Figure 4.3 presents the relative molar flux of water to ammonia for the four operating conditions, with a lower  $J_W/J_A$  signifying better selectivity for ammonia transport. The magnitude of  $J_W/J_A$  for conventional operation is

significantly higher than the isothermal processes (negative values for IMD reflect the reversed direction of water vapor permeation). For every mole of ammonia volatilized from the feed stream, 54 and 31 moles of water are simultaneously evaporated in CMD-DI and CMD-AC, respectively, underscoring that thermal energy input for vaporization enthalpy is predominantly consumed for H<sub>2</sub>O and not the intended NH<sub>3</sub> (detailed energy analysis is presented in a later section). The poor selectivity of CMD is attributed to the concentration of water being about 100× higher than ammonia in the simulated urine stream ( $\approx 55.5$  mol-H<sub>2</sub>O/L compared to 0.5 mol-NH<sub>3</sub>/L), overwhelming the effect of greater volatility of ammonia than water. The transport of water in isothermal MD was suppressed by up to 68× compared to conventional operation ( $-0.803$  and  $-3.02$  mol-H<sub>2</sub>O/mol-NH<sub>3</sub> for IMD-DI and IMD-AC, respectively), highlighting the enhanced selectivity of IMD for ammonia separation and recovery. The relative vapor flux in kg-H<sub>2</sub>O/mol-NH<sub>3</sub> is presented in Figure C.4 of Appendix C.

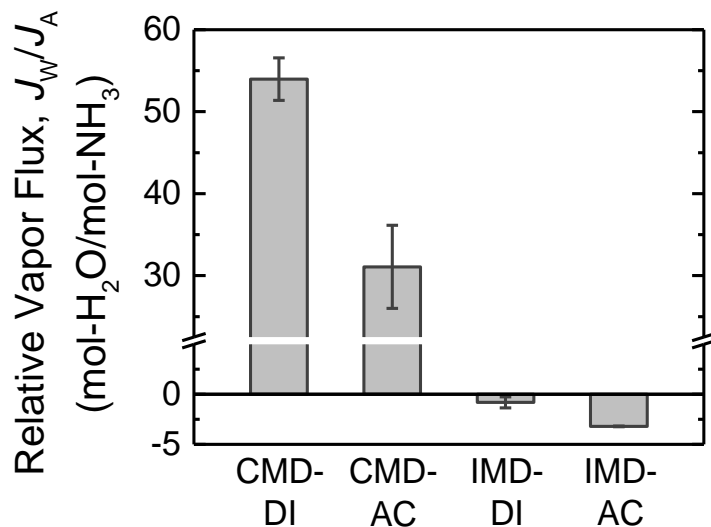


**Figure 4.3.** Relative molar flux of water to ammonia for the four operations, CMD-DI, CMD-AC, IMD-DI, and IMD-AC. IMD-DI and IMD-AC exhibit negative relative fluxes because water vapor permeation was in opposite direction, from collector to feed side. Error bars indicate standard deviations of duplicate experiments with different membrane coupon.

**Acidic Collector Enhances Ammonia Vapor Flux.** Under acidic collector operation, CMD-AC and IMD-AC, ammonia vapor fluxes were, on average, 46.5% higher than with DI water, CMD-DI and IMD-DI (green patterned columns, left vertical axis of Figure 4.2). As ammonia permeates from feed to collector, pH of the collector rose above 10 when DI water is used, but remained below 4 with acetic acid as collector (Figure C.5). At solution temperatures of 20 and 40 °C,  $pK_A$  of  $NH_{3(aq)}$  is 9.4 and 8.8, respectively. Consequentially, ammoniacal nitrogen is predominantly in the form of ammonia,  $NH_{3(aq)}$ , in DI water collector, whereas ammonia protonates to nonvolatile ammonium,  $NH_4^+$ , in the acidic collectors.

Because ammonia present in the DI water collector exhibits vapor pressure, i.e.,  $P_{C,A} > 0$ , the driving force for  $NH_3$  permeation,  $P_{F,A} - P_{C,A}$ , is lowered. However, vapor pressure generated by  $NH_{3(aq)}$  in the DI water collector is marginal and, hence, does not fully account for the difference in  $J_A$  between DI water and acidic collector. At the end of the hour-long experiments, ammonia concentration in the collector only reached 8.43 mM and 8.66 mM for CMD-DI and IMD-DI, respectively, equivalent to a reduction in ammonia vapor pressure gradient of 1.5 and 3.8% (drop for isothermal operation is higher because the collector stream is at 40 °C, as opposed to 20 °C for conventional operation). In contrast, the decrease in ammonia vapor fluxes when the collector is DI water instead of acetic acid was 31.6% and 32.0% for CMD and IMD, respectively. Therefore, the slight decline in  $P_A$  gradient when TAN is present as  $NH_{3(aq)}$  does not adequately explain the considerably smaller  $J_A$  with DI water collector.

An increase in ammonia vapor flux when acidic solutions were utilized as collector had been reported,<sup>219, 248</sup> but the mechanism was not discussed. We postulate that the  $J_A$  enhancement is due to the acidic solution improving the kinetics of ammonia vapor dissolution into the aqueous phase. At the collector side vapor-liquid interface, some ammonia molecules incident on the liquid

surface are reflected back into the vapor phase, i.e., condensation coefficient  $< 1$ ,<sup>249</sup> resulting in the  $\text{NH}_{3(\text{g})}$  solubilization rate being slower than the initial rate of ammonia permeation. The molecular reflection builds up the partial vapor pressure of ammonia at the interface and results in  $P_{\text{C,A}} > K_{\text{HCC,A}}$ , where  $K_{\text{H}}$  is Henry's constant for  $\text{NH}_3$ .<sup>249</sup> That is, the vapor-liquid interface at the collector side is not at thermodynamic equilibrium. When a non-acidic solution, such as DI water, is employed for the collector stream, the ammonia solubilization kinetics is slow and the eventual steady-state effective driving force is considerably lessened due to the elevated interfacial  $P_{\text{C,A}}$ . On the other hand,  $\text{NH}_{3(\text{g})}$  dissolves significantly faster into an acidic solution,<sup>250</sup> i.e., condensation coefficient is increased, giving rise to a larger  $P_{\text{F,A}} - P_{\text{C,A}}$  and yielding markedly enhanced ammonia vapor flux. Therefore, the use of AC beneficially improves ammonia separation and recovery by mitigating the kinetic limitation of ammonia dissolution.

**Ammonia Vapor Flux Increases with Greater Feed Temperature.** To investigate the influence of temperature on IMD-AC performance, ammonia and water vapor fluxes were characterized as a function of feed and collector solution temperature and presented in Figure 4.4 (green square symbols, left vertical axis and blue circle symbols, right vertical axis, respectively). Ammonia vapor flux monotonically increased from 5.60 to 22.8  $\text{molm}^{-2}\text{h}^{-1}$  (approximately 4-fold) as operating temperatures were raised from 20 to 60 °C. Critically, the magnitude of water vapor flux was suppressed to below  $\approx 2 \text{ kgm}^{-2}\text{h}^{-1}$  across the assessed temperature range, substantially smaller compared to  $J_{\text{W}}$  in CMD (blue triangle symbol in Figure 4.4 for feed and collector solutions at 40 and 20 °C, respectively). As discussed earlier, the direction of water vapor permeation in IMD operation is reversed, i.e., from collector to feed side. This reverse water vapor flux increased with increasing temperature. This is because ammonia permeation is enhanced at higher temperatures and, thus, more heat of vaporization was transferred from the feed to collector side,

causing more severe temperature polarization at the solution-membrane interfaces (previously elaborated and illustrated by Figure C.3 of Appendix C). Hence, the transmembrane temperature gradient is more pronounced at higher temperatures, resulting in greater reverse water vapor permeation.

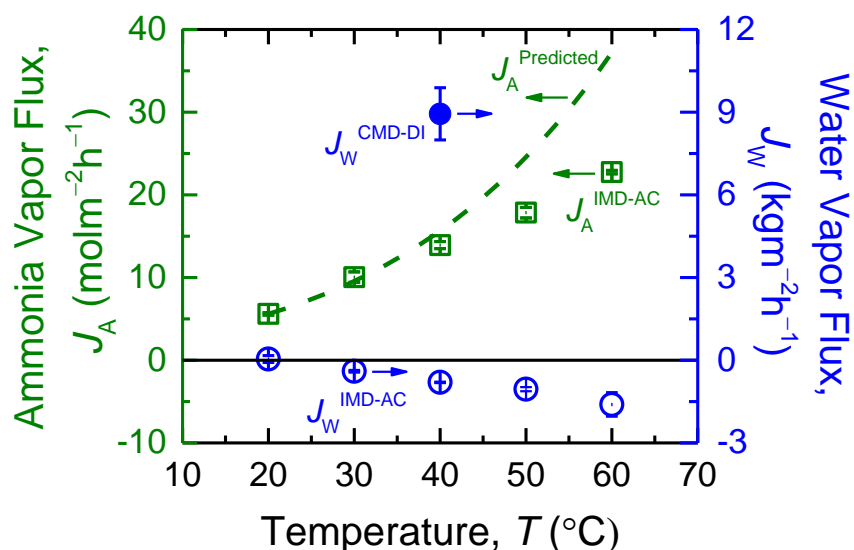


**Figure 4.4.** Experimental IMD-AC ammonia and water vapor fluxes (green square symbols, left vertical axis and blue circle symbols, right vertical axis, respectively) as a function of operating temperature. Predicted ammonia vapor flux, calculated using eqn (4.1) with membrane vapor permeability coefficient at 20 °C ( $L_A = 0.021 \text{ molm}^{-2}\text{h}^{-1}\text{pa}^{-1}$ ), is represented by the green dashed line. For comparison, the water vapor flux in IMD-DI with feed and collector solutions at 40 and 20 °C, respectively, is denoted by the blue triangle symbol. Error bars indicate standard deviations of duplicate experiments with different membrane coupon.

Low relative vapor flux of water to ammonia for IMD-AC was, again, consistently attained across the temperatures investigated (Figure C.6 of Appendix C). Magnitude of relative flux increased slightly with higher temperatures, but was maintained below  $-0.1 \text{ kg-H}_2\text{O/mol-NH}_3$  (marginally positive  $J_W/J_A$  at 20 °C is attributed to inherent experimental uncertainties in measuring very small water fluxes). Crucially, ammonia permeation was obtained with adequate  $\text{NH}_3\text{-H}_2\text{O}$  flux selectivity even at the lowest investigated temperature of 20 °C, which is effectively

ambient condition. Hence, the separation and recovery of ammonia from hydrolyzed urine can potentially be achieved, albeit at slower rates, without heating the feed and collector streams to elevate the temperatures.

With negligible  $\text{NH}_{3(\text{aq})}$  concentration in the collector stream, the higher vapor pressure of ammonia at the feed side due to the greater solution temperature results in an augmented driving force for  $\text{NH}_{3(\text{g})}$  permeation. However,  $J_A$  enhancements with increasing temperature is poorly predicted by the governing flux equation, eqn (4.1), and the Clausius-Clapeyron relation. Using the ammonia vapor pressure gradient at each temperature and membrane vapor permeability coefficient at 20 °C ( $L_A = 0.022 \text{ molm}^{-2}\text{h}^{-1}\text{Pa}^{-1}$ ), ammonia vapor fluxes were computed and shown in Figure 4.4 as the green dashed line. Theoretical calculations overestimate the experimental ammonia vapor fluxes, with greater deviations observed at higher temperatures. Theory forecast an exponential increase in  $J_A$  with rising temperature, due to the exponential dependence of vapor pressure on temperature, but an effectively linear increase in experimental ammonia vapor flux was seen.

One potential explanation for the experimental deviation from expected trend is kinetic limitations for ammonia solubilization into the collector solution (as discussed in the preceding section) being more pronounced at higher temperatures. Alternatively/additionally,  $\text{NH}_3$  volatilization from the feed solution can be a rate-limiting factor. In the earlier section, we discussed that the liquid and vapor phases at the solution-membrane interfaces are not in equilibrium because ammonia vapor transport across the membrane pores is faster than  $\text{NH}_3$  volatilizing from the feed stream and/or dissolving into the collector stream.<sup>249, 251, 252</sup> Therefore the effective vapor pressures of ammonia at the feed and collector interfaces are lower and higher, respectively, than the equilibrium  $P_A$  as governed by Henry's law, i.e.,  $P_{F,A} < K_{\text{HCF,A}}$  and  $P_{C,A} >$

$K_{HC,A}$ . Given larger ammonia vapor fluxes are obtained at higher IMD operating temperatures, the effect of volatilization and solubilization kinetic limitations is, thus, expected to be more amplified. Consequently, the relative reduction in effective driving force,  $P_{F,A} - P_{C,A}$ , is greater and actual  $J_A$  deviates further from prediction (Figure 4.4).

Another possible cause contributing to the observed disagreement is that water vapor transport in the reverse direction during IMD hinders ammonia permeation. As described by Maxwell-Stefan diffusion, mutual interaction between the  $NH_3$  and  $H_2O$  molecules results in frictional drag on the transport of ammonia by water vapor permeating in the opposite direction.<sup>253-</sup>  
<sup>255</sup> This resistance to  $NH_{3(g)}$  transport scales with the magnitude of reverse  $H_{2O(g)}$  flux. Reverse water vapor transport is greater at higher operating temperatures (blue circle symbols of Figure 4.4) and, hence, the discrepancy between theoretical and experimental fluxes is wider.

A third phenomenon that causes experimental fluxes to diverge from calculated  $J_A$  is temperature polarization.<sup>245, 246</sup> As discussed earlier, although the bulk solution streams are at the same temperature in IMD, a transmembrane temperature gradient is set up from the collector to feed sides (Figure C.3 of Appendix C), due to the transfer of  $NH_3$  volatilization/condensation enthalpy. Interfacial temperature at the feed and collector sides are, hence, lower and higher, respectively, than the bulk solution temperatures. Thus, the effective driving force for ammonia permeation,  $P_{F,A} - P_{C,A}$ , is lesser than the calculated value using bulk solution temperatures. The observed reverse water vapor flux is greater at higher temperatures, indicating that the transmembrane temperature gradient is steeper, i.e., temperature polarization is more acute. Therefore, the deviation between experimental and predicted  $J_A$  is anticipated to be larger with increasing temperatures. This mechanism is supported by previous studies that reported decreased

apparent membrane vapor transport coefficient with higher temperatures, (i.e., temperature polarization effects incorporated into  $L$ ).<sup>211, 213</sup>

**High Ammonia Recovery can be Achieved using IMD-AC.** To investigate the potential ammonia recovery yield achievable with IMD-AC from source-separated urine, a batch experiment was conducted with closed-loop recirculation of the solutions across the bench-scale membrane cell, which equivalently simulates co-current flow configuration in a process-scale membrane module. Feed stream TAN ( $= \text{NH}_3 + \text{NH}_4^+$ ) concentration is 500 mM to represent hydrolyzed urine, whereas collector stream is 750 mM acetic acid (higher concentration was employed to avoid pH increases limiting ammonia transport) and 500 mM TAN, i.e., total ammoniacal nitrogen is equal on both sides. TAN concentration of the feed and collector streams in IMD-AC at 40 °C as a function of time is presented in Figure 4.5 (green circle and square symbols, respectively).

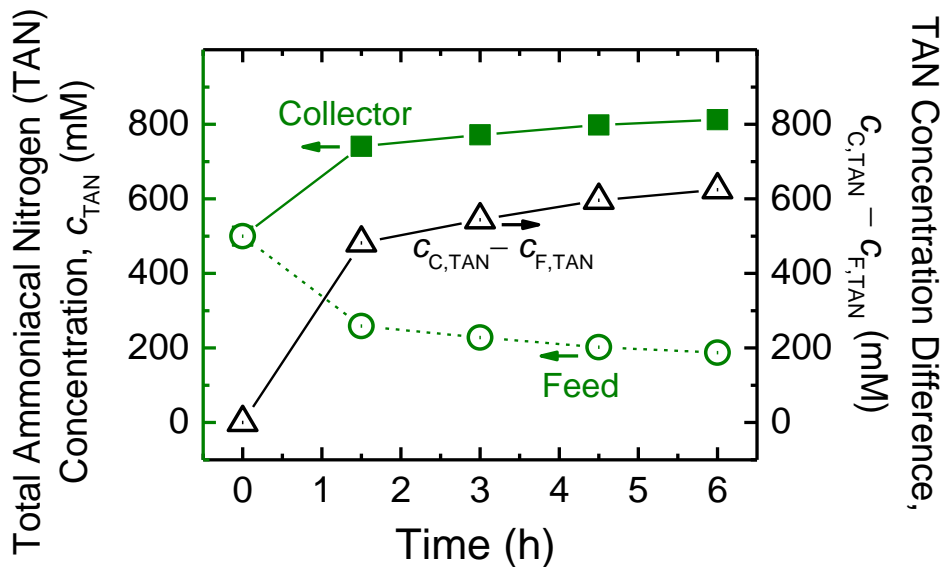


**Figure 4.5.** Total ammoniacal nitrogen, TAN, concentration in the feed and collector streams in IMD-AC operation at 40 °C as a function of time (left vertical axis, green circle and square symbols, respectively). Feed stream has 500 mM TAN to simulate hydrolyzed urine and collector solution is 500 mM TAN and 750 mM acetic acid (i.e., same initial TAN concentrations for both feed and collector

solutions). The black triangle symbols (right vertical axis) represent the difference between the concentration of TAN in the collector and feed streams, i.e.,  $c_{C,TAN} - c_{F,TAN}$ .

After 1.5 h, collector TAN concentration increased to 741 mM while  $c_{F,TAN}$  dropped to 259 mM, representing  $\text{NH}_3$  separation and recovery of 48.2%. Comparatively, TAN recovery in IMD at 40 °C with a DI water collector stream was only 2.7% for the same time period (projected using  $J_A$  of the first 60 min). At the end of 6 h,  $\approx 60\%$  of TAN in the simulated urine was removed and captured in the collector stream, demonstrating the potential for high ammonia recovery using IMD-AC. Water flux was practically negligible and solution volumes are effectively unchanged ( $< 1\%$  difference after 6 h). As ammonia permeates from the feed to collector side, TAN concentration and, correspondingly, volatile  $\text{NH}_{3(aq)}$  concentration of the feed solution decreases. Consequently, ammonia vapor pressure,  $P_{F,A}$ , falls and the driving force for ammonia permeation,  $P_{F,A} - P_{C,A}$ , declines over time, which is evident by the diminishing rate of change of TAN. Final pH of the collector solution is 3.5. Given the  $pK_a$  of ammonia at 40 °C is 8.8, effectively 100% of TAN in the bulk collector solution was present as nonvolatile ammonium,  $\text{NH}_4^+$ . Hence,  $\text{NH}_{3(aq)}$  concentration was negligible, i.e.,  $c_{C,A} \approx 0$ , and ammonia vapor pressure in the collector,  $P_{C,A}$ , is practically zero.

Crucially, the difference in TAN between the collector and feed solutions,  $c_{C,TAN} - c_{F,TAN}$ , increased from 0 to  $\approx 600$  mM (black triangle symbols of Figure 4.5), indicating transport of ammoniacal nitrogen up a concentration gradient. The “uphill” transport of TAN shows IMD-AC can concentrate ammoniacal nitrogen significantly above the initial  $c_{F,TAN}$ . In actual module-scale operation, the feed and collector streams will be circulated in counter-current flow and higher recovery yields of ammonia can be achieved with lower acid concentrations in the collector solution.

**Substantial Energy Saving is Obtained with IMD.** In membrane distillation, thermal energy is required for the vaporization enthalpy of volatile components that permeate across the membrane.<sup>212, 247, 256</sup> Convective heat flux of component  $i$  is the product of the vaporization enthalpy,  $\Delta H_i$ , and the flux,  $J_i$ .<sup>212</sup> Figure 4.6 shows the vaporization energy for ammonia and water (green patterned and blue solid columns, respectively) in the four operating modes. To exclude the influence of different kinetics (i.e., different  $\text{NH}_{3(g)}$  fluxes),  $\Delta H_i J_i$  is divided by  $J_A$  to yield energy per mole of ammonia recovered,  $E_{V,i}$ . Sum of the ammonia and water components gives the net normalized vaporization energy (black patterned columns),

$$\left| \sum E_{V,i} \right| = \left| J_A^{-1} \sum \Delta H_i J_i \right| = \left| \Delta H_A + \Delta H_W J_W / J_A \right|$$

(note that  $J_i$  can be negative and the impact on energy required is discussed later). Determination of enthalpy of ammonia vaporization from an aqueous solution, as opposed to a pure liquid, is presented in Appendix C.2, and  $\Delta H_i$  at the relevant stream temperatures were used in the analysis.<sup>257, 258</sup>

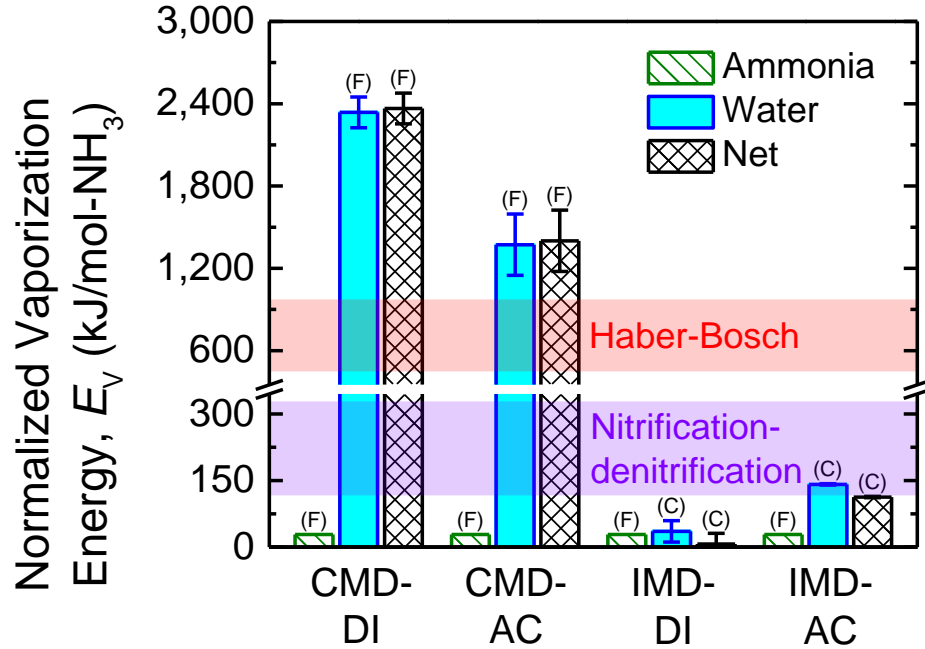


**Figure 4.6.** Vaporization energy for ammonia and water (green patterned and blue solid columns, respectively) per mole of ammonia separated and recovered in CMD-DI, CMD-AC, IMD-DI, and IMD-AC. Labels (F) and (C) above the columns denote heat supply to feed and collector streams, respectively. Patterned black columns represent the net vaporization energies of ammonia and water, i.e.,  $\left| \sum E_{V,(F)} - \sum E_{V,(C)} \right|$ . Error bars for vaporization of water are standard deviations of duplicate water vapor flux measurements. For comparison, the red- and violet-shaded regions indicate energy required by the Haber-Bosch process, 448-973 kJ/mol-NH<sub>3</sub> (8.89-19.3 kWh/kg-N), and nitrification-denitrification, 116-328 kJ/mol-NH<sub>3</sub> (2.3-6.5 kWh/kg-N), respectively.

Whereas normalized energy demand for the vaporization of ammonia,  $E_{V,A}$ , in the four different operating conditions are the same at 28.4 kJ/mol-NH<sub>3</sub> (due to normalization by  $J_A$ ), the heat to vaporize water,  $E_{V,w}$ , varies markedly because it is dependent on the relative vapor flux of water to ammonia (Figure 4.3). In the conventional MD operations of CMD-DI and CMD-AC, considerable thermal energy of 2,340 and 1,370 kJ/mol-NH<sub>3</sub> (46.4 and 27.2 kWh/kg-N), respectively, is required to evaporate water from the feed solution, 82.4 and 48.2× the energy to volatilize ammonia. The high heat input is because of the large magnitude of inevitable water vapor flux in conventional MD. In contrast, due to suppression of water transport in isothermal MD,  $E_{V,w}$  is substantially lessened to 35.4 and 141 kJ/mol-NH<sub>3</sub> (0.702 and 2.80 kWh/kg-N) for IMD-DI and

IMD-AC, respectively. Since direction of  $J_w$  is from the collector to feed side in IMD, i.e., reversed, heat is required for water vaporization at the collector stream (instead of feed side) and is indicated by the label (C). Thermal energy for enthalpy of vaporization is transferred to the other side as enthalpy of condensation when the vapor permeates across the membrane and solubilizes into the aqueous stream. Therefore, the net normalized energy input is the difference between  $E_V$  on the feed and collector sides (black patterned columns). Compared to CMD-DI, IMD-AC requires 95.2% less heat input for vaporization to separate and recover the same amount of ammonia by inhibiting undesired water flux (Figure 4.2). Higher energy savings of 99.7% is achievable with IMD-DI, but  $\text{NH}_3$  recovery yield would be constrained (as discussed in preceding section).

In addition to convective heat flux discussed above, conduction of heat through the membrane is another thermal energy requirement.<sup>256, 259, 260</sup> Conductive heat flux is proportional to the transmembrane temperature differential. Conventional MD necessitates a temperature difference between the feed and collector solutions, whereas the bulk stream temperatures are equal in isothermal MD. Therefore, the temperature gradient across the membrane in IMD is significantly smaller than CMD (Figures 4.1 and C.3) and consequently, conductive heat loss is expected to be minimized in isothermal operation. Moreover, transmembrane heat conduction drives the feed and collector solutions toward temperature equilibrium, which is the working principle of isothermal MD but is against the operation of conventional MD.

Overall, isothermal MD favorably reduces the energy consumption for ammonia removal and reuse by substantially lowering both convective and conductive heat input. Compared to energy demand for the current linear economy management of nitrogen, i.e., production by the Haber-Bosch process and removal by conventional nitrification-denitrification, the vaporization

energy required for  $\text{NH}_3$  recovery in IMD is significantly lower. Energy demand for N fixation by the Haber-Bosch process, the principal ammonia production method, is 8.9-19.3 kWh/kg-N (448-973 kJ/mol- $\text{NH}_3$ , indicated by the red-shaded region in Figure 4.6). Conventional removal of nitrogen by nitrification and denitrification at wastewater treatment plants demands 2.3-6.5 kWh/kg-N (116-328 kJ/mol- $\text{NH}_3$ , indicated by the violet-shaded region). Vaporization energy needed for isothermal MD is around an order of magnitude lower than the Haber-Bosch energy consumption benchmark and is in the same range as nitrification-denitrification. Actual energy requirement for a practical IMD-AC system to remove and recover ammonia from diverted urine will have to factor in auxiliary components (e.g., pumping cost, conductive losses, and heat exchanger efficiency) and module-scale effects, but the first-order energy analysis conducted here highlights potential of the technology to be a competitive alternative to current  $\text{NH}_3$  production and removal methods.

#### **4.5 Implications**

Removal of ammonia from wastewaters is imperative for environmental, ecological, and public health protection. At the same time, nitrogen is a principal component of fertilizer. The high ammonia content in urine offers attractive opportunities to simultaneously recover the resource and remove the contaminant from the waste stream. To align with the principles of green engineering and realize viable implementation, the ammonia separation and recovery approach needs to be energy-efficient.<sup>196</sup> This study demonstrates isothermal membrane distillation with acidic collector can achieve i) selective removal and capture of ammonia from hydrolyzed urine with ii) low thermal energy requirements and iii) high recovery yield.

Importantly, because only mild temperatures are needed to drive the process, isothermal MD can utilize low-grade heat from locally-available waste flows (e.g., warm bathwater runoff or

hot stream of cooling water systems) or onsite low-concentration solar thermal collectors,<sup>59-61</sup> further enhancing sustainability of the technology. The study also showed that ammonia separation and recovery is possible even at ambient temperatures, i.e., without further warming up the feed and collector streams, at the expense of lower fluxes. Acid for the collector solution can be from unwanted effluent streams, such as spent pickling brine, which is effectively vinegar (i.e., acetic acid), from the food industry.<sup>261, 262</sup> This study examined the use of acetic acid, but other suitable acids from waste/low-cost sources can be employed. Additionally, IMD-AC can drive the uphill transport of ammoniacal nitrogen to achieve highly concentrated  $\text{NH}_3$  solutions as product, favorably minimizing the liquid volume for handling and transport. Crucially, vaporization energy requirement for isothermal MD is substantially below the energy demand for fossil fuel-driven Haber-Bosch process, the dominant ammonia production method, and comparable to energy consumption for N removal at conventional WWTPs. Further techno-economic assessments are needed to quantify the capital and operating expenditure of IMD-AC, but the technology shows initial promise to be a cost-competitive and environmentally-sensible technique for removing and recovering ammonia from source-separated urine.

With the projected urban influx of 2.5 billion people by 2050,<sup>263</sup> the population density of cities is expected to increase dramatically. At the same time, providing improved sanitation to the 2.3 billion people globally who are currently unserved will necessitate the installation of new toilets, wastewater facilities, and sanitation infrastructure.<sup>264</sup> These population and sanitation trends present ideal opportunities for the introduction of decentralized urine diversion facilities for nutrient recovery, without costly retrofits or overhauls of the existing system, shifting wastewater management to a more sustainable and efficient paradigm.

Other potential applications of the technology include the selective separation/recovery of compounds that speciate between volatile and nonvolatile forms at different pH. An environmentally-relevant example is H<sub>2</sub>S in domestic and industrial wastewaters.<sup>265</sup> Because of the pH-dependent volatility, H<sub>2</sub>S<sub>(g)</sub> permeates across the MD membrane and speciates to nonvolatile HS<sup>-</sup><sub>(aq)</sub> in a basic collector (equivalent to NH<sub>3(g)</sub> transport and speciation to NH<sub>4</sub><sup>+</sup><sub>(aq)</sub>), thus, enabling selective removal, capture, and concentration.

## Chapter 5: Integrated Membrane Processes to Capture Orthophosphate and Ammonia from Human Urine

### Chapter Abstract

There is a critical need to shift from the existing linear nutrient economy to more sustainable circular nutrient economy rooted in phosphorous and nitrogen recovery from wastewater. The high concentrations of orthophosphate,  $H_xPO_4^{(3-x)-}$ , in fresh source-separated urine and ammoniacal nitrogen,  $NH_4^+/NH_3$ , in hydrolyzed urine offer propitious opportunities for P and N recovery. Donnan dialysis (DD), an ion-exchange membrane-based process, demonstrates initial promise for  $H_xPO_4^{(3-x)-}$  recovery from fresh urine and membrane distillation (MD) demonstrates initial promise for volatile  $NH_3$  recovery from hydrolyzed urine. This study elucidates the impact of fresh and hydrolyzed urine solution pHs and resultant nutrient speciation ( $H_2PO_4^-/HPO_4^{2-}$  and  $NH_4^+/NH_3$ ) on DD and MD performances. Bipolar membrane electrodialysis, BPM-ED, a technique that utilizes electrolytes and electricity to generate acids and bases *in situ*, is employed to strategically control pH to enhance the performances of DD and MD for P and N recovery, respectively. For orthophosphate recovery, BPM-ED can decrease the pH of fresh urine, increasing the fraction of  $H_xPO_4^{(3-x)-}$  present as monovalent  $H_2PO_4^-$ , which improves  $H_xPO_4^{(3-x)-}$  flux by 34.8% and selectivity for  $H_xPO_4^{(3-x)-}$  by 16.5% in DD with a monovalent ion selective membrane compared to operation without BPM-ED. For ammoniacal nitrogen recovery, BPM-ED can increase the pH of hydrolyzed urine, increasing the fraction of N present as volatile  $NH_3$ , which enhances  $NH_3$  flux in MD by 138% compared to operation without BPM-ED. Furthermore, BPM-ED produces an acidic solution, which can be strategically employed as the collector solution in MD, enabling nearly 2× higher N recovery potential. Critically, the specific energy consumption of the integrated approaches of BPM-ED + DD for P recovery and BPM-ED + MD for N recovery

can be lower than the practical energy consumption of the conventional linear economy model for P and N, respectively. This study shows the promising potential of an integrated membrane technology approach for both P and N recovery from source-separated urine.

## 5.1 Introduction

For the reasons presented in Chapter 1, the existing approach to nutrient management is untenable, and more sustainable approaches are critically needed.<sup>131-133</sup> The challenges facing nutrient management can be approached through a circular economy model, which advocates for the simultaneous removal and capture of nutrients from wastewaters.<sup>62-65</sup> In a circular economy model, orthophosphate,  $H_xPO_4^{(3-x)-}$ , and ammonia,  $NH_3$ , can be removed and recovered from wastewater and recycled back into the food chain. Closing the nutrient loop can lessen the reliance on industrial fertilizer production and alleviate nutrient pollution of aquatic environments.

As presented in Chapter 2, the theoretical minimum energy for nutrient recovery, governed by thermodynamic principles, is considerably lower for feeds rich in P and N compared with other diluted wastewaters.<sup>134</sup> Specifically, P recovery from fresh diverted urine, which is concentrated in P (total orthophosphate,  $TOP = 19-48 \times 10^{-3} \text{ mol/L}$ ),<sup>44, 89, 92, 96</sup> is  $\approx 13-34\%$  less energy-intensive than treated wastewater effluent, which is over 1–2 orders of magnitude more dilute.<sup>134</sup> Likewise, N recovery from hydrolyzed urine, which is concentrated in N (total ammoniacal nitrogen,  $TAN = 270-580 \times 10^{-3} \text{ mol/L}$ ),<sup>89, 91-96</sup> is  $\approx 40-68\%$  less energy-intensive than treated wastewater effluent, which is over 2–5 orders of magnitude more dilute.<sup>134</sup> Note that hydrolyzed urine has been stored for  $\approx 2-7$  d to enable the hydrolysis of urea in urine to form ammonium and bicarbonate, which also raises pH.<sup>89, 90</sup> There has been considerable efforts to advance nutrient recovery from diverted urine, with the prevailing practice being mineral precipitation of slow-release fertilizers, such as struvite,  $NH_4MgPO_4 \cdot 6H_2O$ .<sup>67, 68, 72, 89, 90, 114, 115, 135</sup> However, mineral precipitation leads to risks for

contamination by pharmaceuticals, endocrine disrupting compounds, and opportunistic pathogens.<sup>136-141</sup> Membranes can serve as a barrier, retaining these contaminants of concern in the urine feed<sup>167-172, 266, 267</sup> and enabling the capture of targeted P and N species.

For orthophosphate recovery: Donnan dialysis (DD) using ion-exchange membranes (IEMs) is a promising technique for orthophosphate,  $H_xPO_4^{(3-x)-}$ , separation from urine, achieving recovery yields >90%.<sup>268</sup> Work in Chapter 3 examined DD for orthophosphate recovery from fresh urine at pH = 6, which is the low-end of typical fresh urine pH and contains orthophosphate predominantly as  $H_2PO_4^-$ . However, actual urine solutions can range from pH of 6–7.5, i.e., mid-point pH = 6.75, depending on a person's diet.<sup>44, 89, 91-96</sup> Higher pHs  $\gg$   $pK_{a2}$  of phosphate can shift the predominant orthophosphate species to  $HPO_4^{2-}$ . In DD, the speciation of  $H_xPO_4^{(3-x)-}$  as  $H_2PO_4^-$  or  $HPO_4^{2-}$ , which is dependent on solution pH, can influence orthophosphate transport, particularly if the IEM selects for monovalent ions over multivalent ions, as monovalent ion-selective membranes do.<sup>161-164, 268</sup> For N recovery: membrane distillation (MD) is a promising technique for the selective and energy-efficient recovery of ammoniacal nitrogen from hydrolyzed urine.<sup>74</sup> In MD, volatile  $NH_3$  in hydrolyzed urine is driven across a hydrophobic microporous membrane.<sup>74, 214-216</sup> Work in Chapter 4 examined MD for  $NH_3$  recovery from simulated hydrolyzed urine, which contained approximately 50% TAN as  $NH_3$  and 50% as  $NH_4^+$ .<sup>74</sup>  $NH_3$  is a volatile form of N, while  $NH_4^+$  is ionic and nonvolatile, so  $NH_3$  is the preferred N species for ammoniacal nitrogen recovery using MD. Similar to orthophosphate speciation, ammoniacal nitrogen speciation as  $NH_3$  or  $NH_4^+$  is pH-dependent; higher pHs  $\gg$   $pK_a$  of ammonia shift predominance to  $NH_3$ . Strategically manipulating fresh and hydrolyzed urine pHs can potentially benefit the performances of DD and MD for orthophosphate and ammoniacal nitrogen recovery, respectively. Another membrane technique of bipolar membrane electrodialysis, which generates acids and bases using electrolyte

solution, can be leveraged to rationally manipulate solution pHs in DD and MD for nutrient recovery.

In this study, we assess the performance of an integrated bipolar membrane electro dialysis (BPM-ED), Donnan dialysis, and isothermal membrane distillation (IMD) system to drive the separation and recovery of orthophosphate and ammoniacal nitrogen from human urine. First, the working principles DD and IMD for respective orthophosphate and ammonia recovery are discussed, and the importance of nutrient speciation ( $\text{H}_2\text{PO}_4^-/\text{HPO}_4^{2-}$  and  $\text{NH}_4^+/\text{NH}_3$ ) is highlighted. Next, BPM-ED is introduced as a technique to generate acids and bases *in situ* to strategically control the speciation of  $\text{H}_2\text{PO}_4^-/\text{HPO}_4^{2-}$  in fresh urine and  $\text{NH}_4^+/\text{NH}_3$  in hydrolyzed urine, which serve as the respective feed solutions to DD and IMD. The potential to utilize BPM-ED to decrease the pH of fresh urine and enhance  $\text{H}_x\text{PO}_4^{(3-x)-}$  flux and selectivity for  $\text{H}_x\text{PO}_4^{(3-x)-}$  in DD is explored for different durations of BPM-ED operation. Then, the potential of BPM-ED to increase the pH of hydrolyzed urine and improve  $\text{NH}_3$  flux in IMD was assessed for different BPM-ED operating current densities. Next, the influence of an acidic collector, generated using BPM-ED, on  $\text{NH}_3$  flux and recovery potential in IMD was assessed. The study evaluated the specific energy consumptions (SECs) of BPM-ED, DD, and IMD techniques and compared SECs to conventional nutrient removal and production techniques. Finally, implications of the integrated membrane technique on decentralized nutrient recovery efforts are discussed.

## 5.2 Working Principles

**Donnan Dialysis for Orthophosphate Recovery.** Detailed working principles of Donnan dialysis (DD) can be found in literature<sup>142-144, 146-148, 151-154</sup> and are explained in Chapter 3. Here, the principles are briefly presented with a focus on orthophosphate recovery from source-separated urine. The flux of  $\text{Cl}^-$  driver ions down a concentration gradient, across an anion exchange

membrane (AEM), sets up an electrochemical potential gradient that drives transport of target  $\text{H}_x\text{PO}_4^{(3-x)-}$  ions in the opposite direction.<sup>142-144, 146-148</sup> AEMs are polymeric thin-films with a high density of positively-charged functional groups to enable the selective permeation of negatively-charged ions (referred to as *counterions*, i.e., oppositely-charged to the AEM), while retaining positively-charged ions (referred to as *co-ions*, i.e., like-charge of the AEM).<sup>149, 150</sup> The AEM divides the feed solution (FS), in this study source-separated urine, and receiver solution (RS), in this study a solution of high chloride content.  $\text{Cl}^-$  ions permeate from the higher concentration RS to the lower concentration FS, while cations,  $\text{M}^+$ , are rejected by the AEM. To preserve electroneutrality target  $\text{H}_x\text{PO}_4^{(3-x)-}$  ions from the urine FS migrate across the membrane in the opposite direction.<sup>142, 143, 146, 151-154</sup> Note that the charge fluxes of  $\text{Cl}^-$  and  $\text{H}_x\text{PO}_4^{(3-x)-}$  must be equal to maintain electroneutrality, i.e., one  $\text{H}_x\text{PO}_4^{(3-x)-}$  ion exchanges with  $(3-x)$   $\text{Cl}^-$  ion(s).

#### **Isothermal Membrane Distillation with Acidic Collector for Ammonia Recovery.**

Working principles of membrane distillation (MD) and isothermal membrane distillation with acidic collector (IMD-AC) are detailed in literature and in Chapter 4,<sup>74, 211, 212</sup> and are briefly explained here with a focus on ammonia separation and recovery from urine. In MD, volatile compounds are driven across a hydrophobic microporous membrane while nonvolatile components are retained in the feed stream. As such, the technique can be used to separate volatile ammonia from hydrolyzed urine.<sup>74, 214-216, 232, 240</sup> The driving force for a compound,  $i$ , to volatilize from the feed, permeate across the membrane, and condense in the collector stream is the transmembrane vapor pressure difference,  $P_{F,i} - P_{C,i}$  (subscripts F and C denote feed and collector sides, respectively). Partial vapor pressure of component  $i$  is dependent on solution temperature, as described by the Clausius-Clapeyron relation,<sup>238</sup> and the concentration of species  $i$  in the solution. Vapor flux of component  $i$ ,  $J_i$ , is described by eqn (5.1):<sup>212</sup>

$$J_i = L_i (P_{F,i} - P_{C,i}) \quad (5.1)$$

where membrane vapor permeability coefficient,  $L_i$ , characterizes the transport of compound  $i$  per unit driving force and is dependent on the vapor molecule, membrane structural properties and membrane chemistry, feed and collector compositions, as well as operating conditions, such as temperature.<sup>211-213</sup>

In the work presented in Chapter 4, IMD-AC was developed to overcome the limitations of CMD for separating volatile compounds from aqueous solutions, including ammonia recovery from hydrolyzed urine. The *isothermal* feature of IMD-AC establishes equal temperatures for feed (F) and collector (C) streams, i.e.,  $T_F = T_C$ , which effectively eliminates  $P_{F,W} - P_{C,W}$ , the driving force for water vapor transport. As a result, the selectivity for ammonia transport is significantly increased relative to CMD. Additionally, Chapter 4 reported that isothermal operation achieved  $\approx 95\%$  savings in energy for vaporization relative to CMD due to suppressed water permeation.<sup>74</sup> The *acidic collector* feature maintains a low pH that is below the  $pK_a$  of ammonia (8.8 for solution temperature of 40 °C),<sup>243</sup> effectively converting all ammonia,  $NH_3$ , that has permeated over to the collector to ionic ammonium,  $NH_4^+$ , which is nonvolatile.<sup>214, 215, 218-231</sup> Critically, IMD-AC can transport  $NH_3$  against a total ammoniacal nitrogen concentration gradient, achieving uphill transport.<sup>74</sup> Additionally, Chapter 4 reports that operation with an acidic collector enhanced ammonia vapor flux by an average of 46.5% compared to using a deionized water collector.<sup>74</sup> Overall, the isothermal and acidic collector features of IMD-AC can, respectively, minimize undesired permeation of water vapor, thus preventing undesired dilution in the collector and reducing heat energy requirements, and eliminate  $P_{C,A}$ , to maximize the driving force for ammonia transport,  $P_{F,A} - P_{C,A}$ , and enable uphill transport of ammoniacal nitrogen. For this reason, IMD-AC, rather than CMD, operation is utilized in this study.

## Opportunities to Incorporate Bipolar Membrane Electrodialysis for Performance

**Improvements.** The performances of DD and IMD-AC for nutrient recovery are dependent on the speciation of orthophosphates,  $\text{H}_2\text{PO}_4^-/\text{HPO}_4^{2-}$ , in fresh urine and ammoniacal nitrogen,  $\text{NH}_4^+/\text{NH}_3$ , in hydrolyzed urine. For DD, the speciation of orthophosphate impacts the charge density and ionic radius, which has implications for kinetics and selectivity over other anions. At a pH = 6.75 (the mid-point of the typical fresh urine pH range),<sup>44, 89, 92, 96</sup> orthophosphate in fresh urine (total orthophosphate, TOP =  $30 \times 10^{-3}$  mol/L) is present as  $\approx 75\%$   $\text{H}_2\text{PO}_4^-$  and  $\approx 25\%$   $\text{HPO}_4^{2-}$ .<sup>44, 89, 92, 96</sup> Changing the pH of the urine solution can drastically alter the predominance of one orthophosphate valency over the other. For examples, increasing the pH of fresh urine above the  $\text{p}K_{a,2}$  of phosphate (7.2 for DD solution temperature of 20 °C) to 9.2, i.e., the high-end of typical wastewater pH range,<sup>89, 91-97</sup> shifts the speciation of orthophosphate to  $\approx 99\%$   $\text{HPO}_4^{2-}$ , while decreasing the pH to 6.0, i.e., the low-end of typical wastewater pH range,<sup>89, 91-97</sup> shifts the speciation of orthophosphate to  $\approx 94\%$   $\text{H}_2\text{PO}_4^-$ . The role of pH and orthophosphate speciation on DD performance has not been elucidated for solutions simulating the composition of major anions in fresh urine (i.e.,  $30 \times 10^{-3}$  mol/L  $\text{H}_2\text{PO}_4^-$ ,  $16 \times 10^{-3}$  mol/L  $\text{SO}_4^{2-}$ , and  $100 \times 10^{-3}$  mol/L  $\text{Cl}^-$ ). Therefore, it remains unclear which form of orthophosphate,  $\text{H}_2\text{PO}_4^-$  or  $\text{HPO}_4^{2-}$ , is more favorable for P recovery using DD. However, in DD with a monovalent ion permselective membrane (MIPM), which is selective for transport of monovalent ions, such as  $\text{H}_2\text{PO}_4^-$ , over multivalent ions, such as  $\text{SO}_4^{2-}$ , presumably it is favorable for the urine stream pH to be less than  $\text{p}K_{a,2}$ , such that monovalent  $\text{H}_2\text{PO}_4^-$  is the predominant orthophosphate.

For IMD-AC,  $\text{NH}_{3(\text{aq})}$  is the favorable form of ammoniacal N in the feed solution because ammonia is volatile and can vaporize and permeate across the hydrophobic microporous membrane. Holding other conditions constant (operation temperatures, concentration of total

ammoniacal nitrogen, and collector composition), the higher the fraction of total ammoniacal nitrogen, TAN, present as  $\text{NH}_{3(\text{aq})}$ , the higher the driving force for ammonia permeation,  $P_{\text{F,A}} - P_{\text{C,A}}$ . For hydrolyzed urine at 40 °C and pH = 8.8,<sup>89, 96</sup> ammoniacal nitrogen (TAN =  $495 \times 10^{-3}$  mol/L) is present as  $\approx 50\%$   $\text{NH}_4^+$  and  $\approx 50\%$   $\text{NH}_3$ . Increasing the pH of hydrolyzed urine above the  $\text{p}K_{\text{a}}$  of ammonia (8.8 for IMD solution temperature of 40 °C)<sup>243</sup> to 10.5, for example, shifts the speciation of ammoniacal nitrogen to 98%  $\text{NH}_3$ , which can beneficially increase  $P_{\text{F,A}} - P_{\text{C,A}}$ . On the collector side,  $\text{NH}_4^+$  is the favorable form of ammoniacal N because ionic ammonium is nonvolatile<sup>214, 215, 218-231</sup> and does not contribute to  $P_{\text{C,A}}$ , which would decrease the driving force for ammonia transport. For this reason, a low pH acidic collector solution was applied in Chapter 4 to enable the transport of ammonia against a TAN concentration gradient.<sup>74</sup>

Controlling the pH of fresh urine, hydrolyzed urine, and the collector solution of MD can potentially benefit DD and IMD-AC performance for P and N recovery, respectively. Acids and bases can be dosed in the streams to strategically influence pH, but this contributes to additional chemical and transportation costs. Utilizing waste chemicals, such as spent pickling brine (effectively acetic acid), can mitigate some chemical costs, but still relies on the transportation of these chemicals to the treatment site and can potentially introduce unwanted contaminants into the system. Alternatively, acids and bases can be generated *in situ* using widely available, low-cost salts or waste salts using bipolar membrane electrodialysis (BPM-ED).

Working principles of BPM-ED are detailed in literature<sup>149, 269-275</sup> and briefly presented here with a focus on acid and base production for application in DD and IMD-AC for nutrient recovery from urine. BPM-ED is an emerging electrodialysis technique that leverages the electro-dissociation of water within the interfacial layer of a bipolar membrane (BPM) to generate acids and bases. A BPM is a polymeric thin film composed of a negatively charged cation-exchange

layer and a positively charged anion-exchange layer. In a BPM-ED system, a cation exchange membrane (CEM) and anion exchange membrane (AEM) are placed on either side of the BPM (Figure D.1). MX salt solution(s) are sent to outer electrolyte channels that are in contact with the CEM and AEM and a current is applied across the cell. The ionic current cannot be sustained from ions in the bulk electrolyte solutions because  $X^-$  cannot pass through the negatively-charged layer and  $M^+$  cannot pass through the positively-charged layer of the BPM. To carry out the ionic current, water is electro-dissociated into  $H^+$  and  $OH^-$  at the interfacial layer, or bipolar junction, inside the BPM, and  $H^+$  and  $OH^-$  ions migrate to the acid and base chambers, respectively. Electroneutrality in the acid and base chambers is maintained by  $X^-$  and  $M^+$  ion migration from the electrolyte solution(s) across the AEM and CEM, respectively. Redox reactions of  $H^+ \rightarrow 0.5H_2$  and  $OH^- \rightarrow 0.25 O_2 + 0.5 H_2O$  in the electrolyte solution(s) balance the loss of  $X^-$  and  $M^+$  ions, respectively. As a result, BPM-ED can simultaneously produce HX in the acid chamber and MOH in the base chamber.

Acid and base generation in BPM-ED can be leveraged to favorably control the pH of the urine feed in DD and the hydrolyzed urine feed and collector of IMD-AC. HX, here in this study HCl, production within fresh urine will decrease the pH of the solution further shifting the orthophosphate predominance to  $H_2PO_4^-$ , which is presumably beneficial for DD with MIPM. MOH, here in this study NaOH, production within hydrolyzed urine will increase the pH of the solution shifting the ammoniacal nitrogen predominance to  $NH_3$ , which will improve the driving force for ammonia transport. At the same time, BPM-ED can produce an acidic stream, which can be employed as the collector solution of IMD-AC, thereby replacing the need to supply and transport acids to the treatment system. In this study, the acidic stream comprises  $H_2SO_4$  for the generation of an aqueous ammonium sulfate solution as fertilizer.

Figure 5.1 presents the integration of BPM-ED, DD, and IMD-AC for P and N recovery from human urine. First, BPM-ED is employed to decrease the pH of fresh urine. Next, orthophosphate is separated from fresh urine in the DD step. The remaining urine is then stored for  $\approx 2-7$  d days to enable the hydrolysis of urea,  $\text{CH}_4\text{N}_2\text{O}$ , to form  $\text{NH}_3$  and  $\text{HCO}_3^-$ , thereby generating hydrolyzed urine. A second BPM-ED cell is employed to simultaneously increase the pH of hydrolyzed urine and generate a low pH acidic collector solution for IMD-AC. Finally, in IMD-AC,  $\text{NH}_3$  is separated from hydrolyzed urine and recovered in the acidic collector effluent. The remaining hydrolyzed urine is discharged into the sewer.

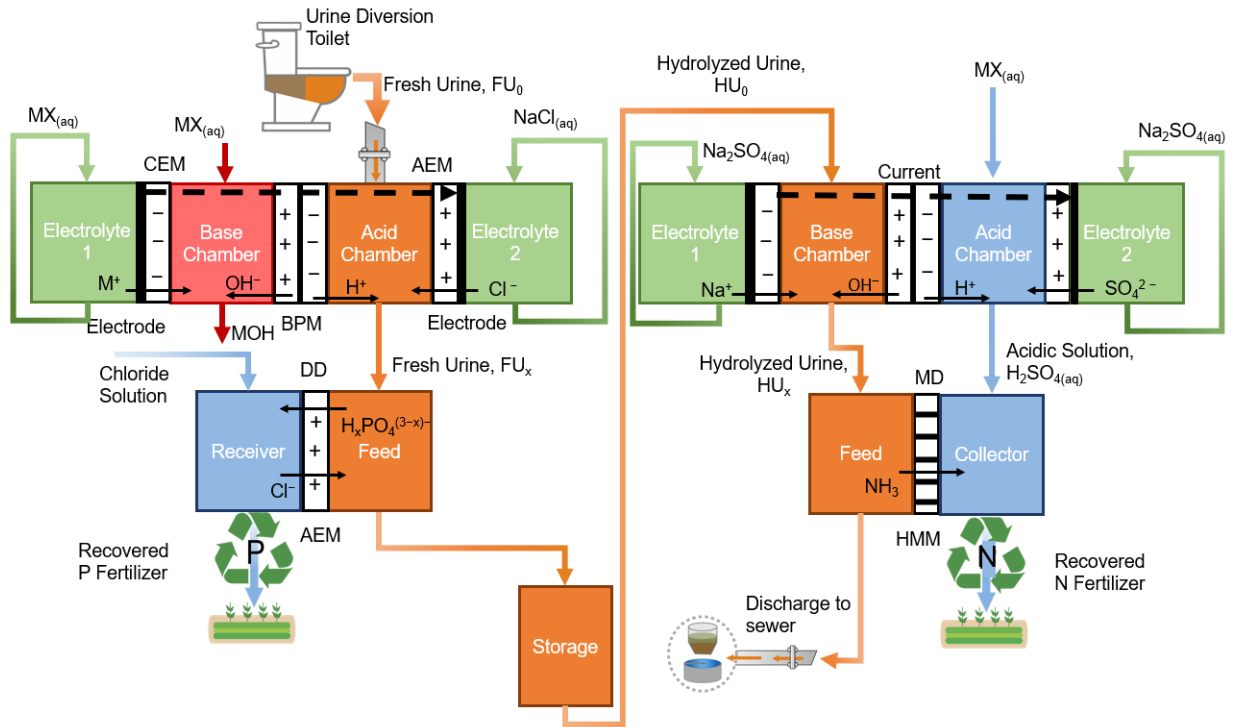


**Figure 5.1.** Schematic of the integrated membrane technology approach of Donnan dialysis (DD) for  $\text{H}_x\text{PO}_4^{(3-x)-}$  recovery, isothermal membrane distillation (IMD) for  $\text{NH}_3$  recovery, and bipolar membrane electro dialysis (BPM-ED) to strategically modify the pH of various streams. First, in a BPM-ED cell, source-separated fresh urine, termed  $\text{FU}_0$ , is directed to the acid chamber, salt solutions of choice are directed to base chamber and electrolyte 1 chambers, and  $\text{NaCl(aq)}$  is directed to the electrolyte 2 chamber. A current is applied across the stack from the electrodes in contact with electrodes 1 and 2, which are connected to positive and negative terminals of a power supply, respectively. Water is electro-

dissociated into protons and hydroxide at the interfacial layer, or bipolar junction, and HCl can be generated within the acid chamber, thereby decreasing the pH of fresh urine. The effluent of the BPM-ED acid chamber, i.e., fresh urine + HCl, termed  $FU_X$ , is then directed to the feed solution to a Donnan dialysis cell, while a salt solution comprising a high concentration of  $Cl^-$  is supplied as the receiver solution. In DD,  $Cl^-$  ions, which are “driver ions”, transport down a concentration gradient from the high concentration RS to low concentration FS. The DD anion exchange membrane prevents the permeation of  $M^+$  cations. Therefore, to maintain electroneutrality,  $H_xPO_4^{(3-x)-}$  ions transport from FS to RS, which enables  $H_xPO_4^{(3-x)-}$  recovery in the receiver solution effluent of the DD cell. The FS effluent of the DD step, i.e., the remaining fresh urine solution, is then directed to storage. In storage, urea,  $CH_4N_2O$ , in urine hydrolyzes to form  $NH_3$  and  $HCO_3^-$ , thereby generating “hydrolyzed urine”, termed  $HU_0$ . Then, in a second BPM-ED cell hydrolyzed urine is directed to the base chamber, the salt solution of choice is directed to the acid chamber, and  $Na_2SO_4$  is directed to both electrolyte chambers. NaOH is generated within the base chamber, thereby increasing the pH of hydrolyzed urine, while  $H_2SO_4$  is simultaneously generated in the acid chamber. The effluent of the BPM-ED base chamber, i.e., hydrolyzed urine + NaOH, termed  $HU_X$ , and the effluent of the acid chamber, i.e.,  $H_2SO_4$  solution, are directed as the feed and collector solutions, respectively, in membrane distillation. In the MD step,  $NH_3$  from the feed solution is driven across a hydrophobic microporous membrane (HMM) and is captured within the collector solution. The effluent of the MD feed stream is then discharged to a sewage system.

### 5.3 Materials and Methods

**Materials and Chemicals.** A bipolar membrane electro dialysis cell and a Donnan dialysis cell were fabricated using Mars Pro MSLA 3D Printer acquired from Elegoo (China). As demonstrated in Figure D.1 of Appendix D the bipolar membrane electro dialysis cell consists of a Neosepta CMB cation exchange membrane between the first electrolyte and base chambers, a Neosepta BP-1E bipolar membrane between the base and acid chambers, and a Neosepta AHA anion exchange membrane between the acid and second electrolyte chambers. All membranes were procured from Ameridia Innovative Solutions (Napa, CA) and have an effective area of  $12.56\text{ cm}^2$ . Graphite electrodes are placed between the CEM and first electrolyte channel and between the AEM and

second electrolyte channel. The power is supplied by Agilent single output DC power supply (U8002A, Santa Clara, CA).

A commercial, monovalent ion-selective AEM, the Selemion ASVN, was procured from Asahi Glass Co. (Japan) and utilized in all Donnan dialysis experiments. The effective membrane area in the Donnan dialysis cell was  $9.0 \text{ cm}^2$  and the feed and collector solution volumes were both 40 mL. A commercial microporous hydrophobic polyvinylidene fluoride (PVDF) membrane of  $0.22 \text{ }\mu\text{m}$  pore-size, GVHP14250, was acquired from MilliporeSigma (Burlington, MA) and utilized for all membrane distillation experiments.

$\text{Na}_2\text{HPO}_4 \cdot 7\text{H}_2\text{O}$ ,  $\text{Na}_3\text{PO}_4 \cdot 12\text{H}_2\text{O}$ , and NaCl salts were obtained from Alfa Aesar (Ward Hill, MA). 85%  $\text{H}_3\text{PO}_4$  solution, urea,  $\text{CO}(\text{NH}_2)_2$ , and  $\text{NH}_4\text{OH}$ ,  $\text{Na}_2\text{SO}_4$ , and  $\text{NH}_4\text{HCO}_3$  salts were provided by Fisher Scientific (Waltham, MA). KCl salt and 2.5 M  $\text{H}_2\text{SO}_4$  solution were acquired from Lab Chem (Zelienople, PA), and Titripur (St. Louis, MO), respectively. All chemicals are ACS grade and were used as received. All solutions were prepared using deionized (DI) water from a Milli-Q ultrapure water purification system (Millipore Co., Burlington, MA).

**Bipolar Membrane Electrodialysis.** BPM-ED experiments were operated in two modes: the first to generate HCl in simulated fresh urine solution and the second to generate NaOH in simulated hydrolyzed urine solution while simultaneously generating  $\text{H}_2\text{SO}_4$  in the acid chamber. Table 5.1 summarizes the BPM-ED operation conditions (mode, initial acid chamber solution, initial base chamber solution, electrolytes, and current density) and target product solutions generated from each operation. In the first mode, 100 mL simulated fresh urine at  $\text{pH} = 6.75$  ( $24 \times 10^{-3} \text{ mol/L Na}_2\text{HPO}_4 \cdot 7\text{H}_2\text{O}$ ,  $6 \times 10^{-3} \text{ mol/L Na}_3\text{PO}_4 \cdot 12\text{H}_2\text{O}$ ,  $40 \times 10^{-3} \text{ mol/L NaCl}$ ,  $60 \times 10^{-3} \text{ mol/L KCl}$  and  $16 \times 10^{-3} \text{ mol/L H}_2\text{SO}_4$ , and  $250 \times 10^{-3} \text{ mol/L urea}$ ),<sup>44, 89, 92, 96</sup> termed  $\text{FU}_0$ , was directed to the acid chamber, 100 mL 0.4 M  $\text{Na}_2\text{SO}_4$  was directed to the base chamber, 200 mL

0.4 M Na<sub>2</sub>SO<sub>4</sub> was directed to the first electrolyte chamber, and 200 mL 0.8 M NaCl was directed to the second electrolyte chamber. The power supply was operated in constant current mode with current set to 125.6 mA to achieve an applied current density of 10 mA/cm<sup>2</sup>. Every 5 minutes for 30 minutes the acid chamber pH was measured using a pH Meter (Orion Star, ThermoFisher Scientific), and 100 μL samples were collected from the acid chamber. Cation and anion concentrations of the acid chamber were analyzed using ion chromatography, IC (Dionex Aquion, Thermo Fisher Scientific, Waltham, MA).

**Table 5.1.** BPM-ED experimental operating conditions and target solutions utilized in downstream processes of Donnan dialysis and isothermal membrane distillation. Note mode 1 products are generated at constant current density and varied duration, while mode 2 products are generated at varied current density for a constant duration.

No.	Mode	Initial Acid Chamber	Initial Base Chamber	Initial First Electrolyte	Initial Second Electrolyte	Applied Current Density (mA/cm <sup>2</sup> )	Duration (hours)	Target Solutions
1	1	FU <sub>0</sub>	0.4 M Na <sub>2</sub> SO <sub>4</sub>	0.4 M Na <sub>2</sub> SO <sub>4</sub>	0.8 M NaCl	10	10	Acid chamber: FU <sub>1</sub> (DD FS)
2	1	FU <sub>0</sub>	0.4 M Na <sub>2</sub> SO <sub>4</sub>	0.4 M Na <sub>2</sub> SO <sub>4</sub>	0.8 M NaCl	10	15	Acid Chamber: FU <sub>2</sub> (DD FS)
3	1	FU <sub>0</sub>	0.4 M Na <sub>2</sub> SO <sub>4</sub>	0.4 M Na <sub>2</sub> SO <sub>4</sub>	0.8 M NaCl	10	20	Acid Chamber: FU <sub>3</sub> (DD FS)
4	2	0.6 M KCl	HU <sub>0</sub>	0.4 M Na <sub>2</sub> SO <sub>4</sub>	0.4 M Na <sub>2</sub> SO <sub>4</sub>	20	4	Base Chamber: HU <sub>1</sub> and Acid Chamber: AC <sub>1</sub> (IMD F and C, respectively)
5	2	0.6 M KCl	HU <sub>0</sub>	0.4 M Na <sub>2</sub> SO <sub>4</sub>	0.4 M Na <sub>2</sub> SO <sub>4</sub>	40	4	Base Chamber: HU <sub>2</sub> (IMD F)

In the second mode, 100 mL simulated hydrolyzed urine at pH = 9.2 ( $6.56 \times 10^{-3}$  mol/L  $\text{Na}_2\text{HPO}_4 \cdot 7\text{H}_2\text{O}$ ,  $93.11 \times 10^{-3}$  mol/L NaCl,  $60 \times 10^{-3}$  mol/L KCl and  $1.16 \times 10^{-3}$  mol/L  $\text{H}_2\text{SO}_4$ ,  $247.5 \times 10^{-3}$  mol/L  $\text{NH}_4\text{HCO}_3$ , and  $247.5 \times 10^{-3}$  mol/L  $\text{NH}_4\text{OH}$ ),<sup>89, 96</sup> termed  $\text{HU}_0$ , was directed to the base chamber, 100 mL 0.6 M KCl was directed to the acid chamber, and 400 mL 0.4 M  $\text{Na}_2\text{SO}_4$  was directed to both electrolyte chambers. Note that  $\text{HU}_0$  simulates the composition of the urine solution after the Donnan dialysis step is driven to Donnan equilibrium, which is predicted in Chapter 3,<sup>268</sup> and urea hydrolysis to 99% completion, which occurs after  $\approx 2-7$  d of storage.<sup>89, 90</sup> The electrolyte solution was replenished with fresh solution every hour to maintain sufficient  $\text{Na}^+$  and  $\text{SO}_4^{2-}$  concentrations for BPM-ED operation over time. The power supply was operated in constant current mode with currents set to either 251.2 mA or 502.4 mA for current densities of 20 and 40 mA/cm<sup>2</sup>, respectively. Every 30 minutes for 6.0 hours, the acid and base chamber pH was measured and 100  $\mu\text{L}$  samples from the base and acid chambers were collected to determine ion concentrations in each solution.

**Orthophosphate Recovery with DD.** Anion fluxes from urine feed solution (FS) to product receiver solution (RS) were examined in Donnan dialysis kinetic experiments. Fluxes were determined from the rate of change of anion concentrations in the RS over 6.0 h. 175  $\mu\text{L}$  samples were collected from each solution and the anion concentrations were analyzed using IC. Water transport across the AEM during the kinetic experiments was not observed and deemed to be practically negligible. The change in moles of anion in the RS over time normalized by the membrane area yields flux,  $J_i$ , where subscript  $i$  denotes orthophosphate, P, or sulfate, S. Relative flux,  $J_P/J_S$ , is defined as the flux of orthophosphate divided by the flux of sulfate.

To investigate the role of FS pH on orthophosphate flux and selectivity  $J_P$  and  $J_S$  were assessed in Donnan dialysis experiments using  $600 \times 10^{-3}$  mol/L NaCl RS and two urine feed

solutions containing the same ion species at pH = 6.0 and 9.2. The low and high pHs reflect the typical pH range of wastewater (low-end of fresh urine and high-end of hydrolyzed urine, respectively) and respectively contain predominantly monovalent orthophosphate,  $\text{H}_2\text{PO}_4^-$ , and divalent orthophosphate,  $\text{HPO}_4^{2-}$ .<sup>44, 89, 92, 96</sup> Both FS simulate the orthophosphate, sulfate, and chloride concentrations in urine. FS at pH = 6.0 is composed of  $24 \times 10^{-3}$  mol/L  $\text{Na}_2\text{HPO}_4 \cdot 7\text{H}_2\text{O}$ ,  $6 \times 10^{-3}$  mol/L  $\text{Na}_3\text{PO}_4 \cdot 12\text{H}_2\text{O}$ ,  $100 \times 10^{-3}$  mol/L NaCl, and  $16 \times 10^{-3}$  mol/L  $\text{H}_2\text{SO}_4$ , and FS at pH = 9.2 is composed of  $30 \times 10^{-3}$  mol/L  $\text{Na}_2\text{HPO}_4 \cdot 7\text{H}_2\text{O}$ ,  $100 \times 10^{-3}$  mol/L NaCl, and  $16 \times 10^{-3}$  mol/L  $\text{Na}_2\text{SO}_4$ .

Additionally, anion fluxes and relative fluxes were assessed using  $600 \times 10^{-3}$  mol/L KCl RS with FS of  $\text{FU}_0$  and three FS simulating target streams from mode 1 BPM-ED operation (Table 5.1 No. 1–3). These FS are acid chamber effluents of BPM-ED mode 1 at a current density of 10 mA/cm<sup>2</sup> for 10, 15, and 20 minutes of operation, and are termed  $\text{FU}_1$ ,  $\text{FU}_2$ , and  $\text{FU}_3$ , respectively.  $\text{FU}_0$  simulates typical fresh urine at pH = 6.75, which is the midpoint of fresh urine pH,<sup>44, 89, 92, 96</sup> while the other three FS are at lower pHs due to HCl production in the BPM-ED acid chamber.

**Ammonia Recovery with IMD-AC.** Ammonia and water vapor fluxes were evaluated in isothermal membrane distillation (IMD) operation with three different feed solutions and DI water collector solution. The feed solutions are  $\text{HU}_0$  and two solutions simulating target streams from BPM-ED mode 2 (Table 5.1 No. 4–5 F). These FS are base chamber effluents after four hours of BPM-ED mode 2 at current densities of 20 mA/cm<sup>2</sup> and 40 mA/cm<sup>2</sup>, termed  $\text{HU}_1$  and  $\text{HU}_2$ , respectively.  $\text{HU}_0$  simulates typical hydrolyzed urine at pH = 9.2,<sup>89, 96</sup> while the other two solutions are at higher pHs due to NaOH production in the BPM-ED base chamber. To investigate the applicability of the low pH solution generated in the acid chamber during BPM-ED an additional IMD experiment was conducted using  $\text{HU}_1$  feed solution and an acidic collector solution, termed

AC<sub>1</sub>. This solution simulates the acid chamber effluent after four hours of BPM-ED mode 2 at a current density of 20 mA/cm<sup>2</sup> (Table 5.1 No. 4 C) diluted by a factor of 10. Note that the dilution was necessary to avoid extremely low pH solutions that can damage the IMD system.

All experiments were conducted in a custom-built bench-scale MD unit. The volume of the feed and collector solutions were approximately 2.0 L each and were circulated countercurrently at crossflow velocities of 22.2 cm/s and 20.0 cm/s, respectively, across the active membrane area of 19.0 cm<sup>2</sup> in a custom-built membrane cell. The operating temperatures for the feed and collector solutions,  $T_F$  and  $T_C$ , respectively, were consistently 40 °C.  $T_F$  and  $T_C$  were regulated with heated and refrigerated circulators (PolyScience, Warrington, PA), respectively, through heat exchangers. Temperatures at the inlet and outlet of the membrane cell on the feed and collector sides were monitored using thermocouples (Omega Engineering, Norwalk, CT), and the solutions within the cells were maintained within  $\pm 1.5$  °C of the target temperature throughout all experimental runs.

Ammonia vapor flux was determined from the rate of change of total ammoniacal nitrogen (TAN = NH<sub>3</sub>+NH<sub>4</sub><sup>+</sup>) in the collector stream. Four 1 mL samples were taken every 15 min, and TAN concentrations were measured following the Indophenol blue method.<sup>244</sup> Ammonia salicylate and ammonia cyanurate reagent powder were added in excess to DI water-diluted samples and analyzed using a calibrated colorimeter (ThermoFisher Scientific). The change in moles of ammonia over time normalized by the membrane area yields  $J_A$ . Water flux was calculated as the average rate of change in the feed and collector solution weights normalized by membrane area, accounting for the transferred ammonia and evaporative loss from bulk solution tanks. The change in weight of the feed and collector bulk solution tanks were automatically logged every 10 seconds using digital microbalances (AX5202, Ohaus, Parsippany, NJ).

## 5.4 Results and Discussion

**Lower Urine pH is more Favorable for Orthophosphate Recovery using Donnan Dialysis with Monovalent Ion-Selective Membrane.** To investigate the influence of solution pH and  $H_xPO_4^{(3-x)-}$  speciation on DD for orthophosphate recovery, DD experiments were conducted using an initial RS of  $600 \times 10^{-3}$  mol/L  $Cl^-$  and two FS of fresh urine at pH = 6.0 and pH = 9.2. Both solutions simulate the composition of major anions in fresh urine (i.e.,  $H_xPO_4^{(3-x)-}$ ,  $SO_4^{2-}$ , and  $Cl^-$  ion concentrations are  $30 \times 10^{-3}$ ,  $16 \times 10^{-3}$ , and  $100 \times 10^{-3}$  mol/L). Figure 5.2 shows the fluxes of orthophosphate and sulfate,  $J_P$  and  $J_S$ , respectively, for DD operation with FS at pHs of 6.0 and 9.2.  $J_P$  is 78.6% higher with FS at pH = 6.0, where orthophosphate is predominantly  $H_2PO_4^-$ , relative to FS at pH = 9.2, where orthophosphate is predominantly  $HPO_4^{2-}$ . The ion-selective coating on the ASVN membrane selects for monovalent ions, i.e.,  $H_2PO_4^-$  in FS at pH = 6.0, and hinders the permeation of multivalent ions, i.e.,  $HPO_4^{2-}$  in FS at pH = 9.2. Therefore, DD with  $H_xPO_4^{(3-x)-}$  as predominantly  $H_2PO_4^-$ , which is the case in solutions at pH  $\ll pK_{a2}$  of phosphate (7.2 at 20°C), results in more favorable orthophosphate transport.

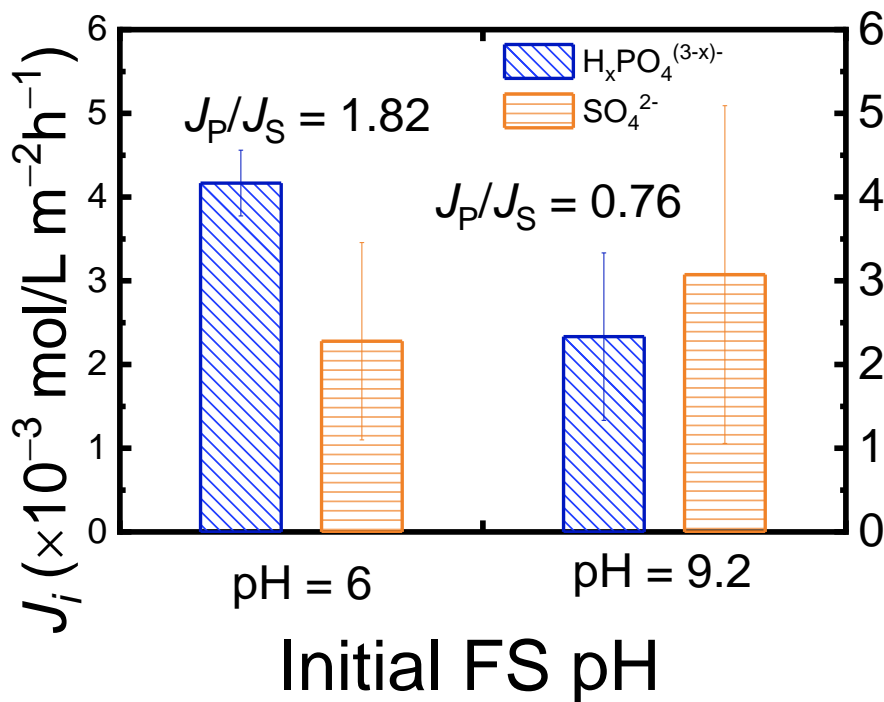


**Figure 5.2.** Flux of orthophosphate,  $J_P$ , and flux of sulfate,  $J_S$ , (patterned blue and orange columns, respectively) in Donnan dialysis kinetic experiments with initial simulated urine feed solutions at pHs of 6.0 and 9.2. Relative flux,  $J_P/J_S$  is depicted above the blue columns. FS at pH = 6.0 is composed of  $24 \times 10^{-3} \text{ mol/L Na}_2\text{HPO}_4 \cdot 7\text{H}_2\text{O}$ ,  $6 \times 10^{-3} \text{ mol/L Na}_3\text{PO}_4 \cdot 12\text{H}_2\text{O}$ ,  $100 \times 10^{-3} \text{ mol/L NaCl}$ , and  $16 \times 10^{-3} \text{ mol/L H}_2\text{SO}_4$ , and FS at pH = 9.2 is composed of  $30 \times 10^{-3} \text{ mol/L Na}_2\text{HPO}_4 \cdot 7\text{H}_2\text{O}$ ,  $100 \times 10^{-3} \text{ mol/L NaCl}$ , and  $16 \times 10^{-3} \text{ mol/L Na}_2\text{SO}_4$ . All experiments were operated with  $600 \times 10^{-3} \text{ mol/L NaCl}$  as the receiver solution. Error bars indicate standard deviations of duplicate experiments.

Relative to DD with FS at pH of 9.2, operation with FS at pH of 6.0 resulted in 25.9% lower  $J_S$ . Because both  $\text{H}_x\text{PO}_4^{(3-x)-}$  and  $\text{SO}_4^{2-}$  can transport from FS to RS to balance  $\text{Cl}^-$  driver ion transport in the opposite direction,  $\text{H}_x\text{PO}_4^{(3-x)-}$  and  $\text{SO}_4^{2-}$  transport is competitive. Previous studies<sup>159, 268</sup> and analysis in Chapter 3 demonstrated that anions compete to sorb into an AEM, and increased sorption of one anion is accompanied by decreased sorption of another. Ion flux,  $J_i$ , is directly proportional to the concentration of species  $i$  in the membrane, therefore reducing the sorption of  $i$  also decreases  $J_i$ .  $\text{H}_x\text{PO}_4^{(3-x)-}$  sorption to a MIPM, which comprises a monovalent ion-selective coating, is higher when monovalent  $\text{H}_2\text{PO}_4^-$ , rather than multivalent  $\text{HPO}_4^{2-}$ , is the

predominant orthophosphate species. Therefore,  $H_xPO_4^{(3-x)-}$  sorption to the AEM can be higher in the solution of pH = 6.0 ( $H_2PO_4^-$  is predominant) compared to pH = 9.2 ( $HPO_4^{2-}$  is predominant). Consequently,  $SO_4^{2-}$  sorption may follow the opposite trend, i.e.,  $SO_4^{2-}$  sorption in FS of pH = 9.2 > FS of pH = 6.0. Because  $J_S$  is directly proportional to  $SO_4^{2-}$  concentration within the AEM, lower  $J_S$  is observed in DD with the FS of pH = 6.0.

It should be noted that initially we anticipated that DD with the two FS would yield equivalent charge flux (meq/m<sup>2</sup>h) from the FS to RS, which is the sum of orthophosphate and sulfate charge fluxes, i.e.,  $(3-x)J_P + 2J_S$ , to balance the flux of  $Cl^-$  in the opposite direction. The preliminary presumption was that the flux of  $Cl^-$  from RS to FS would not be impacted by different FS pH because the driving force for chloride transport,  $[Cl^-]_{RS} - [Cl^-]_{FS}$ , is constant across both operations. However, the driver ion concentration gradient,  $[Cl^-]_{RS} - [Cl^-]_{FS}$ , is not the only factor influencing ion transport in DD. For example, the preceding paragraph highlights the implications of differences in ion partitioning into the AEM on transport kinetics.

Higher  $J_P$  and lower  $J_S$  for DD with FS of pH = 6.0, yields increased relative flux,  $J_P/J_S$  (depicted above the blue columns in Figure 5.2) compared with FS of pH = 9.2. Importantly, in operation with FS of pH = 6.0,  $J_P/J_S > 1$  (i.e.,  $J_P > J_S$ ), which indicates that the membrane preferentially passes  $H_2PO_4^-$  over  $SO_4^{2-}$ , while in operation with FS of pH = 9.2,  $J_P/J_S < 1$  (i.e.,  $J_P < J_S$ ), which indicates that the membrane preferentially passes  $SO_4^{2-}$  over  $HPO_4^{2-}$ . For the purposes of orthophosphate recovery from urine, higher  $J_P$  and  $J_P/J_S$  are more favorable. The experimental results, which demonstrate improved  $J_P$  and  $J_P/J_S$  with FS at pH = 6.0 compared to 9.2, suggest that it is advantageous for the FS to be at a lower pH where  $H_2PO_4^-$  is the predominant form of orthophosphate. For this reason, this study explores the application of BPM-ED for the

production of acids to decrease the pH of fresh urine, initially at 6.75, and increase the predominance of  $\text{H}_2\text{PO}_4^-$ , initially at  $\approx 75\%$ .

### **Bipolar Membrane Electrodialysis can Adjust the pH of Diverted Urine Streams.**

BPM-ED experiments were operated in two modes. The first mode decreases the pH of fresh urine by the generation of  $\text{H}^+$  (with concomitant production of  $\text{Cl}^-$ ) in the urine solution. The second mode increases the pH of hydrolyzed urine by the generation of  $\text{OH}^-$  (with concomitant production of  $\text{Na}^+$ ) in the urine solution, while simultaneously producing a separate  $\text{H}_2\text{SO}_4$  solution. The effluent of the acid chamber of mode 1 is utilized downstream as the feed solution in DD for P recovery, while the effluents of the base chamber and diluted acid chamber of mode 2 are utilized downstream as the feed and collector solutions, respectively, in IMD-AC for N recovery. Note that mode 1 also generates a NaOH solution in the base chamber; however, this solution is not utilized in any downstream operations. Figure 5.3A shows experimental  $[\text{H}_2\text{PO}_4^-]$ ,  $[\text{HPO}_4^{2-}]$ , and pH of the acid chamber (i.e., containing fresh urine solution + HCl generated) over time in mode 1. In BPM-ED mode 1, water is electro-dissociated at the bipolar junction, and  $\text{H}^+$  ions migrate toward the acid chamber, which initially contains fresh urine, while  $\text{Cl}^-$  ions from the NaCl electrolyte solution transport across the AEM to the acid chamber to maintain electroneutrality. The generation of HCl within fresh urine decreases the solution pH and increases the fraction of orthophosphate present as  $\text{H}_2\text{PO}_4^-$ . After 30 mins of operation at a current density of  $10 \text{ mA/cm}^2$ , the pH decreased from 6.75 to 3.01, the amount of orthophosphate present as  $\text{H}_2\text{PO}_4^-$  increased from  $\approx 75\%$  to  $\approx 100\%$ , and the amount of orthophosphate present as  $\text{HPO}_4^{2-}$  decreased from  $\approx 25\%$  to  $\approx 0\%$ . The aim of BPM-ED mode 1 is to shift orthophosphate speciation toward the predominance of monovalent  $\text{H}_2\text{PO}_4^-$  to benefit  $\text{H}_x\text{PO}_4^{(3-x)-}$  flux and selectivity over  $\text{SO}_4^{2-}$  in downstream DD.

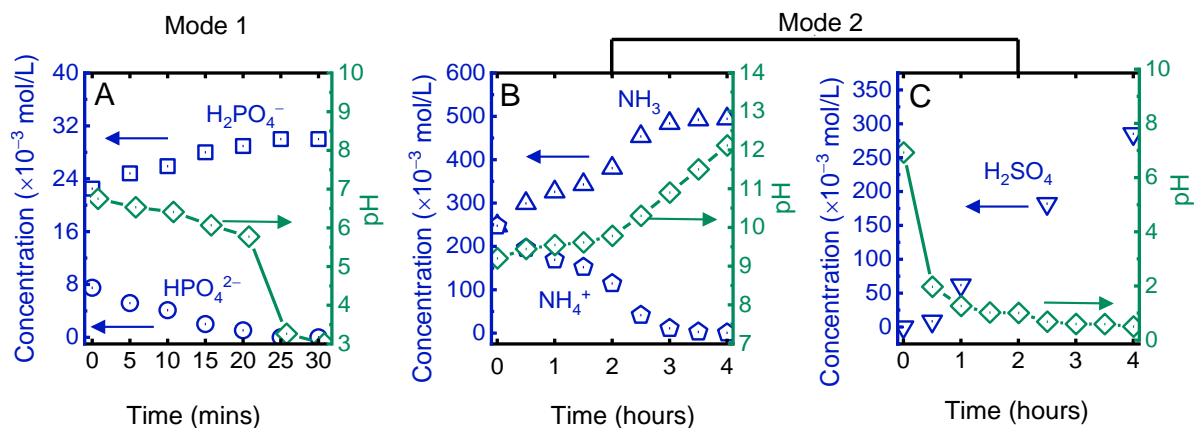


**Figure 5.3.** Concentration of key species (left vertical axis) of  $\text{HPO}_4^{2-}$  and  $\text{H}_2\text{PO}_4^-$  (A),  $\text{NH}_3$  and  $\text{NH}_4^+$  (B), and  $\text{H}_2\text{SO}_4$  (C), as well as pH (right vertical axis) of the product solution during BPM-ED operation in different modes over time. In mode 1, the pH of the fresh urine solution is decreased by the generation of HCl in the acid chamber (A). In mode 2, the pH of the hydrolyzed urine feed solution is increased by the generation of NaOH in the base chamber (B), and at the same time  $\text{H}_2\text{SO}_4$  is generated in the acid chamber (C). Here, BPM-ED modes 1 and 2 operate with respective current densities of 10 and 40  $\text{mA}/\text{cm}^2$ .

Figure 5.3B shows  $[\text{NH}_3]$ ,  $[\text{NH}_4^+]$ , and pH of the base chamber (i.e., containing hydrolyzed urine + NaOH generated) and Figure 5.3C shows the  $[\text{H}_2\text{SO}_4]$  and pH of the acid chamber over time in mode 2. In BPM-ED mode 2, water is electro-dissociated at the bipolar junction and  $\text{H}^+$  ions migrate toward the acid chamber, while  $\text{OH}^-$  ions migrate toward the base chamber, which initially contains hydrolyzed urine. Electroneutrality is maintained by the migration of  $\text{SO}_4^{2-}$  ions from the  $\text{Na}_2\text{SO}_4$  electrolyte across the AEM to the acid chamber and  $\text{Na}^+$  from the electrolyte across the CEM to the base chamber. The NaOH generation within hydrolyzed urine increases the pH of the solution and increases the fraction of TAN present as  $\text{NH}_3$ . After 4 h of operation at current density 40  $\text{mA}/\text{cm}^2$ , the pH of hydrolyzed urine increased from 9.2 to 12.1, the amount of TAN present as  $\text{NH}_3$  increased from  $\approx 50\%$  to 99.9%, and the amount of TAN present as  $\text{NH}_4^+$  decreased from  $\approx 50\%$  to 0.1%. Note that the temperature of BPM-ED operation is 20°C, and the  $\text{p}K_a$  for ammonia at this temperature is 9.2. A higher current density and duration are applied in

mode 2 than in mode 1 because the significant TAN and bicarbonate content in hydrolyzed urine makes modifying the pH of hydrolyzed urine more difficult compared to fresh urine. The TAN and bicarbonate species buffer the solution, such that a higher NaOH dose, which can be achieved by increasing BPM-ED duration or current density, is needed to substantially alter the pH. An aim of BPM-ED mode 2 is to shift the TAN speciation toward near-complete predominance of  $\text{NH}_3$  to increase the driving force for ammonia transport,  $P_{F,A} - P_{C,A}$ , in downstream IMD-AC.

BPM-ED mode 2 simultaneously generates NaOH in the base chamber and  $\text{H}_2\text{SO}_4$  in the acid chamber. Figure 5.3C shows  $[\text{H}_2\text{SO}_4]$  and pH of the acid chamber over time. The pH of the solution starkly decreases immediately upon BPM-ED operation because the initial solution in the acid chamber, 0.6 M  $\text{KCl}_{(\text{aq})}$ , has a low buffering capacity. As a result, only a small  $\text{H}_2\text{SO}_4$  dose is needed to significantly impact pH. The resultant low pH solution can be applied as the acidic collector in downstream IMD-AC to protonate  $\text{NH}_3$  transported from the feed to  $\text{NH}_4^+$ , which avoids a buildup of  $P_{C,A}$  over time. To avoid extremely low pH, the final  $\text{H}_2\text{SO}_4$  solution generated in BPM-ED must be diluted prior to use as the acidic collector in IMD-AC. BPM-ED can generate  $\text{H}^+$  and  $\text{OH}^-$  *in situ* to strategically modify solution pH, which can displace the requirement to supply external acids and bases.

**Urine pH can be Rationally Modified by BPM-ED to Enhance Productivity and Selectivity in Donnan Dialysis Orthophosphate Recovery.** DD experiments were conducted using a constant RS of  $600 \times 10^{-3}$  mol/L KCl and four FS of fresh urine at pH = 6.75, termed  $\text{FU}_0$ , and acid chamber effluents of BPM-ED mode 1 at current density  $10 \text{ mA/cm}^2$  for 10, 15, and 20 minutes of operation, which are termed  $\text{FU}_1$ ,  $\text{FU}_2$ , and  $\text{FU}_3$ , respectively. Orthophosphate and sulfate fluxes,  $J_P$  and  $J_S$ , respectively, in each operation are shown in Figure 5.4A. Note that longer BPM-ED operations generate more HCl, meaning solution pH progressively decreases, and the

fraction of TOP present as  $\text{H}_2\text{PO}_4^-$  progressively increases during BPM-ED operation. As a result,  $\text{FU}_0$ ,  $\text{FU}_1$ ,  $\text{FU}_2$ , and  $\text{FU}_3$  are of pHs of 6.5, 6.1, and 5.75, respectively, and contain respectively 75.0%, 86.3%, 93.3%, and 96.5% TOP as monovalent  $\text{H}_2\text{PO}_4^-$ .  $J_P$  increases from  $\text{FU}_0$  to  $\text{FU}_1$  (i.e., with 10 min BPM-ED duration), then decreases from  $\text{FU}_1$  to  $\text{FU}_2$  and to  $\text{FU}_3$  (i.e., with 15- and 20-min BPM-ED duration). As previously discussed, increased  $[\text{H}_2\text{PO}_4^-]_{\text{FS},0}$  benefits the performance of DD with MIPM, which should drive higher  $J_P$  at longer BPM-ED operation (i.e.,  $\text{FU}_3 > \text{FU}_2 > \text{FU}_1 > \text{FU}_0$ ). However, longer BPM-ED operations also increase  $[\text{Cl}^-]_{\text{FS},0}$ , which can be detrimental to orthophosphate transport.<sup>159, 268</sup> Higher chloride content in the FS decreases the chloride concentration gradient,  $[\text{Cl}^-]_{\text{RS}} - [\text{Cl}^-]_{\text{FS}}$ , which lowers driving force for  $\text{Cl}^-$  transport from RS to FS and  $\text{H}_x\text{PO}_4^{(3-x)-}$  transport in the opposite direction. Using the method from Chapter 3,<sup>268</sup> the driving force for  $J_P$ ,  $\Delta[\text{H}_x\text{PO}_4^{(3-x)-}] \equiv [\text{H}_x\text{PO}_4^{(3-x)-}]_{\text{FS},0} - [\text{H}_x\text{PO}_4^{(3-x)-}]_{\text{FS},f}$ , defined as the difference between initial and final (at Donnan equilibrium) TOP concentrations in the feed solution, was predicted for DD with different chloride content in the FS. Specifically,  $\Delta[\text{H}_x\text{PO}_4^{(3-x)-}]$ , which is the equivalent amount of orthophosphate ions that should transport from FS to RS in DD, was predicted for DD with fresh urine containing  $[\text{Cl}^-]_{\text{FS},0} = 100 \times 10^{-3} \text{ mol/L}$ , i.e., the chloride content prior to BPM-ED, and with  $[\text{Cl}^-]_{\text{FS},0} = 112.5 \times 10^{-3} \text{ mol/L}$ , i.e., the chloride content in  $\text{FU}_3$  after 20 min BPM-ED operation. The result of the analysis was only a 1.6% decrease in  $\Delta[\text{H}_x\text{PO}_4^{(3-x)-}]$  with the inclusion of additional  $\text{Cl}^-$  in FS of  $\text{FU}_3$ , despite 12.5% higher  $[\text{Cl}^-]_{\text{FS},0}$ . In this case,  $\Delta[\text{H}_x\text{PO}_4^{(3-x)-}]$  is not significantly impacted by the additional chloride content in the FS because  $[\text{Cl}^-]_{\text{RS},0}$ , i.e., driver ion concentration in the RS, is still significantly larger than  $[\text{Cl}^-]_{\text{FS},0}$ .

However, additional  $\text{Cl}^-$  ions in  $\text{FU}_3$  (and likewise  $\text{FU}_1$  and  $\text{FU}_2$ ) can contribute to reduced orthophosphate flux due to another mechanism. Monovalent  $\text{Cl}^-$  ions can sorb into the MIPM,

which hinders the ability for  $\text{H}_x\text{PO}_4^{(3-x)-}$  ions to partition into the membrane. Higher  $[\text{Cl}^-]_{\text{FS},0}$  will result in a more pronounced reduction in  $\text{H}_x\text{PO}_4^{(3-x)-}$  sorption. Chapter 3 reported that competition from  $\text{Cl}^-$  sorption significantly lowers  $\text{H}_x\text{PO}_4^{(3-x)-}$  sorption (e.g., 92.8% reduction in total orthophosphate ions sorbed into a conventional AEM, Selemion AMV, upon the inclusion of  $100 \times 10^{-3}$  mol/L in the urine matrix).<sup>268</sup> Because  $J_P$  is directly proportional to  $\text{H}_x\text{PO}_4^{(3-x)-}$  concentration within the AEM, the decreased  $\text{H}_x\text{PO}_4^{(3-x)-}$  sorption results in lower  $J_P$ . In the case of the results presented in Chapter 3,  $J_P$  was reduced by 85.9% with the inclusion of  $\text{Cl}^-$  ions in the FS, demonstrating that the phenomenon of competitive ion sorption can significantly impair orthophosphate transport. There is a tradeoff between beneficially higher  $[\text{H}_2\text{PO}_4^-]$  and detrimentally higher  $[\text{Cl}^-]$  with longer BPM-ED operation. As a result of these competing factors,  $J_P$  increases initially with operation of BPM-ED (i.e., 34.8% increase for 10 min operation prior to DD,  $\text{FU}_1$  in Figure 5.4A), but decreases thereafter with longer BPM-ED durations (i.e.,  $\text{FU}_1 > \text{FU}_2 > \text{FU}_3$ ).

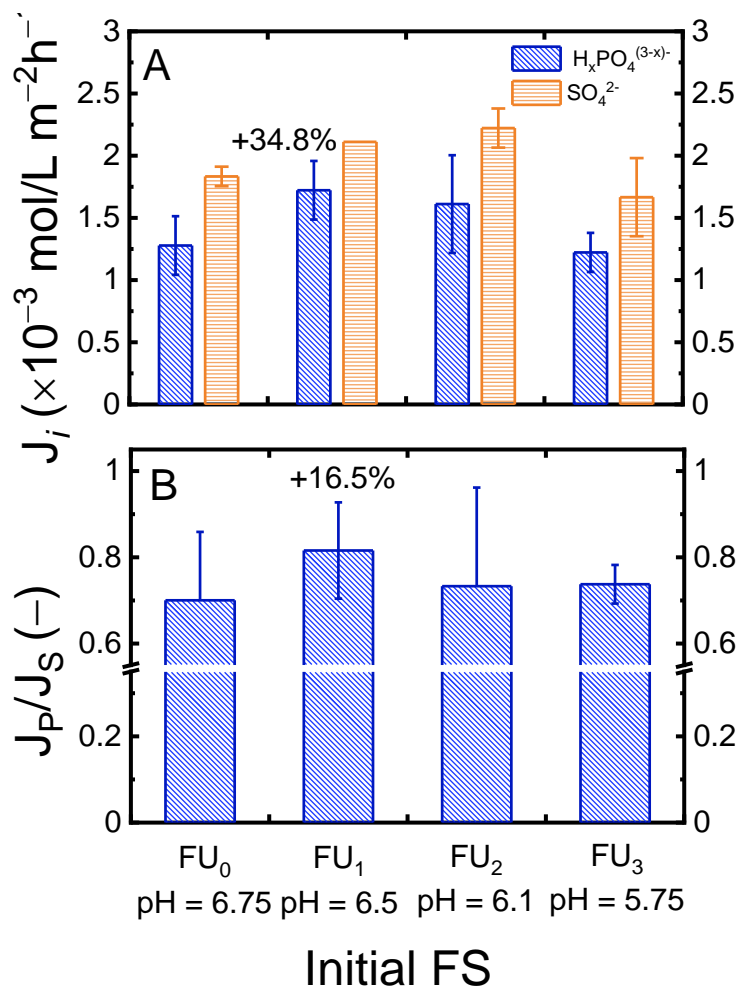


**Figure 5.4.** Ion fluxes  $J_P$  and  $J_S$  (A, patterned blue and orange columns, respectively), and relative fluxes,  $J_P/J_S$  (B, patterned blue column), in DD kinetic experiments with different feed solutions of FU<sub>0</sub> (simulated fresh urine, pH = 6.75), FU<sub>1</sub> (simulated fresh urine +  $6.25 \times 10^{-3}$  mol/L HCl, pH = 6.5), FU<sub>2</sub> (simulated fresh urine +  $7.50 \times 10^{-3}$  mol/L HCl, pH = 6.1), and FU<sub>3</sub> (simulated fresh urine +  $12.5 \times 10^{-3}$  mol/L HCl, pH = 5.75). FU<sub>0</sub> is simulated fresh urine without BPM-ED operation, and FU<sub>1</sub>, FU<sub>2</sub>, and FU<sub>3</sub> model the acid chamber effluents of BPM-ED operation mode 1 at current density 10 mA/cm<sup>2</sup> for 10, 15, and 20 minutes of operation, respectively. All DD experiments were operated with  $600 \times 10^{-3}$  mol/L KCl as the receiver solution. Error bars indicate standard deviations of duplicate experiments. Labels above select columns indicate the percent increase in  $J_P$  and  $J_P/J_S$  relative to operation with FU<sub>0</sub> FS.

The relationship between sulfate flux,  $J_S$ , and DD FS is less clear. There is an initial slight increase in  $J_S$  with BPM-ED, i.e., operations at 10 and 15 min, which produce FU<sub>1</sub> and FU<sub>2</sub>, followed by a decrease at 20 min, i.e., FU<sub>3</sub>. In the discussion accompanying Figure 5.2, the

mechanism of competitive  $\text{H}_x\text{PO}_4^{(3-x)-}$  and  $\text{SO}_4^{2-}$  sorption and transport is provided. This factor drove a lower  $J_S$  with a higher  $J_P$ . However, the results of Figure 5.4A do not follow the same clear trend. One point to consider is that there are less significant variations in  $J_P$  in the experiments presented in Figure 5.4A (i.e., largest difference is 34.8%) compared to experiments in Figure 5.2 (i.e., difference of 78.6%) because pH differences in orthophosphate speciation are less pronounced in the FS of Figure 5.4A (FU<sub>0</sub>, FU<sub>1</sub>, FU<sub>2</sub>, and FU<sub>3</sub>) relative to Figure 5.2 (fresh urine at pHs of 6.0 and 9.2). As a result, the relative differences in  $J_S$  in DD with different FS are smaller for the experiments in Figure 5.4A. Another factor to consider is the progressively higher  $\text{Cl}^-$  concentration from FU<sub>0</sub> to FU<sub>1</sub>, FU<sub>2</sub>, and FU<sub>3</sub> as more HCl is generated during BPM-ED operation. Chloride content can present competition for both  $\text{H}_x\text{PO}_4^{(3-x)-}$  and  $\text{SO}_4^{2-}$  ion sorption, which consequently can hinder both  $\text{H}_x\text{PO}_4^{(3-x)-}$  and  $\text{SO}_4^{2-}$  transport. This factor drives a decrease in  $J_S$  with longer BPM-ED operation, i.e., higher  $[\text{Cl}^-]_{\text{FS},0}$ . However, these mechanisms do not explain the slightly higher  $J_S$  for DD with FU<sub>1</sub> and FU<sub>2</sub> relative to the other FS of FU<sub>0</sub> and FU<sub>3</sub>. Future studies can examine additional FS pH and chloride content to further explore this trend.

Figure 5.4B presents the relative flux of orthophosphate to sulfate,  $J_P/J_S$ , in DD with each FS. The competing factors that impact  $J_P$  and the multifaceted influences on  $J_S$  result in a complex  $J_P/J_S$  trend across the different FS. The highest  $J_P/J_S$  was achieved in operation with FU<sub>1</sub> (i.e., 10 min BPM-ED operation at 10 mA/cm<sup>2</sup>), which resulted in 16.5% improvement on average from operation with raw fresh urine, FU<sub>0</sub> (i.e., fresh urine without BPM-ED treatment). This operation also resulted in the greatest improvement to orthophosphate flux of 34.8% relative to raw fresh urine. BPM-ED can alter the pH of urine to facilitate higher P flux and selectivity, but the gains are relatively small. Nevertheless, because high  $J_P$  and  $J_P/J_S$  are advantageous for orthophosphate recovery, subsequent sections employ the best performance operation with FU<sub>1</sub>.

**BPM-ED can Enhance Ammonia Transport in Membrane Distillation by Purposefully Tuning the pH of Hydrolyzed Urine.** As discussed in previous subsections, IMD feed solution pH impacts TAN speciation between  $\text{NH}_3$  and  $\text{NH}_4^+$ , and thereby influencing  $P_{F,A} - P_{C,A}$ , the driving force for ammonia transport. Figure 5.5A demonstrates  $[\text{NH}_3]$ ,  $[\text{NH}_4^+]$ , and ammonia vapor pressure,  $P_{F,A}$ , as dashed red, dashed blue, and solid green lines, respectively, in hydrolyzed urine at various pHs with a constant concentration of TAN. Note that these calculations consider a solution temperature of  $40^\circ\text{C}$  for IMD operation, which shifts the pH,  $pK_a$ , and resultant TAN speciation compared to solutions at  $20^\circ\text{C}$ . As pH increases, the fraction of TAN present as  $\text{NH}_3$  increases and as  $\text{NH}_4^+$  decreases. At  $\text{pH} \approx 10.5$ , almost complete predominance of  $\text{NH}_3$  over  $\text{NH}_4^+$  is reached, and higher pH only marginally increases  $[\text{NH}_3]$ . At constant  $[\text{TAN}]$  (as in Figure 5.5), higher solution pH beneficially increases  $P_{F,A}$ .

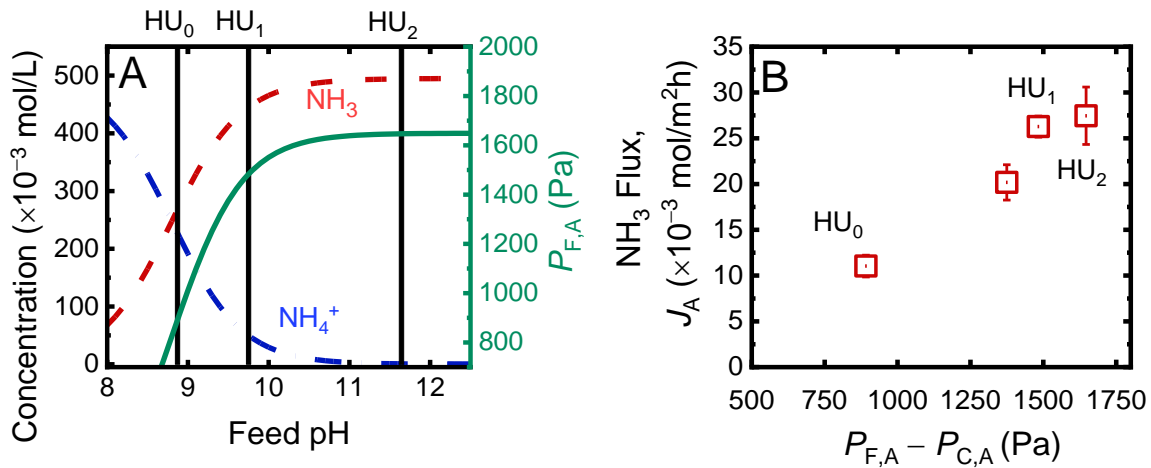


**Figure 5.5.** Concentration of ammoniacal nitrogen species of  $\text{NH}_3$ , depicted as a dashed red line, and  $\text{NH}_4^+$ , depicted as a dot-dashed blue line, (A, left vertical axis) and ammonia vapor pressure in the solution,  $P_{F,A}$ , depicted as a solid green line (A right vertical axis), as a function of IMD initial feed solution pH. Solid black columns designate solution pH, ammoniacal nitrogen speciation, and  $P_{F,A}$  of the hydrolyzed urine solutions of  $\text{HU}_0$ ,  $\text{HU}_1$ , and  $\text{HU}_2$ , which are hydrolyzed urine without BPM-ED, base chamber effluent of BPM-ED operation with hydrolyzed urine at a current density of  $20 \text{ mA/cm}^2$  for four hours ( $\text{HU}_0 + 335 \times 10^{-3} \text{ mol/L NaOH}$ ), and base chamber effluent of BPM-ED operation with

hydrolyzed urine at a current density of 40 mA/cm<sup>2</sup> for four hours (HU<sub>0</sub> + 527.5×10<sup>-3</sup> mol/L NaOH), respectively. Experimental ammonia vapor flux from feed to collector,  $J_A$ , versus ammonia vapor pressure gradient across the membrane,  $P_{F,A} - P_{C,A}$ , in operation with constant collector solution of DI water and varied hydrolyzed urine feed solution pHs (B). Feed solutions HU<sub>0</sub>, HU<sub>1</sub>, and HU<sub>2</sub> are designated in text. An additional point depicts operation with feed solution HU<sub>0</sub> + 250×10<sup>-3</sup> mol/L NaOH. Note that the analysis considers the total ammoniacal nitrogen concentration in all hydrolyzed urine solutions (495×10<sup>-3</sup> mol/L) and the membrane distillation operating temperature of 40°C.

Vertical black lines intersect [NH<sub>3</sub>], [NH<sub>4</sub><sup>+</sup>], and  $P_{F,A}$  for solutions of HU<sub>0</sub>, HU<sub>1</sub>, and HU<sub>2</sub>, which respectively represent typical hydrolyzed urine and base chamber effluents of four hours of mode 2 BPM-ED experiments at current densities of 20 mA/cm<sup>2</sup> and 40 mA/cm<sup>2</sup>. As discussed in previous subsections, BPM-ED mode 2 operation generates NaOH in the base chamber to increase the pH of hydrolyzed urine. Driving the pH of hydrolyzed urine from ≈8.9 (HU<sub>0</sub>) to ≈9.8 (HU<sub>1</sub>) with BPM-ED at 20 mA/cm<sup>2</sup> increases [NH<sub>3</sub>] and  $P_{F,A}$  by 66.3%. Doubling the BPM-ED current density to 40 mA/cm<sup>2</sup> shifts the hydrolyzed urine pH to ≈11.6 (HU<sub>2</sub>), yet only increases [NH<sub>3</sub>] and  $P_{F,A}$  by 10.0% relative to HU<sub>1</sub>. Higher BPM-ED current density more significantly increases the pH of hydrolyzed urine, but there are diminishing returns with respect to improving [NH<sub>3</sub>] and  $P_{F,A}$ . In other words, increasing the pH beyond a certain point only marginally increases [NH<sub>3</sub>] and results in negligible improvements to the driving force for ammonia transport. Another study reported a “critical pH” where near complete predominance of NH<sub>3</sub> is achieved and further NaOH generation in BPM-ED does not increase [NH<sub>3</sub>].<sup>269</sup>

The driving force for ammonia transport in IMD,  $P_{F,A} - P_{C,A}$  is directly proportional to the ammonia vapor pressure in the hydrolyzed urine feed solution,  $P_{F,A}$ . Note that analysis in Chapter 4 and Appendix C demonstrates that the build-up of ammonia vapor pressure in the collector solution,  $P_{C,A}$ , is marginal during the short experimental duration.<sup>74</sup> Therefore, greater  $P_{F,A}$ , achieved using BPM-ED is expected to increase  $P_{F,A} - P_{C,A}$  and enhance ammonia vapor flux in

IMD. To experimentally demonstrate the relationship between  $P_{F,A}-P_{C,A}$  and ammonia flux,  $J_A$ , IMD was operated at 40°C using DI water collector solution and various hydrolyzed urine solutions (constant TAN =  $495 \times 10^{-3}$  mol/L) at different pHs. The hydrolyzed urine solutions are HU<sub>0</sub> (i.e., simulating hydrolyzed urine without BPM-ED operation; pH = 8.8), HU<sub>1</sub> (i.e., simulating hydrolyzed urine solution after 4 h BPM-ED operation at 20 mA/cm<sup>2</sup>, which generated  $335 \times 10^{-3}$  mol/L NaOH in solution; pH = 9.8), HU<sub>2</sub> (i.e., simulating hydrolyzed urine solution after 4 h BPM-ED operation at 40 mA/cm<sup>2</sup>, which generated  $527.5 \times 10^{-3}$  mol/L NaOH in solution; pH = 11.7), and an additional solution of hydrolyzed urine +  $250 \times 10^{-3}$  mol/L NaOH (pH = 9.5). Figure 5.5B presents  $J_A$  in IMD experiments versus the driving force for ammonia transport,  $P_{F,A}-P_{C,A}$ , in each operation.

Generally,  $J_A$  versus  $P_{F,A}-P_{C,A}$  follows an increasing linear trend in accordance with eqn (5.1) (i.e., an increase in driving force for ammonia transport,  $P_{F,A}-P_{C,A}$ , resulted in greater ammonia flux). Note that the slope of  $J_A$  versus  $P_{F,A}-P_{C,A}$  ( $0.016 \times 10^{-3}$  mol m<sup>-2</sup> h<sup>-1</sup> / Pa) is the measured membrane vapor permeability coefficient,  $L_A$ . As demonstrated in Figure 5.5A, increasing solution pH increases  $P_{F,A}$  and consequently improves the driving force for ammonia permeation,  $P_{F,A}-P_{C,A}$  (with the constant condition of  $P_{C,A} \approx 0$ ). As expected, Figure 5.5B demonstrates that higher  $P_{F,A}-P_{C,A}$  improves experimentally measured NH<sub>3</sub> flux in IMD. BPM-ED can generate NaOH to drive up the pH of the FS and consequently improve ammonia flux by increasing  $P_{F,A}-P_{C,A}$ . Greater NaOH concentration in the hydrolyzed urine solution, as in operation with higher BPM-ED current densities (i.e., HU<sub>2</sub>>HU<sub>1</sub>), can more significantly increase solution pH, thereby driving a larger improvement in  $J_A$ . As a result,  $J_A$  is highest with FS containing  $528 \times 10^{-3}$  mol/L NaOH, i.e., HU<sub>2</sub>, followed by  $335 \times 10^{-3}$  mol/L NaOH, i.e., HU<sub>1</sub>, then  $250 \times 10^{-3}$  mol/L NaOH, and finally  $0 \times 10^{-3}$  mol/L NaOH, i.e., HU<sub>0</sub> (no BPM-ED operation prior to IMD).

Figure 5.6A demonstrates  $J_A$  in IMD with DI water collector and feeds of  $HU_0$ ,  $HU_1$ , and  $HU_2$ , i.e., the same experiments presented in Figure 5.5B, (patterned red columns, left vertical axis) as a function of BPM-ED current density. Employing BPM-ED at a current density of 20  $\text{mA}/\text{cm}^2$  prior to IMD operation, i.e., utilizing  $HU_1$  in IMD, resulted in significant improvements to  $J_A$  (138.0% increase) relative to operation without BPM-ED, i.e.,  $HU_0$ . As previously discussed, BPM-ED generates NaOH in hydrolyzed urine, thereby increasing pH, which favorably enhances  $P_{F,A}-P_{C,A}$ , the driving force for  $\text{NH}_3$  permeation. However, shifting the current density of BPM-ED to 40  $\text{mA}/\text{cm}^2$  resulted in diminishing returns on ammonia flux (i.e., minimal increase of only 4.5% relative to operation with  $HU_1$ ). There are a few factors that contribute to the diminishing returns on ammonia flux with higher BPM-ED current density. First, current density is inversely related to current efficiency, which is a measure of how effectively ions are transported across the IEMs.<sup>275, 276</sup> Therefore, BPM-ED operation at 40  $\text{mA}/\text{cm}^2$  has a lower current efficiency than operation at 20  $\text{mA}/\text{cm}^2$ . For this reason, operation at 40  $\text{mA}/\text{cm}^2$  generates less than double the NaOH as 20  $\text{mA}/\text{cm}^2$  (i.e.,  $HU_2$  contains  $527.5 \times 10^{-3}$  mol/L NaOH and  $HU_1$  contains  $335 \times 10^{-3}$  mol/L NaOH). Second, as previously discussed, increasing the pH of hydrolyzed urine beyond a certain pH results in only marginal increases in  $[\text{NH}_3]$  and  $P_{F,A}$ . The result is a larger increase in the driving force for ammonia permeation,  $P_{F,A}-P_{C,A}$ , between operations with  $HU_1$  (i.e., 20  $\text{mA}/\text{cm}^2$ ) and  $HU_0$  (i.e., 0  $\text{mA}/\text{cm}^2$ ) compared to  $HU_2$  (i.e., 40  $\text{mA}/\text{cm}^2$ ) and  $HU_1$ .

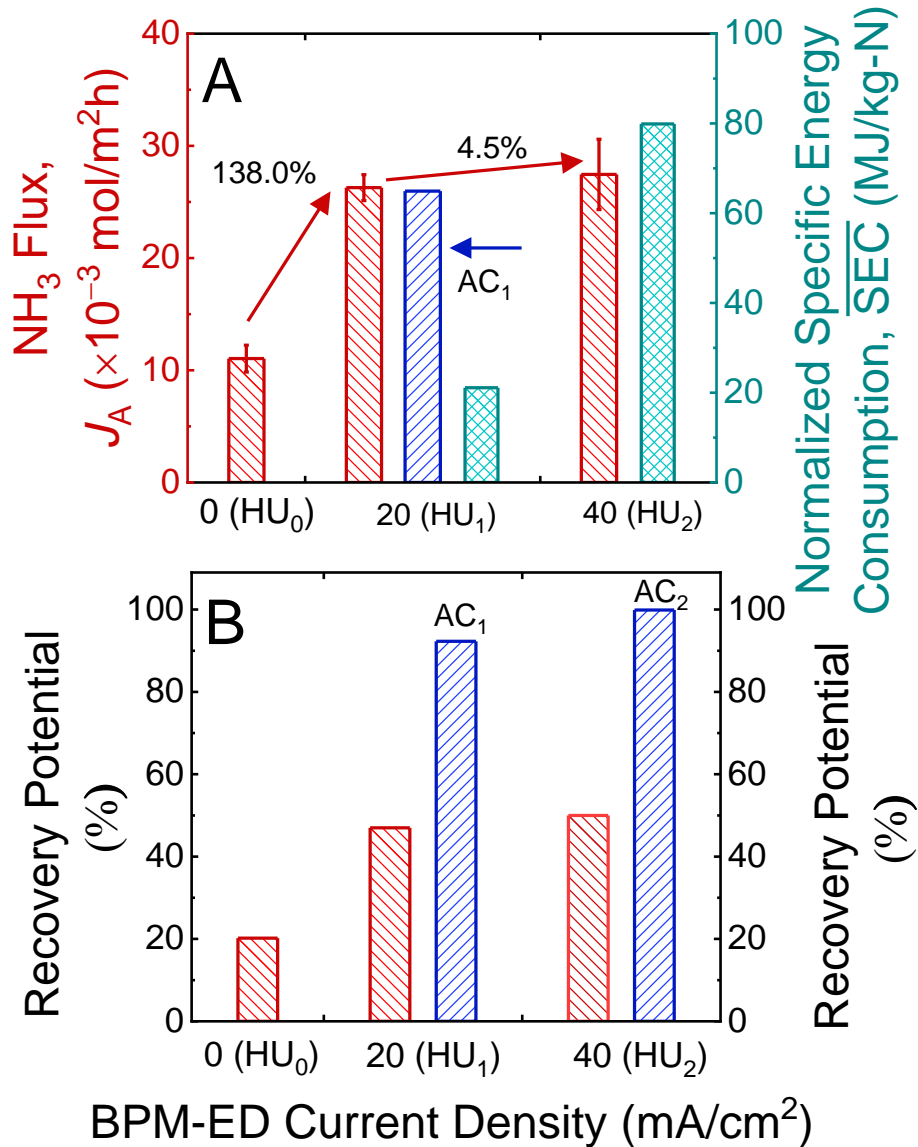


**Figure 5.6.** NH<sub>3</sub> vapor flux,  $J_A$ , (A, left vertical axis, patterned red columns) and specific energy consumption,  $\overline{SEC}$ , of the BPM-ED step (A right vertical axis, patterned green columns) in isothermal membrane distillation experiments with different initial hydrolyzed urine feed solutions of HU<sub>0</sub>, HU<sub>1</sub>, and HU<sub>2</sub> as a function of BPM-ED current density. Solutions HU<sub>0</sub>, HU<sub>1</sub>, and HU<sub>2</sub> are hydrolyzed urine without BPM-ED (i.e., current density = 0 mA/cm<sup>2</sup>), base chamber effluent of BPM-ED operation with hydrolyzed urine at a current density of 20 mA/cm<sup>2</sup> for four hours, and base chamber effluent of BPM-ED operation with hydrolyzed urine at a current density of 40 mA/cm<sup>2</sup> for four hours, respectively. The text coinciding with the red arrow indicates the percent increase in  $J_A$  between operations. All collector solutions are DI water unless otherwise specified as AC<sub>1</sub> (acidic collector).  $J_A$  in operation with HU<sub>1</sub> and AC<sub>1</sub>, which is the acid chamber effluent in BPM-ED operation with  $600 \times 10^{-3}$  mol/L KCl at a current density of 20 mA/cm<sup>2</sup> diluted by a factor of 10, is depicted as patterned blue columns corresponding to

the left vertical axis. TAN recovery potentials in batch operations of isothermal membrane distillation with various feed and collector solutions of equal volumes (B). Recovery potential is determined as the maximum percent TAN from the initial feed solution captured in the collector before the  $\text{NH}_3$  vapor pressure gradient across the membrane,  $P_{F,A} - P_{C,A}$ , is zero, i.e., when the driving force for  $\text{NH}_3$  transport ceases. In all operations, the isothermal operating temperature is  $40^\circ\text{C}$ .  $\text{HU}_0$ ,  $\text{HU}_1$ , and  $\text{HU}_2$  are hydrolyzed urine without BPM-ED, base chamber effluent of BPM-ED operation with hydrolyzed urine at a current density of  $20 \text{ mA/cm}^2$  for four hours, and base chamber effluent of BPM-ED operation with hydrolyzed urine at a current density of  $40 \text{ mA/cm}^2$  for four hours, respectively.  $\text{AC}_1$  and  $\text{AC}_2$  are the acid chamber effluents of BPM-ED operation at  $20 \text{ mA/cm}^2$  and  $40 \text{ mA/cm}^2$ , respectively, both diluted by a factor of 10.

In addition to ammonia flux, the specific energy consumption, SEC, is another key performance metric. SECs, ( $\text{kWh/m}^3$  acid and/or base produced) of 4 h BPM-ED mode 2 at current densities of  $20 \text{ mA/cm}^2$  and  $40 \text{ mA/cm}^2$ , i.e., the operations that produce  $\text{HU}_1$  and  $\text{HU}_2$ , respectively, were calculated using eqn (5.2) (additional details on the methods for calculating SEC are discussed in Appendix D.1).

$$\text{SEC} = \frac{I \int_0^t U(t) dt}{V} \quad (5.2)$$

where  $U$  is voltage across the stack,  $V$  is the volume of the base/acid solution produced (i.e., chamber volumes of 100 mL), and  $t$  is the duration of the experiment.<sup>275</sup> Note this equation assumes a constant current density over time, which was applied in this study.

In this analysis, SEC is divided by the kg-nutrient captured in downstream DD and IMD-AC operations, yielding  $\overline{\text{SEC}}$ . This was accomplished by considering the SEC of the BPM-ED step needed to support the treatment of a person's urine per day. The assumptions in the analysis are the volume of urine captured per day ( $\approx 2\text{L}$ ),<sup>44, 89, 91-96</sup> which is the volume sent to the acid and base chambers in the BPM-ED step, and the amount of P and N excreted in this urine per day (0.93 and 14 g, respectively). Figure 5.6A demonstrates the  $\overline{\text{SEC}}$ s of BPM-ED for productions of the

different hydrolyzed urine feed streams of  $HU_0$ ,  $HU_1$ , and  $HU_2$  (patterned green columns, right vertical axis). Note that because  $HU_0$  is raw hydrolyzed urine without BPM-ED, the  $\overline{SEC}$  for the BPM-ED step is zero.

There is a tradeoff between improvements in  $J_A$  and higher  $\overline{SEC}$  with increasing current density. Applying a higher current,  $I$ , in BPM-ED generates more NaOH, which enhances ammonia flux in downstream IMD operation as previously discussed, but it also demands more electrical energy.<sup>275</sup> Figure 5.6A demonstrates that operation at 40 mA/cm<sup>2</sup> results in approximately 4× higher  $\overline{SEC}$  relative to operation with 20 mA/cm<sup>2</sup>. The inherent tradeoff between faster kinetics for acid/base production and the higher energy consumption is discussed in previous studies.<sup>275, 276</sup> Eqn (5.2) shows that  $\overline{SEC}$  is proportional to the applied current in the operation. In Figure 5.6A, the  $\overline{SEC}$  is 4× higher with only a 2× increase in current density (i.e., from 20 to 40 mA/cm<sup>2</sup>) because  $\overline{SEC}$  is also proportional to voltage, where voltage is 1.9× higher at 40 mA/cm<sup>2</sup>. See the Appendix D.1 for more information on the prediction of voltage and  $\overline{SEC}$  in each operation.

**BPM-ED can Improve Ammonia Recovery in Membrane Distillation by Generation of an Acidic Collector.** BPM-ED mode 2 generates NaOH in the base chamber, which produces hydrolyzed urine solutions of  $HU_1$  and  $HU_2$ , while simultaneously generating  $H_2SO_4$  in the acid chamber. This  $H_2SO_4$  solution can be employed as the acidic collector in IMD-AC for N recovery. IMD-AC experiments were conducted using  $HU_1$  feed solution and  $AC_1$  collector solution, which are the base and acid chamber effluents, respectively, of BPM-ED mode 2 operation at 20 mA/cm<sup>2</sup> for 4 h. Figure 5.6A shows  $J_A$  in IMD-AC with  $HU_1$  feed and  $AC_1$  collector (patterned blue column, left vertical axis). Employing  $AC_1$  did not significantly impact  $J_A$  relative to operation

with DI water collector (i.e., >2% difference between the operations). This is a different finding than that of Chapter 4, which reported that using an acidic collector (comprising acetic acid) improved  $J_A$  relative to operation with DI water collector.<sup>74</sup> In Chapter 4, it was postulated that ammonia dissolution into a neutral pH collector is slower than ammonia permeation, resulting in elevated interfacial  $P_{C,A}$  and decreased driving force for ammonia flux,  $P_{F,A}-P_{C,A}$ . That study postulated that applying an acidic collector can mitigate this kinetic limitation of ammonia dissolution and prevents the build-up of interfacial  $P_{C,A}$ , thereby improving ammonia flux.<sup>74</sup>

There are a number of key differences between the two studies that may contribute to this discrepancy. First, the current study simulates all major ion concentrations in raw hydrolyzed urine, while Chapter 4 employed a simpler hydrolyzed urine solution simulating the TAN and bicarbonate concentrations. Second, the current study employs an acidic collector with  $H_2SO_4$ , i.e., a strong acid, at a concentration =  $22 \times 10^{-3}$  mol/L, while work in Chapter 4 utilized an acetic acid, i.e., a weak acid, solution of  $100 \times 10^{-3}$  mol/L. Third, the current study uses  $HU_1$ , which includes  $335 \times 10^{-3}$  mol/L NaOH and has a pH  $\approx 9.8$  at  $40^\circ C$ , while work in Chapter 4 utilized a hydrolyzed urine feed solution without NaOH and a pH  $\approx 8.8$  at the same temperature. As discussed in preceding paragraphs, higher feed pH results in higher  $P_{F,A}$ ; in these cases, there is a 66.4% increase in  $P_{F,A}$  for this study relative to the previous. As a result, it is possible that  $P_{C,A}$  contributes less significantly toward  $P_{F,A}-P_{C,A}$  in this study. However, future studies need to further examine how  $P_{C,A}$  is influenced by ammonia vapor permeation and collector solution pH.

Ammonia recovery potential, i.e., the amount of TAN from the feed that can be recovered in the receiver, is another key performance metric. Analysis was conducted to predict ammonia recovery potential with different feed and collector combinations of:  $HU_0$  and DI water,  $HU_1$  and DI water,  $HU_1$  and  $AC_1$  (i.e., the base and acid chamber effluents, respectively, of 4 h BPM-ED

mode 2 operation at 20 mA/cm<sup>2</sup>), HU<sub>2</sub> and DI water, and HU<sub>2</sub> and AC<sub>2</sub> (i.e., the base and acid chamber effluents, respectively, of 4 h BPM-ED mode 2 operation at 40 mA/cm<sup>2</sup>) and is presented in Figure 5.6B. Recovery potential is determined as the maximum percent of TAN from the initial feed solution captured in the collector before the NH<sub>3</sub> vapor pressure gradient across the membrane,  $P_{F,A} - P_{C,A}$ , is zero, i.e., when the driving force for NH<sub>3</sub> transport ceases. BPM-ED operation at higher current densities increases  $P_{F,A}$ , which enables more ammonia recovery in the collector solution prior to  $P_{F,A} = P_{C,A}$ . For example, ammonia recovery potential is 132.7% higher with current density of 20 mA/cm<sup>2</sup> (HU<sub>1</sub>) relative to no BPM-ED operation (HU<sub>0</sub>) and with DI water collector solutions in both scenarios. As observed with ammonia flux, increasing the current density from 20 to 40 mA/cm<sup>2</sup> results in diminishing returns; for recovery potential only 6.4% higher is predicted in operations with HU<sub>2</sub> relative to HU<sub>1</sub> and using constant collector of DI water.

Introducing the acidic collectors generated in the acid chamber of BPM-ED (i.e., AC<sub>1</sub> and AC<sub>2</sub> for current densities of 20 and 40 mA/cm<sup>2</sup>, respectively) to IMD operation significantly improves ammonia recovery potential. Over 90% ammonia recovery potential was determined for operations with HU<sub>1</sub>/AC<sub>1</sub> and HU<sub>2</sub>/AC<sub>2</sub> (i.e., utilizing both the base and acid chamber effluents of 4 h BPM-ED mode 2 operation at 20 and 40 mA/cm<sup>2</sup>, respectively). Critically, <50% TAN recovery potential can be achieved in batch IMD operation with equal feed and collector volumes without the use of an acidic collector. Operation of IMD with DI water collector elevates  $P_{C,A}$  over time as NH<sub>3</sub> transports from feed to collector. For DI water collectors, the pH increases above the pK<sub>a</sub> of ammonia, meaning NH<sub>3</sub> is the predominant form of ammoniacal nitrogen in DI water collectors. The driving force for ammonia permeation will cease when  $P_{F,A} = P_{C,A}$ , which occurs if 50% NH<sub>3</sub> transports to the collector and remains predominantly NH<sub>3</sub> in the collector. As discussed in a previous section, an acidic collector can maintain pH < pK<sub>a</sub> of ammonia to protonate

NH<sub>3</sub> transported from the feed to NH<sub>4</sub><sup>+</sup>, which is nonvolatile.<sup>16, 17, 25-3</sup> As a result,  $P_{C,A}$  increases to a lesser extent, which enables more ammonia recovery before  $P_{F,A} = P_{C,A}$ .

Operation with HU<sub>2</sub>/AC<sub>2</sub> (i.e., 40 mA/cm<sup>2</sup> current density) resulted in 8.3% higher ammonia recovery potential than operation with HU<sub>1</sub>/AC<sub>1</sub> (i.e., 20 mA/cm<sup>2</sup> current density). This increase is in part due to the aforementioned factor driving higher  $P_{F,A}$  at increased current density. Additionally, higher BPM-ED current densities produce higher acid concentrations in the same timeframe, i.e., more H<sub>2</sub>SO<sub>4</sub> in AC<sub>2</sub> compared to AC<sub>1</sub>. As a result, AC<sub>2</sub> has a higher buffering capacity than AC<sub>1</sub>, so more NH<sub>3</sub> transport is required to drive pH > pK<sub>a</sub> and shift predominance from NH<sub>4</sub><sup>+</sup> to NH<sub>3</sub>. This enables lower  $P_{C,A}$  at the same TAN recovery and ultimately higher ammonia recovery before  $P_{F,A} = P_{C,A}$ .

Importantly, the application of acidic collector does not increase the  $\overline{SEC}$  relative to operation with DI water collector because BPM-ED operation generates these streams in the acid chamber during the same operations that HU<sub>1</sub> and HU<sub>2</sub> are produced, i.e., both the base and acid chamber effluents of BPM-ED are put to use in the IMD step. For this reason, it may be advantageous to utilize the acid chamber effluent of BPM-ED as an acidic collector in IMD to enhance ammonia recovery potential, demonstrated in Figure 5.6B, even though Figure 5.6A demonstrates that the operation may not benefit kinetics.

**Energy Consumption of the BPM-ED, DD, and IMD Integrated Membrane Process for Nutrient Recovery is Competitive with Linear Economy Approaches.** The membrane techniques applied for P and N recovery of BPM-ED, DD, and IMD require chemical and energy inputs for operation. The following analysis presents the specific energy requirements for each nutrient recovery technology normalized by mol-nutrient recovered. Note that chemical inputs can contribute significantly to the operating costs and environmental footprint of a system and can be

considered in future analysis, but are not considered in this analysis. Similarly, pumping costs and module-scale effects are neglected in this analysis because these are dependent on system-specific conditions.

First, for P recovery, the BPM-ED step requires electric energy to supply the current that is applied across the cell.<sup>269-275</sup> For the DD step, an electrochemical potential gradient setup by a high concentration of chloride ions in the RS drives orthophosphate transport from FS to RS and an external electric source is not required to drive the exchange of driver and target ions. For P recovery, the sum of  $\overline{SEC}$ s for 10 min BPM-ED at 10 mA/cm<sup>2</sup> for HCl generation in fresh urine (i.e., FU<sub>1</sub> stream) and DD is presented (termed BPM-ED + DD) in Figure 5.7. For comparisons, Figure 5.7 also presents the ranges in energy requirements for the conventional methods for P fertilizer production and P removal at WWTPs (i.e., the linear economy approach) of phosphate rock mining and enhanced biological phosphate removal (EBPR)<sup>277</sup>, respectively.

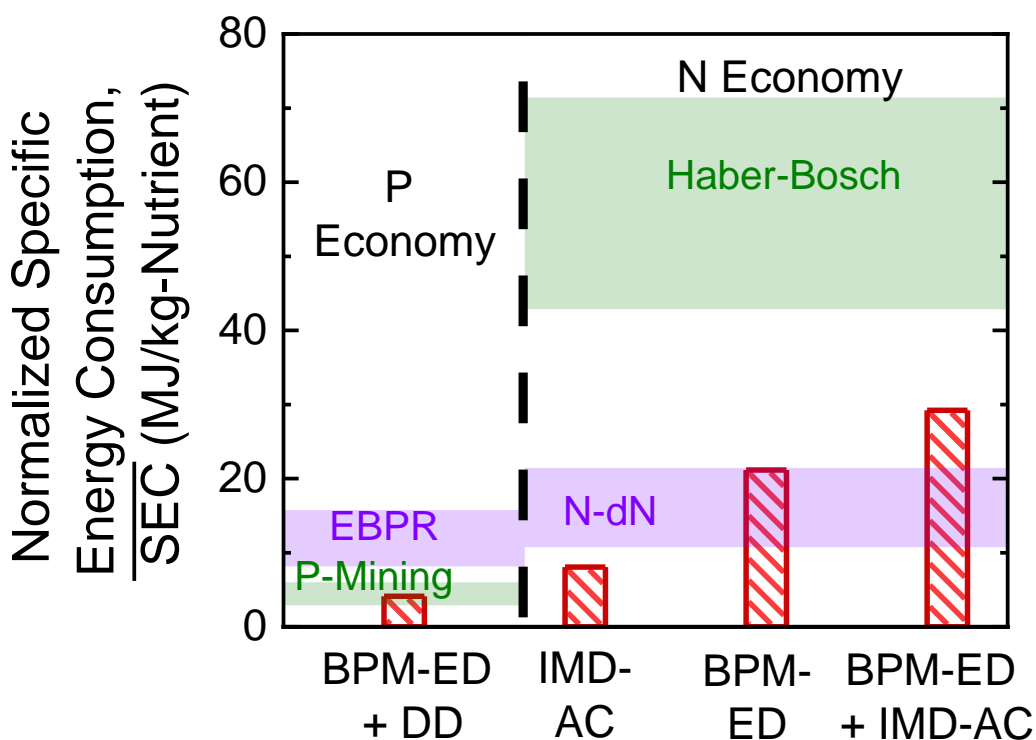


**Figure 5.7.** Specific energy consumption,  $\overline{SEC}$ , (MJ/mol-P or N) for nutrient recovery technologies is depicted as patterned red columns. For orthophosphate recovery,  $\overline{SEC}$  for the combined bipolar membrane electro dialysis (BPM-ED) operation at current density 10 mA/cm<sup>2</sup> for 10 minutes (i.e., production of FU<sub>1</sub> stream) and Donnan dialysis (DD) technology is shown. For nitrogen recovery,  $\overline{SEC}$  s for isothermal membrane distillation with acidic collector (IMD-AC), BPM-ED operation at current density 20 mA/cm<sup>2</sup> for four hours (i.e., production of HU<sub>1</sub> and AC<sub>1</sub> streams), and the combined BPM-ED + IMD-AC technologies are shown. Note that the calculations do not include the chemical energies from the chemicals that are supplied to the systems. For comparison, the range in practical energy requirements for production of nutrients by conventional methods, i.e., phosphate rock mining (P-mining) and nitrogen fixation by the Haber-Bosch process, are depicted as green-shaded regions. Additionally, the range in energy requirements for conventional nutrient removal processes at wastewater treatment plants of enhanced biological phosphate removal (EBPR)<sup>277</sup> and nitrification-denitrification (N-dN), are depicted as violet shaded regions.

The  $\overline{SEC}$  for combined BPM-ED + DD for P recovery (where only the BPM-ED process contributes to  $\overline{SEC}$ ) can be below the practical energy requirements of EBPR for P removal and within the range for P mining. Note that P recovery closes the nutrient loop, enabling both production and removal. When compared against the sum of the practical energy requirements of the linear P economy (i.e., P mining and EBPR), the  $\overline{SEC}$  of BPM-ED + DD is 53.3–82.7% lower. Techno-economic assessments are needed to gauge the complete energy requirements for a BPM-ED + DD system (i.e., including pumping costs and module scale effects) as well as material and chemical costs. Additional assessments can evaluate the benefits and costs of employing BPM-ED prior to DD compared to DD alone. Such analysis can consider the benefits of improved orthophosphate transport and selectivity, which can decrease the membrane area required for the same orthophosphate productivity and increase the orthophosphate recovery potential, respectively, at the cost of capital requirements and electrical energy use for the BPM-ED system.

Next, for N recovery,  $\overline{SEC}$ s of IMD-AC, BPM-ED, and combined BPM-ED + IMD are determined. In IMD-AC, thermal energy is required for the vaporization of components that can transport across the membrane, which are  $NH_3$  and  $H_2O$  in this study. Convective heat flux of species  $i$  is the product of the vaporization enthalpy,  $\Delta H_i$ , and the flux,  $J_i$ , and the total convective heat flux is the sum of the individual components, i.e.,  $\sum \Delta H_i J_i$ .<sup>212</sup> To determine the  $\overline{SEC}$  of the IMD step,  $\sum \Delta H_i J_i$  is divided by  $J_A$  to yield energy consumption per mole of ammonia recovered. Note that the method for determining thermal energy requirements IMD is further detailed in Chapter 4 and Appendix C.<sup>74</sup> Figure 5.7 presents the  $\overline{SEC}$  of the IMD-AC technique. For comparisons, Figure 5.7 also presents the ranges in energy requirements for the conventional methods for N fertilizer production and N removal at WWTPs (i.e., the linear economy approach) of Haber-Bosch for N fixation and nitrification-denitrification (N-dN)<sup>48, 183-185</sup>, respectively.

The  $\overline{SEC}$  for IMD-AC for N recovery can be below the energy requirements for N production via conventional means of the Haber-Bosch process as well as N removal by conventional means of nitrification-denitrification. However, IMD-AC without BPM-ED employs an acidic collector supplied by external chemicals, which can contribute to operating costs. An alternative N recovery technique examined in this study is first employing BPM-ED at  $20 \text{ mA/cm}^2$  for production of acids/bases *in situ* to generate  $HU_1$  (i.e., higher pH hydrolyzed urine) and  $AC_1$  (acidic collector stream), which are then utilized in downstream IMD process for N recovery. Figure 5.7 presents the  $\overline{SEC}$  of the BPM-ED step as well as the combined technique of BPM-ED + IMD.

The  $\overline{SEC}$  of BPM-ED process for the production of  $HU_1$  and  $AC_1$  (in the N recovery technique) is  $\approx 5\times$  that of the BPM-ED process for the production of  $FU_1$  (in the P recovery

technique). As previously discussed, hydrolyzed urine has a higher buffering capacity than fresh urine, and as a result requires more acid or base to alter pH. Therefore, higher current density and duration are required for the production of enough base to reach the desired pH of  $HU_1$  relative to the acid required to reach the desired pH of  $FU_1$ . Consequently, the BPM-ED step in the N recovery technique has a higher  $\overline{SEC}$  than the BPM-ED step of the P recovery technique.

Applying the BPM-ED technique prior to IMD (i.e., the combined BPM-ED + IMD technique for N recovery) does introduce considerable energy consumption of 38.1% increase relative to IMD-AC alone. However, using BPM-ED generates  $AC_1$ , which replaces the need for supplemental chemicals as the acidic collector, and simultaneously increases the pH of hydrolyzed urine to improve ammonia flux. Furthermore, BPM-ED + IMD achieves higher ammonia fluxes than IMD-AC alone, which decreases the membrane area required for the same productivity of ammonia transport. Techno-economic assessments can evaluate the benefits and costs of employing BPM-ED prior to IMD compared to IMD alone.

Despite higher  $\overline{SEC}$  relative to IMD-AC only, the combined BPM-ED and IMD-AC technique for N recovery are still 31.8–59.1% lower than the practical energy needed for the Haber-Bosch process for N production. The  $\overline{SEC}$  for the N recovery technique is, however, higher than the practical energies for nitrification-denitrification. Note that the technology performs both tasks of removing N as a contaminant and producing a valuable fertilizer. A comparison of the sum of the linear N economy, i.e., Haber Bosch + nitrification-denitrification (53.6–92.9 MJ/mol-N), and the BPM-ED + IMD-AC technique demonstrates that the  $\overline{SEC}$  of the N recovery approach is 45.5–68.6% lower than the practical energy of the linear N economy.

## 5.5 Implications

Closing the nutrient loop by capturing P and N from waste streams can reduce nutrient emissions to aquatic environments and help prevent harmful algal blooms. At the same time, recovering these nutrients as value-added fertilizer products can lessen the reliance on the conventional methods for fertilizer production, P mining and N fixation by the Haber-Bosch process, which are currently practiced at unsustainable levels. High concentrations of orthophosphate,  $H_xPO_4^{(3-x)-}$ , and ammonia,  $NH_3$ , in fresh and hydrolyzed urine, respectively, offer opportunities for recovery using DD and IMD, respectively. This study elucidated the role of solution pH and nutrient speciation ( $H_2PO_4^-/HPO_4^{2-}$  and  $NH_4^+/NH_3$ ) on DD and IMD performance. For DD with a monovalent ion-selective membrane, orthophosphate flux and selectivity are improved with feed  $pH \ll pK_{a2}$  of phosphate in which the predominant orthophosphate species is monovalent  $H_2PO_4^-$ , which is preferentially passed by the monovalent ion-selective membrane. For IMD, ammonia flux and recovery are improved with feed  $pH \gg pK_a$  of ammonia where the predominant ammoniacal N species is  $NH_3$ , which is volatile and can transport across the hydrophobic microporous membrane. BPM-ED is a technique for acid/base production *in situ* and was employed here to strategically control the pHs of various solutions for the benefit of DD and IMD performances. BPM-ED can leverage low-cost/waste resources of salt solutions to provide electrolyte for acid/base production, which can benefit the economic feasibility of the approach.

Orthophosphate flux and selectivity in DD with a MIPM can be enhanced by first employing BPM-ED for HCl production to decrease the pH of fresh urine. However, this study found that high doses of HCl can detrimentally impact orthophosphate flux by increasing the chloride sorption to the AEM, which consequently hinders the sorption and transport of

orthophosphate. Furthermore, generating higher amount of HCl in BPM-ED either through increased duration, as in this study, or with higher current density will increase the  $\overline{\text{SEC}}$  of the BPM-ED step. Crucially, the specific energy consumption for P recovery with BPM-ED + DD performance can be lower than the practical energy of P removal at centralized WWTP by EBPR, the primary advanced P removal technique. The  $\overline{\text{SEC}}$  of BPM-ED + DD is also comparable to practical energies of P-mining, the primary P fertilizer production method. Furthermore, P recovery both removes P as a contaminant and produces P fertilizer, therefore the  $\overline{\text{SEC}}$  should be compared against the sum of EBPR and P-mining, i.e., the linear P economy. Importantly, the  $\overline{\text{SEC}}$  for P recovery by BPM-ED + DD is 53.3–82.7% lower than the sum of the practical energies of the linear economy approach to P management.

Ammonia flux and recovery potential in IMD can be improved by first employing BPM-ED to generate NaOH and increase the pH of hydrolyzed urine. In a solution of sufficiently high pH, ammoniacal nitrogen is predominantly  $\text{NH}_3$ , which is a volatile form of N and can transport across the hydrophobic microporous membrane used in MD. Higher BPM-ED current densities more significantly increase hydrolyzed urine pH, which drives higher fraction of TAN as  $\text{NH}_3$  and beneficially improves the driving force for ammonia transport,  $P_{\text{F,A}} - P_{\text{C,A}}$ . However, the study observed diminishing returns in both flux and recovery potential with higher operating current densities in BPM-ED. Beyond a certain pH only a slight increase in  $P_{\text{F,A}}$  is predicted and as a result improvements to ammonia flux and recovery are minimal. Furthermore, operation at higher BPM-ED current densities has a larger  $\overline{\text{SEC}}$ .

BPM-ED simultaneously generates an acidic solution (i.e., in the same operation that NaOH is produced) that can be employed as the acidic collector solution in IMD. An acidic

solution protonates the  $\text{NH}_3$  transported over to the collector to  $\text{NH}_4^+$ , which beneficially enables uphill transport of TAN and improves N recovery potential. Importantly, employing the acidic solution produced in BPM-ED as the collector of IMD can enable N recoveries up to 99.9%, whereas the maximum N recovery without an acidic collector is 50%. In this study,  $\text{H}_2\text{SO}_{4(\text{aq})}$  was strategically generated in the BPM-ED step to enable the recovery of N as ammonium sulfate fertilizer solution in the IMD step. Thoughtful selection of the electrolyte solution in the BPM-ED step enables flexibility in tailoring the water chemistry and desired profile of the recovered N fertilizer. The improvements in  $\text{NH}_3$  flux and N recovery potential realized with the integration of BPM-ED and IMD-AC relative to IMD-AC alone are at the cost of 38.1% higher  $\overline{\text{SEC}}$ . Nevertheless, the  $\overline{\text{SEC}}$  for BPM-ED + IMD-AC is 31.8–59.1% lower than the practical energy needed in the conventional approach to N fertilizer production in the linear nutrient economy, the Haber-Bosch process. The  $\overline{\text{SEC}}$  is, however, higher than the practical energy of the conventional approach to N removal from wastewater in the N economy, nitrification-denitrification. Importantly, in a comparison against the practical energy requirement of the linear N economy (i.e., the sum of Haber-Bosch and nitrification-denitrification), the  $\overline{\text{SEC}}$  of BPM-ED + IMD-AC is 45.5–68.6% lower.

Future techno-economic assessments are needed to quantify the practical energy requirements, chemical costs, and capital costs of the integrated approach of BPM-ED + DD and BPM-ED + IMD to predict the overall expenditure in comparison to the linear economy methods. However, the integrated membrane approach does offer initial promise as a cost-competitive and environmentally-sensible technique for nutrient removal and recovery from source-separated urine. The economic viability of the technique can be further enhanced by employing low-cost/waste resources, such as seawater, desalination brine, and wastewater softening regenerant

rinse, as the electrolyte in BPM-ED and as the receiver solution in DD. Similarly, waste thermal energy can be supplied to drive  $\text{NH}_3$  transport in the IMD step.

Additional techno-economic assessments can examine the costs and benefits of different BPM-ED configurations (duration prior to DD or IMD and current density) to optimize the overall expenditure and fertilizer revenue. One notable aspect to consider is the tradeoff between higher nutrient fluxes, which decreases membrane area needed for the same productivity of recovery, at the cost of higher electricity consumption in the BPM-ED step. Additionally, the differences in overall expenditure and life-cycle environmental impacts for BPM-ED compared with external acid/base addition, which requires chemicals and energy inputs for production and transportation, for pH control can be assessed. One benefit of BPM-ED for acid/base production is the autonomy of the approach, which can be particularly beneficial if nutrient recovery is applied on a small-scale decentralized level. In contrast, external acid/base addition has added logistical concerns associated with transportation and safety.

The insights from this study are broadly applicable to other BPM-ED, DD, and MD systems. The study demonstrated that BPM-ED can be applied to strategically control the pH of fresh and hydrolyzed urine, which can have extended applications to other nutrient recovery approaches. For example, mineral precipitation of N and/or P fertilizers can be favored in certain pH ranges; BPM-ED can be used in place of external acid/base addition to drive the desired mineral precipitation. The study demonstrated that monovalent ion transport in DD with MIPM can be enhanced by strategically decreasing feed pH using BPM-ED. A similar approach can be considered when multivalent species are present together with target ions that are monovalent at certain pH ranges. An environmentally relevant example is  $\text{NH}_4^+$  recovery from wastewater. Additionally, this study elucidated the impacts of MD feed and collector pHs on the transport of

compounds that speciate between volatile and nonvolatile forms at different pHs. An environmentally relevant example is H<sub>2</sub>S (volatile as H<sub>2</sub>S and nonvolatile as HS<sup>-</sup>) removal from domestic or industrial wastewaters.

# **Chapter 6: Evaluation of Costs and Benefits of Nutrient Recovery in Onsite Wastewater Management**

## **Chapter Abstract**

The high concentrations of orthophosphate and ammonia in diverted human urine present significant opportunities for nutrient capture. Membrane-based processes have shown potential to recover the nutrients cost-effectively. In particular, Donnan dialysis (DD) for P recovery and membrane distillation (MD) for N recovery have demonstrated promising performance in terms of flux, selectivity, and recovery potential. In this study, the economic costs and benefits of building-scale onsite nutrient recovery using DD and MD are evaluated. The results of this analysis suggest a >70% reduction in operating costs by leveraging widely-available sources of recycled chemicals and recovered thermal energy. The primary capital expenditures are due to urine diversion toilets and additional piping for source-separation. Overall, the assessment predicts a total capital expenditure (CAPEX) of \$419K (annualized cost of \$27K over 30 years) and operating cost of \$2.7K/year for the production of 360 and 2700 kg-P and N-fertilizer/year, respectively. The predicted revenue from the fertilizer production is \$6.6K/year, which alone is not enough to cover the capital and operating expenditures of the system. However, the analysis presents a preliminary estimate of \$41K/year savings at downstream wastewater treatment plants, through avoided inputs for nutrient removal, achievable through onsite nutrient recovery. If downstream savings in wastewater treatment can be realized as an additional revenue source, potentially through policy incentives, then the modeled onsite urine diversion and nutrient recovery system can achieve nearly \$19K/year of net profit. Finally, the study considers an integration of onsite non-potable water reuse, thermal energy recovery, and nutrient recovery at a building modeling the specifications of the Solaire and predicts approximately \$23K/year net profit.

## 6.1 Introduction

As highlighted in previous chapters, the linear economy model to nutrient management where fertilizer is produced at immense energy costs and downstream nutrient waste is removed from wastewater at additional cost is inefficient. A more sustainable approach is the circular nutrient economy where P and N are captured from wastewater and utilized as fertilizer feedstock. Closing the nutrient loop enables simultaneous removal and capture of P and N preventing nutrient pollution and lessening the reliance on industrial fertilizer production.<sup>62-65</sup>

Analysis in chapter 2 demonstrates that the theoretical minimum energy cost for nutrient recovery, governed by thermodynamic principles, is substantial lower for nutrient-rich waste streams compared to diluted wastewaters.<sup>134</sup> Chapter 2 reports >10% and >40% reductions in the theoretical energy cost for P and N recovery from fresh and hydrolyzed urine, respectively, compared to diluted treated wastewater effluent.<sup>134</sup> Note that the primary form of N in fresh urine is urea,  $\text{CH}_4\text{N}_2\text{O}$ , which hydrolyzes to bicarbonate and bioavailable ammoniacal N, forming hydrolyzed urine, during  $\approx 2-7$  days of storage.<sup>89,90</sup> Mineral precipitation of slow-release fertilizers in urine is a promising nutrient recovery method.<sup>67, 68, 72, 89, 90, 114, 115, 135</sup> However, the technique incurs contamination risks from opportunistic pathogens, endocrine disrupting compounds, and pharmaceuticals.<sup>136-141</sup> Membrane techniques offer a barrier that can separate desired P and N species and retain contaminants of concern.<sup>167-172</sup> Chapter 3 and 4<sup>74, 268</sup> have demonstrated the promising potential of membrane-based processes of Donnan dialysis and membrane distillation for orthophosphate,  $\text{H}_x\text{PO}_4^{(3-x)-}$ , and ammonia,  $\text{NH}_3$ , recovery, respectively, from urine. However, for the methods to be feasible and widely-adopted, they must be economically viable. A paradigm shift from the existing wastewater infrastructure to urine diversion and nutrient recovery will

require capital investment and additional expenditures on chemical/energy/material inputs that need to be considered.

In this study, the economic costs and benefits of onsite nutrient recovery in a model residential building are assessed. First, the methods of Donnan dialysis for P recovery and membrane distillation for N recovery are described and the nutrient recovery infrastructure is detailed. Then, the capital expenditures of the nutrient recovery system are quantified and key contributors to cost are highlighted. Operating expenditures for Donnan dialysis and membrane distillation are determined and opportunities to employ recycled chemicals and recovered thermal energy to reduce these costs are explored. Next, nutrient recovery revenue is predicted from fertilizer prices and estimated savings in nutrient removal costs at downstream centralized wastewater treatment. Capital costs, operating costs, revenue, and net profits are predicted for a residential nutrient recovery system and a workplace nutrient recovery system of equivalent occupancy. Additionally, the analysis presents the costs, revenue, and profits for onsite wastewater management systems of 1. non-potable water reuse, 2. non-potable water reuse and thermal energy recovery, and 3. non-potable water reuse, thermal energy recovery, and nutrient recovery. Finally, the economic and environmental implications of the onsite wastewater management systems are discussed and directions for future analysis are offered.

## **6.2 Description of Onsite Nutrient Recovery**

This work examines the economic costs and benefits of implementing an onsite nutrient recovery system into a residential building. For the analysis, a building with equivalent capacity and specifications as the Solaire in New York City (NYC) will be considered, but the general method can be broadly extended to other premises. The Solaire was selected as a model building for this analysis because it presents a typical residential capacity for a high-density NYC apartment

complex and its existing sustainability initiatives have earned Leadership in Energy and Environmental Design (LEED) Gold certifications. For examples, the building has photovoltaic cells that generate electricity, energy efficient appliances, a non-potable water treatment and reuse system, and a thermal energy recovery unit for water heating. Like the proposed onsite nutrient recovery from human urine, the water reuse and thermal energy recovery units at the Solaire are systems of decentralized wastewater management. For this reason, this work examines the costs and benefits of the integration of all three features (i.e., non-potable water reuse, thermal energy recovery, and nutrient recovery) as onsite wastewater management.

In this model for onsite recovery of nutrients from human urine, two membrane-based techniques are utilized: Donnan dialysis (DD) for P recovery (introduced in Chapter 3) and membrane distillation (MD) for N recovery (introduced in Chapter 4). The working principles of DD are detailed in literature and Chapter 3<sup>142-144, 146-148, 151-154</sup> and are briefly explained here with a focus on orthophosphate recovery from diverted urine. In the proposed configuration of DD, fresh urine is the feed solution and a salt solution of high chloride content is the receiver solution. The flux of driver ions, in this study  $\text{Cl}^-$ , across and anion exchange membrane (AEM), from the high concentration receiver solution to the low concentration feed solution set up an electrochemical potential to drive the transport of target orthophosphate,  $\text{H}_x\text{PO}_4^{(3-x)-}$ , ions in the opposite direction.<sup>142-144, 146-148</sup> As such, orthophosphate is recovered in the receiver solution as P fertilizer product.

Likewise, the working principles of MD are detailed in literature and Chapter 4,<sup>74, 211, 212</sup> and are briefly explained here with focus on ammonia recovery from hydrolyzed urine. As previously mentioned, hydrolyzed urine is urine that has been stored for a number of days to enable the hydrolysis of urea to form ammoniacal N and bicarbonate. In the proposed configuration of

MD, hydrolyzed urine is the feed solution and an acidic solution is the collector solution. Volatile ammonia,  $\text{NH}_3$ , in hydrolyzed urine is driven across a hydrophobic microporous membrane to the collector solution by the difference in ammonia vapor pressure,  $P_A$ , between the feed, F, and collector, C, solutions, i.e.,  $P_{A,F}-P_{A,C}$ . Nonvolatile components in hydrolyzed urine are retained in the feed stream.<sup>74, 214-216, 232, 240</sup>  $\text{NH}_3$  transported to the acidic collector solution is then protonated to  $\text{NH}_4^+$ , which is nonvolatile.<sup>214, 215, 218-231</sup> This minimizes  $P_{A,C}$ , and enables the driving force for ammonia permeation,  $P_{A,F}-P_{A,C}$ , to persist over time. As such, MD enables ammonia recovery in the collector solution as an N fertilizer product.

Based on Chapter 4, operation of membrane distillation as *isothermal* membrane distillation (IMD), i.e., equivalent feed and collector temperature, yields  $\approx 95\%$  savings in energy for vaporization relative to conventional membrane distillation (CMD), which imposes a transmembrane temperature gradient.<sup>74</sup> The temperature gradient in CMD sets up an  $\text{H}_2\text{O}$  vapor pressure gradient across the membrane, which results in undesired water permeation that demands thermal energy and dilutes the N captured in the collector. Instead, in IMD, the  $\text{H}_2\text{O}$  vapor pressure gradient across the membrane is minimized and the undesired water permeation is suppressed. At the same time, IMD achieves nearly equal  $\text{NH}_3$  as the conventional operation of MD.<sup>74</sup> For these reasons, this work models the IMD operation of MD for N recovery from hydrolyzed urine.

Figure 6.1 presents a schematic of the onsite nutrient recovery system depicting collection of urine with urine diversion toilets, Donnan dialysis for P recovery, and membrane distillation for N recovery. First, fresh urine is collected at the source using urine diversion toilets and transferred to the onsite nutrient recovery system through source-separations piping in the building. In the first nutrient recovery step, DD, fresh urine is directed to the feed chamber and a receiver solution of high chloride content is directed to the receiver chamber using pumps 1 and 2, respectively.

Orthophosphate is recovered as P fertilizer in the DD receiver stream effluent. The effluent from the DD feed is then sent to storage to enable the hydrolysis of urea to ammonium and bicarbonate, forming hydrolyzed urine. Then, hydrolyzed urine is warmed using steam or waste thermal energy from hot waste water, through heat exchanger, HEx, 1. For the MD step, the warmed hydrolyzed urine is directed to the feed chamber and a warmed acidic collector solution is directed to the collector chamber using pumps 3 and 4, respectively. The acidic collector solution is also warmed using steam or waste thermal energy from hot waste water, through HEx 2. Pumps 5 and 6 direct the thermal energy source to hex 1 and 2, respectively. In MD, ammonia is recovered as N fertilizer in the collector stream effluent. The MD feed chamber effluent, i.e., remaining urine, is then discharged to the sewer.

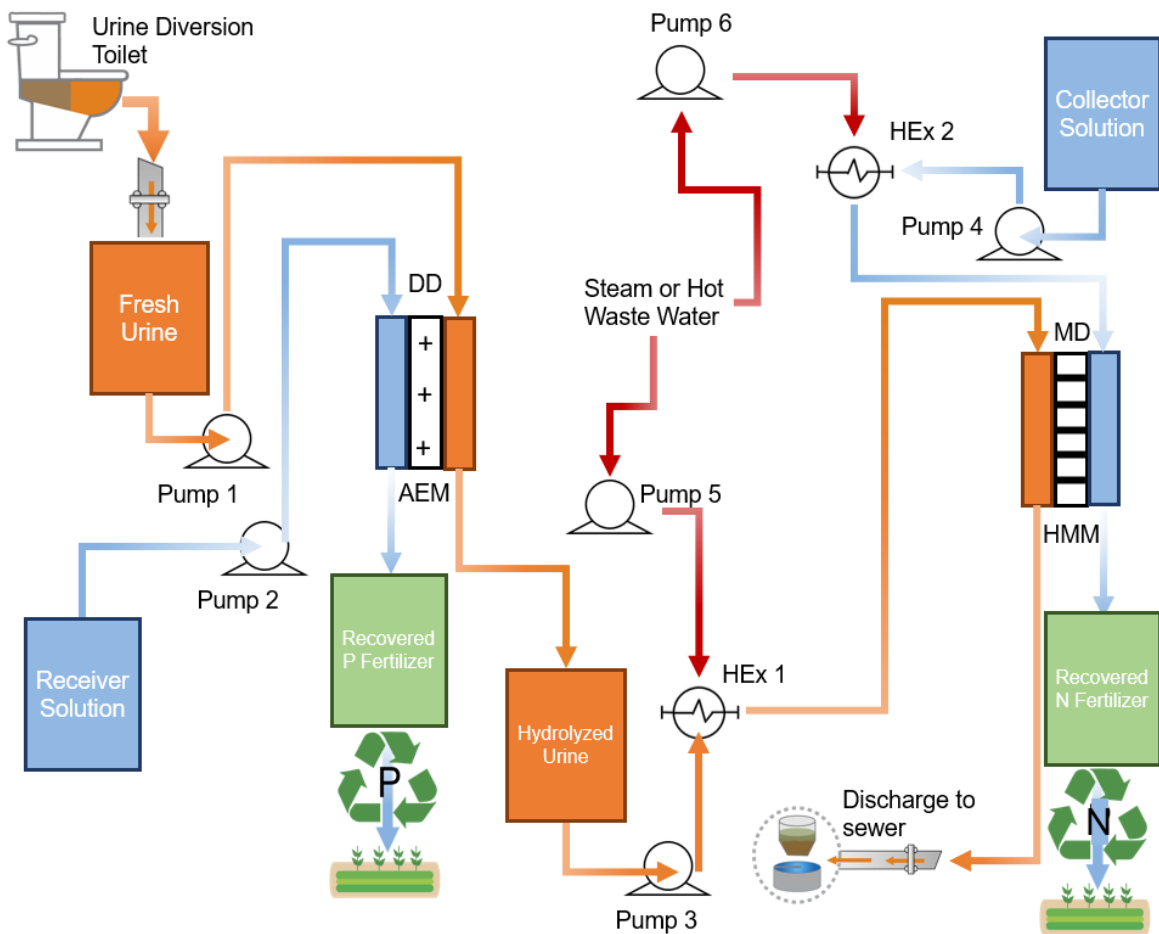


**Figure 6.1.** Schematic of the proposed onsite nutrient recovery system. First, urine is separated at the source using urine diversion toilets. Then, urine is pumped to the feed chamber of a Donnan dialysis (DD) system, while the receiver solution, which consists of a solution of high chloride content, is pumped to the receiver chamber of the DD system. In DD,  $\text{Cl}^-$  transports from the receiver solution across the anion exchange membrane (AEM) to the feed solution, while target  $\text{H}_x\text{PO}_4^{(3-x)-}$  ions transport in the opposite direction. The recovered orthophosphate solution in the receiver effluent can then be utilized as fertilizer. The feed side effluent of DD is then stored to hydrolyze the remaining urine solution. The hydrolyzed urine is then heated using heat exchanger 1, HEx 1, while the collector solution, which comprises an acidic solution, is heated using heat exchanger 2, HEx 2. Either steam or hot waste water can be used to provide thermal energy. For simplicity the other streams involved in the heat exchanger processes are not included in this figure. The hydrolyzed urine and collector solution are then sent to the feed and collector chambers, respectively, of the membrane distillation (MD) system. In MD,  $\text{NH}_3$  transports from the feed solution across the hydrophobic microporous membrane (HMM) to the collector solution. The recovered N in the effluent of the collector side of MD can be utilized as fertilizer. The effluent of the feed solution is discharged to the sewer. Note that pumps 1 and 2 are utilized to pump the feed and receiver solutions, respectively, to the DD system, pumps 3 and 4 are utilized to send the feed and collector solutions, respectively, to the MD system, and pumps 5 and 6 are used to pump the steam or hot water streams to the heat exchanger system. Storage tanks

### 6.3 Assessment Methods and Assumptions

**Capital Cost for Onsite Nutrient Recovery.** Capital cost, or capital expenditures (CAPEX), includes direct costs of the process equipment and indirect capital (construction, overhead, insurance, and contingency costs). In this analysis, the indirect capital costs are estimated as 10% of the total direct cost.<sup>278</sup> Assumptions for direct costs of toilets, piping, tanks, process control, pumps, heat exchangers, membranes, and membrane modules are outlined in Table E.1 of Appendix E. The number of toilets, size of tanks, membrane areas, sizes of pumps, and heat exchanger area are determined by the following methods. The analysis models a building of similar specifications as the Solaire (i.e., 293 apartments) and assuming an average of 2 toilets per apartment (i.e., 596 toilets in the building). There are 6 tanks in total (two for DD, two for MD, and two for product storage), which each have a capacity for 7 days of the building's total urine production. Urine production in the building,  $Q_P$ , is predicted with the assumptions of an average

of 3 people per apartment, and 60% of a person's daily urination occurring at home (i.e., 1.2 L-person/day collected in the apartment building and a total building flow of 1054.8 L/day). Note that the flow rate from urine produced in the building is also used to size the pumps using the assumptions in Table E.1.

Membrane areas,  $A_m$  for the DD and MD steps are calculated using eqn (6.1) and the experimentally measured orthophosphate (subscript P) and ammonia (subscript A) fluxes presented in Chapters 3 and 4, respectively, of  $J_P = 0.0145 \text{ mol/m}^2\text{h}$  and  $J_A = 13.92 \text{ mol/m}^2\text{h}$ , respectively.<sup>74, 279</sup> Note that urine is assumed to contain nutrient concentrations,  $C_i$ , of 30 mmol-orthophosphate/L and 500 mmol-total ammoniacal nitrogen/L.

$$A_m = \frac{Q_P C_i}{J_i} \quad (6.1)$$

The heat exchangers area,  $A_{\text{HEX}}$ , is calculated using eqn (6.2) where  $Q_T$  is the rate of heat transfer between the target stream and hot stream and is calculated by eqn (6.3),  $U$  is the overall heat transfer coefficient (assumptions provided in Table E.2), and  $\Delta T_{\text{lm}}$  log mean temperature difference calculated by eqn (6.4).<sup>280</sup> Note that  $m$  is mass flow rate,  $C_p$  is heat capacity,  $T$  is temperature, and subscripts H, C, in, and out refer to the hot stream, cold stream (or target stream), and inlet and outlet conditions, respectively.  $T_{\text{H,in}}$ ,  $T_{\text{C,in}}$ , and  $T_{\text{C,out}}$  (i.e., temperature of hot stream initially, temperature of cold stream initially, and target temperature for the warmed stream, respectively) for different operations are provided in Table E.3.

$$A_{\text{HEX}} = \frac{Q_T}{U \Delta T_{\text{lm}}} \quad (6.2)$$

$$Q_T = m_H C_{p_H} (T_{\text{H,in}} - T_{\text{H,out}}) = m_C C_{p_C} (T_{\text{C,in}} - T_{\text{C,out}}) \quad (6.3)$$

$$\Delta T_{lm} = \frac{(T_{H,in} - T_{C,out}) - (T_{H,out} - T_{C,in})}{\ln \frac{(T_{H,in} - T_{C,out})}{(T_{H,out} - T_{C,in})}} \quad (6.4)$$

Capital cost is annualized by  $CAPEX_{Annual} = F_{Amortization} CAPEX$  where the amortization factor,  $F_{Amortization}$ , is calculated using eqn (6.5), with assumptions for interest rate,  $i$ , and plant lifetime,  $n$ , provided in Table E.4 of Appendix E.<sup>279</sup>

$$F_{Amortization} = \left( \frac{i(1+i)^n}{(1+i)^n - 1} \right) \quad (6.5)$$

**Operating Cost of Nutrient Recovery.** Operating cost, or operating expenditure (OPEX), for the Donnan Dialysis for P recovery is the sum of the chemical cost, electricity for pumping, as well as additional costs for membrane replacement, spares, and labor (grouped as “other” in the analysis). Assumptions for the costs of these items are provided in Table E.5. The electricity for pumping,  $E_p$ , is calculated by eqn (6.6), where pressure difference is calculated as  $\Delta P = \rho g \Delta h$  ( $\rho$  is the density of liquid,  $g$  is the acceleration of gravity, and  $\Delta h$  is pump head), and  $\eta$  is pump efficiency; see Table E.6 of Appendix E for assumptions.<sup>279</sup>

$$E_p = \frac{Q\Delta P}{\eta} \quad (6.6)$$

Another major expenditure in DD is the chemicals to provide chloride in the receiver solution. This chemical cost assumes 1 L of 600 mM  $Cl^-$  required for every 1 L of urine treated (i.e., the conditions of Donnan dialysis for P recovery from fresh urine in Chapter 3). Table E.5 provides cost per volume of receiver solution as well as the costs for the other inputs in the DD system (membrane replacement, spares, and labor).

OPEX of membrane distillation for N recovery from hydrolyzed urine is the sum of energy costs (i.e., electricity for pumping and thermal energy provided by natural gas for heating), chemical cost, as well as additional costs for membrane replacement, spares, and labor (grouped as “other” in the analysis). Electricity for pumping is calculated by eqn (6.6) and using assumptions in Table E.6. The specific thermal energy consumption of the MD step, i.e., external heating requirement and internal heating requirement for convective and conductive heat loss,<sup>74, 212, 213, 245, 247, 256, 259, 260, 281, 282</sup> and associated costs are detailed in Appendix E.1. The chemical cost assumes equivalent volume of acid (chemical input) as the urine that is treated. Table E.7 provides the prices for all expenditures of the MD step.

**Fertilizer Revenue and Savings at Centralized Wastewater Treatment Plants.** The revenue from P and N fertilizer, recovered by DD and MD, respectively, are predicted on per kg-nutrient basis (i.e., \$/kg-P and \$/kg-N). The ranges in prices of various P and N fertilizers<sup>283</sup> (e.g.,  $\text{Ca}(\text{H}_2\text{PO}_4)_2$  and anhydrous  $\text{NH}_3$ ) are normalized by kg of target nutrient of P or N, see Table E.8 of Appendix E for the complete list of fertilizers and estimated prices per kg-nutrient. The range and average in fertilizer price on a per kg-nutrient basis, i.e., \$/kg-P or \$/kg-N, are utilized as the fertilizer revenue.

Another potential revenue source for nutrient recovery is the avoided costs on energy/chemical/other inputs for nutrient removal at downstream centralized WWTPs. In other words, savings at centralized WWTPs can be potentially realized as a revenue source for nutrient recovery in the form of fiscal incentives. For P, enhanced biological phosphorous removal (EBPR) is the prevailing practice for advanced nutrient removal. A previous study estimated that urine diversion and P recovery can result in \$93–134/kg-P avoided expenditure for EBPR at WWTPs.<sup>284</sup> For N, nitrification-denitrification is the prevailing practice for N removal at WWTPs. This

technique requires significant electricity inputs of 1.2–12.5 kWh/kg-N.<sup>81</sup> Potentially, some expenditures for nitrification-denitrification can be avoided if N is recovered. A previous study reports that 33% of electricity requirements for aeration at WWTPs can be avoided with 90% urine diversion. However, future studies need to be conducted to understand how changing nutrient profiles in wastewater by complete urine diversion will impact N removal at downstream WWTPs. For the preliminary techno-economic assessment, avoided electricity expenditures, i.e., 33% reduction, for nitrification-denitrification downstream WWTPs are assumed to be the source of savings for N recovery from urine.

#### **6.4 Implementation of Nutrient Recovery**

**Capital Expenditures for Nutrient Recovery.** Figure 6.2 presents the contribution of different capital components within the nutrient recovery system toward the total CAPEX of \$419K. The cost for urine diversion itself, i.e., the added cost for urine diversion toilets and dual piping, is approximately 75% of the total cost. Within the treatment systems (i.e., DD and MD components), the DD membrane and membrane module are the largest contributors. As consequence of the low  $H_xPO_4^{(3-x)-}$  flux in DD experiments presented in Chapter 3, a large anion exchange membrane of approximately 90 m<sup>2</sup> is needed to separate the P from the urine produced in the model building, while the MD membrane requirement for N separation is much smaller at 1.5 m<sup>2</sup>. Furthermore, the anion exchange membrane utilized in DD is 2× more expensive per unit area than the hydrophobic microporous membrane utilized in MD experiments.

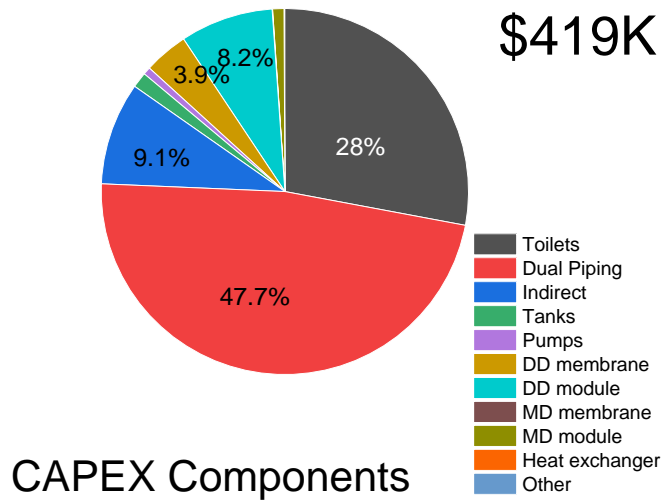


**Figure 6.2.** Contribution of different components toward the total capital cost (CAPEX) for implementation of nutrient recovery. Note that the analysis does not consider retrofit costs because it considers nutrient recovery to be implemented in a new building with the Solaire as a model.

**Operating Cost and Revenue Opportunities.** Operating cost (OPEX) was determined for DD for P recovery and MD for N recovery under different operating conditions. For DD, the “Baseline” condition utilizes KCl provided by external chemicals as the receiver stream, while the “Waste Chemical” condition utilizes a recycled stream of waste water softening regenerant rinse or desalination brine supplied from local sources. Likewise, for MD, the “Baseline” condition uses a sulfuric acid solution sourced from external chemicals as the collector stream, while the “Waste Chemical” condition utilizes a recycled stream of pickling brine (effectively acetic acid) supplied from local sources. The “Waste Heat” condition in MD utilizes recovered thermal energy from hot water streams produced at the Solaire in addition to the waste chemicals. Figure 6.3A and 6.3B present the operating cost for DD on a per kg-P recovered basis and for MD on a per kg-N recovered basis, respectively, as blue columns. Contributions to OPEX from chemical, energy (for

DD electricity for pumping and for MD electricity for pumping + thermal energy) and other costs are depicted as unfilled, patterned, and solid blue overlaid columns, respectively.

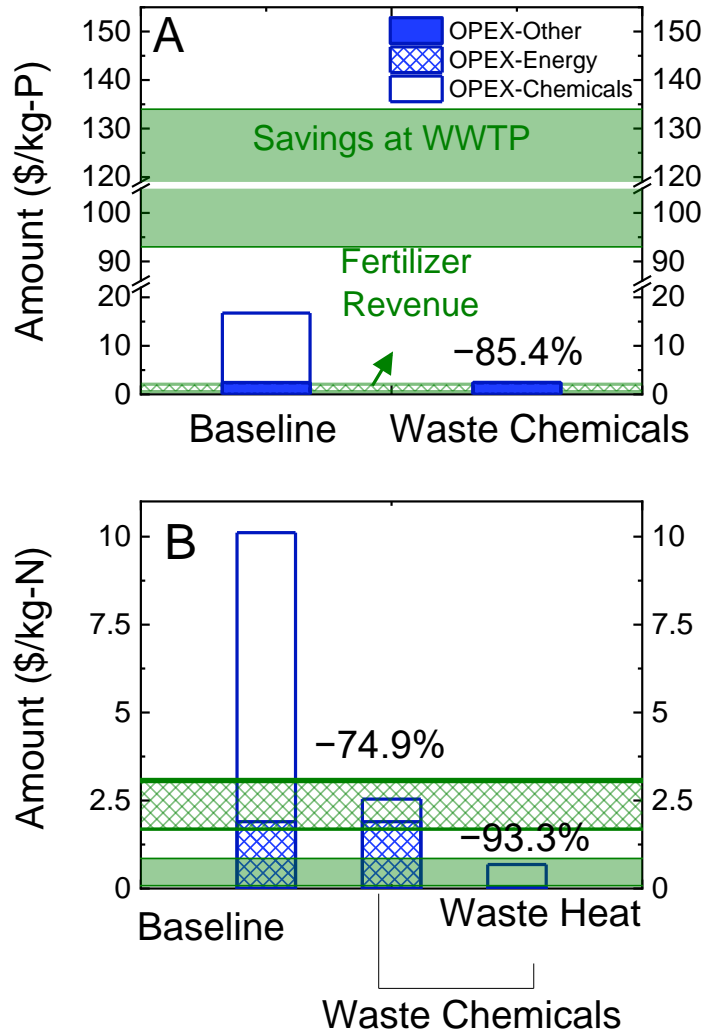


**Figure 6.3.** Operating cost (OPEX) of P and N recovery via Donnan dialysis (2A) and membrane distillation (2B), respectively, under different operations. The different operations for DD are baseline (supplying a KCl solution as the receiver) and utilizing waste chemicals. The different operation for MD are: i.) baseline (isothermal 40°C with heating provided by natural gas), ii.) utilizing waste chemicals of acetic acid, and iii.) utilizing waste acetic acid and waste heat harnessed with the Solaire’s thermal energy recovery unit. OPEX components are broken down into energy, chemical, and other

(including spares, membrane replacements, and labor). Revenue associated with fertilizer production is depicted as patterned regions and downstream savings at WWTP are depicted as green shaded regions.

Figures 6.3A and 6.3B both demonstrate considerable savings in OPEX (>70%) with the use of waste chemicals in nutrient recovery systems (i.e., reductions of 85.4% and 74.9% DD and MD, respectively). In place of purchasing KCl salt and sulfuric acid, locally sourced recycled waste streams can supply the chloride content for the receiver solution of DD and acid for collector solution of MD, which significantly reduces the chemical cost for nutrient recovery. Furthermore, for the MD system (Figure 6.3B), employing recovered thermal energy (i.e., waste heat) can yield additional savings in OPEX for a total savings of 93.2% relative to the baseline approach without utilizing recycled chemicals and/or recovered thermal energy. Employing waste heat can lessen the dependence on natural gas for the production of steam to heat MD streams, thereby reducing energy cost of the MD operation for N recovery. Analysis in subsequent subsections employs the best performance conditions for DD and MD (i.e., waste chemical and waste heat + chemical, respectively).

The range in fertilizer revenue (patterned green regions) for P and N fertilizer products are depicted in Figures 6.3A and 6.3B, respectively. P fertilizer revenue is nearly equivalent to the magnitude of OPEX for DD with waste chemicals and N fertilizer revenue is larger than the magnitude OPEX for MD with waste chemicals and waste heat. In addition to the revenue from fertilizer products, potential downstream savings at WWTP through reduced nutrient loading can be considered as a possible revenue source. The predicted savings at WWTPs with P and N recovery are depicted as green shaded regions in Figures 6.3A and 6.3B, respectively. The WWTP savings realized with onsite P recovery are considerable and larger than OPEX for DD, which can greatly benefit the economic viability of the technique. The WWTP savings realized with N recovery are small, but can still benefit the economic viability of MD.

### **Annualized CAPEX, OPEX, Revenue, and Profits of Different Source-Separation**

**Scales.** The analysis presented in the preceding subsection presents operating costs and revenue of nutrient recovery on a per kg-nutrient recovered basis. The following analysis annualizes those values by considering the yearly production of urine and nutrient excretions, which were provided in a previous section. Capital cost was also annualized using the amortization factor as described previously. Finally, net profit, defined as revenue - total costs, was determined. Figure 6.4A presents the annualized CAPEX (patterned orange column), OPEX divided into DD and MD systems (solid and patterned blue columns, respectively), revenue divided into P and N fertilizer products (solid and patterned green columns, respectively), and profits (solid red column). Also depicted are revenue from both fertilizer and savings at WWTPs, marked on the horizontal axis, which are divided into P and N components (solid and patterned green columns, respectively), and the resultant profit, red column, if downstream savings at WWTP are realized as a revenue source.

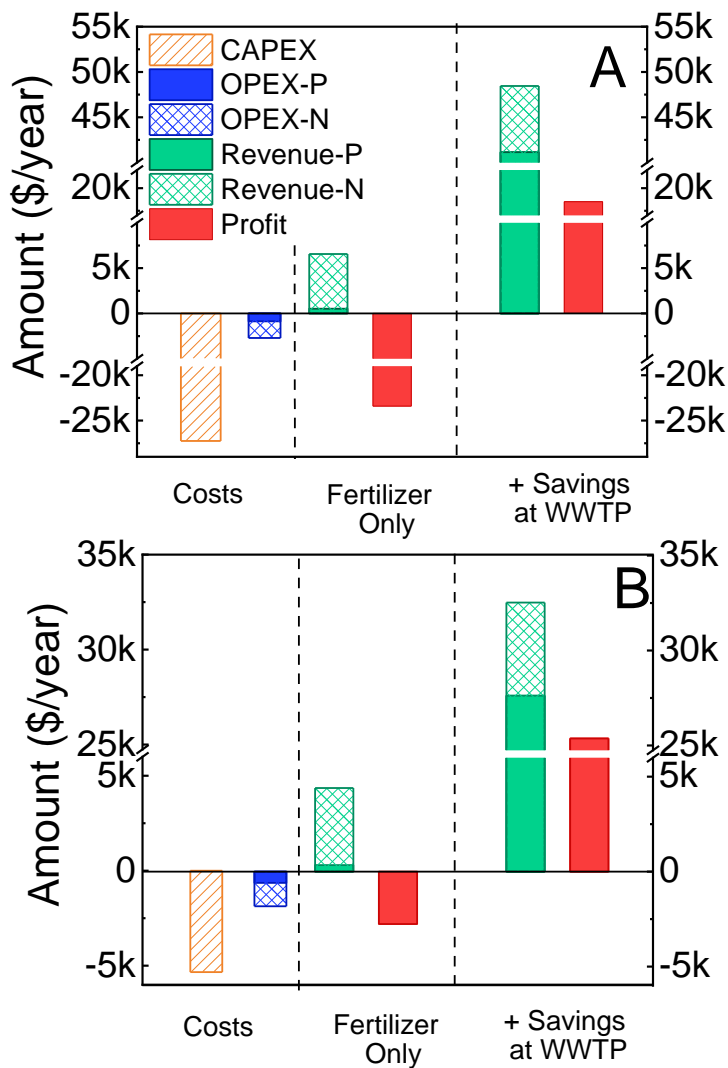


**Figure 6.4.** Annualized capital cost (CAPEX), operating cost (OPEX) separated into P recovery and N recovery components, revenue separated into P and N recovery components, and net profit for the implementation of nutrient recovery systems under different operations (options 1 and 2). Option 1, 4A, is installation of urine diverting toilets and piping in all apartments of a building modeling the Solaire with the assumption that 60% of a resident’s urination occurs in their apartment. Option 2, 4B, models a work building of similar occupancy as the Solaire, but with 10% the number of toilets and piping length and with the assumption that 40% daily urination occurs at the workplace. Net profit is the revenue – total cost. Revenue and profits are shown assuming only fertilizer revenue and including the savings at centralized WWTPs as additional revenue. Note that the mid-point values for fertilizer revenue and savings at the centralized WWTP are utilized.

Note that while N fertilizer revenue and P fertilizer revenue are comparable on a kg-nutrient basis (Figure 6.3), N fertilizer revenue  $\gg$  P fertilizer revenue on an annual basis (Figure 6.4A). This is because the N content is over 10 $\times$  more than the P content in urine, and as a result more N fertilizer is produced from the onsite nutrient recovery system on an annual basis. For the same reason, annualized OPEX MD  $>$  annualized OPEX DD system even though OPEX MD on kg-N basis  $<$  OPEX DD kg-P basis.

As a consequence of expensive toilets and piping required for source-separation of urine, annualized CAPEX is considerable and significantly larger than OPEX (i.e., CAPEX is approximately 10 $\times$  OPEX). Although the magnitude of total fertilizer revenue  $>$  magnitude of operating costs, the high capital cost drives a negative profit (i.e., a net cost). However, realizing downstream savings at WWTPs as a revenue source can increase revenue by approximately 7 $\times$  and yield net positive profits of greater than \$18K/year.

If the scale of source-separation components (i.e., number of toilets and length of piping) is lessened, the CAPEX cost can be reduced. Potentially, such reduction can be realized if nutrient recovery is implemented in a high-density building with communal restrooms, such as a work building, where less toilets per person are needed compared to a residential building with private sanitation rooms. Annualized CAPEX, OPEX, revenue, and profits were predicted for urine diversion and nutrient recovery in a workplace building assuming the same occupancy of the Solaire, 10% toilets and piping length as the Solaire, and 40% of an occupants' daily urination occurring in this workplace. Figure 6.4B presents the same analysis as in Figure 6.4A, but for this workplace nutrient recovery model.

The CAPEX for urine diversion and nutrient recovery in the workplace building (Figure 6.4B, orange patterned column) is 80.5% lower than the CAPEX in apartment buildings modeling

the Solaire (Figure 6.4A, orange patterned column) because of significant savings in toilets and piping. OPEX and revenue, from both fertilizer and downstream savings at WWTP, are approximately 33% lower in the workplace building than in the apartment building. This is because of the assumption that an occupant releases 40% of their urine at work and 60% of their urine at home (i.e., 33% less urine released in the work building). The profits of the workplace building nutrient recovery system are slightly negative, i.e., net cost, if only fertilizer revenue is considered. However, the magnitude of this cost is 88% lower than that of the cost (negative profits) of the apartment building nutrient recovery system. Furthermore, if downstream savings at WWTP are realized, then the workplace nutrient recovery effort can yield positive profits that are 37% higher than that of the apartment nutrient recovery effort.

**Combined Water, Thermal Energy, and Nutrient Management.** There are opportunities to capture and utilize other valuable resources from wastewater. Water can be reclaimed from wastewater and repurposed onsite in non-potable applications, such as flush, cooling, laundry. Thermal energy can be harnessed from hot waste streams and applied for water heating in the building. The Solaire building has existing onsite non-potable water reuse and thermal energy recovery systems. Analysis examined the costs and benefits of the existing onsite wastewater management practices at the Solaire and in a proposed model with nutrient recovery in addition to the aforementioned onsite wastewater management practices.

CAPEX, OPEX, revenue, and profits of the different systems were estimated based on the following methods. Capital costs for water and thermal energy recovery at the Solaire are determined based on the expenditures for the non-potable water treatment (NPWT) system and thermal energy recovery unit, see Table E.9 of Appendix E for assumptions. Table E.10 provides relevant operational data (i.e., potable water demand, wastewater sent to WWTP, and reuse flow)

for the Solaire as well as a reference building of equivalent capacity and water demands, but without a non-potable water reuse system. Operating expenditures were determined from records detailing chemical, energy, and other (materials, spares, labor, etc) inputs to the systems. Table E.11 provides assumptions on the costs for water service, material, chemical, electricity, and natural gas. Additionally, Figure E.1 of Appendix E shows the cost of components that contribute to energy component of OPEX (i.e., natural gas for water heating, electricity for the operation of NPWT, electricity for the hydronic loop of the thermal energy recovery system) and the total cost of energy inputs for the reference system, water recovery system at the Solaire, and water + thermal energy recovery systems at the Solaire.

Revenues for the Solaire systems are defined as savings achieved relative to a reference building of equivalent capacity without water, thermal energy, or nutrient recovery. For water recovery for non-potable reuse, the revenue source is savings in water service (i.e., drinking water supply from the city and wastewater treatment service at a centralized plant). For thermal energy recovery for water heating, the revenue source is savings in natural gas used to heat water for residential use. To prevent double-counting of OPEX in the determination of profit, net profit for each scenario is calculated as: total costs of the reference system – the total cost of the scenario under examination. Figure E.2 of Appendix E demonstrates the expenditures in the reference system on water service and water heating and the annualized CAPEX, OPEX, revenue, and net profits of the water and water + thermal energy recovery systems at the Solaire

Figure 6.5 presents CAPEX (patterned orange columns), OPEX (patterned blue columns), revenue (patterned green columns), and net profits (solid red columns) for operations with water recovery, water + thermal energy recovery, and water + thermal energy + nutrient recovery. Note that this analysis does not consider how separate urine collection, and the resultant change in

nutrient profile, will impact the onsite water recovery system, but future work can include such considerations for a more accurate prediction of OPEX. For nutrient recovery, additional revenue and resultant profits from downstream savings at WWTPs are depicted as unfilled green and red columns, respectively.

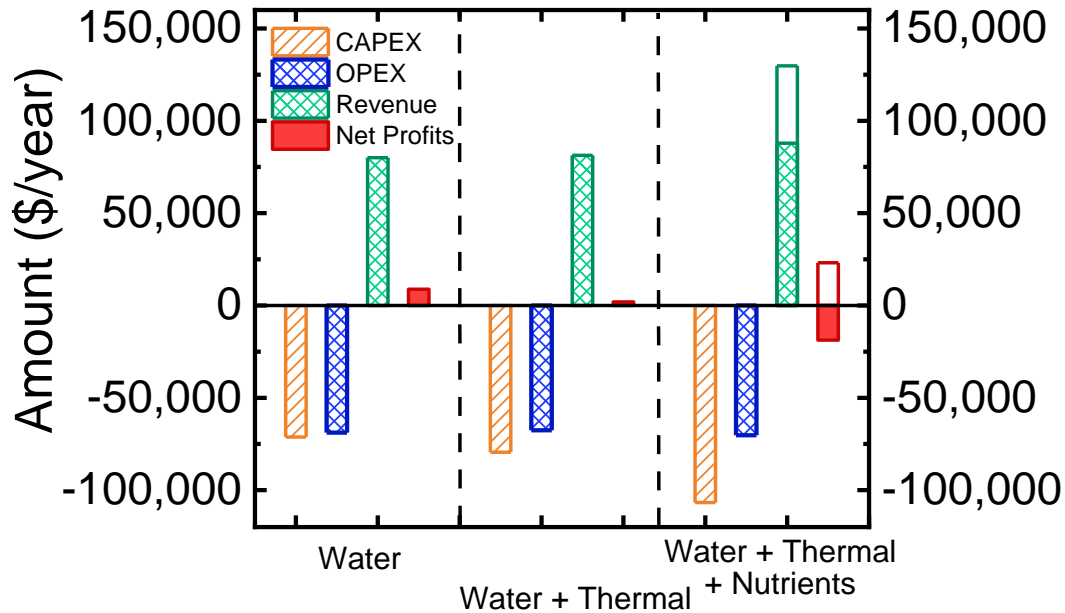


**Figure 6.5.** Annualized capital cost (CAPEX), operating cost (OPEX), revenue, and net profit for the implementation of non-potable water reuse, non-potable water reuse + thermal energy recovery, and non-potable water reuse + thermal energy recovery + nutrient recovery in a building modeling the Solaire. Revenue for non-potable water reuse is calculated as reduction in OPEX relative to a baseline building without non-potable water reuse (i.e., savings) and for thermal energy recovery as reduction in OPEX relative to a baseline building without either water reuse or thermal energy recovery. Revenue for the additional nutrient recovery component is fertilizer revenue (patterned green column) and additional savings as reduction in OPEX for nutrient removal efforts at centralized WWTPs (unfilled green column). Profit is calculated as revenue – total cost. Two profits are depicted for the case with nutrient recovery: the red shaded region is considering only fertilizer revenue and the unfilled red column considers added revenue from savings at WWTP. Note that the optimal conditions for nutrient recovery (i.e., option 1 to implement toilets in all apartments) and utilizing waste chemicals and thermal energy recovery) were applied for the analysis.

Non-potable water recovery at the Solaire results in significant savings in external water service (approximately 88%) driving a net profit of \$8.8K/year. Thermal energy recovery at the Solaire saves 10% of the expenditures on natural gas, but does introduce additional CAPEX for the thermal energy recovery unit and OPEX of electricity for the hydronic loop. The result is lower net profit than the water recovery system alone (\$1.9K/year). It is important to consider that the thermal energy recovery unit at the Solaire building is an initial model system that limits the amount of thermal energy that is able to be recovered. As a result, the savings from lessened natural gas usage are stunted and the profit is limited. Future iterations of the thermal energy recovery system can increase capacity to realize higher revenue.

Adding nutrient recovery to a building modeling the specifications of the Solaire considerably increases the CAPEX by 34% relative to the existing onsite wastewater management (i.e., water + thermal energy recovery units). These additional capital expenditures are primarily due to the high costs of urine diversion toilets and dual piping. The increase in OPEX with the practice of nutrient recovery is more marginal at 4%. The flow of urine to the nutrient recovery systems is approximately 20× less than the flow of wastewater to the non-potable water treatment system, therefore the inputs to the nutrient recovery system are much less. Importantly, the thermal energy recovery unit can be applied to source the thermal energy required for the MD system, which enables significant reduction in OPEX (as detailed with the use of waste heat in Figure 6.3). Revenue from fertilizer production is only an additional 8% compared to the savings from water + thermal energy recovery. This additional revenue source does not cover the increased CAPEX and OPEX with nutrient recovery, and the result is net negative profits, or costs, of approximately \$19K/year. However, if downstream savings at WWTPs can be realized as an additional revenue

source, then implementing nutrient recovery with the other onsite wastewater management practices can achieve net positive profits of approximately \$23K/year.

## **6.5 Implications**

The existing approach to nutrient management, i.e., the linear economy model, is inefficient and unsustainable. Closing the nutrient loop by recovering P and N from nutrient rich human urine can reduce nutrient emissions to aquatic environments and lessen the dependence on industrial fertilizer production (i.e., P mining and N fixation by the Haber-Bosch process). However, the feasibility of urine diversion and nutrient recovery is dependent on the economic viability of the approach. This study presents an initial techno-economic assessment of onsite nutrient recovery in a high-density residential apartment building using membrane-based process of Donnan dialysis for P recovery and membrane distillation for N recovery. The analysis predicts that the model onsite urine diversion and nutrient recovery system has total capital cost of \$419K (annualized cost of \$27K) and operating cost of \$2.7K/year (with the configuration of lowest cost) for the production of 360 and 2700 kg-P and N-fertilizer/year, respectively. The predicted revenue from the fertilizer production is \$6.6K/year, which alone is not enough to cover the capital and operating expenditures of the system. However, the analysis presents a preliminary estimate of \$41K/year savings at downstream wastewater treatment plants achievable through onsite nutrient recovery. These savings result from lessened expenditures for removal of P and N at centralized WWTPs by conventional means (i.e., biological treatment). If these savings can be realized as a revenue source for the stakeholders of the onsite nutrient recovery system, possibly through policy incentives like subsidies, then the onsite urine diversion and nutrient recovery system can achieve \$19K/year of net profit (i.e., revenue > total costs).

The study also examines the costs and benefits of onsite wastewater management at the Solaire with systems of 1. non-potable water reuse, 2. non-potable water reuse and thermal energy recovery, and for a model building of 3. non-potable water reuse, thermal energy recovery, and nutrient recovery. Analysis reveals that relative to a reference building without water, thermal energy, or nutrient recovery, wastewater management systems of 1, 2, and 3 can yield \$8.8K, \$1.9K, and \$23 K profits/year, respectively, achieved through savings in water service, lower natural gas demand for water service, and fertilizer revenue and savings at WWTPs for nutrient removal. Future iterations of the thermal energy recovery unit can have expanded capacities to realize higher savings in natural gas and improve economic viability.

The economic assessment of nutrient recovery sheds light on opportunities to reduce costs in the nutrient recovery systems by leveraging widely-available low-cost/waste resources in place of more expensive chemicals. The operating costs of Donnan dialysis and membrane distillation can be reduced by 85.4 and 74.9%, respectively, with the use of locally-sourced waste streams relative to operations with purchased KCl and sulfuric acid. For membrane distillation, costs can be further lessened to a total of 93.3% less than the baseline condition by tapping into recovered thermal energy to heat the streams. The Solaire building has a thermal energy recovery unit that captures heat from waste streams to lessen natural gas usage for water heating; a similar unit can supply thermal energy for the membrane distillation system.

This analysis highlights the highest cost components of an onsite nutrient recovery: the urine diversion system (i.e., source-separation toilets and an additional piping infrastructure). These expenditures are approximately 75% of the CAPEX and 68% of the total annualized cost. It is important to note that the analysis models the implementation of nutrient recovery into a new building of equivalent specifications of the Solaire, therefore the costs do not include retrofit for

installation of toilets and piping into an existing building. Such expenditures can be significant and should be considered if incorporating nutrient recovery into an existing building. For this reason, nutrient recovery may be more economically viable if implemented into new buildings. Population growth and sanitation trends necessitate the construction of new urban buildings and sanitation infrastructure, which present opportunities to introduce onsite nutrient recovery systems into these new facilities. Population projections predict an urban influx of 2.5 billion people by 2050,<sup>263</sup> which will increase the population density of cities and necessitate new residential buildings. Additionally, 2.3 billion people globally do not have access to sufficient sanitation infrastructure and wastewater treatment,<sup>264</sup> therefore installation of urine diversion toilets and onsite nutrient recovery presents an opportunity to benefit the sanitation needs of developing communities without overhauls of existing systems and retrofit for the new systems.

This preliminary assessment utilized figures for financial savings at WWTPs achieved with onsite P recovery (i.e., avoided costs for enhanced biological phosphorous removal)<sup>284</sup> and avoided costs on electricity for N removal at centralized WWTPs by nitrification-denitrification.<sup>81</sup> Removal of P and N from urine will impact nutrient profiles of the remaining wastewater, which can change the inputs needed for biological treatment both onsite non-potable water reuse systems and centralized wastewater treatment facilities. The exact nature of these changes can be predicted in future assessments to examine how separate urine collection and nutrient recovery will impact energy, chemical, and other demands for treatment of the remaining wastewater. Additionally, future assessments can include a sensitivity analysis that examines how uncertainty in prices, particularly for toilets, piping, and fertilizer revenue, and assumptions, particularly volume of urine collected and urine composition, can impact the expenditures, revenue, and net profit of onsite nutrient recovery.

Another area for future work is the examination and optimization of the scale of urine diversion and nutrient recovery that achieves the most economic benefit. This preliminary assessment briefly compared two urine diversion configurations: one in a residential building with private restrooms and one in a work building with communal restrooms. The residential building model includes source-separation toilets in all apartments and an additional piping infrastructure for separate urine collection. The workplace building assumes less toilets and piping infrastructure because restrooms are public. This resulted in considerable CAPEX savings, however, slightly lower revenue was achieved due to lower urine flow. However, the assumption that 60% of urine flow occurs at home and the remaining at work can be revisited with future studies, especially in light of increased practice of working from home. Note that the assumptions regarding the number of toilets, length of piping, and volume of urine collected each day can also be revisited in a sensitivity analysis to examine the accuracy of cost and profit predictions. Additionally, different scales (block, community, etc) can be considered to optimize the net profits of nutrient recovery. Nevertheless, the initial analysis provides strong evidence that urine diversion and nutrient recovery from communal spaces may minimize CAPEX and be more economically strategic than implementation in private residences.

Outside of economic benefits, the onsite wastewater systems may offer environmental and resource-security advantages. The non-potable water reuse system reclaims and repurposes wastewater as non-potable water fit-for-purpose. This approach can potentially avoid some impacts associated with centralized water and wastewater treatment and conveyance, diversion of water away from sensitive ecosystems, and discharge of wastewater into sensitive aquatic environments.<sup>285-287</sup> For the Solaire building in NYC, in particular, lessened wastewater loading to centralized WWTPs can potentially reduce combined sewage overflow instances, which have

known harmful environmental consequences.<sup>288</sup> Additionally, water reuse may improve resource-security if practiced in regions facing drought or water-shortages.<sup>285</sup> The thermal energy recovery system lessens the dependence on natural gas for water heating at the Solaire. As previously discussed, nutrient recovery can avoid impacts associated with P mining and N fixation as well as nutrient pollution of aquatic environments. Moreover, nutrient recovery may benefit resource-security, particularly in the midst of depleting phosphate rock reserves.

However, when considering the potential environmental advantages of non-potable water reuse, thermal energy recovery, and nutrient recovery, it is also important to consider potential negative environmental impacts that are introduced by these methods. These systems all demand new infrastructure, construction, chemicals, and energy, which introduce environmental consequences. For example, the thermal energy unit avoids some impacts associated with natural gas, but introduces additional electricity requirements to support the hydronic loop. Similarly, water reuse and nutrient recovery may avoid impacts from the conventionally practiced approaches, but the methods introduce new aspects (e.g., treatment systems, chemical inputs, electricity demands) that may or may not have larger environmental burdens.<sup>31, 289-293</sup> Future life-cycle assessments should quantify the environmental impacts (e.g., global warming potential, eutrophication potential, resource depletion) of the onsite wastewater management systems at the Solaire compared to reference systems of buildings without water or thermal energy recovery. Additionally, these assessments can consider life-cycle cost and benefits of implementing nutrient recovery at the Solaire or a similar new building compared to the reference linear economy approach.

## Chapter 7: Conclusions

### 7.1 Summary

The work presented in this dissertation elucidated strategic methods for nutrient capture and advanced membrane technologies for nutrient recovery from human urine. The studies i.) approached nutrient recovery on a system-level to recognize optimal waste streams to target for P and N separation ii.) advanced membrane-based processes for nutrient recovery iii.) examined the economic viability of the nutrient recovery techniques.

In chapter 2, optimal nutrient recovery configurations were identified based on a thermodynamic and energetic analysis. The minimum energies required to recover various P and N fertilizer products from waste streams of fresh and hydrolyzed urine, greywater, domestic wastewater, and secondary treated wastewater effluent were quantified using the Gibbs free energy of separation. The analysis illustrated the degree to which recovering P and N from nutrient-dense waste streams, such as fresh and hydrolyzed urine, compared to other more dilute sources is advantageous. The study also revealed the practical efficiencies required by separation techniques for nutrient recovery to be lower than the current approaches of Haber-Bosch and phosphate rock mining. The chapter highlighted that strategic selection of waste stream, i.e., fresh urine for P recovery and hydrolyzed urine for N recovery, and fertilizer product can reduce energy intensities for nutrient recovery.

In Chapter 3, the performance potential of Donnan dialysis (DD) for orthophosphate recovery from diverted human urine was examined. The exchange of  $\text{H}_2\text{PO}_4^-$  and  $\text{Cl}^-$  across an anion-exchange membrane is demonstrated in DD experiments driven by the ion concentration gradient between the urine feed solution containing orthophosphate and a receiver solution of high chloride content. Importantly,  $\text{H}_2\text{PO}_4^-$  transported against an orthophosphate concentration

gradient. By adopting higher feed to receiver volume ratios, DD enriched orthophosphate in the receiver solution above the initial urine feed concentration. Additionally, the study elucidated the impact of other anions in urine on orthophosphate flux and recovery yield, specifically,  $\text{SO}_4^{2-}$  and  $\text{Cl}^-$  in fresh urine, and  $\text{SO}_4^{2-}$ ,  $\text{Cl}^-$ , and  $\text{HCO}_3^-$  in hydrolyzed urine. Reductions in orthophosphate flux, selectivity, and recovery yield were observed upon the inclusion of other anions in the feed solution. Selectivity for  $\text{H}_2\text{PO}_4^-$  transport over  $\text{SO}_4^{2-}$  was enhanced using a monovalent ion permselective membrane. The chapter demonstrated that abundantly available low-cost/waste streams of high  $\text{Cl}^-$  content can be utilized as the receiver solution in DD to enable P reclamation from urine.

In Chapter 4, novel isothermal membrane distillation with acidic collector (IMD-AC) was developed for the selective and energy efficient recovery of ammonia from human urine. Ammonia and water vapor fluxes in different membrane distillation configurations, isothermal and conventional, were examined. The innovative isothermal operation, i.e., same feed and collector temperatures, suppressed undesired water vapor permeation, while favorably maintaining ammonia vapor flux relative to conventional operation. Resultingly, isothermal membrane distillation significantly improved selectivity for  $\text{NH}_3$  permeation over  $\text{H}_2\text{O}$ . The study revealed that an acidic solution as the collector stream enhanced ammonia vapor flux by an average of 46.5% compared to using a deionized water collector. Importantly, against a total ammoniacal nitrogen concentration gradient, i.e., uphill transport, ammonia recovery of  $\approx 60\%$  was attained, highlighting the prospect of the technology for high-yield recovery. Critically, suppressed water permeation in IMD-AC resulted in 95% savings in vaporization energy consumption relative to conventional MD. The resulting vaporization energy requirement is lower than the linear economy approaches of Haber-Bosch process for N fixation and N removal by nitrification-denitrification.

This chapter demonstrated that IMD-AC overcomes the limitations of conventional membrane distillation and is a promising technique for selective and energy-efficient recovery of ammonia from source-separated urine.

Chapter 5 proposed an integrated membrane approach of bipolar membrane electro dialysis (BPM-ED), DD, and IMD-AC for P and N recovery from human urine. The chapter elucidates the role of pH and nutrient speciation, i.e.,  $\text{H}_2\text{PO}_4^-$  versus  $\text{HPO}_4^{2-}$  and  $\text{NH}_4^+$  versus  $\text{NH}_3$ , on the performance of DD and IMD-AC. BPM-ED is introduced as a technique to generate acids and bases *in situ* to leverage the speciation between  $\text{H}_2\text{PO}_4^-/\text{HPO}_4^{2-}$  in fresh urine and  $\text{NH}_4^+/\text{NH}_3$  in hydrolyzed urine to favorably impact DD and IMD-AC performance. BPM-ED was used to decrease the pH of fresh urine and enhance DD  $\text{H}_x\text{PO}_4^{(3-x)-}$  flux and selectivity for  $\text{H}_x\text{PO}_4^{(3-x)-}$  up to 34.8% and 16.5%, respectively. Then, BPM-ED was used to increase the pH of hydrolyzed urine and improve  $\text{NH}_3$  flux in IMD up to 148.7%. The acidic collector solution generated by BPM-ED increased the ammonia recovery potential in IMD from < 50% to > 90%. The study established that the specific energy consumptions of the integrated membrane process can be competitive with or comparable to the conventional linear nutrient economy approaches to P and N management.

Chapter 6 provided a preliminary techno-economic assessment on onsite nutrient recovery using DD and IMD-AC. The analysis revealed that operating costs can be reduced >70% by using waste chemicals, such as waste water softening regenerant rinse, and recovered thermal energy from warm waste streams, such as bathwater. The largest contributions to capital cost are the source-separation toilets and dual piping system. These expenditures can potentially be alleviated by implementing urine diversion in public restrooms rather than private apartments. Realizing the downstream savings at WWTP associated with reduction in nutrient loading as a revenue source,

potentially through policy incentives, in addition to fertilizer revenue can improve the economic viability of nutrient recovery and enable net positive profits.

## 7.2 Novel Contributions

The quantitative thermodynamic and energy analysis of nutrient recovery from various waste streams demonstrated that **P and N capture from nutrient rich sources, such as human urine, has lower energy intensity than recovery from more dilute sources.**<sup>134</sup> The theoretical minimum energy of recovery, quantified using Gibbs free energy of separation, can be reduced through **strategic selection of waste stream and product.** Analysis unearthed that waste stream pH and nutrient density are important factors governing the energy intensity. This thesis also shed light on potential practical energy requirements for P and N recovery and revealed efficiencies in separation processes required for the energy intensity to be lower than the conventional production methods of P mining and Haber-Bosch, respectively. A first-order analysis underlined the potential energy savings achievable by nutrient recovery from human urine compared with the existing linear economy approach. **The framework to determine the minimum energy of separation can be applied to other resource recovery efforts to guide the selection of waste streams and products.**

Next, this work demonstrated the ability of Donnan dialysis with a high driver ion content in the receiver solution to enable **orthophosphate recovery against a concentration gradient, i.e., uphill transport.**<sup>268</sup> The study demonstrated diminishing returns in phosphorous recovery with increased driver ion,  $\text{Cl}^-$ , content in the receiver solution. Higher  $[\text{Cl}^-]_{\text{RS}}$  resulted in increased co-ion (cation) transport and osmosis from FS to RS. **Orthophosphate was enriched in the receiver solution** to higher concentrations of urine by leveraging feed and receiver volumes. This thesis systematically explored the impact of anions in fresh and hydrolyzed urine on

orthophosphate flux, selectivity, and P recovery. The analysis provides strong evidence that **ions compete to partition into the IEM and exchange with driver ions in the receiver solution**. The work revealed the rationale for using fresh, rather than hydrolyzed urine, for P recovery: the high bicarbonate content of the latter source is detrimental to orthophosphate flux and selectivity. Selectivity for monovalent ions,  $\text{H}_2\text{PO}_4^-$  in fresh urine, over multivalent ions,  $\text{SO}_4^{2-}$  in fresh urine, can be enhanced using monovalent ion selective membranes. The insights from this work are broadly applicable to DD for other resource recovery or contaminant removals efforts, particularly from streams with multiple anions and/or cations, such as  $\text{NH}_4^+$  recovery from wastewater and removal of  $\text{NO}_3^-$  and  $\text{H}_x\text{AsO}_4^{(3-x)-}$  from drinking water.

The thesis **presented IMD-AC as a promising and energy-efficient technique for selective recovery of ammonia from human urine.**<sup>74</sup> The isothermal feature, i.e., equal feed and collector operating temperatures, minimized the driving force for water vapor permeation and resultingly **suppressed undesired  $\text{H}_2\text{O}$  transport and improved selectivity for  $\text{NH}_3$** . The acidic collector feature of IMD-AC drove the protonation of  $\text{NH}_3$  to  $\text{NH}_4^+$  and **enabled the transport of  $\text{NH}_3$  vapor against an ammoniacal nitrogen concentration gradient**. The acidic collector also increased ammonia flux compared to operation with a DI water collector. This thesis postulated that the kinetics of ammonia vapor dissolution is influenced by pH and is more favorable in an acidic collector solution. By suppressing water vapor transport **IMD-AC achieved 95% savings in vaporization energy consumption relative to conventional MD**. The study also demonstrated that ammonia recovery is possible using IMD-AC at ambient temperatures, which can reduce thermal energy requirements, though at the expense of lower kinetics. Critically, the **vaporization energy requirement of the IMD-AC technique for N separation and recovery can be lower**

**than the practical energy requirements of the linear economy approach** of nitrification-denitrification for N removal and Haber-Bosch the N fixation.

DD and IMD-AC can be practiced in sequence to capture both P and N from human urine. **Nutrient speciation, i.e.,  $\text{H}_2\text{PO}_4^-/\text{HPO}_4^{2-}$  and  $\text{NH}_4^+/\text{NH}_3$ , in urine can be favorably leveraged to improve DD and IMD-AC performance.**<sup>294</sup> The work elucidated the role of feed pH and orthophosphate speciation on DD performance. Orthophosphate transport and recovery in DD with a monovalent ion selective membrane is beneficially improved at  $\text{pH} \ll \text{p}K_{\text{a},2}$  of phosphate, where monovalent  $\text{H}_2\text{PO}_4^-$  is the predominant orthophosphate species. This thesis also underscored the role of feed pH and ammoniacal nitrogen speciation on MD performance. Higher pH of hydrolyzed urine beneficially increased the fraction of ammoniacal nitrogen as volatile  $\text{NH}_3$ , which enhanced ammonia permeation in MD. The thesis applied **bipolar membrane electrodialysis to generate acids and bases *in situ* to strategically control the pHs** of urine feed stream in DD and urine feed and acidic collector streams in IMD-AC. As a result, **orthophosphate flux and selectivity in DD was increased and  $\text{NH}_3$  vapor flux in IMD-AC was enhanced**. At the same time, an **acidic stream benefiting N recovery was produced *in situ* using low-cost/waste salt solutions**.

The techno-economic assessment of implementing DD and IMD-AC for nutrient recovery from source-separated urine into onsite wastewater management **revealed opportunities to improve the economic viability for decentralized nutrient recovery. Utilization of waste resources, such as waste low-grade heat and waste chemicals, significantly decreased costs of operation.**<sup>295</sup> Thermal energy recovery from warm waste streams produced onsite offer propitious opportunities as low-grade heat in MD for N recovery. Analysis revealed that accounting for the benefits of nutrient recovery to downstream wastewater treatment is key to economic viability of the technique. The analysis demonstrates that the capital costs from urine

diversion itself, i.e., toilet and piping, are larger than the nutrient recovery technologies of DD and MD. Urine diversion in public restrooms may be more economically favorable than urine diversion in private restrooms.

### 7.3 Resulting Publications

The following publications are associated with the work presented in this dissertation.

1. S. N. McCartney, N. S. Watanabe, N. Y. Yip. Thermodynamic and energy analysis of nitrogen and phosphorous recovery from wastewaters, *Environmental Science: Water Research and Technology*, 2021, 11.
2. S. N. McCartney, H. Fan, N. S. Watanabe, Y. Huang, N. Y. Yip. Donnan Dialysis for Phosphate Recovery from Diverted Urine, *Environmental Science and Technology: Water*,
3. S. N. McCartney, N. A. Williams, C. Boo, X. Chen, N. Y. Yip, Novel Isothermal Membrane Distillation with Acidic Collector for Selective and Energy-Efficient Recovery of Ammonia from Urine, *ACS Sustainable Chemistry and Engineering*, 2020, 8, 19, 7324–7334
4. S. N. McCartney, H. Fan, N. S. Watanabe, Y. Huang, N. Y. Yip. Integrated Membrane Processes to Capture Orthophosphate and Ammonia from Human Urine. *Manuscript under preparation*.
5. S. N. McCartney, S. Chu, Z. Gallagher, E. Clerico, N. Y. Yip. Evaluation of Costs and Benefits of Decentralized Management of Wastewater: Non-Potable Water Reuse, Thermal Energy Recovery, and Nutrient Recovery. *Manuscript under preparation*.

## 7.4 Implications and Future Directions

The existing linear economy approach to nutrient management has clear shortcomings of high expenditures for production of fertilizer by Haber-Bosch for N fixation and phosphate mining and high chemical and energy cost for nutrient removal at downstream WWTPs to prevent the pollution of aquatic environments. Further compounding these issues is the reliance on other regions to support fertilizer demand, which leaves fertilizer economies vulnerable to the consequences of international conflicts (e.g., Russia's invasion of Ukraine and resultant sanctions on fertilizer exports).<sup>296, 297</sup> Additionally, phosphate rock reserves are a finite and depleting resource. At the same time, the global population is projected to drive  $\approx 50\text{--}85\%$  increase in fertilizer demand by 2050.<sup>296</sup> A more sustainable circular economy promotes the recovery of nutrient from waste streams for reuse, to lower the dependence on industrial P and N fertilizer production from current unsustainable levels, and simultaneously protect aquatic environments from harmful nutrient emissions. The purpose of this work is to critically inform nutrient recovery approaches and advance membrane-based processes for P and N capture to support the paradigm shift from an inefficient linear nutrient economy to a sustainable circular nutrient economy.

The findings of the thermodynamic and energy assessment guide the selection of waste stream and product for nutrient recovery efforts. Based on inherent energy requirements for separation, strategic nutrient recovery efforts should target source-separated urine rather than diluted centralized sources of wastewater. Therefore, instead of reliance on the incumbent centralized sanitation infrastructure, decentralized urine diversion and nutrient recovery efforts may be more viable. While decentralized nutrient recovery from urine will demand new infrastructure (e.g., urine diversion toilets, dual piping, and onsite treatment systems), projected population and sanitation trends present ideal opportunities to introduce urine diversion and onsite

nutrient recovery facilities. The projected urban influx of 2.5 billion people by 2050 and current 2.3 billion people without adequate sanitation will necessitate the installation of new sanitation systems and wastewater treatment facilities.<sup>298</sup> Incorporation of onsite nutrient recovery from source-separated urine into these new facilities would not require costly replacements and retrofit of existing sanitation systems.

This thesis unearthed that it is possible for nutrient recovery to out-compete the energy requirements of the conventional linear economy production methods, i.e., Haber-Bosch for N fixation and phosphate rock mining, if separation processes achieve efficiency benchmarks. Critical to the adoption of nutrient recovery is the development and advancement of technologies capable of high nutrient recovery potential with low energy intensities and expenditures. Studies on membrane-based process of DD, IMD-AC, and BPM-ED, i.e., Chapters 3, 4, and 5, reveal considerations for applying the technologies to nutrient recovery from urine and present opportunities to advance performance and cost-competitiveness. However, future studies are needed to determine the energy efficiencies of separation techniques, DD and IMD-AC relative to the thermodynamic minimum energy for nutrient separation and recovery.

For P recovery with DD, supplying sufficient chloride driver ion content in the receiver solution can enable orthophosphate transport against a concentration gradient, i.e., achieve uphill P transport, to reach practically feasible high P recovery yields.<sup>268</sup> Performance, in terms of orthophosphate recovery, selectivity, and kinetics, can be enhanced if DD is performed immediately following urine diversion and collection, prior to the hydrolysis of urea, which generates a high bicarbonate content that proved detrimental to orthophosphate transport.<sup>268</sup> Furthermore, a monovalent ion permselective membrane offers an approach to improve the selectivity for monovalent orthophosphate over sulfate, but at the cost of decreased kinetics.<sup>268</sup>

Future work can also consider the impact of membrane properties, such as fixed charged density and swelling degree, on the transport of different ions and selectivity for phosphate over other ions. The design of a DD system for P recovery should consider both desired P recovery yields and membrane requirements, which is reflected in tradeoff between economic benefits with capital and operating costs. Another consideration for DD design is to capture orthophosphate within a smaller receiver solution volume relative to the feed to enrich P above the initial concentration of urine. An enriched orthophosphate solution is of greater economic value and facilitates transportation of the P fertilizer.

Operation of isothermal, i.e., equal feed and collector temperature, membrane distillation with acidic collector, or IMD-AC, enabled the production of an enriched ammonia solution that is of greater economic value and facilitates transportation of N fertilizer.<sup>74</sup> Crucially, the vaporization energy requirement for IMD-AC can be lower than and comparable to the specific energy requirements of the dominant industrial N fertilizer production method, i.e., Haber-Bosch for N fixation, and N removal at conventional WWTPs by nitrification-denitrification, respectively.<sup>74</sup> The design of IMD-AC for NH<sub>3</sub> recovery can also consider operation at ambient temperatures, i.e., without warming feed and collector stream, which can reduce thermal energy expenditures, though at the expense of slower kinetics.<sup>74</sup> Practically, this is reflected as tradeoff between reduced operating costs and higher capital cost for larger membrane areas required for the same productivity of N recovery.

BPM-ED can be used as a tool to strategically modify solution pH to enhance the performance, in terms of nutrient flux and recovery potential, of DD for P recovery and IMD-AC for N recovery.<sup>294</sup> The approaches of BPM-ED + DD for P recovery and BPM-ED + IMD-AC for N recovery exhibited lower specific energies than the practical energy requirements of the

currently practiced linear P and N economies (i.e., fertilizer production and removal at centralized WWTPs).<sup>294</sup> The integrated membrane approach of DD, IMD-AC, and BPM-ED demonstrated initial promise for P and N recovery from source-separated urine. Future work can employ real samples of human urine to examine the impacts of proteins and biomolecules, which can be potential foulants, on the DD and IMD-AC operations.

For each of the three membrane-based processes, there are propitious opportunities to apply low-cost and/or recycled waste streams to source chemical and/or energy requirements for operation, thereby enhancing economic viability and/or sustainability of the techniques. The DD study revealed that a variety of solutions with high chloride content, including low-cost and recycled streams, can supply sufficient driver ions to facilitate orthophosphate recovery. For example, waste water softening regenerant rinse, which contains a high concentration of chloride, produced in high-density buildings can be repurposed and used onsite as the receiver solution. Alternatively, desalination brine or sweater can be used to supply chloride content driving orthophosphate recovery in DD. Additionally, the selection of receiver solution in DD is flexible and can be tailored to the desired nutrient profile of the fertilizer product. The IMD-AC study demonstrated that only mild temperatures are needed to drive  $\text{NH}_3$  recovery from urine. Crucially, low-grade heat from locally-available waste flows (e.g., warm bathwater runoff or hot stream of cooling water systems) or onsite solar thermal collectors can supply the necessary thermal energy to drive N recovery in IMD-AC. The cost of operation can be further reduced and sustainability enhanced by supplying acid for the collector solutions from unwanted effluent streams, such as spent pickling brine, which contains acetic acid. Alternatively, an acidic solution can be generated by BPM-ED, replacing the need to source the acid from external sources. In BPM-ED, salt solutions providing electrolyte for acid or base generation can also be sourced from low-cost or

waste resources. Future work can examine the impact of the strength of acid generated via BPM-ED (i.e., weak versus strong acids) on IMD-AC performance. Tapping into unwanted effluents streams to provide chemicals and/or energy for DD, IMD-AC, and BPM-ED can promote circular economies of these other resources. Repurposing these resources to membrane-based processes for nutrient recovery may enhance the cost-competitiveness and environmentally-sensibility of these techniques.

The economic benefits and costs of onsite nutrient recovery using DD and IMD-AC are assessed in a preliminary techno-economic assessment, Chapter 6. The proposed system leverages on the ecosystem of waste utilization and economies of scale in high-density urban population centers. Operation costs can be reduced by utilizing waste heat and chemicals to drive IMD-AC and locally-available waste chemicals to drive DD.<sup>295</sup> However, the high capital costs from toilets and piping infrastructure present challenges for economic feasibility.<sup>295</sup> Preliminary analysis revealed that these costs can be mitigated through urine diversion in public, rather than private restrooms, which require fewer toilets and less piping length.<sup>295</sup> While fertilizer production provides a small source of revenue, potentially, future policy can incentivize decentralized nutrient recovery efforts on the basis of reduced costs downstream at centralized WWTPs.

Additional analysis can consider the energy requirement and cost for disposal of waste streams produced during nutrient recovery. Future techno-economic studies are needed to compare and optimize the scale of urine diversion, i.e., number and location of toilets, to enhance the economic feasibility of nutrient recovery from source-separated urine. Additionally, future life cycle assessments are needed to quantify the environmental impacts (e.g., greenhouse gas emissions, eutrophication potential, resource depletion) of nutrient recovery compared to the existing linear economy approach. Realizing environmental benefits for capturing P and N from

urine for reuse as fertilizer may provide compelling justification for the implementation of urine diversion and nutrient recovery. Additionally, future work can assess the economic and environmental impact of urine source-separation and nutrient recovery on centralized wastewater treatment; specifically, how the changed biome impacts requirements for biological treatments steps in wastewater treatment. Outside of cost-competitiveness and environmental impacts, health and hygiene are also vital performance metrics. As such, assessing the presence of contaminants, such as pathogenic microorganisms, organic pollutants, toxic heavy metals, and pharmaceuticals, in the recovered nutrient products is important. Future studies need to be conducted to better understand rejection of contaminants by AEMs, utilized in DD for P recovery, and hydrophobic microporous membranes, utilized in IMD-AC for N recovery. Additionally, the potential presence of unwanted species in receiver and collector solutions supplied from low-cost/waste resources should be examined in future work. Additionally, the potential presence of unwanted or hazardous species in receiver and collector solutions supplied from low-cost/waste resources should be examined in future work. Also, future studies can evaluate if specific membrane chemistries are more favorable for ammonia flux and selectivity and can elucidate the impact of collector stream pH on ammonia transport in IMD-AC.

The insights from this work are broadly applicable to other processes for resource recovery and/or contaminant removal. The thermodynamic and energy analysis framework can be adapted to quantify minimum energies for removal and/or recovery practices and can be employed to guide strategic approaches for separation. Next, the approach for determining ion concentrations in the feed and receiver solution at Donnan equilibrium can be used to predict DD recovery potential or contaminant removal efficiency from mixed electrolyte solutions. Furthermore, the systematic analysis of factors influencing transport of different ions in DD underscores the role of competitive

ion sorption on transport kinetics and can elucidate ion transport behavior in solutions with complex compositions. These findings can be considered in DD systems for  $\text{NH}_4^+$  recovery from wastewater, metal ion recovery from electroplating rinse, and removal of  $\text{NO}_3^-$  and  $\text{H}_x\text{AsO}_4^{(3-x)-}$  from drinking water, as some examples. IMD-AC, developed in this work, can be adopted and applied for selective separation and/or recovery of compounds that speciate between volatile and nonvolatile forms at different. An example of an environmentally-relevant application is  $\text{H}_2\text{S}$  removal from domestic and industrial wastewaters. Like  $\text{NH}_3$ ,  $\text{H}_2\text{S}$  exhibits pH-dependent volatility. In such a system,  $\text{H}_2\text{S}_{(g)}$  permeates across the MD membrane and speciates to nonvolatile  $\text{HS}^-_{(aq)}$  in a basic collector (equivalent to  $\text{NH}_3_{(g)}$  transport and speciation to  $\text{NH}_4^+_{(aq)}$ ), thus, enabling selective removal of the contaminant.

## References

1. Haynes, W. M., *CRC Handbook of Chemistry and Physics* 91 ed.; CRC Press: Boca Raton, FL, 2014.
2. Dean, J. A., *Lange's Handbook of Chemistry*. 15 ed.; McGraw-Hill, Inc. : New York, 1999.
3. La Iglesia, A., Estimating the thermodynamic properties of phosphate minerals at high and low temperature from the sum of constituent units. *Estud Geol-Madrid* **2009**, *65* (2), 109-119.
4. Erisman, J. W.; Sutton, M. A.; Galloway, J.; Klimont, Z.; Winiwarter, W., How a century of ammonia synthesis changed the world. *Nat. Geosci.* **2008**, *1* (10), 636-741.
5. Fowler, D.; Coyle, M.; Skiba, U.; Sutton, M. A.; Cape, J. N.; Reis, S.; Sheppard, L. J.; Jenkins, A.; Grizzetti, B.; Galloway, J. N.; Vitousek, P.; Leach, A.; Bouwman, A. F.; Butterbach-Bahl, K.; Dentener, F.; Stevenson, D.; Amann, M.; Voss, M., The global nitrogen cycle in the Twentyfirst century. *Philos. Trans. R. Soc. B, Biol. Sci.* **2013**, *368* (1621).
6. Chen, J. G.; Crooks, R. M.; Seefeldt, L. C.; Bren, K. L.; Bullock, R. M.; Darensbourg, M. Y.; Holland, P. L.; Hoffman, B.; Janik, M. J.; Jones, A. K.; Kanatzidis, M. G.; King, P.; Lancaster, K. M.; Lyman, S. V.; Pfromm, P.; Schneider, W. F.; Schrock, R. R., Beyond fossil fuel-driven nitrogen transformations. *Science* **2018**, *360* (6391).
7. Reta, G.; Dong, X.; Li, Z.; Su, B.; Hu, X.; Bo, H.; Yu, D.; Wan, H.; Liu, J.; Li, Y.; Xu, G.; Wang, K.; Xu, S., Environmental impact of phosphate mining and beneficiation: review. *Int. J. Hydrol. Sci.* **2018**, *2* (4), 424-431.
8. *ITP Mining: Energy and Environmental Profile of the U.S. Mining Industry* Department of Energy, Office of Energy Efficiency & Renewable Energy: 2002.
9. Smil, V., Phosphorus in the Environment: Natural Flows and Human Interferences. *Annu. Rev. Environ. Resour.* **2000**, *25*, 53-88.
10. Elser, J.; Bennett, E., A broken biogeochemical cycle. *Nature* **2011**, *478* (7367), 29-31.
11. Sandhu, D.; Singh, A.; Duranceau, S. J.; Nam, B. H.; Mayo, T.; Wang, D., Fate and transport of radioactive gypsum stack water entering the Floridan aquifer due to a sinkhole collapse. *Sci. Rep.* **2018**, *8*.
12. Nelson, N. G.; Cuchiara, M. L.; Hendren, C. O.; Jones, J. L.; Marshall, A.-M., Hazardous Spills at Retired Fertilizer Manufacturing Plants Will Continue to Occur in the Absence of Scientific Innovation and Regulatory Enforcement. *Environ. Sci. Technol.* **2021**, *55* (24), 16267–16269.
13. Michalak, A. M.; Anderson, E. J.; Beletsky, D.; Boland, S.; Bosch, N. S.; Bridgeman, T. B.; Chaffin, J. D.; Cho, K.; Confesor, R.; Daloglu, I.; DePinto, J. V.; Evans, M. A.; Fahnenstiel, G. L.; He, L.; Ho, J. C.; Jenkins, L.; Johengen, T. H.; Kuo, K. C.; LaPorte, E.; Liu, X.; McWilliams, M. R.; Moore, M. R.; Posselt, D. J.; Richards, R. P.; Scavia, D.;

- Steiner, A. L.; Verhamme, E.; Wright, D. M.; Zagorski, M. A., Record-setting algal bloom in Lake Erie caused by agricultural and meteorological trends consistent with expected future conditions. *Proc. Natl. Acad. Sci.* **2013**, *110* (16), 6448-6452.
14. Conley, D. J.; Paerl, H. W.; Howarth, R. W.; Boesch, D. F.; Seitzinger, S. P.; Havens, K. E.; Lancelot, C.; Likens, G. E., Ecology - Controlling eutrophication: Nitrogen and phosphorus. *Science* **2009**, *323*, 1014-1015.
15. Diaz, R. J.; Rosenberg, R., Spreading dead zones and consequences for marine ecosystems. *Science* **2008**, *321*, 926-929.
16. Hitzfeld, B. C.; Høger, S. J.; Dietrich, D. R., Cyanobacterial toxins: Removal during drinking water treatment, and human risk assessment. *Environ Health Persp* **2000**, *108*, 113-122.
17. Brooks, B. W.; Lazorchak, J. M.; Howard, M. D. A.; Johnson, M. V. V.; Morton, S. L.; Perkins, D. A. K.; Reavie, E. D.; Scott, G. I.; Smith, S. A.; Steevens, J. A., Are Harmful Algal Blooms Becoming the Greatest Inland Water Quality Threat to Public Health and Aquatic Ecosystems? *Environ. Toxicol. Chem.* **2016**, *35* (1), 6-13.
18. Brooks, B. W.; Lazorchak, J. M.; Howard, M. D. A.; Johnson, M.-V. V.; Morton, S. L.; Perkins, D. A. K.; Reavie, E. D.; Scott, G. I.; Smith, S. A.; Steevens, J. A., Are harmful algal blooms becoming the greatest inland water quality threat to public health and aquatic ecosystems? *Environmental Toxicology and Chemistry* **2016**, *35* (1), 6-13.
19. Anderson, D. M.; Glibert, P. M.; Burkholder, J. M., Harmful algal blooms and eutrophication: Nutrient sources, composition, and consequences. *Estuaries* **2002**, *25* (4), 704-726.
20. Hitzfeld, B. C.; Höger, S. J.; Dietrich, D. R., Cyanobacterial toxins: removal during drinking water treatment, and human risk assessment. *Environmental Health Perspectives* **2000**, *108* (Suppl 1), 113-122.
21. Paerl, H. W.; Gardner, W. S.; McCarthy, M. J.; Peierls, B. L.; Wilhelm, S. W., Algal blooms: Noteworthy nitrogen. *Science* **2014**, *346* (6206), 175-175.
22. Caron, D. A.; Garneau, M.-È.; Seubert, E.; Howard, M. D. A.; Darjany, L.; Schnetzer, A.; Cetinić, I.; Filteau, G.; Lauri, P.; Jones, B.; Trussell, S., Harmful algae and their potential impacts on desalination operations off southern California. *Water Research* **2010**, *44* (2), 385-416.
23. *Water Desalination Report*; Volume 53, Number 31; Global Water Intelligence: 2017.
24. Steffen, W.; Richardson, K.; Rockstrom, J.; Cornell, S. E.; Fetzer, I.; Bennett, E. M.; Biggs, R.; Carpenter, S. R.; de Vries, W.; de Wit, C. A.; Folke, C.; Gerten, D.; Heinke, J.; Mace, G. M.; Persson, L. M.; Ramanathan, V.; Reyers, B.; Sorlin, S., Planetary boundaries: Guiding human development on a changing planet. *Science* **2015**, *347* (6223).
25. Cordell, D.; Rosemarin, A.; Schröder, J. J.; Smit, A. L., Towards global phosphorus security: A systems framework for phosphorus recovery and reuse options. *Chemosphere* **2011**, *84*, 747-754.

26. Grönman, K.; Ypyä, J.; Virtanen, Y.; Kurpp, S.; Soukka, R.; Seuri, P.; Finér, A.; Linnanena, L., Nutrient footprint as a tool to evaluate the nutrient balance of a food chain. *J. Clean. Prod.* **2016**, *112* (4), 2429-2440.
27. Wiel, B. Z. d.; Weijma, J.; Middelaar, C. E. v.; Kleinke, M.; Buisman, C. J. N.; Wichern, F., Restoring nutrient circularity: A review of nutrient stock and flow analyses of local agro-food-waste systems. *Resour Conserv Recycl* **2020**, *160*, 104901.
28. Conley, D. J.; Paerl, H. W.; Howarth, R. W.; Boesch, D. F.; Seitzinger, S. P.; Havens, K. E.; Lancelot, C.; Likens, G. E., Controlling Eutrophication: Nitrogen and Phosphorus. *Science* **2009**, *323* (5917), 1014-1015.
29. Sutton, M. A.; Oenema, O.; Erisman, J. W.; Leip, A.; van Grinsven, H.; Winiwarter, W., Too much of a good thing. *Nature* **2011**, *472* (7342), 159-161.
30. Falk, M. W.; Reardon, D. J.; Neethling, J. B.; Clark, D. L.; Pramanik, A., Striking the Balance between Nutrient Removal, Greenhouse Gas Emissions, Receiving Water Quality, and Costs. *Water Environment Research* **2013**, *85* (12), 2307-2316.
31. Rahman, S. M.; Eckelman, M. J.; Onnis-Hayden, A.; Gu, A. Z., Life-Cycle Assessment of Advanced Nutrient Removal Technologies for Wastewater Treatment. *Environ. Sci. and Technol.* **2016**.
32. Larsen, T. A.; Maurer, M.; Udert, K. M.; Lienert, J., Nutrient cycles and resource management: implications for the choice of wastewater treatment technology. *Water Sci. Technol.* **2007**, *56* (5), 229-37.
33. Winkler, M. K.; Straka, L., New directions in biological nitrogen removal and recovery from wastewater. *Curr. Opin. Biotechnol.* **2019**, *57*, 50-55.
34. Oehmen, A.; Lemos, P. C.; Carvalho, G.; Yuan, Z.; Keller, J.; Blackall, L. L.; Reis, M. A., Advances in enhanced biological phosphorus removal: from micro to macro scale. *Water Res.* **2007**, *41* (11), 2271-300.
35. Yeoman, S.; Stephenson, T.; Lester, J. N.; Perry, R., The removal of phosphorus during wastewater treatment: a review. *Environ. Pollut.* **1988**, *49* (3), 183-233.
36. Smith, A. L.; Stadler, L. B.; Love, N. G.; Skerlos, S. J.; Raskin, L., Perspectives on anaerobic membrane bioreactor treatment of domestic wastewater: a critical review. *Bioresour. Technol.* **2012**, *122*, 149-59.
37. Blackall, L. L.; Crocetti, G. R.; Saunders, A. M.; Bond, P. L., A review and update of the microbiology of enhanced biological phosphorus removal in wastewater treatment plants. *Antonie Van Leeuwenhoek* **2002**, *81* (1-4), 681-91.
38. Zhu, G.; Peng, Y.; Li, B.; Guo, J.; Yang, Q.; Wang, S., Biological removal of nitrogen from wastewater. *Rev Environ Contam Toxicol* **2008**, *192*, 159-95.
39. McCarty, P. L., What is the Best Biological Process for Nitrogen Removal: When and Why? *Environ. Sci. Technol.* **2018**, *52* (7), 3835-3841.

40. Epstein, E., *Land Application of Sewage Sludge and Biosolids*. 1 ed.; CRC Press: Boca Raton, 2002.
41. Lu, Q.; He, Z. L.; Stoffella, P. J., Land Application of Biosolids in the USA: A Review. *Applied and Environmental Soil Science* **2012**.
42. Gao, X.; Shen, T.; Zheng, Y.; Sun, X.; Huang, S.; Ren, Q.; Zhang, X.; Tian, Y.; Luan, G., Practical manure handbook. Chinese Agricultural Publishing House. Beijing: 2002.
43. Jönsson, H.; Vinnerås, B. In *Adapting the nutrient content of urine and faeces in different countries using FAO and Swedish data*, bEcosan—closing the loopQ—Proceedings of the 2nd International Symposium on ecological sanitation, 2003; pp 07-11.
44. Larsen, T. A.; Udert, K. M.; Lienert, J., *Source separation and decentralization for wastewater management*. Iwa Publishing: 2013.
45. Höglund, C. Evaluation of microbial health risks associated with the reuse of source-separated human urine. *Bioteknologi*, 2001.
46. Höglund, C.; Ashbolt, N.; Stenström, T. A.; Svensson, L., Viral persistence in source-separated human urine. *Advances in Environmental Research* **2002**, 6 (3), 265-275.
47. Simha, P.; Ganesapillai, M., Ecological Sanitation and nutrient recovery from human urine: How far have we come? A review. *Sustainable Environment Research* **2017**, 27 (3), 107-116.
48. Maurer, M.; Schwegler, P.; Larsen, T. A., Nutrients in urine: energetic aspects of removal and recovery. *Water Sci Technol* **2003**, 48 (1), 37-46.
49. Maurer, M.; Pronk, W.; Larsen, T. A., Treatment processes for source-separated urine. *Water Research* **2006**, 40 (17), 3151-3166.
50. Liu, Y.; Kumar, S.; Kwag, J.-H.; Ra, C., Magnesium ammonium phosphate formation, recovery and its application as valuable resources: a review. *Journal of Chemical Technology & Biotechnology* **2013**, 88 (2), 181-189.
51. Karak, T.; Bhattacharyya, P., Human urine as a source of alternative natural fertilizer in agriculture: A flight of fancy or an achievable reality. *Resour Conserv Recy* **2011**, 55 (4), 400-408.
52. Larsen, T. A.; Alder, A. C.; Eggen, R. I. L.; Maurer, M.; Lienert, J., Source separation: Will we see a paradigm shift in wastewater handling? *Environ. Sci. Technol.* **2009**, 43 (16), 6121.
53. Tanada, S.; Kabayama, M.; Kawasaki, N.; Sakiyama, T.; Nakamura, T.; Araki, M.; Tamura, T., Removal of phosphate by aluminum oxide hydroxide. *J Colloid Interf Sci* **2003**, 257 (1), 135-140.
54. Xie, J.; Wang, Z.; Lu, S. Y.; Wu, D. Y.; Zhang, Z. J.; Kong, H. N., Removal and recovery of phosphate from water by lanthanum hydroxide materials. *Chem Eng J* **2014**, 254, 163-170.

55. Karageorgiou, K.; Paschalis, M.; Anastassakis, G. N., Removal of phosphate species from solution by adsorption onto calcite used as natural adsorbent. *Journal of Hazardous Materials* **2007**, *139* (3), 447-452.
56. Zhang, G. S.; Liu, H. J.; Liu, R. P.; Qu, J. H., Removal of phosphate from water by a Fe-Mn binary oxide adsorbent. *J. Colloid Interface Sci.* **2009**, *335* (2), 168-174.
57. Lu, J. B.; Liu, H. J.; Liu, R. P.; Zhao, X.; Sun, L. P.; Qu, J. H., Adsorptive removal of phosphate by a nanostructured Fe-Al-Mn trimetal oxide adsorbent. *Powder Technol* **2013**, *233*, 146-154.
58. Maul, G. A.; Kim, Y.; Amini, A.; Zhang, Q.; Boyer, T. H., Efficiency and life cycle environmental impacts of ion-exchange regeneration using sodium, potassium, chloride, and bicarbonate salts. *Chem Eng J* **2014**, *254*, 198-209.
59. Kalogirou, S. A., Solar thermal collectors and applications. *Progress in Energy and Combustion Science* **2004**, *30* (3), 231-295.
60. Wong, L. T.; Mui, K. W.; Guan, Y., Shower water heat recovery in high-rise residential buildings of Hong Kong. *Appl Energ* **2010**, *87* (2), 703-709.
61. Liu, L. B.; Fu, L.; Jiang, Y., Application of an exhaust heat recovery system for domestic hot water. *Energy* **2010**, *35* (3), 1476-1481.
62. Webster, K., *The Circular Economy: a Wealth of Flows*. Ellen MacArthur Foundation: Isle of Wight, 2015.
63. W. McDonough, M. B., *Cradle to Cradle: Remaking the Way We Make Things*. 1 ed.; North Point Press: New York, 2002.
64. Commoner, B., *The Closing Circle: Nature, Man, and Technology*. Random House: New York, 1971.
65. Stahel, W. R., The circular economy. *Nature* **2016**, *531* (7595), 435-8.
66. Maurer, M.; Schwegler, P.; Larsen, T. A., Nutrients in urine: energetic aspects of removal and recovery. *Water Sci. Technol.* **2003**, *48* (1), 37-46.
67. Ronteltap, M.; Maurer, M.; Gujer, W., Struvite precipitation thermodynamics in source-separated urine. *Water Res.* **2007**, *41* (5), 977-84.
68. Maurer, M.; Pronk, W.; Larsen, T. A., Treatment processes for source-separated urine. *Water Res.* **2006**, *40* (17), 3151-3166.
69. Mihelcic, J. R.; Fry, L. M.; Shaw, R., Global potential of phosphorus recovery from human urine and feces. *Chemosphere* **2011**, *84* (6), 832-839.
70. Zhang, J.; She, Q.; Chang, V. W. C.; Tang, C. Y.; Webster, R. D., Mining nutrients (N, K, P) from urban source-separated urine by forward osmosis dewatering. *Environ. Sci. Technol.* **2014**.
71. Liu, Q. L.; Liu, C. H.; Zhao, L.; Ma, W. C.; Liu, H. L.; Ma, J., Integrated forward osmosis-membrane distillation process for human urine treatment. *Water Res.* **2016**, *91*, 45-54.

72. Randall, D. G.; Naidoo, V., Urine: The liquid gold of wastewater. *J. Environ. Chem. Eng.* **2018**, *6* (2), 2627-2635.
73. Tarpeh, W. A.; Barazesh, J. M.; Cath, T. Y.; Nelson, K. L., Electrochemical Stripping to Recover Nitrogen from Source-Separated Urine. *Environ. Sci. Technol.* **2018**, *52* (3), 1453-1460.
74. McCartney, S. N.; Williams, N.; Boo, C.; Chen, X.; Yip, N. Y., Novel Isothermal Membrane Distillation with Acidic Collector for Selective and Energy-Efficient Recovery of Ammonia from Urine. *ACS Sustain. Chem. Eng.* **2020**, *8* (19), 7324-7334.
75. Jagtap, N.; Boyer, T. H., Integrated Decentralized Treatment for Improved N and K Recovery from Urine. *J. Sustain. Water Built Environ.* **2020**, *6* (2).
76. Xu, K. N.; Qu, D.; Zheng, M.; Guo, X. H.; Wang, C. W., Water Reduction and Nutrient Reconciliation of Hydrolyzed Urine via Direct-Contact Membrane Distillation: Ammonia Loss and Its Control. *J Environ Eng* **2019**, *145* (3).
77. Sendrowski, A.; Boyer, T. H., Phosphate removal from urine using hybrid anion exchange resin. *Desalination* **2013**, *322*, 104-112.
78. Kjerstadius, H.; Haghigatafshar, S.; Davidsson, A., Potential for nutrient recovery and biogas production from blackwater, food waste and greywater in urban source control systems. *Environ. Technol.* **2015**, *36* (13), 1707-1720.
79. El-Shafai, S. A.; El-Gohary, F. A.; Nasr, F. A.; van der Steen, N. P.; Gijzen, H. J., Nutrient recovery from domestic wastewater using a UASB-duckweed ponds system. *Bioresour. Technol.* **2007**, *98* (4), 798-807.
80. Hulsen, T.; Batstone, D. J.; Keller, J., Phototrophic bacteria for nutrient recovery from domestic wastewater. *Water Res.* **2014**, *50*, 18-26.
81. Batstone, D. J.; Hulsen, T.; Mehta, C. M.; Keller, J., Platforms for energy and nutrient recovery from domestic wastewater: A review. *Chemosphere* **2015**, *140*, 2-11.
82. Ward, A. J.; Arola, K.; Brewster, E. T.; Mehta, C. M.; Batstone, D. J., Nutrient recovery from wastewater through pilot scale electrodialysis. *Water Res.* **2018**, *135*, 57-65.
83. Theregowda, R. B.; Gonzalez-Mejia, A. M.; Ma, X.; Garland, J., Nutrient Recovery from Municipal Wastewater for Sustainable Food Production Systems: An Alternative to Traditional Fertilizers. *Environ. Eng. Sci.* **2019**, *36* (7), 833-842.
84. Umble, A. K.; Ketchum, L. H., A strategy for coupling municipal wastewater treatment using the sequencing batch reactor with effluent nutrient recovery through aquaculture. *Water Sci. Technol.* **1997**, *35* (1), 177-184.
85. Yetilmezsoy, K.; Sapci-Zengin, Z., Recovery of ammonium nitrogen from the effluent of UASB treating poultry manure wastewater by MAP precipitation as a slow release fertilizer. *J. Hazard. Mater.* **2009**, *166* (1), 260-269.
86. Pastor, L.; Mangin, D.; Ferrer, J.; Seco, A., Struvite formation from the supernatants of an anaerobic digestion pilot plant. *Bioresour. Technol.* **2010**, *101* (1), 118-125.

87. Liu, R. D.; Wang, Y. K.; Wu, G.; Luo, J. N.; Wang, S. G., Development of a selective electrodialysis for nutrient recovery and desalination during secondary effluent treatment. *Chem. Eng. J.* **2017**, *322*, 224-233.
88. Booker, N. A.; Priestley, A. J.; Fraser, I. H., Struvite formation in wastewater treatment plants: Opportunities for nutrient recovery. *Environ. Technol.* **1999**, *20* (7), 777-782.
89. Udert, K. M.; Larsen, T. A.; Biebow, M.; Gujer, W., Urea hydrolysis and precipitation dynamics in a urine-collecting system. *Water Res.* **2003**, *37* (11), 2571-2582.
90. Udert, K. M.; Larsen, T. A.; Gujer, W., Estimating the precipitation potential in urine-collecting systems. *Water Res.* **2003**, *37* (11), 2667-2677.
91. Almeida, M. C.; Bulter, D.; Friedler, E., At-source domestic wastewater quality. *Urban Water* **1999**, *1* (1), 49-55.
92. Simha, P.; Ganesapillai, M., Ecological Sanitation and nutrient recovery from human urine: How far have we come? A review. *Sustain. Environ. Res* **2017**, *27* (3), 107-116.
93. *The Use of Reclaimed Water and Sludge in Food Crop Production*. National Academy Press: Washington, D.C., 1996.
94. Pettygrove, G. S., *Irrigation With Reclaimed Municipal Wastewater - A Guidance Manual*. 1 ed.; CRC Press: Boca Raton, 1985.
95. Friedler, E.; Butler, D.; Alfiya, Y., Wastewater composition. In *Source Separation and Decentralization for Wastewater Management*, Larsen, T. A.; Udert, K. M.; Lienert, J., Eds. IWA Publishing: London, UK, 2013; pp 241-254.
96. Fittschen, I.; Hahn, H. H., Characterization of the municipal wastewater part human urine and a preliminary comparison with liquid cattle excretion. *Water Sci. Technol.* **1998**, *38* (6), 9-16.
97. Wei, X. C.; Viadero, R. C.; Bhojappa, S., Phosphorus removal by acid mine drainage sludge from secondary effluents of municipal wastewater treatment plants. *Water Res.* **2008**, *42* (13), 3275-3284.
98. Liu, C.; Rainwater, K.; Song, L. F., Energy analysis and efficiency assessment of reverse osmosis desalination process. *Desalination* **2011**, *276* (1-3), 352-358.
99. Mistry, K. H.; McGovern, R. K.; Thiel, G. P.; Summers, E. K.; Zubair, S. M.; Lienhard, J. H., Entropy Generation Analysis of Desalination Technologies. *Entropy-Switz* **2011**, *13* (10), 1829-1864.
100. Lin, S.; Yip, N. Y.; Elimelech, M., Direct contact membrane distillation with heat recovery: Thermodynamic insights from module scale modeling. *J. Membr. Sci* **2014**, *453*, 498-515.
101. D Brogioli, L. M., NY Yip, Thermodynamic analysis and energy efficiency of thermal desalination processes. *Desalination* **2018**, *428*, 29-39.

102. Yip, N. Y.; Elimelech, M., Thermodynamic and energy efficiency analysis of power generation from natural salinity gradients by pressure retarded osmosis. *Environ. Sci. Technol.* **2012**, *46* (9), 5230-9.
103. Smith, J. M.; Van Ness, H. C.; Abbott, M. M., *Introduction to Chemical Engineering Thermodynamics*. 7th ed.; McGraw-Hill: New York, 2005; p 840.
104. Sassen, C. L.; Vankwartel, R. A. C.; Vanderkooi, H. J.; Arons, J. D., Vapor-Liquid-Equilibria for the System Ammonia + Water up to the Critical Region. *J. Chem. Eng. Data* **1990**, *35* (2), 140-144.
105. Wang, M.; Ferreira, C. A. I., Absorption heat pump cycles with NH<sub>3</sub> - ionic liquid working pairs. *Appl. Energy* **2017**, *204*, 819-830.
106. Kurhe, D. N.; Dagade, D. H.; Jadhav, J. P.; Govindwar, S. P.; Patil, K. J., Thermodynamic Studies of Amino Acid-Denaturant Interactions in Aqueous Solutions at 298.15 K. *J Solution Chem* **2011**, *40* (9), 1596-1617.
107. Page, E. R., Aqueous Ammonia as a Nitrogen-Fertilizer for Summer Cauliflowers, Compared with Ammonium-Nitrate (Broadcast) and Urea (Broadcast and Injected). *J. Agric. Sci.* **1979**, *92* (Feb), 251-254.
108. Smith, C. J.; Chalk, P. M., Comparison of the Efficiency of Urea, Aqueous Ammonia and Ammonium-Sulfate as Nitrogen Fertilizers. *Plant Soil* **1980**, *55* (2), 333-337.
109. Breitenbeck, G. A.; Bremner, J. M., Effects of Rate and Depth of Fertilizer Application on Emission of Nitrous-Oxide from Soil Fertilized with Anhydrous Ammonia. *Biol. Fertil. Soils* **1986**, *2* (4), 201-204.
110. Broschat, T. K.; Moore, K. K., Release rates of ammonium-nitrogen, nitrate-nitrogen, phosphorus, potassium, magnesium, iron, and manganese from seven controlled-release fertilizers. *Commun. in Soil Sci. Plant Anal.* **2007**, *38* (7-8), 843-850.
111. Mullins, G. L.; Sikora, F. J., Field-Evaluation of Commercial Monoammonium Phosphate Fertilizers. *Fert Res* **1990**, *22* (1), 1-6.
112. Reuveni, M.; Oppenheim, D.; Reuveni, R., Integrated control of powdery mildew on apple trees by foliar sprays of mono-potassium phosphate fertilizer and sterol inhibiting fungicides. *Crop Prot.* **1998**, *17* (7), 563-568.
113. Latifian, M.; Liu, J.; Mattiasson, B., Struvite-based fertilizer and its physical and chemical properties. *Environ. Technol.* **2012**, *33* (24), 2691-2697.
114. Liu, Y.; Kumar, S.; Kwag, J. H.; Ra, C., Magnesium ammonium phosphate formation, recovery and its application as valuable resources: a review. *J Chem Technol Biot* **2013**, *88* (2), 181-189.
115. Rahman, M. M.; Salleh, M. A. M.; Rashid, U.; Ahsan, A.; Hossain, M. M.; Ra, C. S., Production of slow release crystal fertilizer from wastewaters through struvite crystallization - A review. *Arab. J. Chem.* **2014**, *7* (1), 139-155.

116. Zhang, F. F.; Wang, Q. S.; Hong, J. L.; Chen, W.; Qi, C. C.; Ye, L. P., Life cycle assessment of diammonium- and monoammonium-phosphate fertilizer production in China. *J. Clean. Prod.* **2017**, *141*, 1087-1094.
117. Arslanoglu, H.; Tumen, F., Potassium struvite (slow release fertilizer) and activated carbon production: Resource recovery from vinasse and grape marc organic waste using thermal processing. *Process Saf. Environ. Prot.* **2021**, *147*, 1077-1087.
118. Landry, K. A.; Sun, P.; Huang, C. H.; Boyer, T. H., Ion-exchange selectivity of diclofenac, ibuprofen, ketoprofen, and naproxen in ureolyzed human urine. *Water Res.* **2015**, *68*, 510-521.
119. Edahwati, L.; Sutyono, S.; Perwitasari, D. S.; Muryanto, S.; Jamari, J.; Bayuseno, A. P., Effects of the Optimised pH and Molar Ratio on Struvite Precipitation in Aqueous System. In *Matec Web Conf*, 2016; Vol. 58.
120. Widjajanto, D. W., Environmental advantages and disadvantages of different sources of nitrogen in agricultural systems. In *Fertilizers and Environment*, Rodriguez-Barrueco, C., Ed. Salamanca, Spain, 1995; pp 253-257.
121. Hignett, T. P., Some Factors Influencing Choice of Nitrogen Fertilizers. In *Fertilizer Manual*, Kluwer Academic Publishers: Dordrecht, The Netherlands, 1985; pp 136-145.
122. Gnaratnam, A.; McCurdy, M.; Grafton, M.; Jeyakumar, P.; Bishop, P.; Davies, C. *Assessment of Nitrogen Fertilizers Under Controlled Environment – A Lysimeter Design*; Fertilizer and Lime Research Centre; Massey University: 2019.
123. Bleiwas, D. I. *Estimates of Electricity Requirements for the Recovery of Mineral Commodities, with Examples Applied to Sub-Saharan Africa*; 2011–1253; Reston, VA, 2011.
124. Cussler, E. L.; Dutta, B. K., On separation efficiency. *AIChE J.* **2012**, *58* (12), 3825-3831.
125. Korhonen, J.; Honkasalo, A.; Seppälä, J., Circular economy: the concept and its limitations. *Ecol Econ* **2018**, *143*, 36-47.
126. Gao, X.; Shen, T.; Zheng, Y.; Sun, X.; Huang, S.; Ren, Q.; Zhang, X.; Tian, Y.; Luan, G., *Practical manure handbook. In Chinese*. Agricultural Publishing House: Beijing, 2002.
127. H. Jönsson, B. V., Adapting the nutrient content of urine and faeces in different countries using FAO and Swedish data. In *2nd International Symposium on ecological sanitation*, 2004; pp 7-11.
128. Ashley, K.; Cordell, D.; Mavinic, D., A brief history of phosphorus: From the philosopher's stone to nutrient recovery and reuse. *Chemosphere* **2011**, *84* (6), 737-746.
129. Simonova, M.; Gruère, A.; de Sousa, J.; Couturier, V.; Rousseau, O.; Marcel-Monnier, S.; Beltaief, S. *Global Medium-Term Outlook for Fertilizers and Raw Materials: 2020-2024*; Market Intelligence and Agricultural Services: Montreal, Canada, 2020.
130. *World Population Prospects- Data Booklet*; ST/ESA/SER.A/401; 2017.

131. Li, W. W.; Yu, H. Q.; Rittmann, B. E., Chemistry: Reuse water pollutants. *Nature* **2015**, 528 (7580), 29-31.
132. Verstraete, W.; de Caveye, P. V.; Diamantis, V., Maximum use of resources present in domestic "used water". *Bioresour. Technol.* **2009**, 100 (23), 5537-5545.
133. Guest, J. S.; Skerlos, S. J.; Barnard, J. L.; Beck, M. B.; Daigger, G. T.; Hilger, H.; Jackson, S. J.; Karvazy, K.; Kelly, L.; Macpherson, L.; Mihelcic, J. R.; Pramanik, A.; Raskin, L.; Van Loosdrecht, M. C. M.; Yeh, D.; Love, N. G., A new planning and design paradigm to achieve sustainable resource recovery from wastewater. *Environ. Sci. Technol.* **2009**.
134. McCartney, S. N.; Watanabe, N. S.; Yip, N. Y., Thermodynamic and energy analysis of nitrogen and phosphorous recovery from wastewaters. *Environ. Sci.: Water Res. Technol.* **2021**, 7 (11), 2075-2088.
135. Wang, J.; Burken, J. G.; Zhang, X. Q.; Surampalli, R., Engineered struvite precipitation: Impacts of component-ion molar ratios and pH. *J Environ Eng* **2005**, 131 (10), 1433-1440.
136. Ronteltap, M.; Maurer, M.; Gujer, W., The behaviour of pharmaceuticals and heavy metals during struvite precipitation in urine. *Water Res* **2007**, 41 (9), 1859-68.
137. Kemacheevakul, P.; Chuangchote, S.; Otani, S.; Matsuda, T.; Shimizu, Y., Effect of magnesium dose on amount of pharmaceuticals in struvite recovered from urine. *Water Sci. Technol.* **2015**, 72 (7), 1102-10.
138. Lahr, R. H.; Goetsch, H. E.; Haig, S. J.; Noe-Hays, A.; Love, N. G.; Aga, D. S.; Bott, C. B.; Foxman, B.; Jimenez, J.; Luo, T.; Nace, K.; Ramadugu, K.; Wigginton, K. R., Urine Bacterial Community Convergence through Fertilizer Production: Storage, Pasteurization, and Struvite Precipitation. *Environ. Sci. Technol.* **2016**, 50, 11619-11626.
139. Mullen, R. A.; Wigginton, K. R.; Noe-Hays, A.; Nace, K.; Love, N. G.; Bott, C. B.; Aga, D. S., Optimizing extraction and analysis of pharmaceuticals in human urine, struvite, food crops, soil, and lysimeter water by liquid chromatography-tandem mass spectrometry. *Anal. Methods* **2017**, 9.
140. Tang, C.; Liua, Z.; Penga, C.; Chaia, L.-Y.; Kurodac, K.; Okidoc, M.; Song, Y.-X., New insights into the interaction between heavy metals and struvite: Struvite as platform for heterogeneous nucleation of heavy metal hydroxide. *Chem Eng J* **2019**, 365, 60-69.
141. Boer, M. A. d.; Hammerton, M.; Sloopweg, J. C., Uptake of pharmaceuticals by sorbent-amended struvite fertilisers recovered from human urine and their bioaccumulation in tomato fruit. *Water Res* **2018**, 133, 19-26.
142. Chen, S. Y.; Shi, Z.; Song, Y.; Li, X. R.; Hu, Y. L., Phosphate removal from aqueous solution by Donnan dialysis with anion-exchange membrane. *J Cent South Univ* **2014**, 21 (5), 1968-1973.
143. Shashvatt, U.; Amurrio, F.; Portner, C.; Blaney, L., Phosphorus recovery by Donnan dialysis: Membrane selectivity, diffusion coefficients, and speciation effects. *Chem. Eng. J.* **2021**, 419.

144. Trifi, I. M.; Trifi, B.; Ayed, S. B.; Hamrouni, B., Removal of phosphate by Donnan dialysis coupled with adsorption onto calcium alginate beads. *Water Sci. Technol.* **2009**, *80* (1).
145. Zhao, B.; Zhao, H.; Ni, J., Arsenate removal by Donnan dialysis: Effects of the accompanying components. *Sep. Purif. Technol.* **2010**, *72* (3), 250-255.
146. Sarkar, S.; Sengupta, A. K.; Prakash, P., The Donnan Membrane Principle: Opportunities for Sustainable Engineered Processes and Materials. *Environ. Sci. Technol.* **2010**, *44* (4), 1161-1166.
147. Strathmann, H., Electrodialysis and related processes. In *Membrane Science and Technology*, Noble, R. D.; Stern, S. A., Eds. Elsevier: 1995; Vol. 2, pp 213-281.
148. Tanaka, Y., Donnan Dialysis. In *Ion Exchange Membranes: Fundamentals and Applications*, Second ed.; IEM Research: Ibaraki, Japan, 2015; pp 445-457.
149. Strathmann, H., Ion-Exchange Membrane Processes in Water Treatment. *Sustainable Water for the Future: Water Recycling Versus Desalination* **2010**, *2*, 141-199.
150. Strathmann, H., *Ion-Exchange Membrane Separation Processes*. Elsevier: 2004.
151. Yan, G. J.; Bao, Y.; Tan, M.; Cui, Q.; Lu, X. L.; Zhang, Y., Defluorination by Donnan Dialysis with seawater for seafood processing. *J Food Eng* **2018**, *238*, 22-29.
152. Velizarov, S., Transport of arsenate through anion-exchange membranes in Donnan dialysis. *J. Membr. Sci.* **2013**, *425*, 243-250.
153. Hichour, M.; Persin, F.; Sandeaux, J.; Gavach, C., Fluoride removal from waters by Donnan dialysis. *Separation and Purification Technology* **2000**, *18* (1), 1-11.
154. Asante-Sackey, D.; Rathilal, S.; Tetteh, E. K.; Ezugbe, E. O.; Pillay, L. V., Donnan Membrane Process for the Selective Recovery and Removal of Target Metal Ions—A Mini Review. *Membranes* **2021**, *11* (358).
155. J. Veermana, J.; de Jong, R. M.; M., S.; Metz, S. J.; Harmsen, G. J., Reverse electrodialysis: Comparison of six commercial membrane pairs on the thermodynamic efficiency and power density. *J. Membr. Sci.* **2009**, *343* (1-2), 7-15.
156. Spiegler, K. S., Transport processes in ionic membranes. *Trans. Faraday Soc.* **1958**, *54*, 1408-1428.
157. Beck, A.; Ernst, M., Kinetic modeling and selectivity of anion exchange in Donnan dialysis. *J. Membr. Sci.* **2015**, *479*, 132-140.
158. Pessoa-Lopes, M.; Crespo, J. G.; Velizarov, S., Arsenate removal from sulphate-containing water streams by an ion-exchange membrane process. *Sep. Purif. Technol.* **2016**, *166*, 125-134.
159. Malewitz, T.; Pintauro, P. N.; Rear, D., Multicomponent absorption of anions in commercial anion-exchange membranes. *J. Membr. Sci.* **2007**, *301*, 171-179.

160. Galizia, M.; Benedetti, F. M.; Paula, D. R.; Freeman, B. D., Monovalent and divalent ion sorption in a cation exchange membrane based on cross-linked poly (p-styrene sulfonate-co-divinylbenzene). *J. Membr. Sci.* **2017**, *525*, 132-142.
161. Saracco, G.; Zanetti, M. C., Ion transport through monovalent-anion-permselective membranes. *Ind Eng Chem Res* **1994**, *33* (1), 96-101.
162. Saracco, G., Transport properties of monovalent-ion-permselective membranes. *Chem. Eng. Sci.* **1997**, *52* (17), 3019-3031.
163. Lu, H.-Y.; Lin, C.-S.; Lee, S.-C.; Ku, M.-H.; Hsu, J.-P.; Tseng, S.; Lin, S.-H., Preparation of Mineral Source Water From Deep Sea Water: Reduction of Sulfate Ion Using Selemion ASV Membrane. *AIChE Journal* **2011**, *5* (4), 1033-1042.
164. Fan, H.; Huang, Y.; Billinge, I. H.; Bannon, S. M.; Geise, G. M.; Yip, N. Y., Counterion Mobility in Ion-Exchange Membranes: Spatial Effect and Valency-Dependent Electrostatic Interaction. *ACS EST Engg* **2022**.
165. Kronzucker, H. J.; Coskun, D.; Schulze, L. M.; Wong, J. R.; Britto, D. T., Sodium as nutrient and toxicant. *Plant Soil* **2013**, *369*, 1-23.
166. Genc, Y.; McDonald, G. K.; Tester, M., Reassessment of tissue Na<sup>+</sup> concentration as a criterion for salinity tolerance in bread wheat. *Plant Cell Environ* **2007**, *30*, 1-23.
167. Arola, K.; Ward, A.; Mänttäri, M.; Kallioinen, M.; Batstone, D., Transport of pharmaceuticals during electro dialysis treatment of wastewater. *Water Res* **2019**, *161*, 496-504.
168. Banasiaka, L. J.; Bruggen, B. V. d.; Schäfer, A. I., Sorption of pesticide endosulfan by electro dialysis membranes. *Chem Eng J* **2011**, *116* (1), 233-239.
169. Pronk, W.; Biebow, M.; Boller, M., Electro dialysis for Recovering Salts from a Urine Solution Containing Micropollutants. *Environ. Sci. Technol.* **2006**, *40* (7), 2414-2420.
170. Ma, L.; Gutierrez, L.; Vooren, T. V.; Vanoppen, M.; Kazemabad, M.; Verliefde, A.; Cornelissen, E., Fate of organic micropollutants in reverse electro dialysis: Influence of membrane fouling and channel clogging. *Desalination* **2021**, *512*, 115114.
171. Ma, L.; Gutierrez, L.; Verbeke, R.; D'Haese, A.; Waqas, M.; Dickmann, M.; Helm, R.; Vankelecom, I.; Verliefde, A.; Cornelissen, E., Transport of organic solutes in ion-exchange membranes: Mechanisms and influence of solvent ionic composition. *Water Res* **2021**, *190*, 116756.
172. Vanoppen, M.; Bakelants, A. F. A. M.; Gaublomme, D.; Schoutteten, K. V. K. M.; Bussche, J. V.; Vanhaecke, L.; Verliefde, A. R. D., Properties Governing the Transport of Trace Organic Contaminants through Ion-Exchange Membranes. *Environ. Sci. Technol.* **2015**, *49* (1), 489-497.
173. Lawlor, D. W.; Milford, G. F. J., The effect of sodium on growth of water-stressed sugar-beet. *Ann. Bot.* **1973**, *37* (3), 597-604.
174. Lv, Y.; Li, Z.; Zhou, X.; Cheng, S.; Zheng, L., Stabilization of source-separated urine by heat-activated peroxydisulfate. *Sci. Total Environ.* **2020**, *749*.

175. Randall, D. G.; Krähenbühl, M.; Köpping, I.; Larsen, T. A.; Udert, K. M., A novel approach for stabilizing fresh urine by calcium hydroxide addition. *Water Res* **2016**, *95*, 361-369.
176. Svane, S.; Sigurdarson, J. J.; Finkenwirth, F.; Eitinger, T.; Karring, H., Inhibition of urease activity by different compounds provides insight into the modulation and association of bacterial nickel import and ureolysis. *Sci. Rep.* **2020**, *10*.
177. Hellström, D.; Johannson, E.; Grennberg, K., Storage of human urine: acidification as a method to inhibit decomposition of urea. *Ecol. Eng.* **1999**, *12* (3-4), 253-269.
178. Ikematsu, M.; Kaneda, K.; Iseki, M.; Yasuda, M., Electrochemical treatment of human urine for its storage and reuse as flush water. *Sci. Total Environ.* **2007**, *382* (1), 159-164.
179. Saettaab, D.; Zhengab, C.; Leyvaac, C.; Boyer, T. H., Impact of acetic acid addition on nitrogen speciation and bacterial communities during urine collection and storage. *Sci. Total Environ.* **2020**, *745*.
180. NAE Grand Challenges for Engineering. <https://www.nae.edu/File.aspx?id=187214> (accessed 02/20/2019).
181. Erisman, J. W.; Sutton, M. A.; Galloway, J.; Klimont, Z.; Winiwarter, W., How a century of ammonia synthesis changed the world. *Nature Geoscience* **2008**, *1* (10), 636-741.
182. Fowler, D.; Coyle, M.; Skiba, U.; Sutton, M. A.; Cape, J. N.; Reis, S.; Sheppard, L. J.; Jenkins, A.; Grizzetti, B.; Galloway, J. N.; Vitousek, P.; Leach, A.; Bouwman, A. F.; Butterbach-Bahl, K.; Dentener, F.; Stevenson, D.; Amann, M.; Voss, M., The global nitrogen cycle in the Twentyfirst century. *Philosophical Transactions of the Royal Society B: Biological Sciences* **2013**, *368* (1621).
183. Mulder, A., The quest for sustainable nitrogen removal technologies. *Water Sci Technol* **2003**, *48* (1), 67-75.
184. Wett, B., Development and implementation of a robust deammonification process. *Water Sci. Technol.* **2007**, *56* (7), 81-88.
185. Schaubroeck, T.; De Clippeleir, H.; Weissenbacher, N.; Dewulf, J.; Boeckx, P.; Vlaeminck, S. E.; Wett, B., Environmental sustainability of an energy self-sufficient sewage treatment plant: Improvements through DEMON and co-digestion. *Water Research* **2015**, *74*, 166-179.
186. Verstraete, W.; de Caveye, P. V.; Diamantis, V., Maximum use of resources present in domestic "used water". *Bioresour. Technol.* **2009**, *100* (23), 5537-5545.
187. Guest, J. S.; Skerlos, S. J.; Barnard, J. L.; Beck, M. B.; Daigger, G. T.; Hilger, H.; Jackson, S. J.; Karvazy, K.; Kelly, L.; Macpherson, L.; Mihelcic, J. R.; Pramanik, A.; Raskin, L.; Van Loosdrecht, M. C. M.; Yeh, D.; Love, N. G., A new planning and design paradigm to achieve sustainable resource recovery from wastewater. In *Environmental Science and Technology*, 2009.

188. Yetilmezsoy, K.; Sapci-Zengin, Z., Recovery of ammonium nitrogen from the effluent of UASB treating poultry manure wastewater by MAP precipitation as a slow release fertilizer. *J. Hazard. Mater.* **2009**, *166* (1), 260-269.
189. Cai, T.; Park, S. Y.; Li, Y. B., Nutrient recovery from wastewater streams by microalgae: Status and prospects. *Renewable & Sustainable Energy Reviews* **2013**, *19*, 360-369.
190. Lin, Y.; Guo, M.; Shah, N.; Stuckey, D. C., Economic and environmental evaluation of nitrogen removal and recovery methods from wastewater. *Bioresour. Technol* **2016**, *215*, 227-238.
191. Bilyk, K.; Bustamante, H.; Connor, M.; deBarbadillo, C.; Downing, L.; Dupont, R.; Fattah, K.; Finch, R.; Gray, D.; Harper, W., Nutrient Recovery: State of the Knowledge. *Water Environment Research Foundation* **2011**, *1*, 1-19.
192. Mehta, C. M.; Khunjar, W. O.; Nguyen, V.; Tait, S.; Batstone, D. J., Technologies to Recover Nutrients from Waste Streams: A Critical Review. *Critical Reviews in Environmental Science and Technology* **2015**, *45* (4), 385-427.
193. Pastor, L.; Mangin, D.; Ferrer, J.; Seco, A., Struvite formation from the supernatants of an anaerobic digestion pilot plant. *Bioresour. Technol.* **2010**, *101* (1), 118-125.
194. Desloover, J.; Abate Woldeyohannis, A.; Verstraete, W.; Boon, N.; Rabaey, K., Electrochemical Resource Recovery from Digestate to Prevent Ammonia Toxicity during Anaerobic Digestion. *Environmental Science & Technology* **2012**, *46* (21), 12209-12216.
195. Ippersiel, D.; Mondor, M.; Lamarche, F.; Tremblay, F.; Dubreuil, J.; Masse, L., Nitrogen potential recovery and concentration of ammonia from swine manure using electro dialysis coupled with air stripping. *Journal of Environmental Management* **2012**, *95*, S165-S169.
196. Anastas, P. T., and Zimmerman, J.B., Design through the Twelve Principles of Green Engineering. *Environmental Science & Technology* **2003**, *37* (5), 94A-101A.
197. Karak, T.; Bhattacharyya, P., Human urine as a source of alternative natural fertilizer in agriculture: A flight of fancy or an achievable reality. *Resources, Conservation and Recycling* **2011**, *55* (4), 400-408.
198. Larsen, T. A.; Alder, A. C.; Eggen, R. I. L.; Maurer, M.; Lienert, J., Source separation: Will we see a paradigm shift in wastewater handling? *Environmental Science and Technology* **2009**, *43* (16), 6121.
199. Gao, X. S., T.; Zheng, Y.; Sun, X.; Huang, S.; Ren, Q.; Zhang, X.; Tian, Y.; Luan, G, *Practical manure handbook. In Chinese*. Agricultural Publishing House: Beijing, 2002.
200. Larsen, T. A. U., K. M.; Lienert, J., *Source separation and decentralization for wastewater management*. Iwa Publishing: 2013.
201. Jönsson, H. V., B. In *Adapting the nutrient content of urine and faeces in different countries using FAO and Swedish data*, Proceedings of the 2nd International Symposium on ecological sanitation, 2003; pp 7-11.

202. Larsen, T. A.; Hoffmann, S.; Lüthi, C.; Truffer, B.; Maurer, M., Emerging solutions to the water challenges of an urbanizing world. *Science* **2016**, *352* (6288), 928-933.
203. Randall, D. G.; Naidoo, V., Urine: The liquid gold of wastewater. *J. Environ. Chem. Eng.* **2018**, *6* (2), 2627-2635.
204. Başakçılardan-Kabakci, S.; İpekoğlu, A. N.; Talinli, I., Recovery of Ammonia from Human Urine by Stripping and Absorption. *Environmental Engineering Science* **2007**, *24* (5), 615-624.
205. Kabdaşlı, I.; Tünay, O.; İşlek, Ç.; Erdinç, E.; Hüskaçar, S.; Tatlı, M. B., Nitrogen recovery by urea hydrolysis and struvite precipitation from anthropogenic urine. *Water Sci Technol* **2006**, *53* (12), 305-312.
206. Ledezma, P.; Kuntke, P.; Buisman, C. J. N.; Keller, J.; Freguia, S., Source-separated urine opens golden opportunities for microbial electrochemical technologies. *Trends in Biotechnology* **2015**, *33* (4), 214-220.
207. Udert, K. M.; Wächter, M., Complete nutrient recovery from source-separated urine by nitrification and distillation. *Water Res* **2012**, *46* (2), 453-464.
208. Kabdaşlı, I.; Tünay, O., Nutrient recovery by struvite precipitation, ion exchange and adsorption from source-separated human urine – a review. *Environmental Technology Reviews* **2018**, *7* (1), 106-138.
209. Udert, K. M.; Larsen, T. A.; Biebow, M.; Gujer, W., Urea hydrolysis and precipitation dynamics in a urine-collecting system. *Water Research* **2003**, *37* (11), 2571-2582.
210. Liu, Y.; Kumar, S.; Kwag, J. H.; Ra, C., Magnesium ammonium phosphate formation, recovery and its application as valuable resources: a review. *J. Chem. Technol. Biotechnol.* **2013**, *88* (2), 181-189.
211. Lawson, K. W.; Lloyd, D. R., Membrane Distillation *J. Membr. Sci.* **1997**, *124* (1), 1-25.
212. Alkhudhiri, A.; Darwish, N.; Hilal, N., Membrane distillation: A comprehensive review. *Desalination* **2012**, *287*, 2-18.
213. Drioli, E.; Ali, A.; Macedonio, F., Membrane distillation: Recent developments and perspectives. *Desalination* **2015**, *356*, 56-86.
214. Zarebska, A.; Nieto, D. R.; Christensen, K. V.; Norddahl, B., Ammonia recovery from agricultural wastes by membrane distillation: Fouling characterization and mechanism. *Water Research* **2014**, *56*, 1-10.
215. Qu, D.; Sun, D.; Wang, H.; Yun, Y., Experimental study of ammonia removal from water by modified direct contact membrane distillation. *Desalination* **2013**, *326*, 135-140.
216. Duong, T.; Xie, Z.; Ng, D.; Hoang, M., Ammonia removal from aqueous solution by membrane distillation. *Water and Environment Journal* **2013**, *27* (3), 425-434.
217. Bodell, B. R., Distillation of Saline Water Using Silicone Rubber Membrane. *United States Patent* **1968**.

218. Ahn, Y. T.; Hwang, Y. H.; Shin, H. S., Application of PTFE membrane for ammonia removal in a membrane contactor. *Water Sci Technol* **2011**, *63* (12), 2944-2948.
219. Ding, Z.; Liu, L.; Li, Z.; Ma, R.; Yang, Z., Experimental study of ammonia removal from water by membrane distillation (MD): The comparison of three configurations. *J. Membr. Sci.* **2006**, *286* (1-2), 93-103.
220. Kartohardjono, S.; Fermi, M. I.; Yuliusman; Elkardiana, K.; Sangaji, A. P.; Ramadhan, A. M., The Removal of Dissolved Ammonia from Wastewater through a Polypropylene Hollow Fiber Membrane Contactor. *International Journal of Technology* **2015**, *6* (7), 1146-1152.
221. Lauterbock, B.; Moder, K.; Germ, T.; Fuchs, W., Impact of characteristic membrane parameters on the transfer rate of ammonia in membrane contactor application. *Separation and Purification Technology* **2013**, *116*, 327-334.
222. Lin, P. H.; Horng, R. Y.; Hsu, S. F.; Chen, S. S.; Ho, C. H., A Feasibility Study of Ammonia Recovery from Coking Wastewater by Coupled Operation of a Membrane Contactor and Membrane Distillation. *International Journal of Environmental Research and Public Health* **2018**, *15* (3).
223. Liu, H. Y.; Wang, J. L., Separation of ammonia from radioactive wastewater by hydrophobic membrane contactor. *Progress in Nuclear Energy* **2016**, *86*, 97-102.
224. Lu, J.; Li, B. A.; Wang, L.; Wang, Y.; Wang, S. C., Utilization of ammonia-containing wastewater by combining membrane absorption and vacuum membrane distillation. *Journal of Chemical Technology and Biotechnology* **2014**, *89* (2), 312-321.
225. Tun, L. L.; Jeong, D.; Jeong, S.; Cho, K.; Lee, S.; Bae, H., Dewatering of source-separated human urine for nitrogen recovery by membrane distillation. *J. Membr. Sci.* **2016**, *512*, 13-20.
226. Xia, Q.; Yun, Y. B.; Chen, J. J.; Qu, D.; Li, C. L.; Zhu, S. W., Treatment of ammonia nitrogen wastewater by membrane distillation using PVDF membranes. *Desalination and Water Treatment* **2017**, *61*, 126-135.
227. Xu, K. N.; Qu, D.; Zheng, M.; Guo, X. H.; Wang, C. W., Water Reduction and Nutrient Reconcentration of Hydrolyzed Urine via Direct-Contact Membrane Distillation: Ammonia Loss and Its Control. *J Environ Eng* **2019**, *145* (3).
228. Daguerre-Martini, S.; Vanotti, M. B.; Rodriguez-Pastor, M.; Rosal, A.; Moral, R., Nitrogen recovery from wastewater using gas-permeable membranes: Impact of inorganic carbon content and natural organic matter. *Water Res* **2018**, *137*, 201-210.
229. Vanotti, M. B.; Dube, P. J.; Szogi, A. A.; García-González, M. C., Recovery of ammonia and phosphate minerals from swine wastewater using gas-permeable membranes. *Water Res* **2017**, *112*, 137-146.
230. Kuntke, P.; Zamora, P.; Saakes, M.; Buisman, C. J. N.; Hamelers, H. V. M., Gas-permeable hydrophobic tubular membranes for ammonia recovery in bio-electrochemical systems. *Environmental Science: Water Research & Technology* **2016**, *2* (2), 261-265.

231. Tarpeh, W. A.; Barazesh, J. M.; Cath, T. Y.; Nelson, K. L., Electrochemical Stripping to Recover Nitrogen from Source-Separated Urine. *Environmental Science & Technology* **2018**, *52* (3), 1453-1460.
232. EL-Bourawi, M. S.; Khayet, M.; Ma, R.; Ding, Z.; Li, Z.; Zhang, X., Application of vacuum membrane distillation for ammonia removal. *Journal of Membrane Science* **2007**, *301* (1-2), 200-209.
233. He, Q. Y.; Tu, T.; Yan, S. P.; Yang, X.; Duke, M.; Zhang, Y. L.; Zhao, S. F., Relating water vapor transfer to ammonia recovery from biogas slurry by vacuum membrane distillation. *Separation and Purification Technology* **2018**, *191*, 182-191.
234. Sarbatly, R.; Chiam, C. K., Ammonia Removal from Saline Water by Direct Contact Membrane Distillation. In *Sustainable Membrane Technology for Energy, Water, and Environment*, Wiley: 2012; pp 309-317.
235. Wu, C. R.; Yan, H. H.; Li, Z. G.; Lu, X. L., Ammonia recovery from high concentration wastewater of soda ash industry with membrane distillation process. *Desalination and Water Treatment* **2016**, *57* (15), 6792-6800.
236. Xie, Z. L.; Duong, T.; Hoang, M.; Nguyen, C.; Bolto, B., Ammonia removal by sweep gas membrane distillation. *Water Research* **2009**, *43* (6), 1693-1699.
237. Liu, Q. L.; Liu, C. H.; Zhao, L.; Ma, W. C.; Liu, H. L.; Ma, J., Integrated forward osmosis-membrane distillation process for human urine treatment. *Water Research* **2016**, *91*, 45-54.
238. Rittner, D. B., R.A., Clausius-Clapeyron equation. In D. Rittner, & R. A. Bailey, Facts on File science encyclopedia: Encyclopedia of chemistry (2nd ed.). **2016**.
239. Wang, P.; Chung, T. S., Recent advances in membrane distillation processes: Membrane development, configuration design and application exploring. *J. Membr. Sci.* **2015**, *474*, 39-56.
240. Rezakazemi, M.; Shirazian, S.; Ashrafizadeh, S. N., Simulation of ammonia removal from industrial wastewater streams by means of a hollow-fiber membrane contactor. *Desalination* **2012**, *285*, 383-392.
241. El-Bourawi, M. S.; Ding, Z.; Ma, R.; Khayet, M., A framework for better understanding membrane distillation separation process. *J. Membr. Sci.* **2006**, *285* (1-2), 4-29.
242. J.M. Smith, H. C. V. N., M. M. Abbott, Introduction to Chemical Engineering Thermodynamics. **2005**, 357-358.
243. Bates, R. G.; Pinching, G. D., Acidic dissociation constant of ammonium ion at 0 to 50 C, and the base strength of ammonia. *Journal of Research of the National Bureau of Standards* **2012**, *42* (5), 419-430.
244. Bolleter, W. T.; Bushman, C. J.; Tidwell, P. W., Spectrophotometric Determination of Ammonia as Indophenol. *Analytical Chemistry* **1961**, *33* (4), 592-594.
245. Schofield, R. W.; Fane, A. G.; Fell, C. J. D., Heat and mass transfer in membrane distillation. *J. Membr. Sci.* **1987**, *33* (3), 299-313.

246. Fane, A. G.; Schofield, R. W.; Fell, C. J. D., The efficient use of energy in membrane distillation. *Desalination* **1987**, *64*, 231-243.
247. Khayet, M., Membranes and theoretical modeling of membrane distillation: A review. *Advances in Colloid and Interface Science* **2011**, *164* (1-2), 56-88.
248. Zhu, Z.; Hao, Z.; Shen, Z.; Chen, J., Modified modeling of the effect of pH and viscosity on the mass transfer in hydrophobic hollow fiber membrane contactors. *J. Membr. Sci.* **2005**, *250* (1-2), 269-276.
249. Deshmukh, A.; Lee, J., Membrane desalination performance governed by molecular reflection at the liquid-vapor interface. *International Journal of Heat and Mass Transfer* **2019**, *140*, 1006-1022.
250. Shi, Q.; Davidovits, P.; Jayne, J. T.; Worsnop, D. R.; Kolb, C. E., Uptake of gas-phase ammonia. 1. Uptake by aqueous surfaces as a function of pH. *Journal of Physical Chemistry A* **1999**, *103* (44), 8812-8823.
251. Eames, I. W.; Marr, N. J.; Sabir, H., The evaporation coefficient of water: A review. *International Journal of Heat and Mass Transfer* **1997**, *40* (12), 2963-2973.
252. Marek, R.; Straub, J., Analysis of the evaporation coefficient and the condensation coefficient of water. *International Journal of Heat and Mass Transfer* **2001**, *44* (1), 39-53.
253. Kerkhof, P. J. A. M., A modified Maxwell-Stefan model for transport through inert membranes: The binary friction model. *Chem Eng J* **1996**, *64* (3), 319-343.
254. Krishna, R.; Wesselingh, J. A., Review article number 50 - The Maxwell-Stefan approach to mass transfer. *Chemical Engineering Science* **1997**, *52* (6), 861-911.
255. Cussler, E., Multicomponent Diffusion. In *Multicomponent Diffusion*, Elsevier: 2013; p 39.
256. Lin, S.; Yip, N. Y.; Elimelech, M., Direct contact membrane distillation with heat recovery: Thermodynamic insights from module scale modeling. *J. Membrane Sci.* **2014**, *453*, 498-515.
257. NIST Chemistry Webook, SRD 69: Ammonia. <https://webbook.nist.gov/cgi/cbook.cgi?ID=7664-41-7> (accessed 02/20/2019).
258. NIST Chemistry Webook, SRD 69: Water. <https://webbook.nist.gov/cgi/cbook.cgi?ID=C7732185> (accessed 02/20/2019).
259. Vanneste, J.; Bush, J. A.; Hickenbottom, K. L.; Marks, C. A.; Jassby, D.; Turchi, C. S.; Cath, T. Y., Novel thermal efficiency-based model for determination of thermal conductivity of membrane distillation membranes. *J. Membr. Sci.* **2018**, *548*, 298-308.
260. Leitch, M. E.; Lowry, G. V.; Mauter, M. S., Characterizing convective heat transfer coefficients in membrane distillation cassettes. *J. Membr. Sci.* **2017**, *538*, 108-121.
261. McFeeters, R., Reuse of fermentation brines in the cucumber pickling industry. Environmental Protection Agency, O. o. R. a. D., Industrial Environmental Research Laboratory, Ed. 1978; Vol. 1.

262. Romero Barranco, C. B. B., M.; Garcia Garcia, P.; Garrido Fernández, A., Management of spent brines or osmotic solutions. *Journal of Food Engineering* **2001**, *49* (2), 237-246.
263. Kammen, D. M.; Sunter, D. A., City-integrated renewable energy for urban sustainability. *Science* **2016**, *352* (6288), 922-8.
264. World Health Organization. Progress on sanitation and drinking water: 2015 update and MDG assessment. 2015.
265. Zhang, L.; De Schryver, P.; De Gusseme, B.; De Muynck, W.; Boon, N.; Verstraete, W., Chemical and biological technologies for hydrogen sulfide emission control in sewer systems: a review. *Water Res* **2008**, *42* (1-2), 1-12.
266. Han, L.; Xiao, T.; Tan, Y. Z.; Fane, A. G.; Chew, J. W., Contaminant rejection in the presence of humic acid by membrane distillation for surface water treatment. *J. Membr. Sci* **2017**, *541*, 291-299.
267. Li, F.; Huang, J.; Xia, Q.; Lou, M.; Yang, B.; Tian, Q.; Liu, Y., Direct contact membrane distillation for the treatment of industrial dyeing wastewater and characteristic pollutants. *Sep. Purif. Technol.* **2018**, *195*, 83-91.
268. McCartney, S. N.; Fan, H.; Watanabe, N.; Huang, Y.; Yip, N. Y., Donnan Dialysis for Phosphate Recovery from Diverted Urine. *Environ. Sci. Technol. Water* **2022**, *Manuscript Under Review*.
269. Li, Y.; Wang, R.; Shi, S.; Cao, H.; Yip, N. Y.; Lin, S., Bipolar Membrane Electrodialysis for Ammonia Recovery from Synthetic Urine: Experiments, Modeling, and Performance Analysis. *Environ. Sci. Technol.* **2021**, *55* (21), 14886-14896.
270. Chiao, Y. C.; Chlanda, F. P.; Mani, K. N., Bipolar Membranes for Purification of Acids and Bases. *J. Membr. Sci* **1991**, *61*, 239–252.
271. Pärnamäe, R.; Mareev, S.; Nikonenko, V.; Melnikov, S.; Sheldeshov, N.; Zabolotskii, V.; Hamelers, H. V. M.; Tedesco, M., Bipolar membranes: A review on principles, latest developments, and applications. *J. Membr. Sci* **2021**, *617*, 118538.
272. Mafé, S.; Ramírez, P.; Alcaraz, A., Electric Field-Assisted Proton Transfer and Water Dissociation at the Junction of a Fixed-Charge Bipolar Membrane. *Chem. Phys. Lett* **1998**, *294*, 406-412.
273. Gao, F.; Wang, L.; Wang, J.; Zhang, H.; Lin, S., Nutrient recovery from treated wastewater by a hybrid electrochemical sequence integrating bipolar membrane electrodialysis and membrane capacitive deionization. *Environ. Sci.: Water Res. Technol.* **2020**, *6* (383).
274. Pronk, W.; Biebow, M.; Boller, M., Treatment of source-separated urine by a combination of bipolar electrodialysis and a gas transfer membrane. *Water Sci Technol.* **2006**, *53* (3), 139–146.
275. Lu, H.; Wang, L.; Wycisk, R.; Pintauro, P. N.; Lin, S., Quantifying the kinetics-energetics performance tradeoff in bipolar membrane electrodialysis. *J. Membr. Sci.* **2020**, *612*, 118279.

276. Szczygielka, M.; Antczak, J.; Prochaska, K., Separation and concentration of succinic acid from post-fermentation broth by bipolar membrane electrodialysis (EDBM). *Sep. Purif. Technol.* **2017**, *181*, 53-59.
277. Kogler, A.; Farmer, M.; Simon, J. A.; Tilmans, S.; Wells, G. F.; Tarpeh, W. A., Systematic Evaluation of Emerging Wastewater Nutrient Removal and Recovery Technologies to Inform Practice and Advance Resource Efficiency. *Acs Est Eng* **2021**, *1* (4), 662-684.
278. Noora, I.; Martin, A.; Dahl, O., Process design of industrial-scale membrane distillation system for wastewater treatment in nano-electronics fabrication facilities. *MethodsX* **2020**, *7*, 101066.
279. Tavakkoli, S.; Lokare, O. R.; Vidic, R. D.; Khanna, V., A techno-economic assessment of membrane distillation for treatment of Marcellus shale produced water. *Desalination* **2017**, *416*, 24-34.
280. Noora, I.; Martin, A.; Dahl, O., Techno-economic system analysis of membrane distillation process for treatment of chemical mechanical planarization wastewater in nano-electronics industries. *Sep. Purif. Technol.* **2020**, *248*, 117013.
281. Jantaporn, W.; Ali, A.; Aimar, P., Specific energy requirement of direct contact membrane distillation. *Chem Eng Res Des* **2017**, *128*, 15-26.
282. Yang, X.; Duke, M.; Zhang, J. H.; Li, J. D., Modeling of heat and mass transfer in vacuum membrane distillation for ammonia separation. *Separation and Purification Technology* **2019**, *224*, 121-131.
283. USDA Agricultural Marketing Service.
284. Bashar, R.; Gungor, K.; Karthikeyan, K. G.; Barak, P., Cost effectiveness of phosphorus removal processes in municipal wastewater treatment. *Chemosphere* **2018**, *197*, 280-290.
285. Bichai, F.; Ryan, H.; Fitzgerald, C.; Williams, K.; Abdelmoteleb, A.; Brotchie, R.; Komatsu, R., Understanding the Role of Alternative Water Supply in an Urban Water Security Strategy: An Analytical Framework for Decision Making. *Urban Water J.* **2015**, *12* (3), 175-189.
286. Daigger, G. T., Evolving Urban Water and Residual Management Paradigms: Water Reclamation and Reuse, Decentralization, and Resource Recovery. *Water Encieon. Res.* **2009**, *81* (8), 809-823.
287. Hering, J. G.; Waite, T. D.; Luthy, R. G.; Drewes, J. E.; Sedlak, D. L., Changing Framework for Urban Water Systems. *Environ. Sci. Technol.* **2013**, *47* (19), 10721-10726.
288. Sousa, M. R. C. D.; Montalto, F. A.; Spatari, S., Using Life Cycle Assessment to Evaluate Green and Grey Combined Sewer Overflow Control Systems. *J. Ind. Ecol.* **2012**, *16* (6).
289. Kavvada, O.; Horvath, A.; Stockes-Draut, J. R.; Hendrickson, T. P.; Eisenstein, W. A.; Nelson, K. L., Assessing Location and Scale of Urban Nonpotable Water Reuse Systems for Life-Cycle Energy Consumption and Greenhouse Gas Emissions. *Environ. Sci. Technol.* **2016**, *50*, 13184-13194.

290. Opher, T.; Friedler, E.; Shapria, A., Comparative life cycle sustainability assessment of urban water reuse at various centralization scales. *Int J Life Cycle Assess* **2019**, *24*, 1319-1332.
291. Hasik, V.; Anderson, N. E.; Collinge, W. O.; Thiel, C. L.; Khanna, V.; Wirick, J.; Piacentini, R.; Landis, A. E.; Bilec, M. M., Evaluating the Life Cycle Environmental Benefits and Trade-Offs of Water Reuse Systems for Net-Zero Buildings. *Environ. Sci. Technol.* **2016**.
292. Balkau, F.; Bezama, A., Life cycle methodologies for building circular economy in cities and regions. *Waste Manag Res* **2019**, *37* (8), 765-766.
293. Dominguez, S.; Laso, J.; Margallo, M.; Aldaco, R.; Rivero, M. J.; Irabien, A.; Ortiz, I., LCA of greywater management within a water circular economy restorative thinking framework. *Sci Total Environ* **2018**, *621*, 1047-1056.
294. McCartney, S. N.; Fan, H.; Watanabe, N.; Huang, Y.; Yip, N. Y., Integrated Membrane Processes to Capture Orthophosphate and Ammonia from Human Urine *Manuscript Under Development* **2022**.
295. McCartney, S. N.; Chu, S.; Gallagher, Z.; Clerico, E.; Yip, N. Y., Preliminary Evaluation of Costs and Benefits of Nutrient Recovery in Onsite Wastewater Management. *Manuscript Under Development* **2022**.
296. Schnitkey, G.; Paulson, N.; Swanson, K.; Colussi, J.; Baltz, J., Nitrogen Fertilizer Prices and Supply in Light of the Ukraine-Russia Conflict. *farmdoc daily* **2022**, *12* (45).
297. Balma, L., Long-run impacts of the conflict in Ukraine on food security in Africa. *Kiel Policy Brief* **2022**, *Ukraine Special 1*.
298. Mogollóna, J. M.; Beusenab, A. H. W.; H.J.Mvan Grinsvenb, H. J.; Westhoekb, H.; Bouwmanab, A. F., Future agricultural phosphorus demand according to the shared socioeconomic pathways. *Glob. Environ. Change* **2018**, *50*, 149-163.
299. Benjamin, M. M., *Water Chemistry*. Waveland Press, Inc: Long Grove, Il, 2015.
300. Gustafsson, J. P. *Visual MINTEQ, Version 3.1*, 3.1; Stockholm, 2013.
301. Kurhe, D. N.; Dagade, D. H.; Jadhav, J. P.; Govindwar, S. P.; Patil, K. J., Thermodynamic Studies of Amino Acid–Denaturant Interactions in Aqueous Solutions at 298.15 K. *Journal of Solution Chemistry* **2011**, *40* (1596).
302. Pickering, M., The Entropy of Dissolution of Urea. *J Chem Educ* **1987**, *64* (8), 723-724.
303. Keller, R. A., *Basic tables in chemistry*. McGraw-Hill: New York, 1967.
304. Purolite: Water Softening Basics. <https://www.purolite.com/application/softening/How-do-water-softeners-work>.
305. *PuroLite Product Guide: Product Characteristics and Applications*; 2021.
306. Michaud, C. F., Factors Affecting the Brine Efficiency of Softeners, Part 1. *Water Conditioning & Purification* **1999**, 36-38.
307. Michaud, C. F., Factors Affecting the Brine Efficiency of Softeners, Part 2. *Water Conditioning & Purification* **1999**, 76-78.

308. Kuda, T.; Yano, T., Mineral Composition of Seawater Bittern Nigari Products and Their Effects on Changing of Browning and Antioxidant Activity in the Glucose/Lysine Maillard Reaction. *Appl Biochem Biotechnol* **2014**, *172*, 2989–2997.
309. Selemion: Ion Exchange Membranes. ACG Engineering Co., LTD: 2018.
310. Bates, R. G.; Pinching, G. D., Acidic dissociation constant of ammonium ion at 0 to 50 C, and the base strength of ammonia. *Journal of Research of the National Bureau of Standards* **2012**.
311. GTG Portable Electric Waterless Toilet. [https://www.buildclub.com/product/bc0\\_41-851655](https://www.buildclub.com/product/bc0_41-851655).
312. TOTO Aquia Dual Flush 1.28 / .8 GPF Floor Mounted Elongated Toilet - Less Toilet Seat. [https://www.build.com/product/summary/1495742?uid=3504964&jmtest=gg-gbav2\\_3504964&inv2=1&&source=gg-gba-pla\\_3504964!c1709211112!a69367404440!dc!ng&gclid=CjwKCAjw6dmSBhBkEiwA\\_W-EoNIVQTOzZWJQ5XMNDmOmBKwIvIDoWPO\\_FWuhPi2zm6h6XAGDbiSrMxoCweoQAvD\\_BwE&gclsrc=aw.ds](https://www.build.com/product/summary/1495742?uid=3504964&jmtest=gg-gbav2_3504964&inv2=1&&source=gg-gba-pla_3504964!c1709211112!a69367404440!dc!ng&gclid=CjwKCAjw6dmSBhBkEiwA_W-EoNIVQTOzZWJQ5XMNDmOmBKwIvIDoWPO_FWuhPi2zm6h6XAGDbiSrMxoCweoQAvD_BwE&gclsrc=aw.ds).
313. Ahdaba, Y. D.; Schuckinga, G.; Rehmana, D.; Lienhard, J. H., Cost effectiveness of conventionally and solar powered monovalent selective electrodialysis for seawater desalination in greenhouses. *Appl. Energy* **2021**, *301*.
314. Hewitt, G. F.; Pugh, S. J., Approximate Design and Costing Methods for Heat Exchangers. *Heat Transf. Eng.* **2011**, *28* (2), 76-86.
315. Banat, F.; Jwaied, N., Economic evaluation of desalination by small-scale autonomous solar-powered membrane distillation units. *Desalination* **2008**, *220* (1-3), 566-573.
316. Al-Obaidani, S.; Curcio, E.; Macedonio, F.; Profio, G. D.; Al-Hinai, H.; Drioli, E., Potential of membrane distillation in seawater desalination: Thermal efficiency, sensitivity study and cost estimation. *J. Membr. Sci* **2008**, *323* (1), 85-98.
317. Kakac, S.; Liu, H., *Heat Exchangers: Selection, Rating and Thermal Design*. CRC Press: 2002.
318. Kuppan, T., *Heat Exchanger Design Handbook*. CRC Press: 2000.
319. Motealleh, B.; Liu, Z.; Masel, R. I.; Sculley, J. P.; Ni, Z. R.; Meroueh, L., Next-generation anion exchange membrane water electrolyzers operating for commercially relevant lifetimes. *Int. J. Hydrog. Energy* **2021**, *46* (5), 3379-3386.
320. U.S. Bureau of Labor Statistics: Average Energy Prices, New York-Newark-Jersey City — February 2022. [https://www.bls.gov/regions/new-york-new-jersey/news-release/averageenergyprices\\_newyorkarea.htm#:~:text=Source%3A%20U.S.%20Bureau%20of%20Labor,area%20compared%20to%20the%20nation](https://www.bls.gov/regions/new-york-new-jersey/news-release/averageenergyprices_newyorkarea.htm#:~:text=Source%3A%20U.S.%20Bureau%20of%20Labor,area%20compared%20to%20the%20nation).
321. Schnitkey, G.; Paulson, N.; Swanson, K. *2021 Fertilizer Price Increases in Perspective, with Implications for 2022 Costs*; Department of Agricultural and Consumer Economics, University of Illinois at Urbana-Champaign: 2021.

322. 93% Sulfuric Acid (NSF approved) - 4200 lb tote. <https://www.chemworld.com/Sulfuric-Acid-NSF-approved-p/66be-4200.htm>.
323. U.S. Energy Information Administration: United States Natural Gas Industrial Price. <https://www.eia.gov/dnav/ng/hist/n3035us3m.htm>.
324. The Official Website of the City of New York: Water and Sewer Rate. <https://portal.311.nyc.gov/article/?kanumber=KA-02465#:~:text=As%20of%20July%201%2C%202021,remains%20at%20%241.27%20per%20day>.
325. Sodium Hydroxide (Liquid Caustic Soda, NaOH, Lye). <https://www.univarsolutions.com/product-categories/essential-chemicals-ingredients/liquid-caustic-soda>.
326. Sodium Hydroxide Beads FCC/Food Grade. <https://www.laballey.com/products/sodium-hydroxide-fcc-beads>.
327. Made In China Superior Quality Industrial Grade Sewage Treatment NaOH 99% Soda Flakes. [https://www.alibaba.com/product-detail/Made-In-China-Superior-Quality-Industrial\\_1600380901334.html?spm=a2700.galleryofferlist.normal\\_offer.d\\_title.4d25125btBW\\_SKE](https://www.alibaba.com/product-detail/Made-In-China-Superior-Quality-Industrial_1600380901334.html?spm=a2700.galleryofferlist.normal_offer.d_title.4d25125btBW_SKE).
328. Aluminum Chlorohydrate ACH Aluminum Chlorohydrate Anhydrous Chemical Raw Materials ALUMINUM CHLO. <https://www.alibaba.com/showroom/price-aluminum-chlorohydrate.html>.

## Appendix A: Supporting Information for Chapter 2

### A.1 Methodology to Determine Molar Minimum Energy of Recovery

To determine the molar minimum energy of nutrient recovery,  $\bar{E}_{\min}$ , mole fractions of species  $i$  in the feed, product, and retentate are required. The mole fractions of species  $i$  in the waste stream feed,  $x_{i,F}$ , are based on literature data.<sup>89, 91-96</sup> The mole fraction and molar ratio of a species in the product,  $x_{i,P}$  and  $n_{i,P}$ , respectively, are dependent on the targeted product, and mole fraction of species in the retentate,  $x_{i,R}$ , is determined by species mole balance. Mole balances are expressed as  $x_{i,F}N_F + x_{i,RXN}N_{RXN} = x_{i,P}N_P + x_{i,R}N_R$  for aqueous products or  $x_{i,F}N_F + n_{i,RXN}N_{RXN} = n_{i,P}N_P + x_{i,R}N_R$  for pure liquid/solid products; where the subscript  $i,RXN$  denotes the species produced or consumed in reactions. To recover products, nutrients and product co-species are consumed. Additionally,  $H_2O$ ,  $OH^-$ , and  $H^+$  may be generated or consumed for the deprotonation and protonation of  $NH_4^+/NH_3$  and  $H_3PO_4/H_2PO_4^-/HPO_4^{2-}/PO_4^{3-}$  species to capture targeted products. For the  $NH_4^+/NH_3$  and  $H_3PO_4/H_2PO_4^-/HPO_4^{2-}/PO_4^{3-}$  species, mole balances are based on TAN and TOP mole fractions, respectively. To utilize the mole balances to solve for  $x_{i,R}$ , scenarios with different recovery yields are modeled. Recovery yield is the amount of species,  $i$ , from the initial feed solution captured as a product, defined by  $Y_{i,P} = x_{i,P}N_P/x_{i,F}N_F$  for aqueous products and  $Y_{i,P} = n_{i,P}N_P/x_{i,F}N_F$  for solid/pure products.

It is important to note that pH and resultant TAN and TOP speciation influence the Gibbs free energy of a solution because of the following three factors: i)  $G_{NH_3(aq)} \neq G_{NH_4^+(aq)}$ ,  $G_{HPO_4^{2-}(aq)} \neq G_{H_2PO_4^-(aq)}$ , ii)  $\gamma_i$  values are dependent on the species, and iii)  $x_i$  is dependent on the concentration of each species. The speciation between ammonium and ammonia,  $NH_4^+ \leftrightarrow NH_3 +$

$H^+$ , is governed by eqn (A.1), and the speciations between the four forms of orthophosphate,  $H_3PO_4 \leftrightarrow H_2PO_4^- + H^+$ ,  $H_2PO_4^- \leftrightarrow HPO_4^{2-} + H^+$ , and  $HPO_4^{2-} \leftrightarrow PO_4^{3-} + H^+$ , are governed by eqns (A.2), (A.3), and (A.4):

$$K_{a,NH_4^+} = \frac{\{NH_3\}\{H^+\}}{\{NH_4^+\}} \approx 10^{-9.24} \quad (A.1)$$

$$K_{a,H_3PO_4,1} = \frac{\{H_2PO_4^-\}\{H^+\}}{\{H_3PO_4\}} \approx 10^{-2.14} \quad (A.2)$$

$$K_{a,H_3PO_4,2} = \frac{\{HPO_4^{2-}\}\{H^+\}}{\{H_2PO_4^-\}} \approx 10^{-7.20} \quad (A.3)$$

$$K_{a,H_3PO_4,3} = \frac{\{PO_4^{3-}\}\{H^+\}}{\{HPO_4^{2-}\}} \approx 10^{-12.37} \quad (A.4)$$

where  $K_a$  is the dissociation constant for the acid and  $\{i\}$  is the activity of species  $i$ . All  $K_a$  values were acquired from literature.<sup>299</sup> Table A.1 presents the range in pH for each waste stream and resultant speciation determined using eqns (A.1)–(A.4).

**Table A.1.** Range in pH of each waste stream<sup>89, 91-97</sup> and resultant speciation of TAN and TOP.  $\alpha_i$  is the fraction of TAN or TOP present as the species denoted by the subscript. The pH range is presented with “H” signifying the high-end and “L” signifying the low-end. Note that only  $\text{H}_2\text{PO}_4^-$  and  $\text{HPO}_4^{2-}$  forms of TOP are presented because  $\text{H}_3\text{PO}_4$  and  $\text{PO}_4^{3-}$  concentrations are negligible in the waste streams.

Waste stream	pH	$\alpha_{\text{NH}_3}$	$\alpha_{\text{NH}_4^+}$	$\alpha_{\text{HPO}_4^{2-}}$	$\alpha_{\text{H}_2\text{PO}_4^-}$	Predominant form of TOP
Greywater H	9	0.365	0.635	0.984	0.016	$\text{HPO}_4^{2-}$
Greywater L	5	$5.75 \times 10^{-5}$	1.00	$6.13 \times 10^{-3}$	0.994	$\text{H}_2\text{PO}_4^-$
2° WW effluent A	7.7	0.028	0.972	0.796	0.204	$\text{HPO}_4^{2-}$
2° WW effluent B	6.8	$3.62 \times 10^{-3}$	0.996	0.334	0.666	$\text{H}_2\text{PO}_4^-$
Domestic WW A	8.5	0.154	0.846	0.984	0.016	$\text{HPO}_4^{2-}$
Domestic WW B	6.5	$1.82 \times 10^{-3}$	$9.49 \times 10^{-7}$	0.163	0.837	$\text{H}_2\text{PO}_4^-$
Fresh Urine A	7.5	0.018	0.982	0.661	0.339	$\text{HPO}_4^{2-}$
Fresh Urine B	6	$5.75 \times 10^{-4}$	0.999	0.058	0.942	$\text{H}_2\text{PO}_4^-$
Hydrolyzed Urine A	9.2	0.477	0.523	0.990	0.010	$\text{HPO}_4^{2-}$
Hydrolyzed Urine B	9.0	0.365	0.635	0.984	0.016	$\text{HPO}_4^{2-}$

**Table A.2.** Concentration of active species (components of products in the analysis), other forms of N, and passive species (components in the waste streams, but not in products) in waste streams examined in the analysis.<sup>89, 91-97</sup> Ranges are provided when available in the literature.

Species	Concentration (mM)				
	Greywater	Fresh Urine	Hydrolyzed Urine	Domestic WW	2° WW effluent
Sulfate (SO <sub>4</sub> <sup>2-</sup> )	0.00156–0.225	0.288–36.7	1.65–17.4	0.469	1.73
Potassium (K <sup>+</sup> )	0.000510–0.0614	20.1–94.5	19.4–56.3	0.619	0.256–0.767
Magnesium (Mg <sup>2+</sup> )	1.48–1.96	4.11		0.453–0.918	0.412–2.058
Nitrate (NO <sub>3</sub> <sup>-</sup> )					0.0714–1.42
Urea (CH <sub>4</sub> N <sub>2</sub> O)		125.9–264.5			
Sodium (Na <sup>+</sup> )			64.9–119		1.41–17.4
Chloride (Cl <sup>-</sup> )			64.9–119		1.41–17.4

## A.2 Molar Minimum Energy Equations

The following provides the expressions for molar minimum energies to recover products from the waste streams as presented in Figures 2.2, 2.3, 2.5, and 2.6.

**Figure 2.2.** To determine  $\bar{E}_{\min}$  for recovering  $\text{NH}_3(l)$  from all waste streams presented in Figure 2, eqn (A.5) was utilized. Note that in Figure 2.2 all TAN was assumed to be present as  $\text{NH}_4^+$ , while analysis presented in Figure 2.3 considers the speciation between  $\text{NH}_4^+$  and  $\text{NH}_3$ .

$$\begin{aligned} \bar{E}_{\min} = & G_{f,\text{NH}_3(l)}^{\circ} \\ & + \frac{N_R}{N_P} \left[ \begin{aligned} & x_{\text{NH}_4^+,\text{R}} G_{\text{NH}_4^+} + x_{\text{H}_2\text{O},\text{R}} G_{\text{H}_2\text{O}} + x_{\text{OH}^-,\text{R}} G_{\text{OH}^-} \\ & + RT \left( \begin{aligned} & x_{\text{NH}_4^+,\text{R}} \ln(\gamma_{\text{NH}_4^+,\text{R}} x_{\text{NH}_4^+,\text{R}}) + x_{\text{H}_2\text{O},\text{R}} \ln(\gamma_{\text{H}_2\text{O},\text{R}} x_{\text{H}_2\text{O},\text{R}}) \\ & + x_{\text{H}^+,\text{R}} \ln(\gamma_{\text{H}^+,\text{R}} x_{\text{H}^+,\text{R}}) + x_{\text{OH}^-,\text{R}} \ln(\gamma_{\text{OH}^-,\text{R}} x_{\text{OH}^-,\text{R}}) \end{aligned} \right) \end{aligned} \right] \quad (\text{A.5}) \\ & - \frac{N_F}{N_P} \left[ \begin{aligned} & x_{\text{NH}_4^+,\text{F}} G_{\text{NH}_4^+} + x_{\text{H}_2\text{O},\text{F}} G_{\text{H}_2\text{O}} + x_{\text{OH}^-,\text{F}} G_{\text{OH}^-} \\ & + RT \left( \begin{aligned} & x_{\text{NH}_4^+,\text{F}} \ln(\gamma_{\text{NH}_4^+,\text{F}} x_{\text{NH}_4^+,\text{F}}) + x_{\text{H}_2\text{O},\text{F}} \ln(\gamma_{\text{H}_2\text{O},\text{F}} x_{\text{H}_2\text{O},\text{F}}) \\ & + x_{\text{H}^+,\text{F}} \ln(\gamma_{\text{H}^+,\text{F}} x_{\text{H}^+,\text{F}}) + x_{\text{OH}^-,\text{F}} \ln(\gamma_{\text{OH}^-,\text{F}} x_{\text{OH}^-,\text{F}}) \end{aligned} \right) \end{aligned} \right] \end{aligned}$$

**Figure 2.3.** For the determination of  $\bar{E}_{\min}$  to recover  $\text{NH}_3(l)$ , the aqueous ammonia products (i.e., 10 M  $\text{NH}_3(\text{aq})$ , 5.0 M  $\text{NH}_3(\text{aq})$ , and 1.0 M  $\text{NH}_3(\text{aq})$ ), and  $(\text{NH}_4)_2\text{SO}_4(\text{s})$ , eqns (A.6), (A.7), and (A.8), respectively, were utilized. The pH of all the aqueous  $\text{NH}_3$  product streams is high ( $>11.7$ ), such that  $>99.7\%$  of TAN is  $\text{NH}_3$  and  $\text{NH}_4^+$  species are negligible. Note that in all calculations Gibbs free energy required for recovery is normalized per mole of TAN recovered.

$$\begin{aligned}
\bar{E}_{\min} &= G_{f,\text{NH}_3(1)}^\circ \\
&+ \frac{N_{\text{R}}}{N_{\text{P}}} \left[ x_{\text{NH}_4^+,\text{R}} G_{\text{NH}_4^+} + x_{\text{NH}_3,\text{R}} G_{\text{NH}_3} + x_{\text{H}_2\text{O},\text{R}} G_{\text{H}_2\text{O}} + x_{\text{OH}^-,\text{R}} G_{\text{OH}^-} \right. \\
&\quad \left. + RT \left( x_{\text{NH}_4^+,\text{R}} \ln(\gamma_{\text{NH}_4^+,\text{R}} x_{\text{NH}_4^+,\text{R}}) + x_{\text{NH}_3,\text{R}} \ln(\gamma_{\text{NH}_3,\text{R}} x_{\text{NH}_3,\text{R}}) \right) \right. \\
&\quad \left. + x_{\text{H}_2\text{O},\text{R}} \ln(\gamma_{\text{H}_2\text{O},\text{R}} x_{\text{H}_2\text{O},\text{R}}) + x_{\text{H}^+,\text{R}} \ln(\gamma_{\text{H}^+,\text{R}} x_{\text{H}^+,\text{R}}) + x_{\text{OH}^-,\text{R}} \ln(\gamma_{\text{OH}^-,\text{R}} x_{\text{OH}^-,\text{R}}) \right) \quad (\text{A.6}) \\
&- \frac{N_{\text{F}}}{N_{\text{P}}} \left[ x_{\text{NH}_4^+,\text{F}} G_{\text{NH}_4^+} + x_{\text{NH}_3,\text{F}} G_{\text{NH}_3} + x_{\text{H}_2\text{O},\text{F}} G_{\text{H}_2\text{O}} + x_{\text{OH}^-,\text{F}} G_{\text{OH}^-} \right. \\
&\quad \left. + RT \left( x_{\text{NH}_4^+,\text{F}} \ln(\gamma_{\text{NH}_4^+,\text{F}} x_{\text{NH}_4^+,\text{F}}) + x_{\text{NH}_3,\text{F}} \ln(\gamma_{\text{NH}_3,\text{F}} x_{\text{NH}_3,\text{F}}) \right) \right. \\
&\quad \left. + x_{\text{H}_2\text{O},\text{F}} \ln(\gamma_{\text{H}_2\text{O},\text{F}} x_{\text{H}_2\text{O},\text{F}}) + x_{\text{H}^+,\text{F}} \ln(\gamma_{\text{H}^+,\text{F}} x_{\text{H}^+,\text{F}}) + x_{\text{OH}^-,\text{F}} \ln(\gamma_{\text{OH}^-,\text{F}} x_{\text{OH}^-,\text{F}}) \right) \quad \left. \right]
\end{aligned}$$

$$\begin{aligned}
\bar{E}_{\min} &= \frac{1}{x_{\text{TAN},\text{P}}} \left[ x_{\text{NH}_3,\text{P}} G_{\text{NH}_3} + x_{\text{H}_2\text{O},\text{P}} G_{\text{H}_2\text{O}} + x_{\text{OH}^-,\text{P}} G_{\text{OH}^-} \right. \\
&\quad \left. + RT \left( x_{\text{NH}_3,\text{P}} \ln(\gamma_{\text{NH}_3,\text{P}} x_{\text{NH}_3,\text{P}}) + x_{\text{H}_2\text{O},\text{P}} \ln(\gamma_{\text{H}_2\text{O},\text{P}} x_{\text{H}_2\text{O},\text{P}}) \right) \right. \\
&\quad \left. + x_{\text{H}^+,\text{P}} \ln(\gamma_{\text{H}^+,\text{P}} x_{\text{H}^+,\text{P}}) + x_{\text{OH}^-,\text{P}} \ln(\gamma_{\text{OH}^-,\text{P}} x_{\text{OH}^-,\text{P}}) \right) \quad \left. \right] \\
&+ \frac{N_{\text{R}}}{x_{\text{TAN},\text{P}} N_{\text{P}}} \left[ x_{\text{NH}_4^+,\text{R}} G_{\text{NH}_4^+} + x_{\text{NH}_3,\text{R}} G_{\text{NH}_3} + x_{\text{H}_2\text{O},\text{R}} G_{\text{H}_2\text{O}} + x_{\text{OH}^-,\text{R}} G_{\text{OH}^-} \right. \\
&\quad \left. + RT \left( x_{\text{NH}_4^+,\text{R}} \ln(\gamma_{\text{NH}_4^+,\text{R}} x_{\text{NH}_4^+,\text{R}}) + x_{\text{NH}_3,\text{R}} \ln(\gamma_{\text{NH}_3,\text{R}} x_{\text{NH}_3,\text{R}}) \right) \right. \\
&\quad \left. + x_{\text{H}_2\text{O},\text{R}} \ln(\gamma_{\text{H}_2\text{O},\text{R}} x_{\text{H}_2\text{O},\text{R}}) + x_{\text{H}^+,\text{R}} \ln(\gamma_{\text{H}^+,\text{R}} x_{\text{H}^+,\text{R}}) + x_{\text{OH}^-,\text{R}} \ln(\gamma_{\text{OH}^-,\text{R}} x_{\text{OH}^-,\text{R}}) \right) \quad (\text{A.7}) \\
&- \frac{N_{\text{F}}}{x_{\text{TAN},\text{P}} N_{\text{P}}} \left[ x_{\text{NH}_4^+,\text{F}} G_{\text{NH}_4^+} + x_{\text{NH}_3,\text{F}} G_{\text{NH}_3} + x_{\text{H}_2\text{O},\text{F}} G_{\text{H}_2\text{O}} + x_{\text{OH}^-,\text{F}} G_{\text{OH}^-} \right. \\
&\quad \left. + RT \left( x_{\text{NH}_4^+,\text{F}} \ln(\gamma_{\text{NH}_4^+,\text{F}} x_{\text{NH}_4^+,\text{F}}) + x_{\text{NH}_3,\text{F}} \ln(\gamma_{\text{NH}_3,\text{F}} x_{\text{NH}_3,\text{F}}) \right) \right. \\
&\quad \left. + x_{\text{H}_2\text{O},\text{F}} \ln(\gamma_{\text{H}_2\text{O},\text{F}} x_{\text{H}_2\text{O},\text{F}}) + x_{\text{H}^+,\text{F}} \ln(\gamma_{\text{H}^+,\text{F}} x_{\text{H}^+,\text{F}}) + x_{\text{OH}^-,\text{F}} \ln(\gamma_{\text{OH}^-,\text{F}} x_{\text{OH}^-,\text{F}}) \right) \quad \left. \right]
\end{aligned}$$

$$\begin{aligned}
\bar{E}_{\min} = & \frac{1}{2} G_{f,(\text{NH}_4)_2\text{SO}_4(\text{s})}^\circ \\
& + \frac{N_{\text{R}}}{2N_{\text{P}}} \left[ +RT \left( \begin{aligned} & x_{\text{NH}_4^+, \text{R}} G_{\text{NH}_4^+} + x_{\text{NH}_3, \text{R}} G_{\text{NH}_3} + x_{\text{SO}_4^{2-}, \text{R}} G_{\text{SO}_4^{2-}} + x_{\text{H}_2\text{O}, \text{R}} G_{\text{H}_2\text{O}} + x_{\text{OH}^-, \text{R}} G_{\text{OH}^-} \\ & x_{\text{NH}_4^+, \text{R}} \ln(\gamma_{\text{NH}_4^+, \text{R}} x_{\text{NH}_4^+, \text{R}}) + x_{\text{NH}_3, \text{R}} \ln(\gamma_{\text{NH}_3, \text{R}} x_{\text{NH}_3, \text{R}}) + \\ & x_{\text{SO}_4^{2-}, \text{R}} \ln(\gamma_{\text{SO}_4^{2-}, \text{R}} x_{\text{SO}_4^{2-}, \text{R}}) + x_{\text{H}_2\text{O}, \text{R}} \ln(\gamma_{\text{H}_2\text{O}, \text{R}} x_{\text{H}_2\text{O}, \text{R}}) + \\ & x_{\text{H}^+, \text{R}} \ln(\gamma_{\text{H}^+, \text{R}} x_{\text{H}^+, \text{R}}) + x_{\text{OH}^-, \text{R}} \ln(\gamma_{\text{OH}^-, \text{R}} x_{\text{OH}^-, \text{R}}) \end{aligned} \right) \right] \\
& - \frac{N_{\text{F}}}{2N_{\text{P}}} \left[ +RT \left( \begin{aligned} & x_{\text{NH}_4^+, \text{F}} G_{\text{NH}_4^+} + x_{\text{NH}_3, \text{F}} G_{\text{NH}_3} + x_{\text{SO}_4^{2-}, \text{F}} G_{\text{SO}_4^{2-}} + x_{\text{H}_2\text{O}, \text{F}} G_{\text{H}_2\text{O}} + x_{\text{OH}^-, \text{F}} G_{\text{OH}^-} \\ & x_{\text{NH}_4^+, \text{F}} \ln(\gamma_{\text{NH}_4^+, \text{F}} x_{\text{NH}_4^+, \text{F}}) + x_{\text{NH}_3, \text{F}} \ln(\gamma_{\text{NH}_3, \text{F}} x_{\text{NH}_3, \text{F}}) + \\ & x_{\text{SO}_4^{2-}, \text{F}} \ln(\gamma_{\text{SO}_4^{2-}, \text{F}} x_{\text{SO}_4^{2-}, \text{F}}) + x_{\text{H}_2\text{O}, \text{F}} \ln(\gamma_{\text{H}_2\text{O}, \text{F}} x_{\text{H}_2\text{O}, \text{F}}) + \\ & x_{\text{H}^+, \text{F}} \ln(\gamma_{\text{H}^+, \text{F}} x_{\text{H}^+, \text{F}}) + x_{\text{OH}^-, \text{F}} \ln(\gamma_{\text{OH}^-, \text{F}} x_{\text{OH}^-, \text{F}}) \end{aligned} \right) \right] \quad (\text{A.8})
\end{aligned}$$

For the determination of  $\bar{E}_{\min}$  to recover different phosphate products,  $\text{KMgPO}_4 \cdot 6 \text{H}_2\text{O}_{(\text{s})}$  (potassium magnesium phosphate),  $\text{NH}_4\text{MgPO}_4 \cdot 6 \text{H}_2\text{O}_{(\text{s})}$  (struvite),  $\text{KH}_2\text{PO}_4_{(\text{s})}$  (potassium phosphate), and  $\text{NH}_4\text{H}_2\text{PO}_4_{(\text{s})}$  (monoammonium phosphate), eqns (A.9), (A.10), (A.11), and (A.12) were respectively employed.

$$\begin{aligned}
\bar{E}_{\min} = & G_{f, \text{KMgPO}_4 \cdot 6 \text{H}_2\text{O}(\text{s})}^\circ \\
& + \frac{N_{\text{R}}}{N_{\text{P}}} \left[ +RT \left( \begin{aligned} & x_{\text{K}^+, \text{R}} G_{\text{K}^+} + x_{\text{Mg}^{2+}, \text{R}} G_{\text{Mg}^{2+}} + x_{\text{H}_2\text{PO}_4^-, \text{R}} G_{\text{H}_2\text{PO}_4^-} + x_{\text{HPO}_4^{2-}, \text{R}} G_{\text{HPO}_4^{2-}} + x_{\text{H}_2\text{O}, \text{R}} G_{\text{H}_2\text{O}} + x_{\text{OH}^-, \text{R}} G_{\text{OH}^-} \\ & x_{\text{K}^+, \text{R}} \ln(\gamma_{\text{K}^+, \text{R}} x_{\text{K}^+, \text{R}}) + x_{\text{Mg}^{2+}, \text{R}} \ln(\gamma_{\text{Mg}^{2+}, \text{R}} x_{\text{Mg}^{2+}, \text{R}}) \\ & + x_{\text{H}_2\text{PO}_4^-, \text{R}} \ln(\gamma_{\text{H}_2\text{PO}_4^-, \text{R}} x_{\text{H}_2\text{PO}_4^-, \text{R}}) + x_{\text{HPO}_4^{2-}, \text{R}} \ln(\gamma_{\text{HPO}_4^{2-}, \text{R}} x_{\text{HPO}_4^{2-}, \text{R}}) \\ & + x_{\text{H}_2\text{O}, \text{R}} \ln(\gamma_{\text{H}_2\text{O}, \text{R}} x_{\text{H}_2\text{O}, \text{R}}) + x_{\text{H}^+, \text{R}} \ln(\gamma_{\text{H}^+, \text{R}} x_{\text{H}^+, \text{R}}) + x_{\text{OH}^-, \text{R}} \ln(\gamma_{\text{OH}^-, \text{R}} x_{\text{OH}^-, \text{R}}) \end{aligned} \right) \right] \\
& - \frac{N_{\text{F}}}{N_{\text{P}}} \left[ +RT \left( \begin{aligned} & x_{\text{K}^+, \text{F}} G_{\text{K}^+} + x_{\text{Mg}^{2+}, \text{F}} G_{\text{Mg}^{2+}} + x_{\text{H}_2\text{PO}_4^-, \text{F}} G_{\text{H}_2\text{PO}_4^-} + x_{\text{HPO}_4^{2-}, \text{F}} G_{\text{HPO}_4^{2-}} + x_{\text{H}_2\text{O}, \text{F}} G_{\text{H}_2\text{O}} + x_{\text{OH}^-, \text{F}} G_{\text{OH}^-} \\ & x_{\text{K}^+, \text{F}} \ln(\gamma_{\text{K}^+, \text{F}} x_{\text{K}^+, \text{F}}) + x_{\text{Mg}^{2+}, \text{F}} \ln(\gamma_{\text{Mg}^{2+}, \text{F}} x_{\text{Mg}^{2+}, \text{F}}) \\ & + x_{\text{H}_2\text{PO}_4^-, \text{F}} \ln(\gamma_{\text{H}_2\text{PO}_4^-, \text{F}} x_{\text{H}_2\text{PO}_4^-, \text{F}}) + x_{\text{HPO}_4^{2-}, \text{F}} \ln(\gamma_{\text{HPO}_4^{2-}, \text{F}} x_{\text{HPO}_4^{2-}, \text{F}}) \\ & + x_{\text{H}_2\text{O}, \text{F}} \ln(\gamma_{\text{H}_2\text{O}, \text{F}} x_{\text{H}_2\text{O}, \text{F}}) + x_{\text{H}^+, \text{F}} \ln(\gamma_{\text{H}^+, \text{F}} x_{\text{H}^+, \text{F}}) + x_{\text{OH}^-, \text{F}} \ln(\gamma_{\text{OH}^-, \text{F}} x_{\text{OH}^-, \text{F}}) \end{aligned} \right) \right] \quad (\text{A.9})
\end{aligned}$$

$$\begin{aligned}
\bar{E}_{\min} &= G_{f,\text{NH}_4\text{MgPO}_4 \cdot 6\text{H}_2\text{O}(\text{s})}^\circ \\
&+ \frac{N_{\text{R}}}{N_{\text{P}}} \left[ \begin{aligned} &\left( x_{\text{NH}_4^+,\text{R}} G_{\text{NH}_4^+} + x_{\text{NH}_3,\text{R}} G_{\text{NH}_3} + x_{\text{Mg}^{2+},\text{R}} G_{\text{Mg}^{2+}} + x_{\text{H}_2\text{PO}_4^-\text{,R}} G_{\text{H}_2\text{PO}_4^-} + \right. \\ &\left. x_{\text{HPO}_4^{2-},\text{R}} G_{\text{HPO}_4^{2-}} + x_{\text{H}_2\text{O},\text{R}} G_{\text{H}_2\text{O}} + x_{\text{OH}^-\text{,R}} G_{\text{OH}^-} \right) \\ &+ RT \left( \begin{aligned} &x_{\text{NH}_4^+,\text{R}} \ln(\gamma_{\text{NH}_4^+,\text{R}} x_{\text{NH}_4^+,\text{R}}) + x_{\text{NH}_3,\text{R}} \ln(\gamma_{\text{NH}_3,\text{R}} x_{\text{NH}_3,\text{R}}) + \\ &x_{\text{Mg}^{2+},\text{R}} \ln(\gamma_{\text{Mg}^{2+},\text{R}} x_{\text{Mg}^{2+},\text{R}}) + x_{\text{H}_2\text{PO}_4^-\text{,R}} \ln(\gamma_{\text{H}_2\text{PO}_4^-\text{,R}} x_{\text{H}_2\text{PO}_4^-\text{,R}}) + \\ &x_{\text{HPO}_4^{2-},\text{R}} \ln(\gamma_{\text{HPO}_4^{2-},\text{R}} x_{\text{HPO}_4^{2-},\text{R}}) + x_{\text{H}_2\text{O},\text{R}} \ln(\gamma_{\text{H}_2\text{O},\text{R}} x_{\text{H}_2\text{O},\text{R}}) + \\ &x_{\text{H}^+,\text{R}} \ln(\gamma_{\text{H}^+,\text{R}} x_{\text{H}^+,\text{R}}) + x_{\text{OH}^-\text{,R}} \ln(\gamma_{\text{OH}^-\text{,R}} x_{\text{OH}^-\text{,R}}) \end{aligned} \right) \end{aligned} \right] \\
&- \frac{N_{\text{F}}}{N_{\text{P}}} \left[ \begin{aligned} &\left( x_{\text{NH}_4^+,\text{F}} G_{\text{NH}_4^+} + x_{\text{NH}_3,\text{F}} G_{\text{NH}_3} + x_{\text{Mg}^{2+},\text{F}} G_{\text{Mg}^{2+}} + x_{\text{H}_2\text{PO}_4^-\text{,F}} G_{\text{H}_2\text{PO}_4^-} + \right) \\ &\left( x_{\text{HPO}_4^{2-},\text{F}} G_{\text{HPO}_4^{2-}} + x_{\text{H}_2\text{O},\text{F}} G_{\text{H}_2\text{O}} + x_{\text{OH}^-\text{,F}} G_{\text{OH}^-} \right) \\ &+ RT \left( \begin{aligned} &x_{\text{NH}_4^+,\text{F}} \ln(\gamma_{\text{NH}_4^+,\text{F}} x_{\text{NH}_4^+,\text{F}}) + x_{\text{NH}_3,\text{F}} \ln(\gamma_{\text{NH}_3,\text{F}} x_{\text{NH}_3,\text{F}}) + \\ &x_{\text{Mg}^{2+},\text{F}} \ln(\gamma_{\text{Mg}^{2+},\text{F}} x_{\text{Mg}^{2+},\text{F}}) + x_{\text{H}_2\text{PO}_4^-\text{,F}} \ln(\gamma_{\text{H}_2\text{PO}_4^-\text{,F}} x_{\text{H}_2\text{PO}_4^-\text{,F}}) + \\ &x_{\text{HPO}_4^{2-},\text{F}} \ln(\gamma_{\text{HPO}_4^{2-},\text{F}} x_{\text{HPO}_4^{2-},\text{F}}) + x_{\text{H}_2\text{O},\text{F}} \ln(\gamma_{\text{H}_2\text{O},\text{F}} x_{\text{H}_2\text{O},\text{F}}) + \\ &x_{\text{H}^+,\text{F}} \ln(\gamma_{\text{H}^+,\text{F}} x_{\text{H}^+,\text{F}}) + x_{\text{OH}^-\text{,F}} \ln(\gamma_{\text{OH}^-\text{,F}} x_{\text{OH}^-\text{,F}}) \end{aligned} \right) \end{aligned} \right] \quad (\text{A.10})
\end{aligned}$$

$$\begin{aligned}
\bar{E}_{\min} &= G_{f,\text{KH}_2\text{PO}_4(\text{s})}^\circ \\
&+ \frac{N_{\text{R}}}{N_{\text{P}}} \left[ \begin{aligned} &x_{\text{K}^+,\text{R}} G_{\text{K}^+} + x_{\text{H}_2\text{PO}_4^-\text{,R}} G_{\text{H}_2\text{PO}_4^-} + x_{\text{HPO}_4^{2-},\text{R}} G_{\text{HPO}_4^{2-}} + x_{\text{H}_2\text{O},\text{R}} G_{\text{H}_2\text{O}} + x_{\text{OH}^-\text{,R}} G_{\text{OH}^-} \\ &+ RT \left( \begin{aligned} &x_{\text{K}^+,\text{R}} \ln(\gamma_{\text{K}^+,\text{R}} x_{\text{K}^+,\text{R}}) + x_{\text{H}_2\text{PO}_4^-\text{,R}} \ln(\gamma_{\text{H}_2\text{PO}_4^-\text{,R}} x_{\text{H}_2\text{PO}_4^-\text{,R}}) + \\ &x_{\text{HPO}_4^{2-},\text{R}} \ln(\gamma_{\text{HPO}_4^{2-},\text{R}} x_{\text{HPO}_4^{2-},\text{R}}) + x_{\text{H}_2\text{O},\text{R}} \ln(\gamma_{\text{H}_2\text{O},\text{R}} x_{\text{H}_2\text{O},\text{R}}) + \\ &x_{\text{H}^+,\text{R}} \ln(\gamma_{\text{H}^+,\text{R}} x_{\text{H}^+,\text{R}}) + x_{\text{OH}^-\text{,R}} \ln(\gamma_{\text{OH}^-\text{,R}} x_{\text{OH}^-\text{,R}}) \end{aligned} \right) \end{aligned} \right] \\
&- \frac{N_{\text{F}}}{N_{\text{P}}} \left[ \begin{aligned} &x_{\text{K}^+,\text{F}} G_{\text{K}^+} + x_{\text{H}_2\text{PO}_4^-\text{,F}} G_{\text{H}_2\text{PO}_4^-} + x_{\text{HPO}_4^{2-},\text{F}} G_{\text{HPO}_4^{2-}} + x_{\text{H}_2\text{O},\text{F}} G_{\text{H}_2\text{O}} + x_{\text{OH}^-\text{,F}} G_{\text{OH}^-} \\ &+ RT \left( \begin{aligned} &x_{\text{K}^+,\text{F}} \ln(\gamma_{\text{K}^+,\text{F}} x_{\text{K}^+,\text{F}}) + x_{\text{H}_2\text{PO}_4^-\text{,F}} \ln(\gamma_{\text{H}_2\text{PO}_4^-\text{,F}} x_{\text{H}_2\text{PO}_4^-\text{,F}}) + \\ &x_{\text{HPO}_4^{2-},\text{F}} \ln(\gamma_{\text{HPO}_4^{2-},\text{F}} x_{\text{HPO}_4^{2-},\text{F}}) + x_{\text{H}_2\text{O},\text{F}} \ln(\gamma_{\text{H}_2\text{O},\text{F}} x_{\text{H}_2\text{O},\text{F}}) + \\ &x_{\text{H}^+,\text{F}} \ln(\gamma_{\text{H}^+,\text{F}} x_{\text{H}^+,\text{F}}) + x_{\text{OH}^-\text{,F}} \ln(\gamma_{\text{OH}^-\text{,F}} x_{\text{OH}^-\text{,F}}) \end{aligned} \right) \end{aligned} \right] \quad (\text{A.11})
\end{aligned}$$

$$\begin{aligned}
\bar{E}_{\min} = & G_{f, \text{NH}_4\text{H}_2\text{PO}_4(\text{s})} \\
& + \frac{N_{\text{R}}}{N_{\text{P}}} \left[ \begin{aligned} & \left( x_{\text{NH}_4^+, \text{R}} G_{\text{NH}_4^+} + x_{\text{NH}_3, \text{R}} G_{\text{NH}_3} + x_{\text{H}_2\text{PO}_4^-, \text{R}} G_{\text{H}_2\text{PO}_4^-} + \right. \\ & \left. x_{\text{HPO}_4^{2-}, \text{R}} G_{\text{HPO}_4^{2-}} + x_{\text{H}_2\text{O}, \text{R}} G_{\text{H}_2\text{O}} + x_{\text{OH}^-, \text{R}} G_{\text{OH}^-} \right) \\ & + RT \left( \begin{aligned} & x_{\text{NH}_4^+, \text{R}} \ln(\gamma_{\text{NH}_4^+, \text{R}} x_{\text{NH}_4^+, \text{R}}) + x_{\text{NH}_3, \text{R}} \ln(\gamma_{\text{NH}_3, \text{R}} x_{\text{NH}_3, \text{R}}) \\ & + x_{\text{H}_2\text{PO}_4^-, \text{R}} \ln(\gamma_{\text{H}_2\text{PO}_4^-, \text{R}} x_{\text{H}_2\text{PO}_4^-, \text{R}}) + x_{\text{HPO}_4^{2-}, \text{R}} \ln(\gamma_{\text{HPO}_4^{2-}, \text{R}} x_{\text{HPO}_4^{2-}, \text{R}}) \\ & + x_{\text{H}_2\text{O}, \text{R}} \ln(\gamma_{\text{H}_2\text{O}, \text{R}} x_{\text{H}_2\text{O}, \text{R}}) + x_{\text{H}^+, \text{R}} \ln(\gamma_{\text{H}^+, \text{R}} x_{\text{H}^+, \text{R}}) + x_{\text{OH}^-, \text{R}} \ln(\gamma_{\text{OH}^-, \text{R}} x_{\text{OH}^-, \text{R}}) \end{aligned} \right) \end{aligned} \right] \\
& - \frac{N_{\text{F}}}{N_{\text{P}}} \left[ \begin{aligned} & \left( x_{\text{NH}_4^+, \text{F}} G_{\text{NH}_4^+} + x_{\text{NH}_3, \text{F}} G_{\text{NH}_3} + x_{\text{H}_2\text{PO}_4^-, \text{F}} G_{\text{H}_2\text{PO}_4^-} + \right. \\ & \left. x_{\text{HPO}_4^{2-}, \text{F}} G_{\text{HPO}_4^{2-}} + x_{\text{H}_2\text{O}, \text{F}} G_{\text{H}_2\text{O}} + x_{\text{OH}^-, \text{F}} G_{\text{OH}^-} \right) \\ & + RT \left( \begin{aligned} & x_{\text{NH}_4^+, \text{F}} \ln(\gamma_{\text{NH}_4^+, \text{F}} x_{\text{NH}_4^+, \text{F}}) + x_{\text{NH}_3, \text{F}} \ln(\gamma_{\text{NH}_3, \text{F}} x_{\text{NH}_3, \text{F}}) \\ & + x_{\text{H}_2\text{PO}_4^-, \text{F}} \ln(\gamma_{\text{H}_2\text{PO}_4^-, \text{F}} x_{\text{H}_2\text{PO}_4^-, \text{F}}) + x_{\text{HPO}_4^{2-}, \text{F}} \ln(\gamma_{\text{HPO}_4^{2-}, \text{F}} x_{\text{HPO}_4^{2-}, \text{F}}) \\ & + x_{\text{H}_2\text{O}, \text{F}} \ln(\gamma_{\text{H}_2\text{O}, \text{F}} x_{\text{H}_2\text{O}, \text{F}}) + x_{\text{H}^+, \text{F}} \ln(\gamma_{\text{H}^+, \text{F}} x_{\text{H}^+, \text{F}}) + x_{\text{OH}^-, \text{F}} \ln(\gamma_{\text{OH}^-, \text{F}} x_{\text{OH}^-, \text{F}}) \end{aligned} \right) \end{aligned} \right] \quad (\text{A.12})
\end{aligned}$$

**Figure 2.5.** For the determination of  $\bar{E}_{\min}$  to recover  $\text{NH}_3(\text{l})$  and 1.0 M  $\text{NH}_3(\text{aq})$  at various recovery yields from hydrolyzed urine and 2° treated WW effluent eqns (A.6) and (A.7) were respectively applied. Inputs of  $x_{\text{NH}_3, \text{F}}$  and  $x_{\text{NH}_4^+, \text{F}}$  are dependent on the speciation of TAN in the feed (i.e., fraction of TAN as  $\text{NH}_3$ ,  $\alpha_{\text{NH}_3}$ , and as  $\text{NH}_4^+$ ,  $\alpha_{\text{NH}_4^+}$ ; where  $x_{\text{NH}_3} = \alpha_{\text{NH}_3} x_{\text{TAN}}$  and  $x_{\text{NH}_4^+} = \alpha_{\text{NH}_4^+} x_{\text{TAN}}$ ). Inputs of  $x_{\text{NH}_3, \text{R}}$  and  $x_{\text{NH}_4^+, \text{R}}$  are dependent on the speciation of TAN in the retentate as well as the TAN material balance,  $x_{\text{TAN}, \text{F}} N_{\text{F}} + x_{\text{TAN}, \text{RXN}} N_{\text{RXN}} = x_{\text{TAN}, \text{P}} N_{\text{P}} + x_{\text{TAN}, \text{R}} N_{\text{R}}$ . For 2° treated WW effluent systems,  $\text{NH}_4^+$  was assumed to be predominant in the feed and retentate due to both streams having  $\text{pH} \ll \text{pK}_a$ . For hydrolyzed urine systems, speciation of TAN in the feed was evaluated using a model urine solution (Table A.7) with Visual Minteq.<sup>300</sup> To calculate  $x_{\text{TAN}, \text{R}}$ , the TAN material balance was

applied. Then,  $x_{\text{NH}_3,\text{R}}$  and  $x_{\text{NH}_4^+,\text{R}}$  were calculated using Visual Minteq to determine pH,  $\alpha_{\text{NH}_3,\text{R}}$ , and  $\alpha_{\text{NH}_4^+,\text{R}}$  (Tables S8 and S9).

**Figure 2.6.** For the determination of  $\bar{E}_{\text{min}}$  to recover 1.0 M  $\text{KNO}_3(\text{aq})$ , 1.0 M  $\text{NH}_4\text{NO}_3(\text{aq})$ ,  $\text{KNO}_3(\text{s})$ , and  $\text{NH}_4\text{NO}_3(\text{s})$  from 2° treated WW effluent, eqns (A.13), (A.14), (A.15), and (A.16), respectively, were used. For 1.0 M  $\text{urea}(\text{aq})$  and  $\text{urea}(\text{s})$  recovery from hydrolyzed urine, eqns (A.17) and (A.18) were used, respectively. In this analysis, all recovery energies were normalized per mole of nitrogen recovered.

$$\begin{aligned}
 \bar{E}_{\text{min}} = & \frac{1}{x_{\text{NO}_3^-, \text{P}}} \left[ x_{\text{K}^+, \text{P}} G_{\text{K}^+} + x_{\text{NO}_3^-, \text{P}} G_{\text{NO}_3^-} + x_{\text{H}_2\text{O}, \text{P}} G_{\text{H}_2\text{O}} + x_{\text{OH}^-, \text{P}} G_{\text{OH}^-} \right. \\
 & + RT \left[ \begin{array}{l} x_{\text{K}^+, \text{P}} \ln(\gamma_{\text{K}^+, \text{P}} x_{\text{K}^+, \text{P}}) \\ + x_{\text{NO}_3^-, \text{P}} \ln(\gamma_{\text{NO}_3^-, \text{P}} x_{\text{NO}_3^-, \text{P}}) + x_{\text{H}_2\text{O}, \text{P}} \ln(\gamma_{\text{H}_2\text{O}, \text{P}} x_{\text{H}_2\text{O}, \text{P}}) \\ + x_{\text{H}^+, \text{P}} \ln(\gamma_{\text{H}^+, \text{P}} x_{\text{H}^+, \text{P}}) + x_{\text{OH}^-, \text{P}} \ln(\gamma_{\text{OH}^-, \text{P}} x_{\text{OH}^-, \text{P}}) \end{array} \right] \\
 & + \frac{N_{\text{R}}}{x_{\text{NO}_3^-, \text{P}} N_{\text{P}}} \left[ x_{\text{K}^+, \text{R}} G_{\text{K}^+} + x_{\text{NO}_3^-, \text{R}} G_{\text{NO}_3^-} + x_{\text{H}_2\text{O}, \text{R}} G_{\text{H}_2\text{O}} + x_{\text{OH}^-, \text{R}} G_{\text{OH}^-} \right. \\
 & + RT \left[ \begin{array}{l} x_{\text{K}^+, \text{R}} \ln(\gamma_{\text{K}^+, \text{R}} x_{\text{K}^+, \text{R}}) \\ + x_{\text{NO}_3^-, \text{R}} \ln(\gamma_{\text{NO}_3^-, \text{R}} x_{\text{NO}_3^-, \text{R}}) + x_{\text{H}_2\text{O}, \text{R}} \ln(\gamma_{\text{H}_2\text{O}, \text{R}} x_{\text{H}_2\text{O}, \text{R}}) \\ + x_{\text{H}^+, \text{R}} \ln(\gamma_{\text{H}^+, \text{R}} x_{\text{H}^+, \text{R}}) + x_{\text{OH}^-, \text{R}} \ln(\gamma_{\text{OH}^-, \text{R}} x_{\text{OH}^-, \text{R}}) \end{array} \right] \\
 & - \frac{N_{\text{F}}}{x_{\text{NO}_3^-, \text{P}} N_{\text{P}}} \left[ x_{\text{K}^+, \text{F}} G_{\text{K}^+} + x_{\text{NO}_3^-, \text{F}} G_{\text{NO}_3^-} + x_{\text{H}_2\text{O}, \text{F}} G_{\text{H}_2\text{O}} + x_{\text{OH}^-, \text{F}} G_{\text{OH}^-} \right. \\
 & + RT \left[ \begin{array}{l} x_{\text{K}^+, \text{F}} \ln(\gamma_{\text{K}^+, \text{F}} x_{\text{K}^+, \text{F}}) \\ + x_{\text{NO}_3^-, \text{F}} \ln(\gamma_{\text{NO}_3^-, \text{F}} x_{\text{NO}_3^-, \text{F}}) + x_{\text{H}_2\text{O}, \text{F}} \ln(\gamma_{\text{H}_2\text{O}, \text{F}} x_{\text{H}_2\text{O}, \text{F}}) \\ + x_{\text{H}^+, \text{F}} \ln(\gamma_{\text{H}^+, \text{F}} x_{\text{H}^+, \text{F}}) + x_{\text{OH}^-, \text{F}} \ln(\gamma_{\text{OH}^-, \text{F}} x_{\text{OH}^-, \text{F}}) \end{array} \right] \quad (\text{A.13})
 \end{aligned}$$

$$\begin{aligned}
\bar{E}_{\min} = & \frac{1}{2x_{\text{TAN,P}}} \left[ \begin{aligned} & x_{\text{NH}_4^+,\text{P}} G_{\text{NH}_4^+} + x_{\text{NH}_3,\text{P}} G_{\text{NH}_3} + x_{\text{NO}_3^-\text{,P}} G_{\text{NO}_3^-} + x_{\text{H}_2\text{O,P}} G_{\text{H}_2\text{O}} + x_{\text{OH}^-\text{,P}} G_{\text{OH}^-} \\ & + RT \left( \begin{aligned} & x_{\text{NH}_4^+,\text{P}} \ln(\gamma_{\text{NH}_4^+,\text{P}} x_{\text{NH}_4^+,\text{P}}) + x_{\text{NH}_3,\text{P}} \ln(\gamma_{\text{NH}_3,\text{P}} x_{\text{NH}_3,\text{P}}) \\ & + x_{\text{NO}_3^-\text{,P}} \ln(\gamma_{\text{NO}_3^-\text{,P}} x_{\text{NO}_3^-\text{,P}}) + x_{\text{H}_2\text{O,P}} \ln(\gamma_{\text{H}_2\text{O,P}} x_{\text{H}_2\text{O,P}}) \\ & + x_{\text{H}^+,\text{P}} \ln(\gamma_{\text{H}^+,\text{P}} x_{\text{H}^+,\text{P}}) + x_{\text{OH}^-\text{,P}} \ln(\gamma_{\text{OH}^-\text{,P}} x_{\text{OH}^-\text{,P}}) \end{aligned} \right) \end{aligned} \right] \\
& + \frac{N_{\text{R}}}{2x_{\text{TAN,P}} N_{\text{P}}} \left[ \begin{aligned} & x_{\text{NH}_4^+,\text{R}} G_{\text{NH}_4^+} + x_{\text{NH}_3,\text{R}} G_{\text{NH}_3} + x_{\text{NO}_3^-\text{,R}} G_{\text{NO}_3^-} + x_{\text{H}_2\text{O,R}} G_{\text{H}_2\text{O}} + x_{\text{OH}^-\text{,R}} G_{\text{OH}^-} \\ & + RT \left( \begin{aligned} & x_{\text{NH}_4^+,\text{R}} \ln(\gamma_{\text{NH}_4^+,\text{R}} x_{\text{NH}_4^+,\text{R}}) + x_{\text{NH}_3,\text{R}} \ln(\gamma_{\text{NH}_3,\text{R}} x_{\text{NH}_3,\text{R}}) \\ & + x_{\text{NO}_3^-\text{,R}} \ln(\gamma_{\text{NO}_3^-\text{,R}} x_{\text{NO}_3^-\text{,R}}) + x_{\text{H}_2\text{O,R}} \ln(\gamma_{\text{H}_2\text{O,R}} x_{\text{H}_2\text{O,R}}) \\ & + x_{\text{H}^+,\text{R}} \ln(\gamma_{\text{H}^+,\text{R}} x_{\text{H}^+,\text{R}}) + x_{\text{OH}^-\text{,R}} \ln(\gamma_{\text{OH}^-\text{,R}} x_{\text{OH}^-\text{,R}}) \end{aligned} \right) \end{aligned} \right] \\
& - \frac{N_{\text{F}}}{2x_{\text{TAN,P}} N_{\text{P}}} \left[ \begin{aligned} & x_{\text{NH}_4^+,\text{F}} G_{\text{NH}_4^+} + x_{\text{NH}_3,\text{F}} G_{\text{NH}_3} + x_{\text{NO}_3^-\text{,F}} G_{\text{NO}_3^-} + x_{\text{H}_2\text{O,F}} G_{\text{H}_2\text{O}} + x_{\text{OH}^-\text{,F}} G_{\text{OH}^-} \\ & + RT \left( \begin{aligned} & x_{\text{NH}_4^+,\text{F}} \ln(\gamma_{\text{NH}_4^+,\text{F}} x_{\text{NH}_4^+,\text{F}}) + x_{\text{NH}_3,\text{F}} \ln(\gamma_{\text{NH}_3,\text{F}} x_{\text{NH}_3,\text{F}}) \\ & + x_{\text{NO}_3^-\text{,F}} \ln(\gamma_{\text{NO}_3^-\text{,F}} x_{\text{NO}_3^-\text{,F}}) + x_{\text{H}_2\text{O,F}} \ln(\gamma_{\text{H}_2\text{O,F}} x_{\text{H}_2\text{O,F}}) \\ & + x_{\text{H}^+,\text{F}} \ln(\gamma_{\text{H}^+,\text{F}} x_{\text{H}^+,\text{F}}) + x_{\text{OH}^-\text{,F}} \ln(\gamma_{\text{OH}^-\text{,F}} x_{\text{OH}^-\text{,F}}) \end{aligned} \right) \end{aligned} \right] \quad (\text{A.14})
\end{aligned}$$

$$\begin{aligned}
\bar{E}_{\min} = & G_{f,\text{KNO}_3(\text{s})}^\circ \\
& + \frac{N_{\text{R}}}{N_{\text{P}}} \left[ \begin{aligned} & x_{\text{K}^+,\text{R}} G_{\text{K}^+} + x_{\text{NO}_3^-\text{,R}} G_{\text{NO}_3^-} + x_{\text{H}_2\text{O,R}} G_{\text{H}_2\text{O}} + x_{\text{OH}^-\text{,R}} G_{\text{OH}^-} \\ & + RT \left( \begin{aligned} & x_{\text{K}^+,\text{R}} \ln(\gamma_{\text{K}^+,\text{R}} x_{\text{K}^+,\text{R}}) + x_{\text{NO}_3^-\text{,R}} \ln(\gamma_{\text{NO}_3^-\text{,R}} x_{\text{NO}_3^-\text{,R}}) \\ & + x_{\text{H}_2\text{O,R}} \ln(\gamma_{\text{H}_2\text{O,R}} x_{\text{H}_2\text{O,R}}) + x_{\text{H}^+,\text{R}} \ln(\gamma_{\text{H}^+,\text{R}} x_{\text{H}^+,\text{R}}) + x_{\text{OH}^-\text{,R}} \ln(\gamma_{\text{OH}^-\text{,R}} x_{\text{OH}^-\text{,R}}) \end{aligned} \right) \end{aligned} \right] \quad (\text{A.15}) \\
& - \frac{N_{\text{F}}}{N_{\text{P}}} \left[ \begin{aligned} & x_{\text{K}^+,\text{F}} G_{\text{K}^+} + x_{\text{NO}_3^-\text{,F}} G_{\text{NO}_3^-} + x_{\text{H}_2\text{O,F}} G_{\text{H}_2\text{O}} + x_{\text{OH}^-\text{,F}} G_{\text{OH}^-} \\ & + RT \left( \begin{aligned} & x_{\text{K}^+,\text{F}} \ln(\gamma_{\text{K}^+,\text{F}} x_{\text{K}^+,\text{F}}) + x_{\text{NO}_3^-\text{,F}} \ln(\gamma_{\text{NO}_3^-\text{,F}} x_{\text{NO}_3^-\text{,F}}) \\ & + x_{\text{H}_2\text{O,F}} \ln(\gamma_{\text{H}_2\text{O,F}} x_{\text{H}_2\text{O,F}}) + x_{\text{H}^+,\text{F}} \ln(\gamma_{\text{H}^+,\text{F}} x_{\text{H}^+,\text{F}}) + x_{\text{OH}^-\text{,F}} \ln(\gamma_{\text{OH}^-\text{,F}} x_{\text{OH}^-\text{,F}}) \end{aligned} \right) \end{aligned} \right]
\end{aligned}$$

$$\begin{aligned}
\bar{E}_{\min} &= \frac{1}{2} G_{f, \text{NH}_4\text{NO}_3}^\circ \\
&+ \frac{N_{\text{R}}}{2N_{\text{P}}} \left[ +RT \left( \begin{aligned} &x_{\text{NH}_4^+, \text{R}} \ln(\gamma_{\text{NH}_4^+, \text{R}} x_{\text{NH}_4^+, \text{R}}) + x_{\text{NH}_3, \text{R}} \ln(\gamma_{\text{NH}_3, \text{R}} x_{\text{NH}_3, \text{R}}) + x_{\text{NO}_3^-, \text{R}} \ln(\gamma_{\text{NO}_3^-, \text{R}} x_{\text{NO}_3^-, \text{R}}) \\ &+ x_{\text{H}_2\text{O}, \text{R}} \ln(\gamma_{\text{H}_2\text{O}, \text{R}} x_{\text{H}_2\text{O}, \text{R}}) + x_{\text{H}^+, \text{R}} \ln(\gamma_{\text{H}^+, \text{R}} x_{\text{H}^+, \text{R}}) + x_{\text{OH}^-, \text{R}} \ln(\gamma_{\text{OH}^-, \text{R}} x_{\text{OH}^-, \text{R}}) \end{aligned} \right) \right] \\
&- \frac{N_{\text{F}}}{2N_{\text{P}}} \left[ +RT \left( \begin{aligned} &x_{\text{NH}_4^+, \text{F}} \ln(\gamma_{\text{NH}_4^+, \text{F}} x_{\text{NH}_4^+, \text{F}}) + x_{\text{NH}_3, \text{F}} \ln(\gamma_{\text{NH}_3, \text{F}} x_{\text{NH}_3, \text{F}}) + x_{\text{NO}_3^-, \text{F}} \ln(\gamma_{\text{NO}_3^-, \text{F}} x_{\text{NO}_3^-, \text{F}}) \\ &+ x_{\text{H}_2\text{O}, \text{F}} \ln(\gamma_{\text{H}_2\text{O}, \text{F}} x_{\text{H}_2\text{O}, \text{F}}) + x_{\text{H}^+, \text{F}} \ln(\gamma_{\text{H}^+, \text{F}} x_{\text{H}^+, \text{F}}) + x_{\text{OH}^-, \text{F}} \ln(\gamma_{\text{OH}^-, \text{F}} x_{\text{OH}^-, \text{F}}) \end{aligned} \right) \right]
\end{aligned} \tag{A.16}$$

$$\begin{aligned}
\bar{E}_{\min} &= \frac{1}{2x_{\text{CO}(\text{NH}_2)_2, \text{P}} N_{\text{P}}} \left[ +RT \left( \begin{aligned} &x_{\text{CO}(\text{NH}_2)_2, \text{P}} \ln(\gamma_{\text{CO}(\text{NH}_2)_2, \text{P}} x_{\text{CO}(\text{NH}_2)_2, \text{P}}) + x_{\text{H}_2\text{O}, \text{P}} \ln(\gamma_{\text{H}_2\text{O}, \text{P}} x_{\text{H}_2\text{O}, \text{P}}) \\ &+ x_{\text{H}^+, \text{P}} \ln(\gamma_{\text{H}^+, \text{P}} x_{\text{H}^+, \text{P}}) + x_{\text{OH}^-, \text{P}} \ln(\gamma_{\text{OH}^-, \text{P}} x_{\text{OH}^-, \text{P}}) \end{aligned} \right) \right] \\
&+ \frac{N_{\text{R}}}{2x_{\text{CO}(\text{NH}_2)_2, \text{P}} N_{\text{P}}} \left[ +RT \left( \begin{aligned} &x_{\text{CO}(\text{NH}_2)_2, \text{R}} \ln(\gamma_{\text{CO}(\text{NH}_2)_2, \text{R}} x_{\text{CO}(\text{NH}_2)_2, \text{R}}) + x_{\text{H}_2\text{O}, \text{R}} \ln(\gamma_{\text{H}_2\text{O}, \text{R}} x_{\text{H}_2\text{O}, \text{R}}) \\ &+ x_{\text{H}^+, \text{R}} \ln(\gamma_{\text{H}^+, \text{R}} x_{\text{H}^+, \text{R}}) + x_{\text{OH}^-, \text{R}} \ln(\gamma_{\text{OH}^-, \text{R}} x_{\text{OH}^-, \text{R}}) \end{aligned} \right) \right] \\
&- \frac{N_{\text{F}}}{2x_{\text{CO}(\text{NH}_2)_2, \text{P}} N_{\text{P}}} \left[ +RT \left( \begin{aligned} &x_{\text{CO}(\text{NH}_2)_2, \text{F}} \ln(\gamma_{\text{CO}(\text{NH}_2)_2, \text{F}} x_{\text{CO}(\text{NH}_2)_2, \text{F}}) + x_{\text{H}_2\text{O}, \text{F}} \ln(\gamma_{\text{H}_2\text{O}, \text{F}} x_{\text{H}_2\text{O}, \text{F}}) \\ &+ x_{\text{H}^+, \text{F}} \ln(\gamma_{\text{H}^+, \text{F}} x_{\text{H}^+, \text{F}}) + x_{\text{OH}^-, \text{F}} \ln(\gamma_{\text{OH}^-, \text{F}} x_{\text{OH}^-, \text{F}}) \end{aligned} \right) \right]
\end{aligned} \tag{A.17}$$

$$\begin{aligned}
\bar{E}_{\min} &= G_{f, \text{CO}(\text{NH}_2)_2}^\circ \\
&+ \frac{N_{\text{R}}}{2N_{\text{P}}} \left[ +RT \left( \begin{aligned} &x_{\text{CO}(\text{NH}_2)_2, \text{R}} \ln(\gamma_{\text{CO}(\text{NH}_2)_2, \text{R}} x_{\text{CO}(\text{NH}_2)_2, \text{R}}) + x_{\text{H}_2\text{O}, \text{R}} \ln(\gamma_{\text{H}_2\text{O}, \text{R}} x_{\text{H}_2\text{O}, \text{R}}) \\ &+ x_{\text{H}^+, \text{R}} \ln(\gamma_{\text{H}^+, \text{R}} x_{\text{H}^+, \text{R}}) + x_{\text{OH}^-, \text{R}} \ln(\gamma_{\text{OH}^-, \text{R}} x_{\text{OH}^-, \text{R}}) \end{aligned} \right) \right] \\
&- \frac{N_{\text{F}}}{2N_{\text{P}}} \left[ +RT \left( \begin{aligned} &x_{\text{CO}(\text{NH}_2)_2, \text{F}} \ln(\gamma_{\text{CO}(\text{NH}_2)_2, \text{F}} x_{\text{CO}(\text{NH}_2)_2, \text{F}}) + x_{\text{H}_2\text{O}, \text{F}} \ln(\gamma_{\text{H}_2\text{O}, \text{F}} x_{\text{H}_2\text{O}, \text{F}}) \\ &+ x_{\text{H}^+, \text{F}} \ln(\gamma_{\text{H}^+, \text{F}} x_{\text{H}^+, \text{F}}) + x_{\text{OH}^-, \text{F}} \ln(\gamma_{\text{OH}^-, \text{F}} x_{\text{OH}^-, \text{F}}) \end{aligned} \right) \right]
\end{aligned} \tag{A.18}$$

For the determination of  $\bar{E}_{\min}$  to recover  $\text{NH}_{3(l)}$  and 1.0 M  $\text{NH}_{3(aq)}$  from waste streams excluding  $\text{Na}^+$  and  $\text{Cl}^-$  species in the analysis, eqns (A.6) and (A.7) were respectively applied. For the determination of  $\bar{E}_{\min}$  to recover  $\text{NH}_{3(l)}$  and 1.0 M  $\text{NH}_{3(aq)}$  from waste streams including  $\text{Na}^+$  and  $\text{Cl}^-$  species in the analysis, eqns (A.19) and (A.20) were respectively applied. The  $\bar{E}_{\min}$  values are presented in Table A.6.

$$\begin{aligned}
\bar{E}_{\min} = & G_{f,\text{NH}_{3(l)}}^{\circ} \\
& + \frac{N_{\text{R}}}{N_{\text{P}}} \left[ \begin{aligned} & x_{\text{NH}_4^+,\text{R}} G_{\text{NH}_4^+} + x_{\text{NH}_3,\text{R}} G_{\text{NH}_3} + x_{\text{H}_2\text{O},\text{R}} G_{\text{H}_2\text{O}} + x_{\text{OH}^-,\text{R}} G_{\text{OH}^-} + x_{\text{Na}^+,\text{R}} G_{\text{Na}^+} + x_{\text{Cl}^-,\text{R}} G_{\text{Cl}^-} \\ & + RT \left( \begin{aligned} & x_{\text{NH}_4^+,\text{R}} \ln(\gamma_{\text{NH}_4^+,\text{R}} x_{\text{NH}_4^+,\text{R}}) + x_{\text{NH}_3,\text{R}} \ln(\gamma_{\text{NH}_3,\text{R}} x_{\text{NH}_3,\text{R}}) \\ & + x_{\text{H}_2\text{O},\text{R}} \ln(\gamma_{\text{H}_2\text{O},\text{R}} x_{\text{H}_2\text{O},\text{R}}) + x_{\text{H}^+,\text{R}} \ln(\gamma_{\text{H}^+,\text{R}} x_{\text{H}^+,\text{R}}) + x_{\text{OH}^-,\text{R}} \ln(\gamma_{\text{OH}^-,\text{R}} x_{\text{OH}^-,\text{R}}) \\ & + x_{\text{Na}^+,\text{R}} \ln(\gamma_{\text{Na}^+,\text{R}} x_{\text{Na}^+,\text{R}}) + x_{\text{Cl}^-,\text{R}} \ln(\gamma_{\text{Cl}^-,\text{R}} x_{\text{Cl}^-,\text{R}}) \end{aligned} \right) \end{aligned} \right] \\
& - \frac{N_{\text{F}}}{N_{\text{P}}} \left[ \begin{aligned} & x_{\text{NH}_4^+,\text{F}} G_{\text{NH}_4^+} + x_{\text{NH}_3,\text{F}} G_{\text{NH}_3} + x_{\text{H}_2\text{O},\text{F}} G_{\text{H}_2\text{O}} + x_{\text{OH}^-,\text{F}} G_{\text{OH}^-} + x_{\text{Na}^+,\text{F}} G_{\text{Na}^+} + x_{\text{Cl}^-,\text{F}} G_{\text{Cl}^-} \\ & + RT \left( \begin{aligned} & x_{\text{NH}_4^+,\text{F}} \ln(\gamma_{\text{NH}_4^+,\text{F}} x_{\text{NH}_4^+,\text{F}}) + x_{\text{NH}_3,\text{R}} \ln(\gamma_{\text{NH}_3,\text{R}} x_{\text{NH}_3,\text{R}}) \\ & + x_{\text{H}_2\text{O},\text{F}} \ln(\gamma_{\text{H}_2\text{O},\text{F}} x_{\text{H}_2\text{O},\text{F}}) + x_{\text{H}^+,\text{F}} \ln(\gamma_{\text{H}^+,\text{F}} x_{\text{H}^+,\text{F}}) + x_{\text{OH}^-,\text{F}} \ln(\gamma_{\text{OH}^-,\text{F}} x_{\text{OH}^-,\text{F}}) \\ & + x_{\text{Na}^+,\text{F}} \ln(\gamma_{\text{Na}^+,\text{F}} x_{\text{Na}^+,\text{F}}) + x_{\text{Cl}^-,\text{F}} \ln(\gamma_{\text{Cl}^-,\text{F}} x_{\text{Cl}^-,\text{F}}) \end{aligned} \right) \end{aligned} \right] \quad (\text{A.19})
\end{aligned}$$

$$\begin{aligned}
\bar{E}_{\min} = & \frac{1}{x_{\text{TAN,P}}} \left[ x_{\text{NH}_3,\text{P}} G_{\text{NH}_3} + x_{\text{H}_2\text{O},\text{P}} G_{\text{H}_2\text{O}} + x_{\text{OH}^-, \text{P}} G_{\text{OH}^-} + x_{\text{Na}^+, \text{P}} G_{\text{Na}^+} + x_{\text{Cl}^-, \text{P}} G_{\text{Cl}^-} \right. \\
& + RT \left( \begin{aligned} & x_{\text{NH}_3,\text{P}} \ln(\gamma_{\text{NH}_3,\text{P}} x_{\text{NH}_3,\text{P}}) + x_{\text{H}_2\text{O},\text{P}} \ln(\gamma_{\text{H}_2\text{O},\text{P}} x_{\text{H}_2\text{O},\text{P}}) \\ & + x_{\text{H}^+, \text{P}} \ln(\gamma_{\text{H}^+, \text{P}} x_{\text{H}^+, \text{P}}) + x_{\text{OH}^-, \text{P}} \ln(\gamma_{\text{OH}^-, \text{P}} x_{\text{OH}^-, \text{P}}) \\ & + x_{\text{Na}^+, \text{P}} \ln(\gamma_{\text{Na}^+, \text{P}} x_{\text{Na}^+, \text{P}}) + x_{\text{Cl}^-, \text{P}} \ln(\gamma_{\text{Cl}^-, \text{P}} x_{\text{Cl}^-, \text{P}}) \end{aligned} \right) \left. \right] \\
& + \frac{N_{\text{R}}}{x_{\text{TAN,P}} N_{\text{P}}} \left[ x_{\text{NH}_4^+, \text{R}} G_{\text{NH}_4^+} + x_{\text{NH}_3, \text{R}} G_{\text{NH}_3} + x_{\text{H}_2\text{O}, \text{R}} G_{\text{H}_2\text{O}} + x_{\text{OH}^-, \text{R}} G_{\text{OH}^-} + x_{\text{Na}^+, \text{R}} G_{\text{Na}^+} + x_{\text{Cl}^-, \text{R}} G_{\text{Cl}^-} \right. \\
& + RT \left( \begin{aligned} & x_{\text{NH}_4^+, \text{R}} \ln(\gamma_{\text{NH}_4^+, \text{R}} x_{\text{NH}_4^+, \text{R}}) + x_{\text{NH}_3, \text{R}} \ln(\gamma_{\text{NH}_3, \text{R}} x_{\text{NH}_3, \text{R}}) \\ & + x_{\text{H}_2\text{O}, \text{R}} \ln(\gamma_{\text{H}_2\text{O}, \text{R}} x_{\text{H}_2\text{O}, \text{R}}) + x_{\text{H}^+, \text{R}} \ln(\gamma_{\text{H}^+, \text{R}} x_{\text{H}^+, \text{R}}) + x_{\text{OH}^-, \text{R}} \ln(\gamma_{\text{OH}^-, \text{R}} x_{\text{OH}^-, \text{R}}) \\ & + x_{\text{Na}^+, \text{R}} \ln(\gamma_{\text{Na}^+, \text{R}} x_{\text{Na}^+, \text{R}}) + x_{\text{Cl}^-, \text{R}} \ln(\gamma_{\text{Cl}^-, \text{R}} x_{\text{Cl}^-, \text{R}}) \end{aligned} \right) \left. \right] \\
& - \frac{N_{\text{F}}}{x_{\text{TAN,P}} N_{\text{P}}} \left[ x_{\text{NH}_4^+, \text{F}} G_{\text{NH}_4^+} + x_{\text{NH}_3, \text{F}} G_{\text{NH}_3} + x_{\text{H}_2\text{O}, \text{F}} G_{\text{H}_2\text{O}} + x_{\text{OH}^-, \text{F}} G_{\text{OH}^-} + x_{\text{Na}^+, \text{F}} G_{\text{Na}^+} + x_{\text{Cl}^-, \text{F}} G_{\text{Cl}^-} \right. \\
& + RT \left( \begin{aligned} & x_{\text{NH}_4^+, \text{F}} \ln(\gamma_{\text{NH}_4^+, \text{F}} x_{\text{NH}_4^+, \text{F}}) + x_{\text{NH}_3, \text{F}} \ln(\gamma_{\text{NH}_3, \text{F}} x_{\text{NH}_3, \text{F}}) \\ & + x_{\text{H}_2\text{O}, \text{F}} \ln(\gamma_{\text{H}_2\text{O}, \text{F}} x_{\text{H}_2\text{O}, \text{F}}) + x_{\text{H}^+, \text{F}} \ln(\gamma_{\text{H}^+, \text{F}} x_{\text{H}^+, \text{F}}) + x_{\text{OH}^-, \text{F}} \ln(\gamma_{\text{OH}^-, \text{F}} x_{\text{OH}^-, \text{F}}) \\ & + x_{\text{Na}^+, \text{F}} \ln(\gamma_{\text{Na}^+, \text{F}} x_{\text{Na}^+, \text{F}}) + x_{\text{Cl}^-, \text{F}} \ln(\gamma_{\text{Cl}^-, \text{F}} x_{\text{Cl}^-, \text{F}}) \end{aligned} \right) \left. \right] \quad (\text{A.20})
\end{aligned}$$

### A.3 Activity Coefficient Models

**Davies Approximation for Ion Activity Coefficients in Dilute Systems.** The Davies approximation, eqn (A.21), is an empirical extension of the Debye-Huckel theory that can be used to estimate activity coefficients in solutions with ionic strengths,  $I$ ,  $<0.5$  M. For solutions with ionic strengths comparable to or lower than hydrolyzed urine, the Davies approximation for activity coefficients resulted in the best agreement with experimental results compared to other methods, including the B-dot and Millero-Scriber methods.<sup>67</sup>

$$\log \gamma = -Az^2 \left( \frac{\sqrt{I}}{1+\sqrt{I}} - 0.3I \right) \quad (\text{A.21})$$

Here,  $A = 1.82 \times 10^6 (\epsilon T)^{-3/2} \approx 0.509$ ,  $z$  is the valency of the ion,  $\epsilon$  is the dielectric constant,  $T$  is absolute temperature.  $I = 0.5 \sum C_i z_i^2$  and  $C$  is the concentration of ion.

The Davies approximation was applied to calculate the activity coefficient for ions, including  $\text{NH}_4^+$ ,  $\text{SO}_4^{2-}$ ,  $\text{H}_2\text{PO}_4^-$ ,  $\text{HPO}_4^{2-}$ ,  $\text{Mg}^{2+}$ ,  $\text{K}^+$ ,  $\text{Na}^+$ ,  $\text{Cl}^-$ , and  $\text{NO}_3^-$ , for all streams that fit the criteria,  $I \leq 0.5$ , which includes the simplified versions of hydrolyzed urine that only include nutrients and co-species components, fresh urine, domestic WW effluent, 2° WW effluent, and greywater. Not that this method is not applicable for determining activity coefficients of neutral components, such as, urea,  $\text{CO}(\text{NH}_2)_2$ .

**Non-Random Two Liquid Model for  $\text{NH}_3$  and  $\text{H}_2\text{O}$  Activity Coefficients in Concentrated Product Streams of 1.0 M, 5.0 M and 10 M  $\text{NH}_3(\text{aq})$ .** The Non-Random Two Liquid (NRTL) model for a binary mixture, eqns (A.22)–(A.24), is widely applied in phase-equilibria calculations for the quantification of activity coefficients. The NRTL method has been used to determine  $\gamma_{\text{H}_2\text{O}}$  and  $\gamma_{\text{NH}_3}$  in binary  $\text{NH}_3/\text{H}_2\text{O}$  systems.<sup>104, 105</sup>

$$\ln \gamma_1 = x_2 \left[ \tau_{21} \left( \frac{G_{21}}{x_1 + x_2 G_{21}} \right)^2 + \frac{\tau_{12} G_{12}}{(x_2 + x_1 G_{12})^2} \right] \quad (\text{A.22})$$

$$\ln \gamma_2 = x_1 \left[ \tau_{12} \left( \frac{G_{12}}{x_2 + x_1 G_{12}} \right)^2 + \frac{\tau_{21} G_{21}}{(x_1 + x_2 G_{21})^2} \right] \quad (\text{A.23})$$

$$\begin{cases} \ln G_{12} = -\alpha_{12} \tau_{12} \\ \ln G_{21} = -\alpha_{21} \tau_{21} \\ \tau_{12} = \tau_{12}^{(0)} + \frac{\tau_{12}^{(1)}}{T} \\ \tau_{21} = \tau_{21}^{(0)} + \frac{\tau_{21}^{(1)}}{T} \end{cases} \quad (\text{A.24})$$

Here,  $G_{12}$  and  $G_{21}$  are interaction energy parameters,  $\tau_{12}$  and  $\tau_{21}$  are dimensionless interaction parameters, at reference point 0 and state point 1, and  $\alpha_{12}$  and  $\alpha_{21}$  are non-randomness parameters. Parameters values from literature were used for the calculations.<sup>104, 105</sup> The NRTL method was applied to determine  $\gamma_{\text{H}_2\text{O}}$  and  $\gamma_{\text{NH}_3}$  in binary TAN/H<sub>2</sub>O streams, where nearly all TAN is present as NH<sub>3</sub>; product streams 1.0 M NH<sub>3(aq)</sub>, 5.0 M NH<sub>3(aq)</sub>, and 10 NH<sub>3(aq)</sub> met these criteria.

**Experimentally Measured Osmotic and Activity Coefficients for Urea-Water Solutions.** To account for nonideal behavior of urea, CO(NH<sub>2</sub>)<sub>2</sub>, and H<sub>2</sub>O, reported literature values for  $\gamma_{\text{CO(NH}_2)_2}$  and  $\gamma_{\text{H}_2\text{O}}$  determined using vapor pressure osmometry data were utilized. For CO(NH<sub>2</sub>)<sub>2</sub> concentrations ranging from 0.0103 to 1.6927 M,  $\gamma_{\text{CO(NH}_2)_2} = -0.0663C_{\text{CO(NH}_2)_2} + 0.9976$  and  $\gamma_{\text{H}_2\text{O}} = -0.0328C_{\text{CO(NH}_2)_2} + 0.9987$ .<sup>106</sup> Urea and water activity coefficients at CO(NH<sub>2</sub>)<sub>2</sub> concentrations relevant to the analysis in this study were calculated with the linear relationships.

**Activity Coefficients for 1.0 M  $\text{KNO}_{3(\text{aq})}$  and 1.0 M  $\text{NH}_4\text{NO}_{3(\text{aq})}$  recovery.** To account for nonideal behavior in systems with  $I > 0.5$  M, specifically, 1.0 M  $\text{KNO}_{3(\text{aq})}$  and 1.0 M  $\text{NH}_4\text{NO}_{3(\text{aq})}$ , activity coefficients based on isopiestic data<sup>301</sup> at compositions relevant to the analysis were utilized.

**Table A.3.** Standard state Gibbs free energy of formation for species in an aqueous solution.<sup>1,2</sup>

Species in Aqueous Solution	$G_i$ (kJ/mol)
$\text{NH}_4^+$	-79.3
$\text{NH}_3$	-26.6
$\text{SO}_4^{2-}$	-744.5
$\text{H}_2\text{PO}_4^-$	-1130.2
$\text{HPO}_4^{2-}$	-1089.2
$\text{PO}_4^{3-}$	-1081.7
$\text{K}^+$	-283.3
$\text{Mg}^{2+}$	-454.8
$\text{NO}_3^-$	-111.3
$\text{H}_2\text{O}$	-237.1
$\text{OH}^-$	-157.2
$\text{H}^+$	0.0

**Table A.4.** Standard state Gibbs free energy of formation for liquid and solid products.<sup>1-3</sup> For urea, CO(NH<sub>2</sub>)<sub>2</sub>, the Gibbs free energy of dissolution, or the change in Gibbs free energy from CO(NH<sub>2</sub>)<sub>2(aq)</sub> to CO(NH<sub>2</sub>)<sub>2(s)</sub>,  $G_{f,\text{CO(NH}_2)_2(s)}^\circ - G_{f,\text{CO(NH}_2)_2(\text{aq})}^\circ$  is presented.<sup>302, 303</sup>

<b>Product</b>	<b><math>G_{f,P}^\circ</math> (kJ/mol)</b>
NH <sub>3(l)</sub>	-16.410
(NH <sub>4</sub> ) <sub>2</sub> SO <sub>4(s)</sub>	-901.7
(NH <sub>4</sub> )H <sub>2</sub> PO <sub>4(s)</sub>	-1210.38
KMgPO <sub>4</sub> ·6H <sub>2</sub> O <sub>(s)</sub>	-3241
NH <sub>4</sub> MgPO <sub>4</sub> ·6H <sub>2</sub> O <sub>(s)</sub>	-3051.1
KH <sub>2</sub> PO <sub>4(s)</sub>	-1415.85
KNO <sub>3(s)</sub>	-394.93
NH <sub>4</sub> NO <sub>3(s)</sub>	-183.9
CO(NH <sub>2</sub> ) <sub>2(s)</sub>	-5.77

**Table A.5.** Molar minimum energies of recovery,  $\bar{E}_{\min}$ , for TAN products from each waste stream presented in Figure 2.3A.  $\bar{E}_{\min}$  values are calculated at low and high TAN concentrations in the waste stream and low and high waste stream pH, i.e., four  $\bar{E}_{\min}$  values calculated for each recovery scenario. The high and low wastewater pH ranges are respectively indicated by H and L, which correspond to the H and L  $\bar{E}_{\min}$  values. Also shown is the percent decrease in  $\bar{E}_{\min}$  of solution L relative to solution H (i.e., from low to high pH range).

Product	Type of WW	High pH (H)	Low pH (L)	$\bar{E}_{\min}$ (kJ/mol-TAN)					
				Low [TAN]			High [TAN]		
				H	L	Decrease from L to H (%)	H	L	Decrease from L to H (%)
<b>(NH<sub>4</sub>)<sub>2</sub>SO<sub>4(s)</sub></b>	Greywater	9	5	59.73	62.24	4.03	43.12	45.66	5.58
	2° WW effluent	7.7	6.8	53.37	53.56	0.36	39.94	39.75	0.47
	Domestic WW	8.5	6.5	43.15	44.28	2.54	38.28	39.44	2.94
	Fresh Urine	7.5	6	36.45	36.59	0.38	29.22	29.35	0.46
	Hydrolyzed Urine	9.2	9	25.45	26.24	2.99	21.02	21.73	3.28
<b>NH<sub>3(l)</sub></b>	Greywater	9	5	83.64	100.38	16.67	72.97	89.72	18.67
	2° WW effluent	7.7	6.8	98.66	99.63	0.97	85.08	86.06	1.13
	Domestic WW	8.5	6.5	82.48	89.11	7.44	77.51	84.16	7.90
	Fresh Urine	7.5	6	79.87	80.54	0.83	77.53	78.20	0.86
	Hydrolyzed Urine	9.2	9	51.63	57.26	9.83	49.81	55.44	10.15
<b>10 M NH<sub>3(aq)</sub></b>	Greywater	9	5	67.64	85.28	20.68	56.97	74.63	23.67
	2° WW effluent	7.7	6.8	83.49	84.52	1.22	69.92	70.95	1.46
	Domestic WW	8.5	6.5	67.00	74.01	9.47	62.03	69.06	10.18
	Fresh Urine	7.5	6	64.73	65.44	1.09	62.39	63.10	1.13
	Hydrolyzed Urine	9.2	9	35.37	41.27	14.30	33.57	39.46	14.93
<b>5.0 M NH<sub>3(aq)</sub></b>	Greywater	9	5	54.14	82.45	34.34	54.14	71.80	24.60
	2° WW effluent	7.7	6.8	80.67	81.70	1.26	67.09	68.12	1.52
	Domestic WW	8.5	6.5	64.17	71.18	9.84	59.20	66.23	10.61
	Fresh Urine	7.5	6	61.90	62.61	1.13	59.56	60.27	1.18
	Hydrolyzed Urine	9.2	9	32.57	38.46	15.32	30.81	36.69	16.01
<b>1.0 M NH<sub>3(aq)</sub></b>	Greywater	9	5	48.10	76.41	37.05	48.10	65.76	26.86
	2° WW effluent	7.7	6.8	74.63	75.65	1.36	61.05	62.09	1.67
	Domestic WW	8.5	6.5	58.13	65.14	10.76	53.17	60.20	11.69
	Fresh Urine	7.5	6	55.86	56.62	1.34	53.52	54.36	1.54
	Hydrolyzed Urine	9.2	9	26.80	33.07	18.96	25.35	32.03	20.86

**Table A.6.** Molar minimum energies of recovery,  $\bar{E}_{\min}$ , for TOP products from each waste stream presented in Figure 2.3B.  $\bar{E}_{\min}$  values are calculated at low and high TOP and co-species concentrations in the waste stream and low and high waste stream pH, i.e., four  $\bar{E}_{\min}$  values calculated for each recovery scenario. The high and low wastewater pH ranges are respectively indicated by H and L, which correspond to the H and L  $\bar{E}_{\min}$  values. Also shown is the percent decrease in  $\bar{E}_{\min}$  of solution L relative to solution H (i.e., from low to high pH range).

Product	Type of WW	High pH (H)	Low pH (L)	$\bar{E}_{\min}$ (kJ/mol-TOP)					
				Low [TOP] and [Co-species]			High [TOP] and [Co-species]		
				H	L	Decrease from L to H (%)	H	L	Decrease from L to H (%)
<b>KMgPO<sub>4</sub>·6(H<sub>2</sub>O)<sub>(s)</sub></b>	Greywater	9	5	126.25	165.50	23.72	99.08	138.28	28.35
	2° WW effluent	7.7	6.8	106.56	125.56	15.13	96.30	114.97	16.24
	Domestic WW	8.5	6.5	90.99	124.47	26.89	87.92	120.80	27.22
	Fresh Urine	7.5	6	88.31	110.12	19.81	83.84	105.53	20.55
	Hydrolyzed Urine	9.2	9						
<b>NH<sub>4</sub>MgPO<sub>4</sub>·6H<sub>2</sub>O<sub>(s)</sub></b>	Greywater	9	5	108.07	147.60	26.78	79.79	119.16	33.04
	2° WW effluent	7.7	6.8	102.84	120.90	14.93	81.54	99.27	17.86
	Domestic WW	8.5	6.5	78.25	110.91	29.45	70.12	102.31	31.46
	Fresh Urine	7.5	6	75.07	95.65	21.52	71.53	91.83	22.11
	Hydrolyzed Urine	9.2	9						
<b>KH<sub>2</sub>PO<sub>4</sub>(s)</b>	Greywater	9	5	91.09	90.47	-0.69	64.68	63.72	-1.51
	2° WW effluent	7.7	6.8	55.81	57.50	2.93	48.54	50.02	2.95
	Domestic WW	8.5	6.5	50.94	51.25	0.61	48.94	48.85	-0.20
	Fresh Urine	7.5	6	37.18	37.69	1.35	32.84	32.15	-2.14
	Hydrolyzed Urine	9.2	9	42.28	41.26	-2.47	38.97	38.00	-2.56
<b>NH<sub>4</sub>H<sub>2</sub>PO<sub>4</sub>(s)</b>	Greywater	9	5	84.26	86.05	2.08	58.97	60.51	2.54
	2° WW effluent	7.7	6.8	65.87	67.74	2.76	49.04	50.43	2.74
	Domestic WW	8.5	6.5	51.90	53.39	2.79	46.14	46.63	1.06
	Fresh Urine	7.5	6	41.77	39.71	-5.18	39.26	35.48	-10.63
	Hydrolyzed Urine	9.2	9	36.48	36.59	0.28	34.45	34.53	0.24

## A.4 Methodology to Determine the Molar Minimum Energy to Recover N from Hydrolyzed Urine at $Y > 0$

For  $\text{NH}_{3(l)}$  and 1.0 M  $\text{NH}_{3(aq)}$  recovery from hydrolyzed urine, the speciation of TAN in the feed and retentate are not equal. Using Visual Minteq, pH and TAN speciation in the feed and retentate systems at various recovery yields were determined. To capture the buffering capacity of typical hydrolyzed urine, a model solution, consisting of typical concentrations of TAN,  $\text{HCO}_3^-$ ,  $\text{SO}_4^{2-}$ , and TOP found in hydrolyzed urine (Table A.7) was applied as the initial feed stream. TAN material balances were used to determine TAN mole fractions in the retentate. Then, Visual Minteq was used to determine the pH,  $\alpha_{\text{NH}_3}$ , and  $\alpha_{\text{NH}_4^+}$  for the feed and retentate streams in each recovery scenario (Tables A.8 for  $\text{NH}_{3(l)}$  recovery and A.9 for 1.0 M  $\text{NH}_{3(aq)}$  recovery). TAN speciation and material balance were used to determine  $\text{NH}_4^+$  and  $\text{NH}_3$  mole fractions in each stream, which were inputted into eqns (A.10) and (A.11) to calculate  $\bar{E}_{\min}$  for  $\text{NH}_{3(l)}$  and 1.0 M  $\text{NH}_{3(aq)}$ , respectively.

**Table A.7.** Model hydrolyzed urine solution composition consisting of typical TAN,  $\text{HCO}_3^-$ ,  $\text{SO}_4^{2-}$ , and TOP concentrations found in hydrolyzed urine. The target pH, 9.1, is the mid-range pH of hydrolyzed urine.

Salt	Concentration (M)
$\text{NH}_4^+$	0.424
$\text{Na}^+$	0.068
$\text{H}^+$	0.066
$\text{CO}_3^{2-}$	0.212
$\text{SO}_4^{2-}$	0.01
$\text{PO}_4^{3-}$	0.024
$\text{Cl}^-$	0.042

**Table A.8.** Visual Minteq outputs for hydrolyzed urine feed and retentate streams in  $\text{NH}_3(\text{l})$  product recovery scenarios at various recovery yields.

Stream	pH	$\alpha_{\text{NH}_3,\text{R}}$	$\alpha_{\text{NH}_4^+,\text{R}}$
Feed	9.106	0.420	0.580
Retentate at $Y = 0$	9.106	0.420	0.580
Retentate at $Y = 0.005$	9.096	0.418	0.582
Retentate at $Y = 0.2$	8.812	0.272	0.728
Retentate at $Y = 0.5$	6.911	$4.666 \times 10^{-3}$	0.995
Retentate at $Y = 0.8$	5.843	$4.007 \times 10^{-4}$	0.999
Retentate at $Y = 1$	2.278	$1.091 \times 10^{-7}$	1.000

**Table A.9.** Visual Minteq outputs for hydrolyzed urine feed and retentate streams in 1.0 M  $\text{NH}_3(\text{aq})$  product recovery scenarios at various recovery yields.

Stream	pH	$\alpha_{\text{NH}_3,\text{R}}$	$\alpha_{\text{NH}_4^+,\text{R}}$
Feed	9.106	0.420	0.580
Retentate at $Y = 0$	9.106	0.420	0.580
Retentate at $Y = 0.005$	9.095	0.417	0.587
Retentate at $Y = 0.2$	8.813	0.272	0.728
Retentate at $Y = 0.5$	6.900	$4.550 \times 10^{-3}$	0.995
Retentate at $Y = 0.8$	5.823	$5.754 \times 10^{-10}$	1.000
Retentate at $Y = 1$	2.097	$5.754 \times 10^{-10}$	1.000

## A.5 Impact of Recovery Yield on Molar Minimum Energy of Recovery

The  $\bar{E}_{\min}$  trends of  $\text{NH}_3(\text{l})$  and 1.0 M  $\text{NH}_3(\text{aq})$  recovery from hydrolyzed urine as a function of recovery yield are not monotonic, but instead exhibit L-shaped rebounds with initial sharp decreases and followed by gradual increases. To further investigate the underlying reasons for these trends,  $\bar{E}_{\min}$  for  $\text{NH}_3(\text{l})$  recovery from hydrolyzed urine, eqn (A.10), was separated into its contributing terms,  $A$  and  $B$ , and term  $B$  is then further separated into terms  $C$  and  $D$  (eqns (A.25), (A.26), (A.27), and (A.28), respectively). The term that contributes most to the L-shape rebound is  $B (= C + D)$ , i.e., the terms  $C$  and  $D$  dictate the change in  $\bar{E}_{\min}$  with different recovery yields.  $C$  represents the difference in Gibbs free energy of formation of  $\text{NH}_4^+(\text{aq})$  moles in the retentate and feed normalized by moles of product captured; similarly,  $D$  is the difference in Gibbs free energy of formation of  $\text{NH}_4^+(\text{aq})$  moles in the retentate and feed normalized by moles of product captured. Note that  $G_{\text{NH}_4^+}$  and  $G_{\text{NH}_3}$  are constant values of  $-79.3$  kJ/mol and  $-26.6$  kJ/mol, respectively.

$$A = G_{f,\text{NH}_3(\text{l})}^0 + \frac{N_{\text{R}}}{N_{\text{P}}} \left[ RT \left( \begin{aligned} &x_{\text{NH}_4^+,\text{R}} \ln(\gamma_{\text{NH}_4^+,\text{R}} x_{\text{NH}_4^+,\text{R}}) + x_{\text{NH}_3,\text{R}} \ln(\gamma_{\text{NH}_3,\text{R}} x_{\text{NH}_3,\text{R}}) \\ &+ x_{\text{H}_2\text{O},\text{R}} \ln(\gamma_{\text{H}_2\text{O},\text{R}} x_{\text{H}_2\text{O},\text{R}}) + x_{\text{H}^+,\text{R}} \ln(\gamma_{\text{H}^+,\text{R}} x_{\text{H}^+,\text{R}}) \\ &+ x_{\text{OH}^-,\text{R}} \ln(\gamma_{\text{OH}^-,\text{R}} x_{\text{OH}^-,\text{R}}) \end{aligned} \right) \right] \\ - \frac{N_{\text{F}}}{N_{\text{P}}} \left[ RT \left( \begin{aligned} &x_{\text{NH}_4^+,\text{F}} \ln(\gamma_{\text{NH}_4^+,\text{F}} x_{\text{NH}_4^+,\text{F}}) + x_{\text{NH}_4^+,\text{F}} \ln(\gamma_{\text{NH}_4^+,\text{F}} x_{\text{NH}_4^+,\text{F}}) \\ &+ x_{\text{H}_2\text{O},\text{F}} \ln(\gamma_{\text{H}_2\text{O},\text{F}} x_{\text{H}_2\text{O},\text{F}}) + x_{\text{H}^+,\text{F}} \ln(\gamma_{\text{H}^+,\text{F}} x_{\text{H}^+,\text{F}}) \\ &+ x_{\text{OH}^-,\text{F}} \ln(\gamma_{\text{OH}^-,\text{F}} x_{\text{OH}^-,\text{F}}) \end{aligned} \right) \right] \quad (\text{A.25})$$

$$- \frac{N_{\text{F}}}{N_{\text{P}}} \left[ x_{\text{NH}_4^+,\text{F}} G_{\text{NH}_4^+} + x_{\text{NH}_3,\text{F}} G_{\text{NH}_3} + x_{\text{H}_2\text{O},\text{F}} G_{\text{H}_2\text{O}} + x_{\text{OH}^-,\text{F}} G_{\text{OH}^-} \right]$$

$$B = \frac{N_{\text{R}}}{N_{\text{P}}} \left[ x_{\text{NH}_4^+,\text{R}} G_{\text{NH}_4^+} + x_{\text{NH}_3,\text{R}} G_{\text{NH}_3} \right] - \frac{N_{\text{F}}}{N_{\text{P}}} \left[ x_{\text{NH}_4^+,\text{F}} G_{\text{NH}_4^+} + x_{\text{NH}_3,\text{F}} G_{\text{NH}_3} \right] \quad (\text{A.26})$$

$$C = \frac{N_R}{N_p} \left[ x_{\text{NH}_4^+, \text{R}} G_{\text{NH}_4^+} \right] - \frac{N_F}{N_p} \left[ x_{\text{NH}_4^+, \text{F}} G_{\text{NH}_4^+} \right] \quad (\text{A.27})$$

$$D = \frac{N_R}{N_p} \left[ x_{\text{NH}_3, \text{R}} G_{\text{NH}_3} \right] - \frac{N_F}{N_p} \left[ x_{\text{NH}_3, \text{F}} G_{\text{NH}_3} \right] \quad (\text{A.28})$$

Figure A.1 displays the contributions of each term toward  $\bar{E}_{\min}$  and shows that  $C$  follows an L-shaped rebound (i.e., a sharp decrease with increasing  $Y$  followed by a more gradual increase with increasing  $Y$ ), which is similar to the  $\bar{E}_{\min}$  trend. Initially,  $C$  decreases as  $Y$  increases, indicating that the difference between moles of  $\text{NH}_4^+$  in the feed and retentate decreases with the initial increase in  $Y$ . This is due to the decline in retentate pH with higher recovery yields, which corresponds to increased  $\alpha_{\text{NH}_4^+, \text{R}}$  and decreased  $\alpha_{\text{NH}_3, \text{R}}$  (see Tables A.8 and A.9 for pH and speciation in the feed and retentate at different recovery yields). Although increased recovery yield results in lower TAN in the retentate, a higher fraction of TAN remaining in the retentate speciates to  $\text{NH}_4^+$ , thus  $C$  initially decreases with higher recovery yield. However, once the pH of the retentate is sufficiently lower than the  $\text{p}K_{\text{a}}$ , such that  $\text{NH}_4^+$  is predominant compared to  $\text{NH}_3$ , additional increase in  $Y$  results in reduced  $\text{NH}_4^+$  in the retentate. At this point,  $C$  begins to increase with higher recovery yield.  $D$  follows the opposite trend as  $C$  with an initial sharp increase with higher recovery yields followed by a gradual decrease with higher recovery yields. Initially,  $\text{NH}_{3(\text{aq})}$  in the retentate are lost to both the product and protonation to  $\text{NH}_4^+$ . Then, once essentially all TAN is present as  $\text{NH}_3$ , increases in  $Y$  no longer result in significant changes to speciation, thus  $D$  increases.

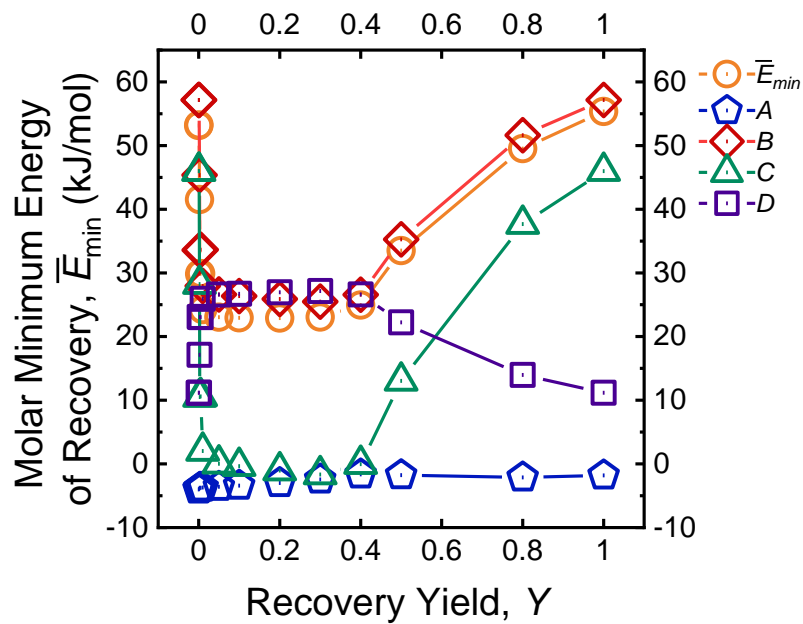


**Figure A.1.** Molar minimum energy,  $\bar{E}_{min}$ , as a function of recovery yield to recover  $\text{NH}_{3(l)}$  from hydrolyzed urine and the contributing terms  $A$ ,  $B$ ,  $C$ , and  $D$ .

**Table A.10.** The change in the sum of the standard state Gibbs free energy of individual ions,  $\sum x_i G_i$ , between the final state (product and retentate) and initial state (waste stream feed); denoted by  $\Delta \sum x_i G_i$ . Note that a range is provided for  $\text{NH}_4\text{NO}_3(\text{aq})$  and  $\text{NH}_4\text{NO}_3(\text{s})$  recoveries because this value is dependent on pH of the waste stream.

<b>Waste Stream</b>	<b>Product</b>	$\Delta \sum x_i G_i$
<b>Secondary wastewater effluent</b>	$\text{KNO}_3(\text{s})$	-0.330
	$\text{NH}_4\text{NO}_3(\text{s})$	5.797–7.569
	$\text{KNO}_3(\text{aq})$	0.000
	$\text{NH}_4\text{NO}_3(\text{aq})$	-0.002
<b>Fresh urine</b>	$\text{Urea}(\text{aq})$	0.000
	$\text{Urea}(\text{s})$	-5.774

**Table A.11.** Molar minimum energy for recovery of select products,  $\text{NH}_{3(l)}$  and 1.0 M  $\text{NH}_{3(aq)}$ , from waste streams of secondary wastewater effluent and hydrolyzed urine calculated with the exclusion and inclusion of passive species,  $\text{Na}^+$  and  $\text{Cl}^-$ . All calculations considered nutrients and co-species of TAN,  $\text{H}_2\text{O}$ ,  $\text{H}^+$ , and  $\text{OH}^-$ . Eqns (A.6) and (A.7) were applied for the determination of  $\bar{E}_{\min}$  to recover  $\text{NH}_{3(l)}$  and 1.0 M  $\text{NH}_{3(aq)}$ , from waste streams excluding  $\text{Na}^+$  and  $\text{Cl}^-$  species. Eqns (A.19) and (A.20) were applied for the determination of  $\bar{E}_{\min}$ . Note that the mid-range pH and TAN concentration in each waste stream were utilized in the analysis, thus the mid-range molar minimum energy of recovery is reported. The percent increase in molar minimum energy for recovery observed when including  $\text{Na}^+$  and  $\text{Cl}^-$  species in the analysis is also presented for each recovery scenario.

Waste Stream	Product	Specific Minimum Energy for Recovery, $\bar{E}_{\min}$ (kJ/mol)		
		Excluding $\text{Na}^+$ and $\text{Cl}^-$ Species	Including $\text{Na}^+$ and $\text{Cl}^-$ Species	Percent Increase (%)
Secondary WW Effluent	$\text{NH}_{3(l)}$	87.45	87.48	0.22
Secondary WW Effluent	1.0 M $\text{NH}_{3(aq)}$	63.46	63.70	0.38
Hydrolyzed Urine	$\text{NH}_{3(l)}$	50.47	50.52	0.10
Hydrolyzed Urine	1.0 M $\text{NH}_{3(aq)}$	26.39	26.89	1.89

## Appendix B: Supporting Information for Chapter 3

### B.1 Donnan Equilibrium

**Binary Systems.** At Donnan equilibrium, the electrochemical potentials of a charged species,  $i$ , in the feed solution, FS, and receiver solution, RS, are equal, as described by eqn (B.1).

$$\mu_i^0 + RT \ln a_{i,RS,f} + z_i F \psi_{RS,f} = \mu_i^0 + RT \ln a_{i,FS,f} + z_i F \psi_{FS,f} \quad (\text{B.1})$$

where  $\mu$  is chemical potential,  $T$  is absolute temperature,  $a$  is activity,  $z$  is ion valence,  $\psi$  is electrical potential,  $R$  is the gas constant, and  $F$  is Faraday's constant; superscript 0 indicates standard state, whereas subscripts  $f$ , FS, and RS refer to final state, feed stream, and receiver stream, respectively. Rearranging eqn (B.1) yields:

$$\frac{F(\psi_{RS,f} - \psi_{FS,f})}{RT} = \ln \left( \frac{a_{i,FS,f}}{a_{i,RS,f}} \right)^{1/z} \quad (\text{B.2})$$

In Donnan dialysis, DD, with initial conditions of  $\text{H}_x\text{PO}_4^{(3-x)-}$  as the sole anion in the FS and  $\text{Cl}^-$  as the sole anion in the RS, the final activities of  $\text{H}_x\text{PO}_4^{(3-x)-}$  and  $\text{Cl}^-$  in the FS and RS are related to the electrical potential between the FS and RS,  $\psi_{RS,f} - \psi_{FS,f}$ .

$$\frac{F(\psi_{RS,f} - \psi_{FS,f})}{RT} = \ln \left( \frac{a_{\text{H}_x\text{PO}_4^{(3-x)-}, \text{FS}, f}}{a_{\text{H}_x\text{PO}_4^{(3-x)-}, \text{RS}, f}} \right)^{1/(3-x)} \quad (\text{B.3})$$

$$\frac{F(\psi_{RS,f} - \psi_{FS,f})}{RT} = \ln \left( \frac{a_{\text{Cl}^-, \text{FS}, f}}{a_{\text{Cl}^-, \text{RS}, f}} \right) \quad (\text{B.4})$$

Because  $\psi_{RS,f} - \psi_{FS,f}$  is the same for the two ions, eqns (B.3) and (B.4) can be combined. Further assuming activity coefficients,  $\gamma$ , approximate to unity simplifies activities to molar concentrations:  $a = \gamma [i] \approx [i]$ , yielding eqn (3.1) in Chapter 3.

$$\frac{[\text{H}_x\text{PO}_4^{(3-x)-}]_{\text{FS},f}}{[\text{H}_x\text{PO}_4^{(3-x)-}]_{\text{RS},f}} = \left( \frac{[\text{Cl}^-]_{\text{FS},f}}{[\text{Cl}^-]_{\text{RS},f}} \right)^{(3-x)} \quad (3.1)$$

The final concentrations at Donnan equilibrium can be determined by applying material balance using initial  $\text{H}_x\text{PO}_4^{(3-x)-}$  and  $\text{Cl}^-$  concentrations, represented by subscript 0. To maintain electroneutrality, one  $\text{H}_x\text{PO}_4^{(3-x)-}$  ion exchanges with  $(3-x)\text{Cl}^-$  ion(s) across the anion exchange membrane. As  $[\text{H}_x\text{PO}_4^{(3-x)-}]_{\text{RS},0} = 0$  and  $[\text{Cl}^-]_{\text{FS},0} = 0$ , and for specific scenario of equal RS and FS volumes, i.e.,  $V_{\text{RS}} = V_{\text{FS}}$ , eqns (B.5)–(B.7) are material balances for the ions.

$$[\text{H}_x\text{PO}_4^{(3-x)-}]_{\text{RS},f} = (3-x)[\text{Cl}^-]_{\text{FS},f} \quad (B.5)$$

$$[\text{H}_x\text{PO}_4^{(3-x)-}]_{\text{FS},f} = [\text{H}_x\text{PO}_4^{(3-x)-}]_{\text{FS},0} - [\text{H}_x\text{PO}_4^{(3-x)-}]_{\text{RS},f} \quad (B.6)$$

$$[\text{Cl}^-]_{\text{FS},f} = [\text{Cl}^-]_{\text{RS},0} - [\text{Cl}^-]_{\text{RS},f} \quad (B.7)$$

Substituting eqns (B.6) and (B.7) into eqn (3.1) yields eqn (B.8).

$$\frac{[\text{H}_x\text{PO}_4^{(3-x)-}]_{\text{FS},0} - [\text{H}_x\text{PO}_4^{(3-x)-}]_{\text{RS},f}}{[\text{H}_x\text{PO}_4^{(3-x)-}]_{\text{RS},f}} = \left( \frac{(3-x)[\text{H}_x\text{PO}_4^{(3-x)-}]_{\text{RS},f}}{[\text{Cl}^-]_{\text{RS},0} - (3-x)[\text{H}_x\text{PO}_4^{(3-x)-}]_{\text{RS},f}} \right)^{(3-x)} \quad (B.8)$$

Therefore, final concentrations of  $\text{H}_x\text{PO}_4^{(3-x)-}$  and  $\text{Cl}^-$  in the FS and RS at Donnan equilibrium can be determined using the initial concentrations.

**Multi-Component Systems.** Following the same approach presented above, the following Donnan equilibrium expression can be derived for DD with the initial FS containing multiple anions of  $\text{H}_x\text{PO}_4^{(3-x)-}$ ,  $\text{SO}_4^{2-}$ , and  $\text{Cl}^-$  by substituting the anions for  $i$ .

$$\left( \frac{[\text{H}_x\text{PO}_4^{(3-x)-}]_{\text{FS}}}{[\text{H}_x\text{PO}_4^{(3-x)-}]_{\text{RS}}} \right)^{1/(3-x)} = \left( \frac{[\text{Cl}^-]_{\text{FS}}}{[\text{Cl}^-]_{\text{RS}}} \right) = \left( \frac{[\text{SO}_4^{2-}]_{\text{FS}}}{[\text{SO}_4^{2-}]_{\text{RS}}} \right)^{1/2} \quad (\text{B.4})$$

Similarly, initial concentrations of  $\text{H}_x\text{PO}_4^{(3-x)-}$ ,  $\text{SO}_4^{2-}$ , and  $\text{Cl}^-$  in the FS and RS can be utilized to determine final ion concentrations at Donnan equilibrium. The following presentation considers equivalent RS and FS volumes. To maintain electroneutrality,  $\text{Cl}^-$  transport from the RS to FS is balanced by  $\text{H}_x\text{PO}_4^{(3-x)-}$  and  $\text{SO}_4^{2-}$  transport from the FS to RS, as described in eqn (B.9). Eqns (B.10)–(B.12) are material balances for the different ions.

$$[\text{Cl}^-]_{\text{FS},f} = (3-x)[\text{H}_x\text{PO}_4^{(3-x)-}]_{\text{RS},f} + 2[\text{SO}_4^{2-}]_{\text{RS},f} + [\text{Cl}^-]_{\text{FS},0} \quad (\text{B.9})$$

$$[\text{H}_x\text{PO}_4^{(3-x)-}]_{\text{FS},f} = [\text{H}_x\text{PO}_4^{(3-x)-}]_{\text{FS},0} - [\text{H}_x\text{PO}_4^{(3-x)-}]_{\text{RS},f} \quad (\text{B.10})$$

$$[\text{SO}_4^{2-}]_{\text{FS},f} = [\text{SO}_4^{2-}]_{\text{FS},0} - [\text{SO}_4^{2-}]_{\text{RS},f} \quad (\text{B.11})$$

$$[\text{Cl}^-]_{\text{FS},f} = [\text{Cl}^-]_{\text{FS},0} + [\text{Cl}^-]_{\text{RS},0} - [\text{Cl}^-]_{\text{RS},f} \quad (\text{B.12})$$

Solving eqns (B.9)–(B.12) gives the final concentrations of  $\text{H}_x\text{PO}_4^{(3-x)-}$ ,  $\text{SO}_4^{2-}$ , and  $\text{Cl}^-$  in the FS and RS.

**Systems with Different FS and RS Volumes.** In the systems presented earlier, the FS and RS volumes are equal. In systems where  $V_{\text{FS}} \neq V_{\text{RS}}$ ,  $[i]_{\text{FS},0} - [i]_{\text{FS},f} \neq [i]_{\text{RS},f} - [i]_{\text{RS},0}$  because of the differences in FS and RS volumes. Factoring in the FS and RS volumes,  $\text{Cl}^-$  transport from the RS to FS is balanced by  $\text{H}_x\text{PO}_4^{(3-x)-}$  and  $\text{SO}_4^{2-}$  transport from the FS to RS:

$$[\text{Cl}^-]_{\text{FS},f} V_{\text{FS}} = (3-x)[\text{H}_x\text{PO}_4^{(3-x)-}]_{\text{RS},f} V_{\text{RS}} + 2[\text{SO}_4^{2-}]_{\text{RS},f} V_{\text{RS}} + [\text{Cl}^-]_{\text{FS},0} V_{\text{FS}} \quad (\text{B.13})$$

The following material balances for the multi-component system, eqn (B.14)–(B.16), account for different FS and RS volumes. Again, knowing the initial ion concentrations enables the final ion concentrations in the FS and RS at Donnan equilibrium to be determined.

$$\left[ \text{H}_x \text{PO}_4^{(3-x)-} \right]_{\text{FS},f} V_{\text{FS}} = \left[ \text{H}_x \text{PO}_4^{(3-x)-} \right]_{\text{FS},0} V_{\text{FS}} - \left[ \text{H}_x \text{PO}_4^{(3-x)-} \right]_{\text{RS},f} V_{\text{RS}} \quad (\text{B.14})$$

$$\left[ \text{SO}_4^{2-} \right]_{\text{FS},f} V_{\text{FS}} = \left[ \text{SO}_4^{2-} \right]_{\text{FS},0} V_{\text{FS}} - \left[ \text{SO}_4^{2-} \right]_{\text{RS},f} V_{\text{RS}} \quad (\text{B.15})$$

$$\left[ \text{Cl}^- \right]_{\text{FS},f} V_{\text{FS}} = \left[ \text{Cl}^- \right]_{\text{FS},0} V_{\text{FS}} + \left[ \text{Cl}^- \right]_{\text{RS},0} V_{\text{RS}} - \left[ \text{Cl}^- \right]_{\text{RS},f} V_{\text{RS}} \quad (\text{B.16})$$

## B.2 Simulated Waste Water Softening Regenerant Rinse

Water softening systems typically utilize salts with a monovalent cation (generally NaCl or KCl) to exchange with the captured polyvalent cations (primarily  $\text{Ca}^{2+}$  and  $\text{Mg}^{2+}$ ) in the regeneration process. The regenerant salts are supplied well in excess of stoichiometry and, thus, the recharge wastewaters, termed waste water softening regenerant rinse, have high concentrations of  $\text{Cl}^-$  (as either NaCl or KCl). A solution of mainly  $\text{KCl}_{(\text{aq})}$  was prepared to simulate the waste water softening regenerant rinse, for use as the receiver solution in DD recovery of orthophosphate. Using the specifications of commercially available water softening products from PuroLite<sup>304, 305</sup> (Table B.1) and material flow of the water softening system (calculated values shown in Table B.2), the composition of typical waste water softening regenerant rinse was determined (Table B.3). Note that hardness was simulated with  $\text{MgCl}_2$  (i.e., no  $\text{Ca}^{2+}$ ).

**Table B.1.** Specifications for commercially available water softening products from PuroLite.<sup>304, 305</sup>

Specification	Value
<b>Maximum theoretical capacity for KCl (grains/lb-KCl)</b> <sup>306, 307</sup>	4,708
<b>Typical Capacity, 65% Max (grains/lb-KCl)</b> <sup>306, 307</sup>	2,660
<b>Typical Dose of KCl (lb/ft<sup>3</sup> resin)</b> <sup>304, 305</sup>	20
<b>Volume of resin (ft<sup>3</sup>)</b> <sup>304, 305</sup>	1
<b>Drain for regeneration, i.e., water volume added to flush (L/ft<sup>3</sup> resin)</b> <sup>304, 305</sup>	189

**Table B.2.** Calculated values based on material flow using the specifications in Table B.1.

Calculation	Value
<b>Typical Dose (Moles of KCl)</b>	122
<b>Typical Capacity (Moles of <math>\text{Ca}^{2+}</math> and <math>\text{Mg}^{2+}</math>/lb resin)</b>	0.45
<b>Divalent Cations (<math>\text{M}^{2+}</math>) Released in Waste stream (Moles of <math>\text{Ca}^{2+}</math> and <math>\text{Mg}^{2+}</math>)</b>	9.09
<b><math>\text{K}^+</math> Ions Remaining (Moles)</b>	103
<b><math>\text{Cl}^-</math> Ions (Moles)</b>	122

**Table B.3.** Composition of a typical waste water softening regenerant rinse, determined using the specifications in Table B.1 and calculated values in Table B.2.

<b>Species</b>	<b>Concentration (<math>\times 10^{-3}</math> mol/L)</b>
<b>KCl</b>	547
<b>MgCl<sub>2</sub></b>	48
<b>Total Cl<sup>-</sup></b>	644

### B.3 Simulated Dilute Bittern

Bittern brine is the liquid stream that remains after the crystallization of table salt from seawater. The composition of bittern brine is shown in Table B.4. Note that bittern brine is highly concentrated in chloride at 6.15 mol/L. To achieve a  $[\text{Cl}^-] \approx 600 \times 10^{-3}$  mol/L, a dilution factor of 10 was utilized, and the composition of the diluted stream is presented in Table B.4. The diluted bittern solution utilized in DD experiments ( $252 \times 10^{-3}$  mol/L  $\text{MgCl}_2 \cdot 6\text{H}_2\text{O}$ ,  $77 \times 10^{-3}$  mol/L KCl,  $25 \times 10^{-3}$  mol/L  $\text{MgSO}_4 \cdot 7\text{H}_2\text{O}$ ,  $26 \times 10^{-3}$  mol/L NaCl, and  $8 \times 10^{-3}$  mol/L  $\text{NH}_4\text{Cl}$ ) accounts for all major ions (excluding  $\text{Ca}^{2+}$  and  $\text{Br}^-$ ).

**Table B.4.** Typical ion concentrations in bittern brine<sup>308</sup> and bittern brine diluted by a factor of 10.

	<b>Bittern Brine (mol/L)</b>	<b>Bittern Brine Diluted by a Factor of 10 (<math>\times 10^{-3}</math> mol/L)</b>
<b>Na<sup>+</sup></b>	0.26	26
<b>NH<sub>4</sub><sup>+</sup></b>	0.08	8
<b>K<sup>+</sup></b>	0.14	14
<b>Mg<sup>2+</sup></b>	2.77	277
<b>Ca<sup>2+</sup></b>	trace	trace
<b>Cl<sup>-</sup></b>	6.15	615
<b>Br<sup>-</sup></b>	trace	trace
<b>SO<sub>4</sub><sup>2-</sup></b>	0.25	25

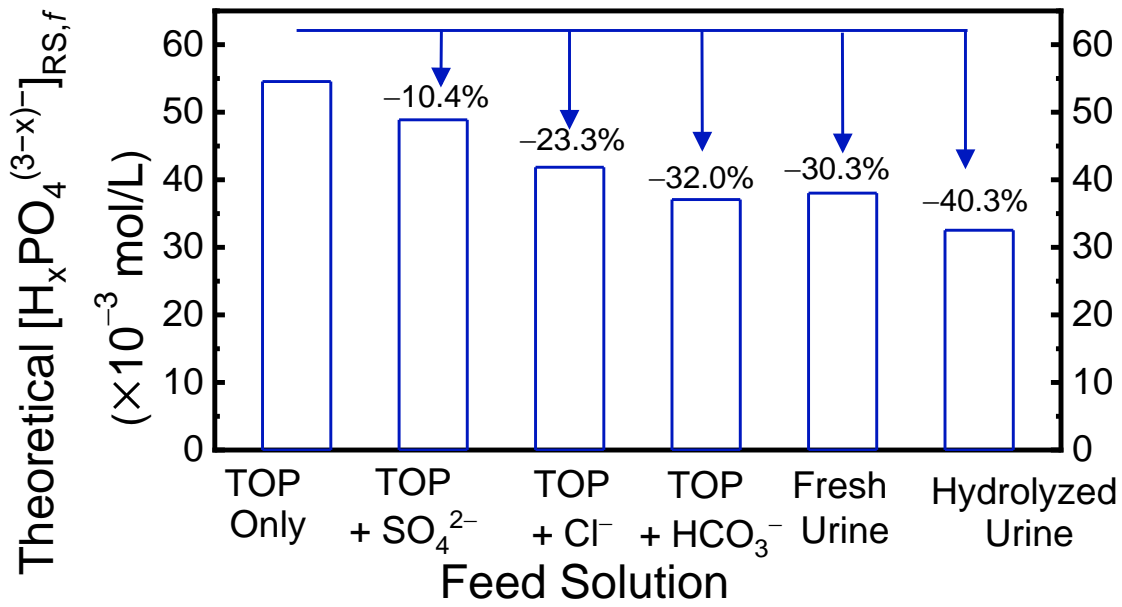


**Figure B.1.** Theoretical  $[\text{H}_x\text{PO}_4^{(3-x)}]_{\text{RS},f}$  in DD operation with FS containing different anions. If present in the FS,  $\text{H}_x\text{PO}_4^{(3-x)-}$ ,  $\text{SO}_4^{2-}$ ,  $\text{Cl}^-$ , and  $\text{HCO}_3^-$  ion concentrations are  $30 \times 10^{-3}$  mol/L,  $16 \times 10^{-3}$  mol/L,  $100 \times 10^{-3}$  mol/L, and  $250 \times 10^{-3}$  mol/L, respectively. The decreases in  $[\text{H}_x\text{PO}_4^{(3-x)-}]_{\text{RS},f}$  relative to the FS containing  $\text{H}_x\text{PO}_4^{(3-x)-}$  only are displayed as labels above the columns.  $V_{\text{FS}}/V_{\text{RS}}$  equal to 2 and receiver solution is  $600 \times 10^{-3}$  mol/L NaCl.

**Table B.5.** Selemion AMV and ASVN membrane characteristics.<sup>6</sup>

<b>Parameter</b>	<b>AMV</b>	<b>ASVN</b>
Characteristic	Standard	Monovalent ion selective
Thickness ( $\mu\text{m}$ )	110	120
Burst Strength (kPa)	200	200
Counterion	$\text{Cl}^-$	$\text{Cl}^-$
Transport Number	>0.96	>0.97

**Table B.6.**  $\Delta[\text{H}_x\text{PO}_4^{(3-x)-}]$  in the feed solution, in operation with FS containing different anions.  $\Delta[\text{H}_x\text{PO}_4^{(3-x)-}] \equiv [\text{H}_x\text{PO}_4^{(3-x)-}]_{\text{FS},0} - [\text{H}_x\text{PO}_4^{(3-x)-}]_{\text{FS},f}$  is defined as the difference between initial and final (at Donnan equilibrium) total orthophosphate concentrations in the feed solution. If present in the FS,  $\text{H}_x\text{PO}_4^{(3-x)-}$ ,  $\text{SO}_4^{2-}$ ,  $\text{Cl}^-$ , and  $\text{HCO}_3^-$  ion concentrations are  $30 \times 10^{-3}$  mol/L,  $16 \times 10^{-3}$  mol/L,  $100 \times 10^{-3}$  mol/L, and  $250 \times 10^{-3}$  mol/L, respectively. The decrease in  $\Delta[\text{H}_x\text{PO}_4^{(3-x)-}]$  relative to the FS containing  $\text{H}_x\text{PO}_4^{(3-x)-}$  only,  $D_{\text{H}_x\text{PO}_4^{(3-x)-}}$ , is also displayed.

FS Anions	$\Delta[\text{H}_x\text{PO}_4^{(3-x)-}]$	$D_{\text{H}_x\text{PO}_4^{(3-x)-}}$ (%)
$\text{H}_x\text{PO}_4^{(3-x)-}$	28.67	N/A
$\text{H}_x\text{PO}_4^{(3-x)-}$ , $\text{SO}_4^{2-}$	27.1	5.26
$\text{H}_x\text{PO}_4^{(3-x)-}$ , $\text{Cl}^-$	24.7	13.7
$\text{H}_x\text{PO}_4^{(3-x)-}$ , $\text{SO}_4^{2-}$ , $\text{Cl}^-$ , i.e., fresh urine	23.4	18.0

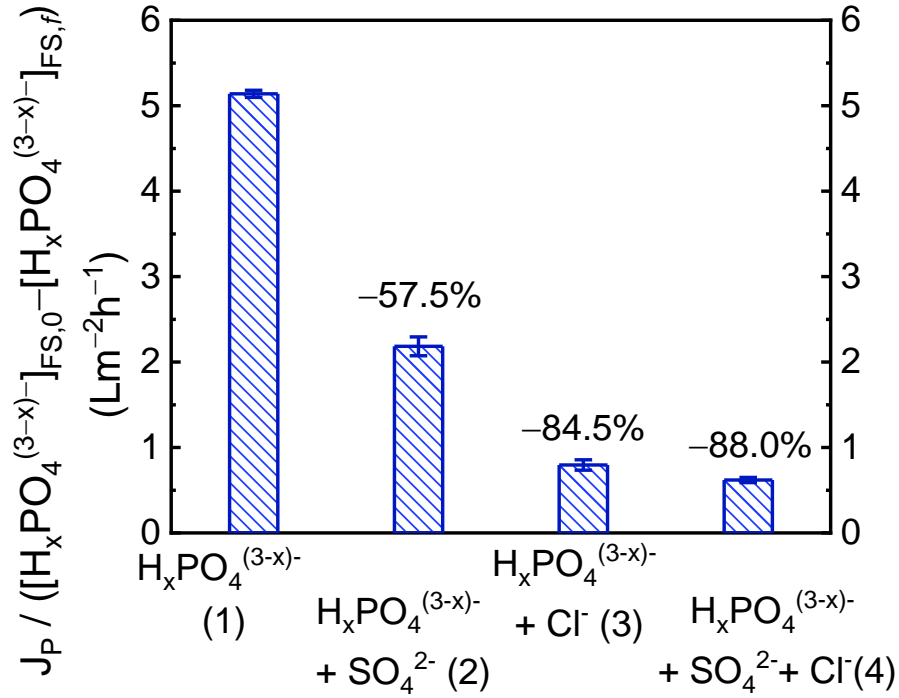


**Figure B.2.** Orthophosphate ion flux,  $J_P$ , normalized by  $[H_xPO_4^{(3-x)-}]_{FS,0} - [H_xPO_4^{(3-x)-}]_{FS,f}$  in DD kinetic experiments with four FS of 1)  $30 \times 10^{-3}$  mol- $H_xPO_4^{(3-x)-}/L$ , 2)  $30 \times 10^{-3}$  mol- $H_xPO_4^{(3-x)-}/L$  and  $16 \times 10^{-3}$  mol- $SO_4^{2-}/L$ , 3)  $30 \times 10^{-3}$  mol- $H_xPO_4^{(3-x)-}/L$  and  $100 \times 10^{-3}$  mol- $Cl^-/L$ , and 4)  $30 \times 10^{-3}$  mol- $H_xPO_4^{(3-x)-}/L$ ,  $100 \times 10^{-3}$  mol- $Cl^-/L$ , and  $16 \times 10^{-3}$  mol- $SO_4^{2-}/L$ . All experiments were operated with  $V_{FS}/V_{RS} = 1$  and  $600 \times 10^{-3}$  mol- $NaCl/L$  as the receiver solution. Data points and error bars are means and standard deviations, respectively, of duplicate experiments. The labels above the columns indicate the change in orthophosphate flux relative to experiments with orthophosphate only feed solution, i.e., FS (1).

#### **B.4 Sorption Experimental Protocol**

AMV membrane coupon of 9.0 cm<sup>2</sup> (0.099 cm<sup>3</sup> volume) was submerged in 50 mL of the feed solution for >24 h to equilibrate. Then, the membrane coupon was transferred to a fresh 50 mL feed solution for another two times for >24 h each, to ensure that previous ion sorption does not interfere with the analysis. Next, the membrane coupon was removed from the feed solution and carefully wiped using a Kimwipe to ensure no residual solution remained on the membrane surface. The membrane coupon was then submerged in 50 mL of DI water for >24 h. After which, the membrane coupon was transferred to 50 mL of 0.10 M NaNO<sub>3</sub> rinse solution for >24 h to enable the desorption of ions. The membrane coupon was immersed in another 50 mL of 0.10 M NaNO<sub>3</sub> rinse solution for >24 h to complete the ion desorption. Ion chromatography was used to analyze the ion concentrations in the DI water and rinse solutions. The total moles in all three solutions were used to determine the total amount of ions sorbed into the AMV membrane. Sorption coefficient,  $X$ , is defined as ions sorbed into the membrane ( $\times 10^{-3}$  moles/cm<sup>3</sup> membrane) normalized by molar concentration in the feed solution.

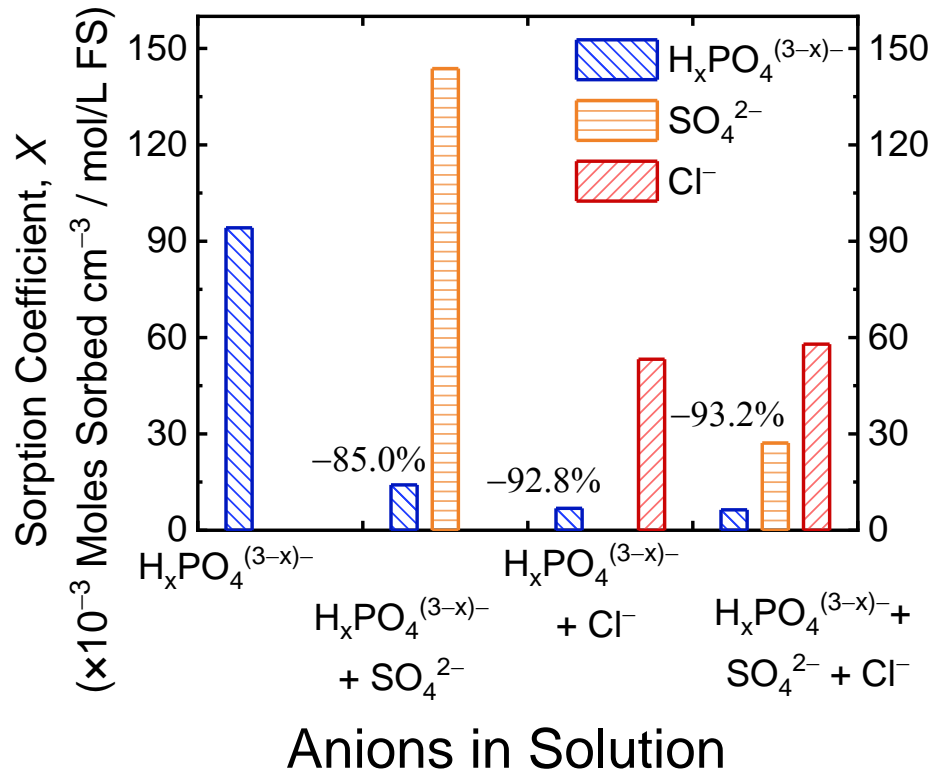


**Figure B.3.** Sorption coefficient,  $X$ , for orthophosphate, sulfate, and chloride into AMV membrane for FS of: 1)  $30 \times 10^{-3}$  mol- $H_xPO_4^{(3-x)-}/L$ , 2)  $30 \times 10^{-3}$  mol- $H_xPO_4^{(3-x)-}/L$  and  $16 \times 10^{-3}$  mol- $SO_4^{2-}/L$ , 3)  $30 \times 10^{-3}$  mol-  $H_xPO_4^{(3-x)-}/L$  and  $100 \times 10^{-3}$  mol- $Cl^-/L$ , and 4)  $30 \times 10^{-3}$  mol-  $H_xPO_4^{(3-x)-}/L$ ,  $100 \times 10^{-3}$  mol- $Cl^-/L$ , and  $16 \times 10^{-3}$  mol- $SO_4^{2-}/L$ , i.e., fresh urine. Sorption coefficient is defined as ions sorbed into the membrane ( $\times 10^{-3}$  moles/cm<sup>3</sup> membrane) normalized by molar concentration in the feed solution.

**Table B.7.** Area specific resistance of Selemion AMV and ASVN membranes for different electrolytes.<sup>309</sup>

<b>Electrolyte</b>	<b>Area Specific Resistance (<math>\Omega \text{ cm}^2</math>)</b>	
	<b>AMV</b>	<b>ASVN</b>
<b>0.5 mol/L NaCl</b>	2.8	3.7
<b>0.25 mol/L Na<sub>2</sub>SO<sub>4</sub></b>	5.5	13
<b>0.5 mol/L HCl</b>	2.5	3.1
<b>0.25 mol/L H<sub>2</sub>SO<sub>4</sub></b>	7.0	9.5

## Appendix C: Supporting Information for Chapter 4

### C.1 Determination of Vapor Pressure

**Vapor Pressure of Water.** The vapor pressure of water in the feed and collector solutions,  $P_{F,W}$  and  $P_{C,W}$ , respectively, in eqn (4.1) of Chapter 4 is determined using the Antoine Equation,  $P_W = \exp[a-b/(T-c)]$ , where unit of  $P_W$  is bar,  $T$  is absolute temperature, and coefficients  $a = 5.204$ ,  $b = 1,734$  K, and  $c = 39.49$  K.<sup>258</sup> Vapor pressure of the mixed systems, i.e., not pure water, is accounted for using Raoult's Law.

**Vapor Pressure of Ammonia.** The vapor pressure of ammonia in the feed and collector solutions,  $P_{F,A}$  and  $P_{C,A}$ , respectively, in eqn (4.1) of Chapter 4 can be estimated using Henry's Law,  $P_A = k_H C_A$ , where  $k_H$  is the Henry's constant for ammonia and  $C_A$  is the ammonia concentration in solution. Henry's constants at different temperatures were calculated based on empirical data from NIST.<sup>257</sup>

**Speciation of Ammoniacal Nitrogen.** The speciation between ammonia and ammonium,  $\text{NH}_4^+ \leftrightarrow \text{NH}_3 + \text{H}^+$ , is governed by eqn (C.1):

$$K_a = \frac{[\text{NH}_3][\text{H}^+]}{[\text{NH}_4^+]} \quad (\text{C.1})$$

where  $K_a$  is the dissociation constant. Total ammoniacal nitrogen, TAN, concentration is the sum of ammonia and ammonium concentrations,  $[\text{TAN}] = [\text{NH}_3] + [\text{NH}_4^+]$ . Speciation of ammoniacal nitrogen between  $\text{NH}_3$  and  $\text{NH}_4^+$  as function of pH for a  $[\text{TAN}] = 500$  mM solution at 25 °C is shown in Figure C.1. When the pH is higher than the  $\text{p}K_a$ , ammonia is the dominant form of ammoniacal nitrogen; conversely, when the pH is lower than the  $\text{p}K_a$ , ammonium is the dominant form. The temperature dependence of  $K_a$  was accounted for using VisualMinteq. At the simulated

urine feed solution pH of 9.4–8.4 for 20–60 °C,  $pK_a$  is 9.4–8.3<sup>310</sup> and, therefore,  $NH_{3(aq)}$  and  $NH_4^+$  are of approximately equal concentrations (i.e.,  $\approx 250$  mM).

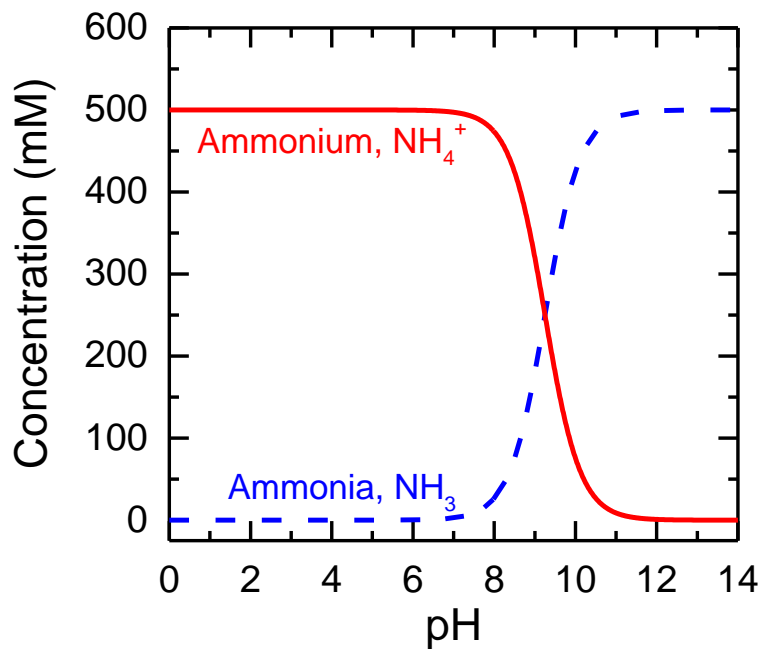


**Figure C.1.** Concentration of ammonia,  $NH_3$ , and ammonium,  $NH_4^+$ , as a function of pH (dashed blue and solid red lines, respectively). Total ammoniacal nitrogen, TAN, concentration of the solution is 500 mM and  $pK_a$  is 9.25 for temperature of 25 °C.

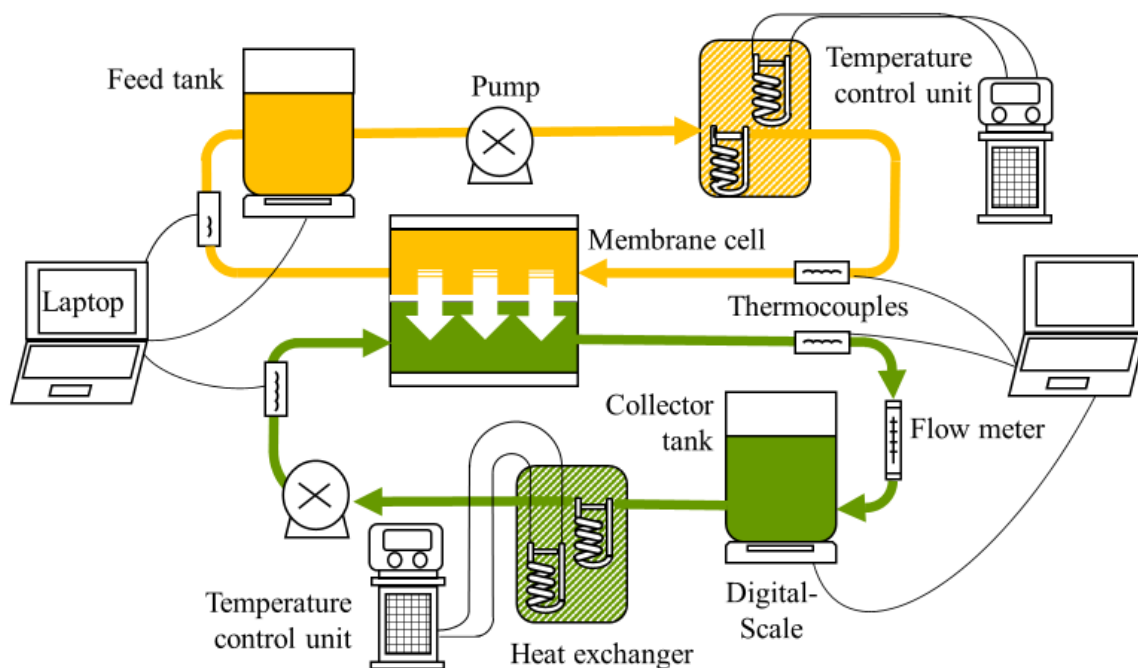


**Figure C.2.** Bench-scale membrane distillation setup utilized in all experiments. Simulated hydrolyzed urine feed solution and collector stream (represented as yellow and green, respectively) are circulated across the membrane cell in countercurrent flow. Digital scales monitor mass changes in the feed and collector tanks and pH of the collector solution is measured periodically. Tanks were enclosed to prevent vapor loss. Heat exchangers are regulated by temperature control units, while thermocouples at the inlets and outlets of the membrane cell record the solution temperature.

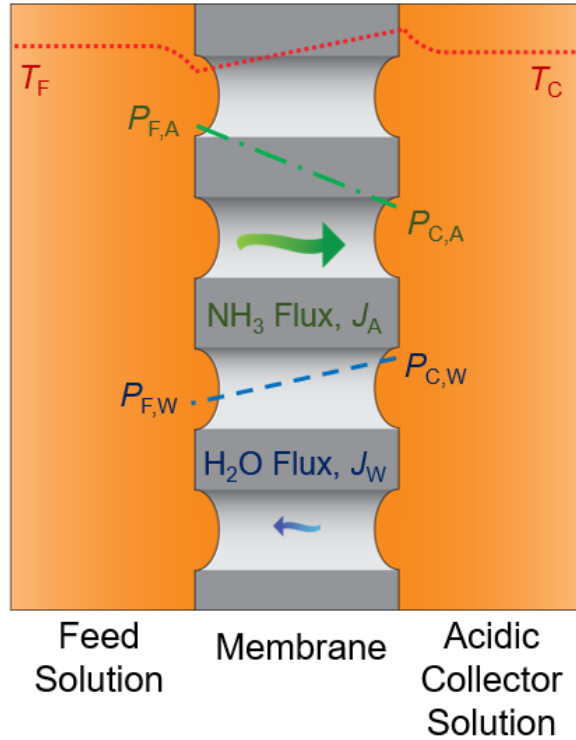


**Figure C.3.** Temperature and vapor pressure profiles in isothermal MD, accounting for temperature polarization at the solution-membrane interfaces. In  $\text{NH}_3$  transport, ammonia in the feed solution vaporizes, permeates across the membrane, and condenses on the collector side. The transfer of  $\text{NH}_3$  volatilization/condensation enthalpy sets up a transmembrane temperature gradient between the collector and feed, i.e., the feed stream is cooled and the collector stream is warmed near the solution-membrane surfaces. The result is a water vapor pressure gradient from collector to feed driving reverse, or negative, water flux.

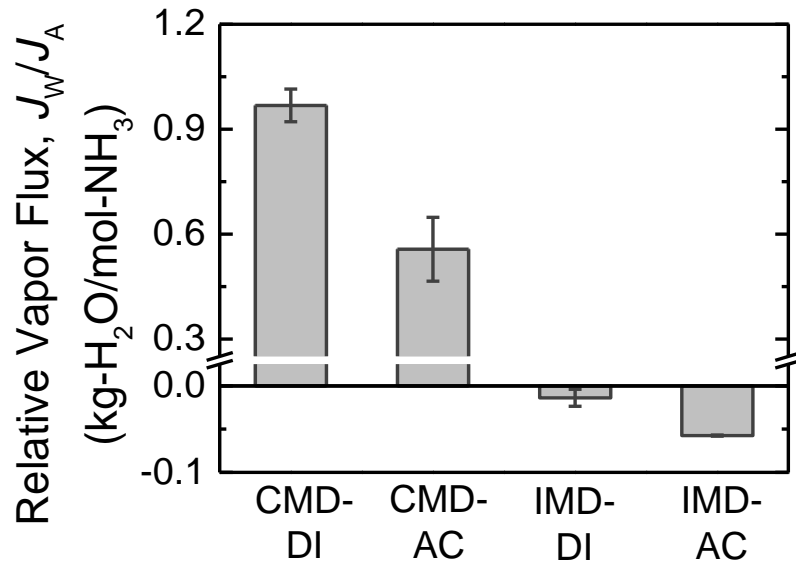


**Figure C.4.** Relative vapor flux of water to ammonia,  $\text{kg-H}_2\text{O/mol-NH}_3$ , for the four operations, CMD-DI, CMD-AC, IMD-DI, and IMD-AC. IMD-DI and IMD-AC exhibit negative relative fluxes because water vapor permeation was in the opposite direction, i.e., from collector to feed side. For CMD, feed and collector solutions are at 40 and 20 °C, whereas both feed and collector solutions are at 40 °C for IMD. Error bars indicate standard deviations of duplicate experiments with different membrane coupon.

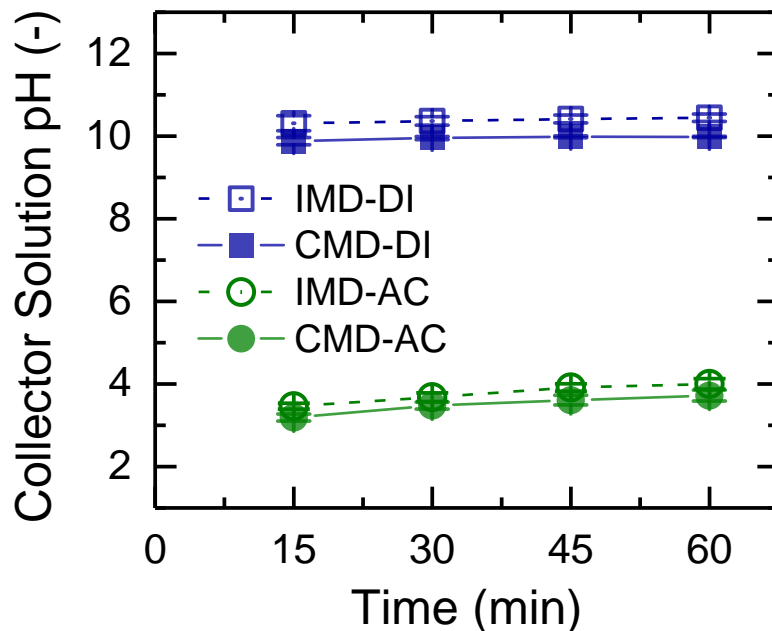


**Figure C.5.** Collector solution pH as a function of time for CMD-DI, CMD-AC, IMD-DI, and IMD-AC experimental runs. Blue square symbols indicate DI water as collector solution, while green circle symbols denote acidic collector of 100 mM acetic acid. Solid and open symbols represent CMD and IMD operation, respectively. For CMD, feed and collector solutions are at 40 and 20 °C, whereas both feed and collector solutions are at 40 °C for IMD. Error bars indicate standard deviations of duplicate experiments with different membrane coupon.

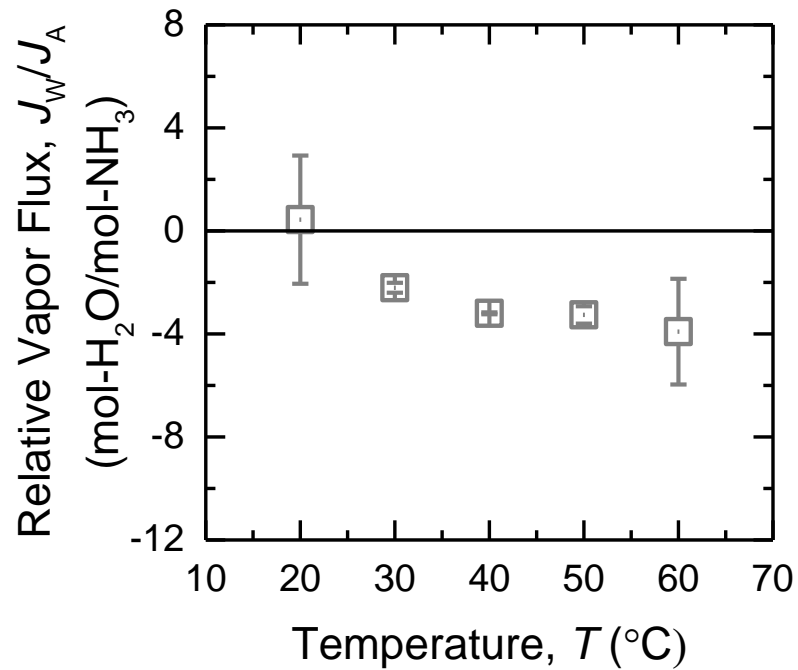
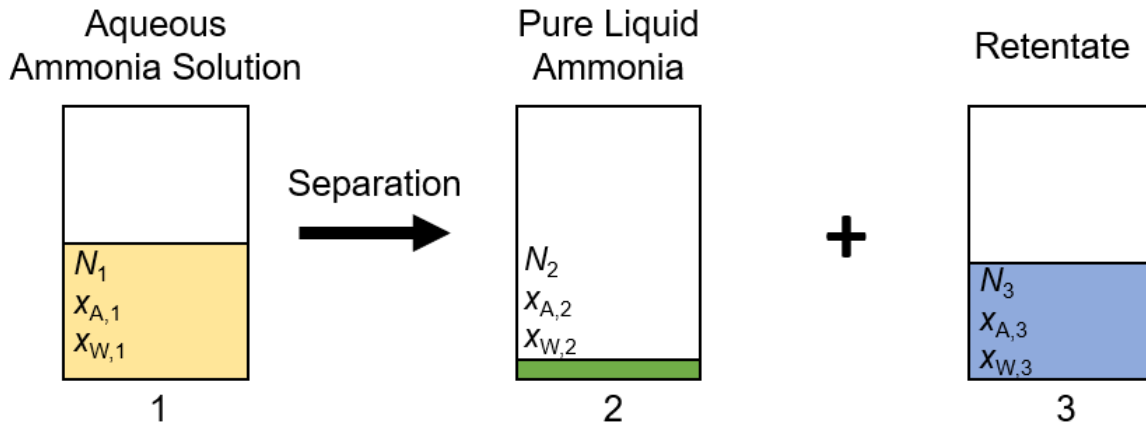


**Figure C.6.** Relative molar flux of water to ammonia in IMD-AC as a function of solution temperature. Negative relative fluxes were exhibited for temperatures between 30–60 °C because water vapor permeation was in the opposite direction, from collector to feed side. Error bars indicate standard deviations of duplicate experiments with different membrane coupons.

## C.2 Vaporization Enthalpy of Ammonia from Aqueous Solutions

**Gibbs Free Energy of Separating Ammonia from Aqueous Solutions.** To determine the enthalpy of ammonia vaporization from an aqueous ammonia solution, as opposed to pure liquid ammonia, the Gibbs free energy of separating pure liquid ammonia from solution is first determined. The separation is depicted in the schematic below:



Aqueous ammonia feed solution, 1, is separated into solution 2, pure liquid ammonia, and solution 3, the retentate with a lower ammonia concentration than the feed solution. Subscripts 1, 2, and 3 represent the respective solutions.  $N$  is total moles of both ammonia and water, i.e.,  $\text{NH}_3(\text{aq})+\text{H}_2\text{O}$ , and  $x$  is the mole fraction of ammonia or water (denoted by subscripts A and W).

The total, ammonia, and water mole balances are expressed in eqns (C.2), (C.3), and (C.4), respectively. Solution 2 is pure liquid ammonia, therefore  $x_{A,2} = 1$  and  $x_{W,2} = 0$ . The fraction of ammonia,  $\text{NH}_3$ , that is separated from the urine feed is defined as  $y$ , eqn (C.5), which can be rearranged to yield eqn (C.6).

$$N_1 = N_2 + N_3 \quad (\text{C.2})$$

$$x_{A,1}N_1 = x_{A,2}N_2 + x_{A,3}N_3 \quad (\text{C.3})$$

$$x_{w,1}N_1 = x_{w,2}N_2 + x_{w,3}N_3 \quad (\text{C.4})$$

$$y \equiv \frac{x_{A,2}N_2}{x_{A,1}N_1} = \frac{N_2}{x_{A,1}N_1} \quad (\text{C.5})$$

$$\frac{N_1}{N_2} = \frac{1}{yx_{A,1}} \quad (\text{C.6})$$

Substituting eqn (C.2) into eqn (C.6) yields eqn (C.7). Combining eqns (C.3), (C.6), and (C.7) gives eqn (C.8) after rearrangement.

$$\frac{N_3}{N_2} = \frac{1}{yx_{A,1}} - 1 \quad (\text{C.7})$$

$$x_{A,3} = \frac{\frac{1}{y} - 1}{\frac{1}{yx_{A,1}} - 1} \quad (\text{C.8})$$

The Gibbs energy of a solution is the sum of the product of the mole fractions of each component,  $i$ , and the Gibbs energy of each respective component, i.e.,  $G = \sum x_i G_i$ . The Gibbs energy of a binary mixture of ammonia and water is expressed as eqn (C.9):

$$G = x_A G_A + x_w G_w + RT \left[ x_A \ln(\gamma_A x_A) + x_w \ln(\gamma_w x_w) \right] \quad (\text{C.9})$$

where  $R$  is the gas constant,  $T$  is temperature, and  $\gamma_i$  is the activity coefficient of component,  $i$ , in the solution. The Gibbs free energy of separation,  $\Delta G_{\text{sep}}$ , is given by eqns (C.10 A)–(C.10D):

$$\Delta G_{\text{sep}} = N_2 G_2 + N_3 G_3 - N_1 G_1 \quad (\text{C.10A})$$

$$G_2 = x_{A,2} G_A + x_{w,2} G_w + RT \left[ x_{A,2} \ln(\gamma_{A,2} x_{A,2}) + x_{w,2} \ln(\gamma_{w,2} x_{w,2}) \right] \quad (\text{C.10B})$$

$$G_3 = x_{A,3}G_A + x_{W,3}G_W + RT \left[ x_{A,3} \ln(\gamma_{A,3}x_{A,3}) + x_{W,3} \ln(\gamma_{W,3}x_{W,3}) \right] \quad (\text{C.10C})$$

$$G_1 = x_{A,1}G_A + x_{W,1}G_W + RT \left[ x_{A,1} \ln(\gamma_{A,1}x_{A,1}) + x_{W,1} \ln(\gamma_{W,1}x_{W,1}) \right] \quad (\text{C.10D})$$

Given that solution 2 is pure liquid ammonia,  $x_{W,2} = 0$  and  $\gamma_{A,2}x_{A,2} = 1$ . For hydrolyzed urine, the concentration of  $\text{NH}_3(\text{aq})$  is relatively dilute (<500 mM) and, thus, solutions 1 and 3 can be simplified using  $\gamma_{W,1}x_{W,1} \approx 1$  and  $\gamma_{W,3}x_{W,3} \approx 1$ . Applying these simplifications and eqns (C.10A)–(C.10D), the Gibbs free energy of separation is approximated to eqn (C.11).

$$\Delta G_{\text{sep}} \approx RT \left[ N_3 x_{A,3} \ln(\gamma_{A,3}x_{A,3}) - N_1 x_{A,1} \ln(\gamma_{A,1}x_{A,1}) \right] \quad (\text{C.11})$$

Normalizing eqn (C.11) by  $N_2$  yields  $\Delta G_{\text{sep},N_2}$ , the energy per mole of  $\text{NH}_3$  separated from the feed solution eqn (C.12).

$$\frac{\Delta G_{\text{sep},N_2}}{RT} \approx \frac{N_3}{N_2} x_{A,3} \ln(\gamma_{A,3}x_{A,3}) - \frac{N_1}{N_2} x_{A,1} \ln(\gamma_{A,1}x_{A,1}) \quad (\text{C.12})$$

For the hydrolyzed urine examined in this study, the ammonia concentration in solutions 1 and 3 are relatively low and the contribution of mole fraction,  $x$ , to the Gibbs free energy of separation is, hence, significantly greater than the effect of activity coefficient,  $\gamma$ . Therefore, the system can be further simplified by assuming  $\gamma_{A,1}$  and  $\gamma_{A,3}$  equal to unity. Finally, substituting eqns (C.6)–(C.8) into eqn (C.12) yields eqn (C.13).

$$\frac{\Delta G_{\text{sep},N_2}}{RT} \approx \left( \frac{1}{y} - 1 \right) \ln(x_{A,3}) - \frac{1}{y} \ln(x_{A,1}) \quad (\text{C.13})$$

The Gibbs free energy to separate an infinitesimally small amount of ammonia from hydrolyzed urine simulated by 500 mM aqueous ammonia solution is calculated to be 9.66 kJ/mol at 40 °C using eqn (C.13).

**Vaporization Enthalpy of Ammonia from Aqueous Solutions.** The enthalpy of vaporization of ammonia from aqueous solutions,  $\Delta H_{A, \text{aq}}$ , is equivalent to the sum of the vaporization enthalpy of pure liquid ammonia,  $\Delta H_{A, \text{l}}$ , and the Gibbs free energy to separate pure liquid ammonia from the aqueous solution, as given by eqn (C.14).

$$\Delta H_{A, \text{aq}} = \Delta H_{A, \text{l}} + \Delta G_{\text{sep}, N_2} \quad (\text{C.14})$$

At the feed temperature during experimental operation, 40 °C,  $H_{A, \text{l}}$  is 18.76 kJ/mol.<sup>257</sup> Hence, the energy required to vaporize an infinitesimally small amount of ammonia from a 500 mM aqueous ammonia solution is 28.42 kJ/mol (i.e., 18.76 + 9.66). This calculated  $\Delta H_{A, \text{aq}}$  is utilized in the energy analysis presented in Figure 4.6 of Chapter 4.

## Appendix D: Supporting Information for Chapter 5

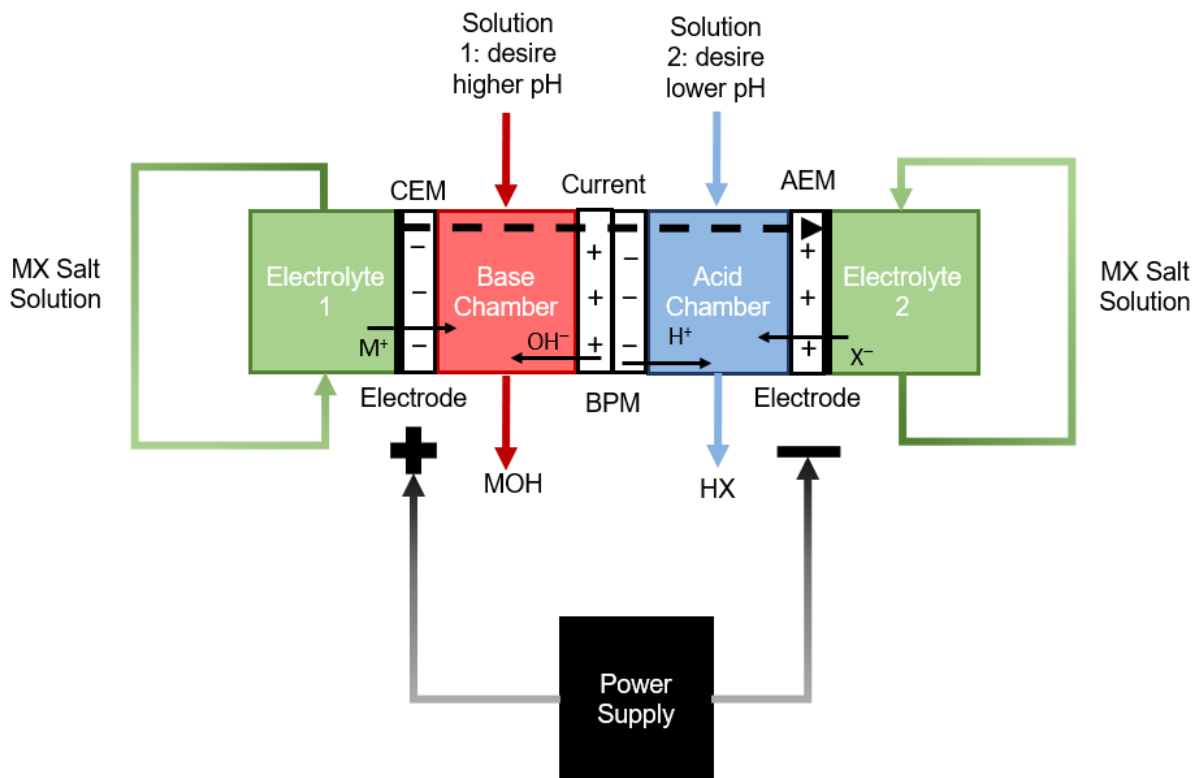


**Figure D.1.** Schematic depicting the setup and working principles of bipolar membrane electro dialysis. Electrolyte solutions of MX salt solution are directed to outer electrolyte chambers. Solution 1, a solution in which the desire is to increase the pH, is directed to the base chamber and solution 2, a solution in which the desire is to decrease the pH, is directed to the acid chamber. Graphite electrodes are placed between the electrolyte chambers and the cation exchange membrane (CEM) and anion exchange membrane (AEM). Next to the CEM and AEM are base and acid chambers, respectively, which are divided by a bipolar membrane (BPM), which contains a positively charged AEM layer facing the base chamber and a negatively charged CEM layer facing the acid chamber. A power supply applies a current between the positive and negative terminals connecting to the electrodes in contact with the CEM and AEM, respectively. The ionic current cannot be sustained by ions in the bulk solution because  $M^+$  cannot pass through the AEM layer of the BPM and  $X^-$  cannot pass through the CEM layer. The current is carried out by electro-dissociation of  $H^+$  and  $OH^-$  at the bipolar junction of the BPM.  $H^+$  and  $OH^-$  ions migrate across the AEM and CEM, respectively, toward the acid and base chambers, respectively. As a result, HX is generated in the acid chamber and MOH is generated in the base chamber.

## D.1 Specific Energy Consumption of BPM-ED

Specific energy consumption of the BPM-ED step is calculated using eqn (5.2) in Chapter 5, here eqn (D.1).<sup>275</sup>

$$\text{SEC} = \frac{I \int_0^t U(t) dt}{V} \quad (\text{D.1})$$

Applied current,  $I$ , is the product of current density,  $j$ , and the area of the bipolar membrane,  $A$ , (i.e.,  $I = jA$ ). The volume of base/acid solution,  $V$ , is based on the experimental conditions (i.e., acid and base chamber volumes, which are 100 mL in this study). Time,  $t$ , is the duration of the BPM-ED step.

The voltage across the stack,  $U$ , is equivalent to the product of current and resistance,  $R$ , across the stack (i.e.,  $U = IR$ ). In this analysis,  $U$  is considered constant over time assuming minimal changes in resistance over the duration of BPM-ED experiments.<sup>275</sup>  $U$  can be measured directly using the power source, Agilent single output DC power supply (U8002A, Santa Clara, CA). However, the custom-built bipolar membrane electro dialysis stack utilized in experiments was not designed to minimize the resistance across the stack and as a result experimentally high voltages were measured ( $\approx 10\text{--}20$  V, Table D.1- experimental voltage drops).

**Table D.1.** Experimental voltage drops across the BPM-ED stack in different BPM-ED operations, which are described by the streams produced, operating mode, and current density as detailed in Chapter 5. Predicted voltage drops based on a more optimized BPM-ED stack based on eqns (D.2)–(D.3) and assumptions presented in Table D.2.

<b>Streams Produced</b>	<b>Operating Mode</b>	<b>Current Density (A/cm<sup>2</sup>)</b>	<b>Predicted U (V)</b>	<b>Experimental U (V)</b>
FU <sub>1</sub>	1	0.01	2.55	10.54
FU <sub>2</sub>	1	0.01	2.50	10.54
FU <sub>3</sub>	1	0.01	2.36	10.54
HU <sub>1</sub> /AC <sub>1</sub>	2	0.02	4.09	13.49
HU <sub>2</sub> /AC <sub>2</sub>	2	0.04	7.73	20.06

The voltage across the stack in a more optimized system can be predicted using the voltages across each component in the stack of anion exchange membrane (AEM), cation exchange membrane (AEM), bipolar membrane, base chamber, acid chamber, and each electrolyte chamber. Note that Table D.1 presents the predicted voltage drops for similar experiments conducted in an optimized system based on analysis presented in subsequent paragraphs. Predicted voltages across the optimized system are  $\approx 61\text{--}78\%$  less than the experimentally measured voltages, which can result in immense savings in energy consumption by eqn (5.2) in Chapter 5. For this reason, the predicted voltages were employed in the analysis.

The predicted voltage drop across the stack,  $U_T$ , is the sum of the voltage drops across the individual components of: chambers  $j$ , the AEM, CEM, and the Donnan potential across the BPM,  $V_D$  (i.e.,  $U_T = \sum U_j + iR_{\text{AEM}} + iR_{\text{CEM}} + V_D$ ). Note that the Donnan potentials across the AEM and CEM are considered negligible and are not considered in this analysis.<sup>275</sup> The Donnan potential across the BPM-ED is determined by eqn (D.2),<sup>275</sup> where  $R$  and  $T$  are the gas constant and temperature,  $Z$  is the dissociation number of the salt,  $C_{\text{H}^+}^{\text{acid}}$  and  $C_{\text{H}^+}^{\text{base}}$  are the concentrations of  $\text{H}^+$

in the acid and base chambers, respectively, and  $\Delta\text{pH}$  is the difference in pH between the chambers as taken by experimentally measured pH.

$$V_D = \frac{RT}{ZF} \ln \frac{C_{H^+}^{acid}}{C_{H^+}^{base}} = 0.0591\Delta\text{pH} \quad (\text{D.2})$$

Voltage drop in each chamber  $j$  can be predicted using  $U_j = iR_j$ . The specific resistance across compartment,  $j$  is calculated by eqn (D.3).<sup>275</sup>

$$R_j = \frac{V_T L_j}{Z_j D_j F C_j} \quad (\text{D.3})$$

where  $V_T$  is the thermal voltage (i.e. 0.0256 V at room temperature),  $L_j$  is the thickness of compartment  $j$  (assumed to be 0.05 cm for each chamber in an optimized system<sup>275</sup>),  $Z_j$  is the dissociation number of the salt in the chamber,  $D$  is the average diffusion coefficient ( $\text{cm}^2/\text{s}$ ),  $F$  is Faraday constant, and  $C_j$  is the concentration of salt in chamber  $j$  taken at the initial point.

Table D.2 presents the assumptions used in the determination of voltage drop across the stack, which are adopted from a previous study.<sup>275</sup>

**Table D.2.** Assumptions utilized for the prediction of voltage drop across the membrane in an optimized BPM-ED stack.

<b>Symbols</b>	<b>Description</b>	<b>Value</b>	<b>Dimension</b>
$A$	Membrane surface area	12.56	$\text{cm}^2$
$D_{acid}$	Effective diffusion coefficient of the acid compartment	0.0001	$\text{cm}^2/\text{s}$
$D_{base}$	Effective diffusion coefficient of the base compartment	$3.32 \times 10^{-5}$	$\text{cm}^2/\text{s}$
$D_{salt}$	Effective diffusion coefficient of the salt compartment	$1 \times 10^{-5}$	$\text{cm}^2/\text{s}$
$R_{AEM}$	Resistance of AEM	2.4	$\Omega \text{ cm}^2$
$R_{CEM}$	Resistance of CEM	3	$\Omega \text{ cm}^2$

## Appendix E: Supporting Information for Chapter 6

**Table E.1.** Assumptions in the calculation of CAPEX for onsite nutrient recovery using Donnan dialysis (DD) for P recovery and membrane distillation (MD) for N recovery. Note that the toilet pricing is the extra cost for the urine diversion toilet relative to a conventional toilet where both toilet prices are based on commercial toilet prices.<sup>311, 312</sup> The piping cost is equal to the total cost for the current collection system for non-potable water reuse at the Solaire building (i.e., dual piping is required for source-separation, therefore an addition piping system is needed), which is provided directly from Natural Systems Utilities.

Component	Cost (\$)	Unit
Toilet <sup>311, 312</sup>	200	Ea.
Piping	200,000	Solaire collection system
Tanks <sup>278-280</sup> (6)	130	Per m <sup>3</sup>
Process Control <sup>278</sup>	140.00	Per m <sup>3</sup> /day
Pumps <sup>278</sup> (6)	5,500.00	Per 100 m <sup>3</sup> /h flow
DD Membrane <sup>313</sup>	180.00	Per m <sup>2</sup>
DD Membrane module <sup>313</sup>	378.00	Per m <sup>2</sup>
Heat Exchanger <sup>278, 314</sup> (2)	325	Per m <sup>2</sup>
MD Membrane <sup>278, 279</sup>	90	Per m <sup>2</sup>
MD Membrane module <sup>280, 315, 316</sup>	2,652.17	Per m <sup>2</sup>

**Table E.2.** Overall heat transfer coefficient,  $U$ , for operations with urine, assumed to have essentially equivalent properties to water, as the target stream to be warmed (i.e., the cold stream) and either steam as the hot stream or hot waste water as the hot stream. Shell and tube heat exchanger is assumed for both operations.<sup>317, 318</sup>

Operation	$U$ (kW/m <sup>2</sup> K)
Steam	2.73
Hot waste water	1.14

**Table E.3.** Temperature of hot stream at the inlet of the heat exchanger,  $T_{H,in}$ , temperature of the cold stream to be warmed at the inlet of the heat exchanger,  $T_{C,in}$ , and target temperature of the warmed stream at the exit of the heat exchanger,  $T_{C,out}$  in heat exchanger operations with steam or hot waste water as the hot stream. Note that  $T_{C,in}$  is assumed to be at room temperature, however, there may be a season effect on this temperature that can be considered in future analysis.  $T_{C,out}$  is the target temperature for operation of isothermal membrane distillation.  $T_{H,in}$  for the hot water is the typical temperature of the hot waste water stream at the Solaire as provided by Natural Systems Utilities.

Operation	Stream	Temperature (°C)
Both	$T_{C,in}$	20
Both	$T_{C,out}$	40
Steam	$T_{H,in}$	150
Hot waste water	$T_{H,in}$	60

**Table E.4.** Assumptions for determining the amortization factor that is required for calculating annualized CAPEX.<sup>279</sup>

<b>Interest rate (per year), <math>i</math></b>	5%
<b>Lifetime Nutrient Recovery System (years), <math>n</math></b>	30
<b>Amortization Factor</b>	0.065

**Table E.5.** Assumptions in the calculation of OPEX of the Donnan dialysis (DD) system for P recovery. Note that KCl is the chemical utilized in the “baseline” operation. In DD with waste chemicals as the chloride source, the costs must consider intake costs, i.e., expenditures for transporting the streams onsite. Chemical costs are based on commercial prices.

	Cost (\$)	Unit
DD Membrane Replacement <sup>319</sup>	5%	membrane cost
Spares <sup>279</sup>	0.033	per m <sup>3</sup> treated urine
Labor <sup>279</sup>	0.03	per m <sup>3</sup> treated urine
Electricity <sup>320</sup>	0.207	per kwh
KCl <sup>321</sup>	350	per ton
Intake of Waste Chemicals (assume 20 mi distance) <sup>279</sup>	0.25	per m <sup>3</sup> transported a mile

**Table E.6.** Assumptions in the calculation of electricity for pumping in the Donnan dialysis and membrane distillation systems.<sup>279</sup>

Symbol	Description	Value
$\rho$	Density of Urine	1017.5 kg/m <sup>3</sup>
$g$	Acceleration of Gravity	9.82 m <sup>2</sup> /s
$\Delta h$	Pump head	45.8 m
$\eta$	Pump Efficiency	62.5

## E.1 Thermal Energy in Membrane Distillation

The specific thermal energy requirement of membrane distillation, SEC, is the sum of the specific energy requirements for external heating, SEC<sub>Ext</sub>, (i.e., increasing stream temperature from ambient temperature to target temperature) and internal heating, SEC<sub>Int</sub> to maintain target temperatures even with heat loss,<sup>281</sup> i.e., eqn (E.1). Note that the analysis in Chapter 6 considers energy requirements and costs associated with those requirements normalized by the recovery rate of N.

$$SEC = SEC_{Ext} + SEC_{Int} \quad (E.1)$$

The specific energy requirements for external heating are calculated using a heat exchanger is calculated using eqn (E.2), where  $Q$  is the mass flow rate,  $Cp$  is heat capacity of the,  $T_A$  is the ambient temperature (assumed to be 20°C) and  $T_T$  is the target temperature (40°C), and subscripts F and C refer to the feed (urine) and collector streams, respectively.

$$SEC_{Ext} = Q_F Cp_F (T_A - T_T) + Q_C Cp_C (T_A - T_T) \quad (E.2)$$

In membrane distillation, heat is “lost” from a stream and transported to another stream by two means: convective and conductive heat transfer. These modes of heat transfer in membrane distillation are elucidated in previous work,<sup>212, 213, 245, 247, 282</sup> but are briefly discussed here in the

context of energy requirements.  $SEC_{Int}$  is the sum of convective and conductive heat transfers,  $Q_E$ , and  $Q_C$ , respectively, i.e., eqn (E.3).

$$SEC_{Int} = Q_E + Q_C \quad (E.3)$$

To support the transportation of volatile components from the feed to collector stream, thermal energy is required for the vaporization enthalpy of volatile components in the feed.<sup>212, 247, 256</sup> Convective heat flux of component  $i$ , is the product of the vaporization enthalpy,  $\Delta H_i$ , and the flux,  $J_i$ , and the total convective heat flux,  $Q_E$ , is the sum of the convective heat flux of all components, i.e., eqn (E.4).<sup>212</sup> Note that  $\Delta H_i$  for species of ammonia and water at the relevant stream temperatures were used in the analysis. Previous work details the determination of convective heat flux in a similar membrane distillation system.<sup>74</sup>

$$Q_E = \left| \sum \Delta H_i J_i \right| \quad (E.4)$$

Conductive heat transport across the membrane also contributes to the thermal energy requirement to maintain target temperatures.<sup>256, 259, 260</sup>  $Q_C$  is calculated by eqn (E.5) where  $k_m$  is thermal conductivity of the membrane, described next,  $\lambda$  is membrane thickness (assumed to be 110 micron), and  $T_{f,m}$  and  $T_{c,m}$  are the temperatures on the feed and collector side of the membrane, respectively, which are determined using methods discussed in subsequent paragraphs.

$$Q_C = \frac{k_m (T_{f,m} - T_{c,m})}{\lambda} \quad (E.5)$$

Thermal conductivity of the membrane is calculated as  $k_m = (1 - \varepsilon)k_{mm} + \varepsilon k_g$ , where  $\varepsilon$  membrane porosity (assumed to be 0.8),  $k_{mm}$  is the thermal conductivity of the membrane material (assumed to be 0.16 W/m<sup>2</sup>K), and  $k_g$  is the thermal conductivity of the gas in the pores of the membrane (assumed to be 0.027 W/m<sup>2</sup>K). The temperatures at the feed and collector side

of the membrane are based on the operation of membrane distillation and is discussed in depth next.

Temperatures at the membrane interface  $T_{f,m}$  and  $T_{c,m}$  can be calculated by eqns (E.6) and (E.7) where  $T_{f,b}$  and  $T_{c,b}$  are the bulk stream temperatures of the feed and collector stream (40°C for both in this analysis),  $h_m$  is the heat transfer coefficient of the membrane (487 W/m<sup>2</sup>K),  $h_f$  is the heat transfer coefficient of the feed stream, urine, (3546 W/m<sup>2</sup>K), and  $h_c$  is the heat transfer coefficient of the collector stream (934 W/m<sup>2</sup>K).<sup>74, 212, 213, 245, 247, 256, 259, 260, 281, 282</sup>

$$T_{f,m} = \frac{h_m \left( T_{c,b} + \frac{h_f}{h_c} T_{f,b} \right) + h_f T_{f,b} - \sum E_{v,i}}{h_m \left( 1 + \frac{h_f}{h_c} \right) + h_f} \quad (\text{E.6})$$

$$T_{f,m} = \frac{h_m \left( T_{f,b} + \frac{h_c}{h_f} T_{c,b} \right) + h_c T_{c,b} + \sum E_{v,i}}{h_m \left( 1 + \frac{h_c}{h_f} \right) + h_c} \quad (\text{E.7})$$

In conventional MD, there is a temperature difference between the feed and collector stream, which results in conductive heat transport from the feed across the membrane to the collector.<sup>74, 212, 213, 245, 247, 256, 259, 260, 281, 282</sup> However, in the analysis presented in Chapter 6, isothermal membrane distillation (i.e., equivalent feed and collector stream bulk temperatures) is utilized. Because the transmembrane temperature gradient is significantly smaller in isothermal membrane distillation, compared to conventional, the conductive heat transport is considerably lower. Although the bulk temperatures are equal, there is still a slight transmembrane temperature gradient due to temperature polarization that drives conductive heat transport. Temperature polarization (i.e., one stream is warmed at the surface of the membrane and the other stream is

cooled) can occur in isothermal membrane distillation due to phase changes of vaporization and condensation, which demand and release heat, respectively.<sup>74</sup>

**Table E.7.** Assumptions in the calculation of OPEX of the membrane distillation (MD) system for N recovery. Note that sulfuric acid is the chemical utilized in the “baseline” operation and for the operation with waste chemicals costs are associated with intake of these chemicals. Sulfuric acid concentration required is 0.355 M and the chemical cost is based on commercial prices.

	<b>Cost (\$)</b>	<b>Unit</b>
MD Membrane Replacement <sup>279</sup>	10%	of membrane cost; annual cost
Spares <sup>279</sup>	0.033	per m <sup>3</sup> treated urine
Labor <sup>279</sup>	0.03	per m <sup>3</sup> treated urine
Sulfuric Acid <sup>322</sup>	3000	per 4200 lbs
Electricity <sup>320</sup>	0.207	per kwh
Natural Gas <sup>323</sup>	8.708	per 1000 ft <sup>3</sup>
Intake of Waste Chemicals (assume 20 mi distance) <sup>279</sup>	0.25	per m <sup>3</sup> transported a mile

**Table E.8.** High and low prices of various P and N fertilizer normalized by kg of target nutrient, P or N. Note that if both P and N are present in the fertilizer, then the value is split between the components on a mole basis. All information is provided by the USDA Agricultural Marketing Service.<sup>283</sup>

<b>Fertilizer</b>	<b>Low</b>		<b>High</b>	
	<b>Price N Fertilizer (\$/kg-N)</b>	<b>value (\$/kg-P)</b>	<b>Price N Fertilizer (\$/kg-N)</b>	<b>value (\$/kg-P)</b>
(NH <sub>4</sub> )H <sub>2</sub> PO <sub>4</sub>	1.69	1.87	1.88	2.08
NH <sub>3</sub> (anhydrous)	1.96		2.08	
(NH <sub>4</sub> ) <sub>2</sub> HPO <sub>4</sub>	2.95	1.47	3.07	1.53
Urea, CH <sub>4</sub> N <sub>2</sub> O	2.07		2.13	
Liquid NH <sub>3</sub> (28%)	2.17		2.48	
Ca(H <sub>2</sub> PO <sub>4</sub> ) <sub>2</sub>		0.55		1.09

**Table E.9.** Assumptions for determining the annualized capital cost of the Solaire non-potable water treatment system and thermal energy recovery unit. The capital costs and lifetime are provided by Natural Systems Utilities.

<b>Total Capital Cost for Non-Potable Water Treatment System at the Solaire</b>	\$2 million
<b>Total Capital Cost for Thermal Energy Recovery Unit at the Solaire</b>	\$150K
<b>Interest rate (per year)</b> <sup>279</sup>	5%
<b>Lifetime Nutrient Recovery System (years)</b>	50
<b>Amortization Factor</b> <sup>279</sup>	0.065

**Table E.10.** Average values of potable water demand, reuse flow from the non-potable water treatment system, and wastewater sent to WWTP at the Solaire from Dec. 2017 to Feb. 2022. For comparison, the same metrics for a reference building (without water reuse) are provided. The reference building has equivalent capacity and water demands as the Solaire, but all water must be sourced from potable water produced in the city rather than the reuse flow. Note all information was provided by Natural System Utilities.

<b>The Solaire</b>	<b>Potable Water Demand (gallons/day)</b>	4,159.76
	<b>Reuse flow (gallons/day)</b>	21,647.68
	<b>Wastewater sent to WWTP (gallons/day)</b>	2,141.85
<b>Reference Building</b>	<b>Potable Water Demand (gallons/day)</b>	25,807.44
	<b>Reuse flow (gallons/day)</b>	0.00
	<b>Wastewater sent to WWTP (gallons/day)</b>	21,823.51

**Table E.11.** Assumptions for determining operating costs for water service, water heating, non-potable water treatment, and thermal energy recovery systems at the Solaire. The distributed annual membrane cost is provided by Natural Systems Utilities. Chemical costs are based on commercial prices.

	<b>Cost (\$)</b>	<b>Unit</b>
<b>Potable water service</b> <sup>324</sup>	0.005481	\$/gallon
<b>Wastewater service</b> <sup>324</sup>	0.008703	\$/gallon
<b>Natural Gas</b> <sup>323</sup>	8.708	\$/1000 ft <sup>3</sup>
<b>Distributed Annual Membrane Cost</b>	3,125	Total
<b>Electricity</b> <sup>320</sup>	0.207	\$/kWh
<b>NaOH</b> <sup>325-327</sup>	8.40	\$/day
<b>Chloro-aluminum hydrate</b> <sup>328</sup>	0.71	\$/day

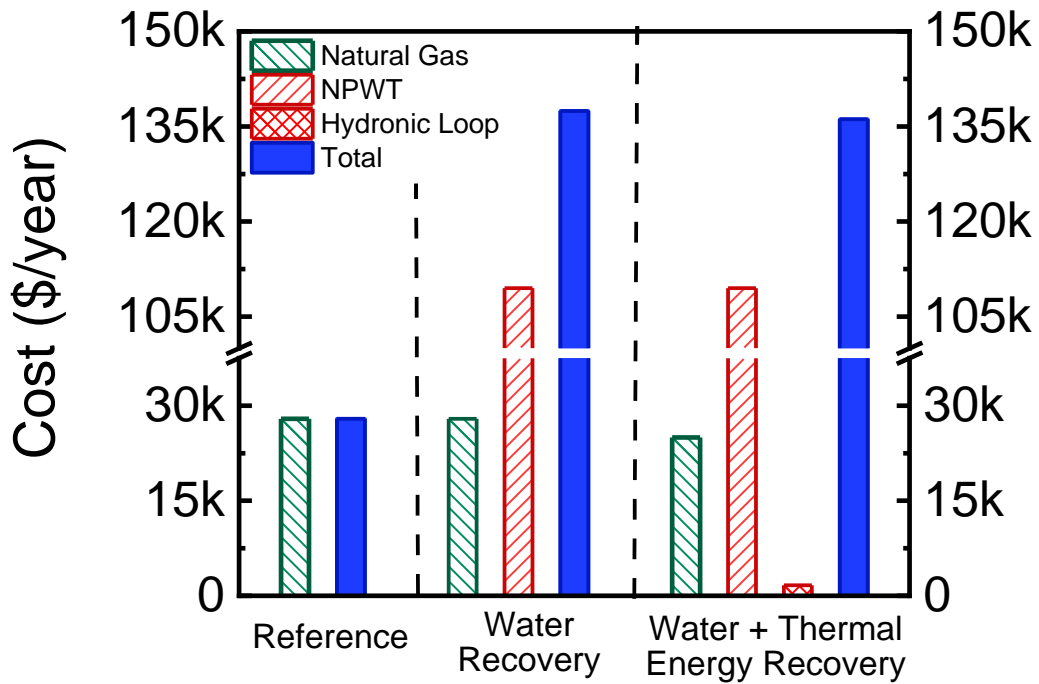


**Figure E.1.** Costs of natural gas, energy use in non-potable water treatment (NPWT), electricity for the hydronic loop, and total energy cost (sum of the aforementioned 3 components) for different scenarios of a reference building without water reuse or thermal energy recovery, the Solaire building with non-potable water reuse (i.e., water recovery), and the Solaire building with non-potable water reuse and thermal energy recovery (i.e., water + thermal energy recovery).

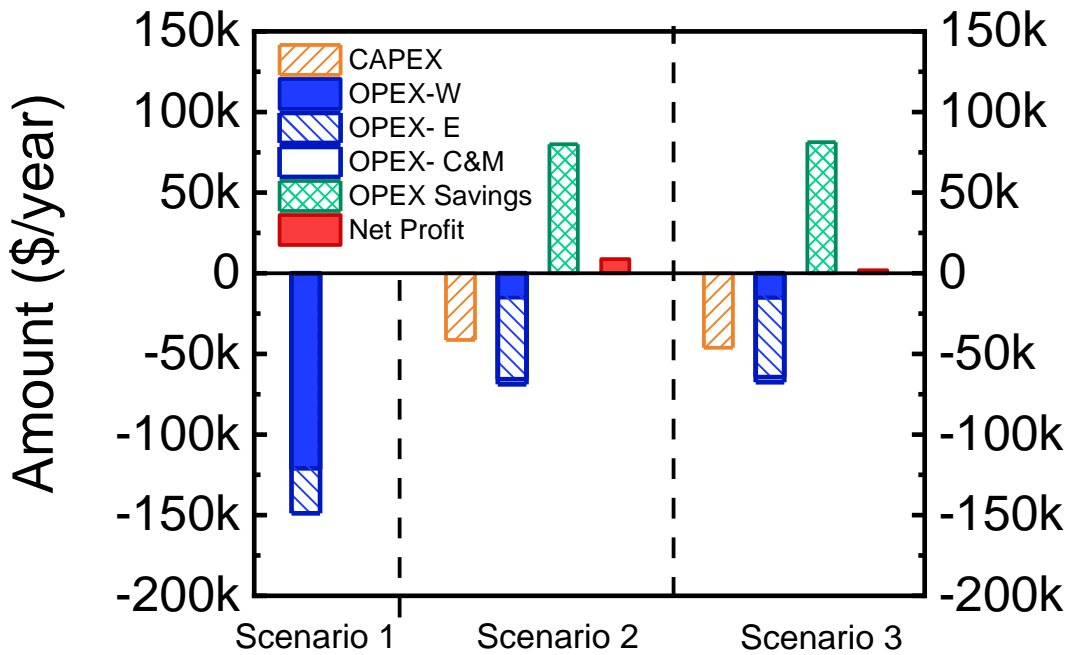


**Figure E.2.** Annualized CAPEX and OPEX broken into energy, water service, and other components for different scenarios of a reference building without water reuse or thermal energy recovery, the Solaire building with non-potable water reuse (i.e., water recovery), and the Solaire building with non-potable water reuse and thermal energy recovery (i.e., water + thermal energy recovery). Note that the CAPEX for the reference system is assumed to be zero because this building is the baseline condition that all other scenarios also have. Water service is the sum of the cost of external drinking water supply and wastewater service. Energy cost is the sum of the costs of natural gas for heating, non-potable water treatment (for scenarios 2 and 3), and electricity for the hydronic loop in the thermal energy recovery unit. Note that OPEX savings for the Solaire systems are relative to the reference case. Net profit of scenario  $x$  is the total costs of reference system - the total cost of scenario  $x$ , where total cost is the sum of annualized CAPEX and OPEX.